UNIVERSIDADE ESTADUAL PAULISTA
"JÚLIO DE MESQUITA FILHO"
Câmpus de São José do Rio Preto

Beatriz de Carvalho Marques

Atividade Antibacteriana de Híbridos Curcumina-cinamaldeído contra Células Planctônicas e Biofilmes de MSSA e MRSA

São José do Rio Preto

2019

Beatriz de Carvalho Marques

Atividade Antibacteriana de Híbridos Curcumina-cinamaldeído contra Células Planctônicas e Biofilmes de MSSA e MRSA

Dissertação apresentada como parte dos requisitos para obtenção do título de Mestre em Microbiologia, junto ao Programa de Pós-Graduação em Microbiologia, do Instituto de Biociências, Letras e Ciências Exatas da Universidade Estadual Paulista "Júlio de Mesquita Filho", Câmpus de São José do Rio Preto.

Financiadoras: FAPESP – Proc. 2017/09245-7

CAPES

Orientador: Prof. Dr. Luis Octavio Regasini

Coorientadora: Dra. Janaina de Cassia Orlandi Sardi

São José do Rio Preto

2019

M357a

Marques, Beatriz de Carvalho

Atividade Antibacteriana de Híbridos Curcumina-cinamaldeído contra Células Planctônicas e Biofilmes de MSSA e MRSA / Beatriz de Carvalho Marques. -- São José do Rio Preto, 2019

166 p. : tabs., fotos

Dissertação (mestrado) - Universidade Estadual Paulista (Unesp), Instituto de Biociências Letras e Ciências Exatas, São José do Rio Preto

Orientador: Luis Octavio Regasini

Coorientador: Janaína de Cassia Orlandi Sardi

1. Microbiologia. 2. Bactérias resistêntes e multirresistentes. 3. Staphylococcus aureus. 4. ESKAPE. 5. Híbridos curcumina-cinamaldeído. I. Título.

Sistema de geração automática de fichas catalográficas da Unesp. Biblioteca do Instituto de Biociências Letras e Ciências Exatas, São José do Rio Preto. Dados fornecidos pelo autor(a).

Essa ficha não pode ser modificada.

Beatriz de Carvalho Marques

Atividade Antibacteriana de Híbridos Curcumina-cinamaldeído contra Células Planctônicas e Biofilmes de MSSA e MRSA

Dissertação apresentada como parte dos requisitos para obtenção do título de Mestre em Microbiologia, junto ao Programa de Pós-Graduação em Microbiologia, do Instituto de Biociências, Letras e Ciências Exatas da Universidade Estadual Paulista "Júlio de Mesquita Filho", Câmpus de São José do Rio Preto.

Financiadoras: FAPESP – Proc. 2017/09245-7

CAPES

Comissão Examinadora

Prof. Dr. Luis Octavio Regasini

UNESP – Instituto de Biociências, Letras e Ciências Exatas - São José do Rio Preto (Orientador)

Profª. Dra. Mara Corrêa Lelles Nogueira

FAMERP – Faculdade de Medicina de São José do Rio Preto - São José do Rio Preto

Profª. Dra. Tais Maria Bauab

UNESP – Faculdade de Ciências Farmacêuticas - Araraquara

São José do Rio Preto

6 de junho de 2019

Dedico esse trabalho à minha mãe, Dilma José de Carvalho, pelo apoio incondicional durante toda a minha vida, e pelo imenso esforço dedicado à minha educação. Dedico ainda, aos meus avós maternos, Anildes e José, e ao meu irmão, Carlos, que sempre me apoiaram, mesmo sem entender muito bem o motivo de eu me dedicar tanto à minha formação.

AGRADECIMENTOS

Primeiramente, agradeço à **Deus**, pela vida, pela saúde, pelas conquistas, por me sustentar nos momentos mais difíceis.

Ao meu orientador, **Prof. Dr. Luis Octávio Regasini**, por todos os ensinamentos e "puxões de orelha" durante os seis anos que estive em seu laboratório. Por ter confiado em mim para a execução deste trabalho. Serei eternamente grata por tudo que aprendi com você.

À minha coorientadora, **Dra. Janaína Sardi**, por me receber em seu laboratório e por me fornecer todo o suporte necessário para a realização dos experimentos biológicos. Obrigada por ser uma coorientadora presente, se preocupando e confiando no meu trabalho. Aprendi muito com você.

Agradeço à minha mãe, **Dilma**, por todo o apoio, incentivo e ensinamentos, por acreditar em mim e me encorajar sempre. Você é meu exemplo de determinação e força de vontade. Sem você nada disso seria possível. Agradeço também ao meu irmão, **Carlos**, e aos meus avós, **Anildes** e **José**, pelo apoio nas horas mais difíceis e por todas as palavras de apoio.

Agradeço ao meu namorado **Luiz Henrique**, pelo companheirismo e compreensão nos momentos mais difíceis. Obrigada por sempre acreditar no meu potencial e me mostrar o lado positivo de todos os acontecimentos da vida.

À todas as pessoas que estão e já passaram pelo Laboratório de Antibióticos e Quimioterápicos (LAQ), por todo o auxílio no cotidiano laboratorial e pela contribuição no meu conhecimento científico. Agradeço, especialmente, à **Mariana**, **Isabelle**, **Carlos**, **Gabriela**, **Mayara**, **Éder**, **Guilherme**, **Ana**, **Daiane**, **Caroline** e **Thaíse**, pela amizade, apoio, ajuda, conversas e momentos de diversão.

Às minhas amigas de graduação, **Gabrielle** e **Gabriela**, por me proporcionarem tantos momentos bons e por estarmos sempre juntas, principalmente nos momentos difíceis. Agradeço muito pelo companheirismo.

Ao **Prof. Dr. Pedro Rosalen**, por ceder seu laboratório e fornecer o suporte necessário para a realização da maioria dos experimentos biológicos, e aos seus alunos da pós-graduação, **Josy**, **Rafaela** e **Diego** por todo apoio e presteza durante o meu período em Piracicaba - SP.

Agradeço à todos os colaboradores deste trabalho. À Profª. Dra. Eleni Gomes e ao **Me. Diego Monteiro**, pelo auxílio durante as análises de Cromatografia Líquida de Alta Eficiência. Ao **Prof. Dr. Fernando Pavan** e à **Me. Gabriela Ayusso**, pela realização do experimento em *Mycobacterium tuberculosis*.

Ao **Centro Multiusuário de Inovação Biomolecular**, Instituto de Biociências, Letras e Ciências Exatas, UNESP/São José Do Rio Preto (FAPESP – processo nº 2009/53989-4), pela utilização dos espectrômetros Bruker Avance III 9,397 t (400 MHz) e 14,095 t (600 MHz). Ao **Laboratório-II de Ressonância Magnética Nuclear**, do Instituto de Química, UNESP/Araraquara, pela utilização do espectrômetro Bruker Fourier (300 MHz).

Agradeço também a todos os **professores** que fizeram parte da minha formação, que me passaram um pouco do conhecimento próprio com tamanha vontade e dedicação. Agradeço, especialmente, à todos os docentes do **Programa de Pós-Graduação em Microbiologia** e ao **IBILCE/UNESP**, local onde passei tanto tempo durante os últimos seis anos e que se tornou a minha segunda casa. Tenho muito orgulho de ter estudado neste câmpus.

À **Fundação de Amparo à Pesquisa do Estado de São Paulo** (FAPESP), pela bolsa concedida durante o mestrado (Processo nº 2017/09245-7) para a realização do presente trabalho.

O presente trabalho foi realizado com apoio da **Coordenação de Aperfeiçoamento de Pessoal de Nível Superior - Brasil** (CAPES) - Código de Financiamento 001.

À **comissão examinadora**, pela disponibilidade e aceite em me ajudar à melhorar este trabalho.

RESUMO

Staphylococcus aureus é uma bactéria Gram-positiva, comensal e patogênica, que coloniza aproximadamente 30% da população humana, apresentando resistência a vários antibióticos. Estudos indicam a bioatividade da curcumina e do cinamaldeído contra *S. aureus*, no entanto, ambos apresentam limitações que impedem seu uso como agente terapêutico. Assim, a fim de otimizar a atividade anti-*S. aureus* da curcumina e do cinamaldeído, bem como suas propriedades químico-biológicas, no presente estudo, duas séries de híbridos curcumina-cinamaldeído foram planejadas e sintetizadas, sendo posteriormente avaliadas contra *S. aureus* sensível e resistente à meticilina (MSSA e MRSA). O híbrido mais ativo foi selecionado para avaliação da sua combinação com antibióticos, e quanto a sua atividade anti-adesão, antibiofilme e no tempo de morte de MSSA e MRSA. A toxicidade *in vivo* deste hídrido também foi avaliada utilizando o invertebrado *Galleria mellonella*. Os híbridos ainda foram avaliados quanto à sua atividade antibacteriana contra outras espécies bacterianas e *Mycobacterium tuberculosis*, e investigados *in silico* quanto às suas propriedades *drug-likeness*. Trinta híbridos foram obtidos com pureza entre 86 e 100%, sendo doze inéditos. Em geral, a hibridação molecular entre a curcumina e o cinamaldeído manteve ou aumentou a atividade antibacteriana dos híbridos quando comparados com a curcumina e com o cinamaldeído, sendo que a lipofilicidade foi um parâmetro central na bioatividade contra MSSA e MRSA. O híbrido **20** apresentou atividade anti-*S. aureus* mais pronunciada, com valores de Concentração Inibitória Mínima (CIM) de 7,8 µg/mL e Concentração Bactericida Mínima (CBM) de 15,6 µg/mL para MSSA, e CIM de 3,9 µg/mL e CBM de 7,8 µg/mL para MRSA, sendo selecionado para os ensaios subsequentes. As associações entre **20** e vancomicina ou meticilina aumentaram a atividade antibacteriana contra MSSA e MRSA. O tratamento com **20** diminuiu a aderência das cepas de MSSA e MRSA aos queratinócitos humanos, quando comparado ao grupo não tratado. Para os biofilmes, após o tratamento com **20**, verificou-se uma diminuição na sua sobrevivência quando comparado ao controle negativo, apresentando atividade antibiofilme similar ou superior à vancomicina e à meticilina. No ensaio de tempo de morte, o tratamento com **20** diminuiu a população bacteriana, indicando ação bactericida. Além disso, **20** apresentou toxicidade a 90 mg/kg, após 72 horas de tratamento, sendo responsável pela morte de 50% da larvas de *Galleria mellonella*. Os híbridos mais lipofílicos demonstraram maior bioatividade contra *Enterococcus faecalis*, *Staphylococcus epidermidis* e *Pseudomonas aeruginosa*. Os híbridos não apresentaram atividade antibacteriana contra *Escherichia coli*. *Acinetobacter baumannii* foi a espécie bacteriana mais suscetível aos híbridos. Contra *Mycobacterium tuberculosis*, verificou-se que a inserção de grupos retiradores de elétrons e lipofílicos aumentou a atividade antimicobacteriana. Com relação aos estudos *in silico*, os híbridos não violaram as regras estabelecidas por Lipinski e Veber, corroborando boas propriedades drug-likeness. Neste estudo, pode-se comprovar a atividade antibacteriana de híbridos de curcumina-cinamaldeído, estimulando o estudo dessas substâncias, a fim de buscar agentes capazes de atuar contra cepas resistentes.

Palavras chave: *Staphylococcus aureus*, curcumina, cinalmaldeído, hibridação molecular

ABSTRACT

Staphylococcus aureus is a gram-positive, commensal and pathogenic bacteria that colonizes approximately 30% of the human population, presenting resistance to several antibiotics. Studies indicate the bioactivity of curcumin and cinnamaldehyde against *S. aureus*, however, both have limitations that prevent its use as a therapeutic agent. Thus, in order to optimize anti-*S. aureus* activity of curcumin and cinnamaldehyde, as well as its chemical-biological properties, in the present study, two series of curcumin-cinnamaldehyde hybrids were planned and synthesized and subsequently evaluated against methicillin-susceptible and methicillin-resistant *S. aureus* (MSSA and MRSA). The most active hybrid was selected for evaluation of its combination with antibiotics, and for its anti-adhesion activity, antibiofilm and the time kill of MSSA and MRSA. *In vivo* toxicity of this hybrid was also evaluated using the *Galleria mellonella* invertebrate. Hybrids were further evaluated for their antibacterial activity against other bacterial species and *Mycobacterium tuberculosis*, and investigated *in silico* for their drug-likeness properties. Thirty hybrids were obtained with purity between 86 and 100%, of which twelve were unpublished. In general, the molecular hybridization between curcumin and cinnamaldehyde maintained or increased the antibacterial activity of hybrids when compared to curcumin and cinnamaldehyde, and lipophilicity was a central parameter in bioactivity against MSSA and MRSA. Hybrid **20** showed more pronounced activity, presented Minimal Inhibitory Concentration (MIC) of 7.8 μg/mL and Minimum Bactericidal Concentration (MBC) of 15.6 μg/mL for MSSA, and MIC of 3.9 μg/mL and MBC of 7,8 μg/mL for MRSA, being selected for subsequent assays. Associations between **20** and vancomycin or methicillin increased the antibacterial activity against MSSA and MRSA. Treatment with **20** decreased the adherence of MSSA and MRSA strains onto human keratinocytes when compared to the untreated group. For biofilms, after treatment with **20**, there was a decrease in their survival when compared to the negative control, presenting antibiofilm activity similar or superior to vancomycin and methicillin. In time kill assay, treatment with **20** decreased the bacterial population, indicating bactericidal action. In addition, **20** presented toxicity at 90 mg/kg, after 72 hours of treatment, being responsible for the death of 50% of *G. mellonella*. Against *Enterococcus faecalis*, *Staphylococcus epidermidis* and *Pseudomonas aeruginosa*, the more lipophilic hybrids demonstrated greater bioactivity. Hybrids showed no antibacterial activity against *Escherichia coli*. *Acinetobacter baumannii* was the bacterial species most susceptible to hybrids. Against *Mycobacterium tuberculosis*, it was found that the insertion of electron withdrawing and lipophilic groups increased the antimycobacterial activity. In relation to *in silico* studies, hybrids did not violate the rules established by Lipinski and Veber, corroborating good drug-likeness properties. In this study, we can prove the antibacterial activity of curcumin-cinnamaldehyde hybrids, stimulating the study of these substances, in order to find agents capable of acting against resistant strains.

Key words: *Staphylococcus aureus*, curcumin, cinalmaldehyde, molecular hybridization

LISTA DE ILUSTRAÇÕES

Capítulo I

Capítulo II

LISTA DE TABELAS

Capítulo II

LISTA DE ABREVIATURAS E SÍMBOLOS

δ - Chemical shift

δ_C - Carbon chemical shift

δ_H - Hydrogen chemical shift

Agr - Accessory gene regulator

Bap protein - Biofilm-associated surface protein

BBB - blood-brain barrier

BHI - Brain Heart Infusion

CBM - Concentração Bactericida Mínima

$CDCl_3$ - deuterated chloroform

CFU/mL - colony-forming unities per mL

CIM - Concentração Inibitória Mínima

ClfB - Clumping factor B

^{13}C NMR - ^{13}C Nuclear Magnetic Resonance

CWA proteins - Cell Wall Anchored Proteins

d: doublet

dd: doublet of doublets

ddd: doublet of doublet of doublets

DMEM: Dulbecco's Modified Eagle's Medium

DMSO - dimethylsulfoxide

DMSO-d_6 - hexadeuterated dimethylsulfoxide

ESKAPE - *Enterococcus faecium*, *Staphylococcus aureus*, *Klebsiella pneumoniae*, *Acinetobacter baumannii*, *Pseudomonas aeruginosa*, and *Enterobacter* species

FDA - Food and Drug Administration

FnBPs – Fibrinogen Binding Proteins

HBA: Hydrogen Bond Acceptors

HBD: Hydrogen Bond Donors

HIA: Human Intestinal Absorption

^{1}H NMR: Hydrogen Nuclear Magnetic Resonance

HPLC-PAD: High Performance Liquid Chromatography with Photodiode Array Detection

J - coupling constant

Log $P_{o/w}$: partition coefficient *n*-octanol/water

m - multiplet

MBC: Minimum Bactericidal Concentration

MIC: Minimum Inhibitory Concentration

MRSA - Methicillin-resistant *Staphylococcus aureus*

MSSA - Methicillin-sensitive *Staphylococcus aureus*

MW: Molecular Weight

NROTB: Number of Routable Bonds

PIA - Polysaccharide Intercellular Adhesin

s - singlet

SasG - Surface protein G

SD - Standard Deviation

SdrC - Serine-aspartate repeat-containing protein C

SEM - Scanning Electron Microscopy

SpA - Protein A

TLC: Thin-Layer Chromatography

TSA - Tryptic Soy Agar

TSB - Tryptic Soy Broth

VISA - Vancomycin-Intermediate *Staphylococcus aureus*

VRSA - Vancomycin-Resistant *Staphylococcus aureus*

SUMÁRIO

CAPÍTULO I

1. INTRODUÇÃO E REVISÃO BIBLIOGRÁFICA

1.1. *Staphylococcus aureus* e sua importância clínica

As infecções nosocomiais, também conhecidas como infecções hospitalares, são infecções que podem ocorrer durante os cuidados de saúde para outras doenças ou mesmo após a alta de paciente (KHAN, AHMAD; MEHBOOB, 2015; KHAN, BAIG; MEHBOOB, 2017). Em 2011, nos Estados Unidos, foram relatados cerca de 722.000 casos e 75.000 mortes decorrentes de infecções nosocomiais (MAGILL et al., 2014), sendo que as bactérias são responsáveis por cerca de 90% desses casos, enquanto protozoários, fungos, vírus e micobactérias representam, aproximadamente 10% (KHAN, AHMAD; MEHBOOB, 2015). Essas infecções podem ter como origens, fatores exógenos ou endógenos, podendo ser transferidas por contato direto ou indireto entre pacientes, profissionais de saúde, objetos contaminados, visitantes ou até mesmo por fontes ambientais (SANTAJIT; INDRAWATTANA, 2016).

Um dos principais microrganismos envolvido em infecções nosocomiais é *Staphylococcus aureus*, uma bactéria Gram-positiva, comensal e patogênica, que coloniza aproximadamente 30% da população humana (TONG et al., 2015). Embora a colonização geralmente não seja prejudicial, esse microrganismo pode romper as defesas inatas do hospedeiro e obter acesso aos tecidos mais profundos, causando uma variedade de infecções superficiais e sistêmicas (BALASUBRAMANIAN et al., 2017).

Em indivíduos saudáveis, *S. aureus* frequentemente causa infecções menos graves, como o impetigo, foliculite e abscessos cutâneos. Infecções mais graves incluem piomiosite, fascite necrosante (TONG et al., 2015) e pneumonia necrosante (SADER et al., 2016; KALE; DHAWAN, 2016). No entanto, são nos ambientes de cuidados com a saúde, que se concentram os casos mais graves de infecções por *S. aureus*, sendo que estas podem ser iniciadas em locais cirúrgicos ou a partir de dispositivos médicos implantados, incluindo válvulas cardíacas, cateteres, próteses e implantes ortopédicos (BROOKS; JEFFERSON, 2012), resultando em bacteremia, um dos estágios mais complicados da infecção por *S. aureus* (TONG et al., 2015).

A capacidade desse patógeno persistir em uma grande variedade de nichos nos hospedeiros, que variam de pele (MONTGOMERY, DAVID; DAUM 2015), dispositivos

abióticos (SCHERR et al. 2014) a tecidos profundos dificulta a sua eliminação, resultando em infecções recorrentes e de difícil tratamento (BALASUBRAMANIAN et al., 2017).

1.2. Biofilmes de *Staphylococcus aureus*

Biofilme consiste em uma comunidade de microrganismos, representada por células que estão aderidas a um substrato, interface, ou entre si. Este conjunto de células está disperso em uma matriz polimérica, exibindo fenótipos alterados em relação ao crescimento, expressão gênica e produção proteica (DONLAN; COSTERTON, 2002). Embora a formação de biofilme não seja um pré-requisito para a infecção persistente, ela ocorre na maioria dos casos, requerendo tratamento mais específico e, muitas vezes, com a associação de fármacos (KRISTIAN et al., 2004).

A formação de um biofilme pode ser caracterizada por uma sucessão de eventos, que incluem: adesão, maturação e dispesão (Figura 1, p. 28). Primeiramente, as bactérias planctônicas de uma infecção aderem-se à uma superfície favorável à sua sobrevivência. Essa adesão dependerá da espécie do patógeno, da composição da superfície (hidrofobicidade, composição química, tensão superficial, cargas eletrostáticas, temperatura), fatores ambientais e produtos gênicos essenciais ao desenvolvimento microbiano (DUNNE, 2002). Em uma infecção de *S. aureus*, essa adesão é mediada por uma ligação entre o patógeno e o hospedeiro, mediada por proteínas CWA (do inglês, *Cell Wall Anchored Proteins*), tais como: ClfB, FnBPs, SdrC, Bap, SasG e SpA (DAYAN et al., 2016).

Após a adesão, inicia-se a maturação, que consiste no desenvolvimento da estrutura multicelular do biofilme, por meio da divisão celular, produção de uma matriz extracelular polimérica e pela desaceleração do metabolismo (O'TOOLE; KAPLAN; KOLTER, 2000). A maturação tem início quando as células bacterianas induzem o mecanismo de *quorum-sensing* que pode ativar ou inibir o desenvolvimento de biofilme, criando uma agregação intercelular por meio da produção da matriz (FOSTER et al., 2014). Essa matriz é composta por fatores do hospedeiro, polissacarídeos, proteínas associadas à superfície e DNA extracelular (MONTANARO et al., 2011). A maturação da comunidade microbiana promove a formação de canais de fluido que são vitais para

fornecer nutrientes às células presentes nas camadas mais profundas do biofilme (COSTERTON et al., 1995).

Após o desenvolvimento, pode ocorrer o desprendimento de células individuais e aglomerados celulares a partir do biofilme formado sob condições ambientais favoráveis ou em caso de expansão, disseminando-se para novos locais de infecção (OTTO, 2013). Esse desprendimento é baseado em forças mecânicas, bem como na interrupção da produção e destruição de parte da matriz extracelular (PERIASAMY et al., 2012). Pequenas variantes de colônia associadas a biofilmes ajudam o *S. aureus* a sobreviver em um estado de metabolismo reduzido, facilitando infecções persistentes, recorrentes e graves (VON EIFF, PETERS; BECKER, 2006).

Figura 1. Formação e dispersão do biofilme de *S. aureus*. Fonte: Adaptado de ENANY; ALEXANDER, 2017

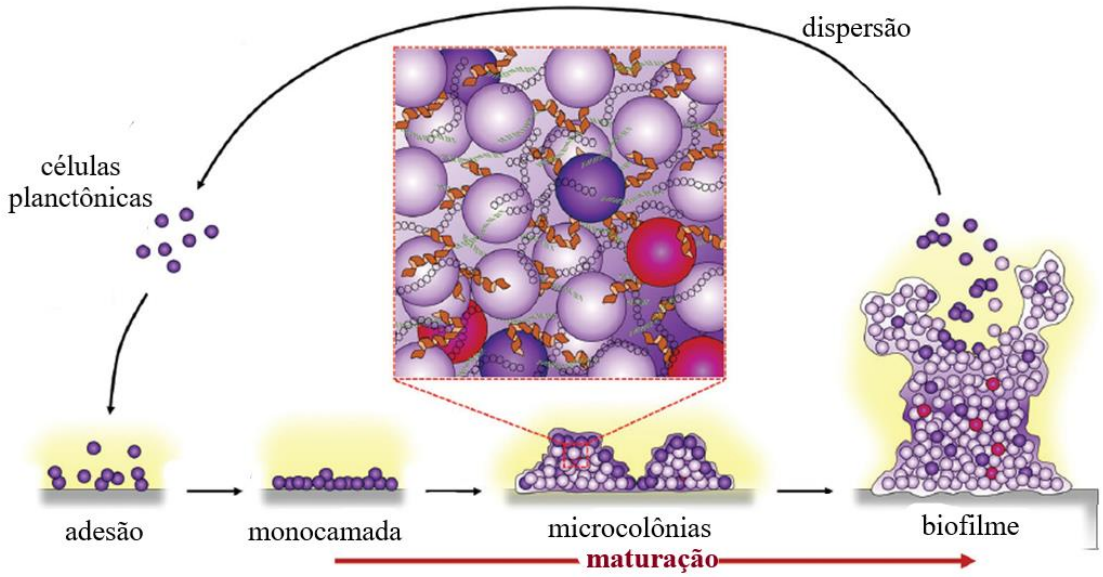

A formação e a dispersão do biofilme de *S. aureus*, assim como de outros patógenos, é influenciada pela atuação do sistema imunológico do hospedeiro e pela presença ou ausência de nutrientes. A glicose e o pH do hospedeiro, por exemplo, podem ativar o desenvolvimento do biofilme de *S. aureus* por regular o funcionamento do sistema Agr (do inglês, *Accessory gene regulator*), principal sistema de *quórum-sensing* desse patógeno Além disso, a presença da matriz presente na estrutura de um biofilme

pode proteger os microrganismos incorporados de todas essas variações e pressões seletivas proporcionadas pelo hospedeiro (BOLES; HORSWILL, 2008).

Assim, o modo de crescimento de *S. aureus*, rigidamente regulado por fatores genéticos complexos, impossibilita uma resposta imunológica efetiva do hospedeiro contra infecções persistentes acompanhadas de biofilmes, culminando em infecções crônicas (ARCHER et al., 2011), bem como dificultando o tratamento devido à natureza recalcitrante dos biofilmes e a resistência aos antibacterianos (GIL et al., 2014).

1.3. Resistência de *Staphylococcus aureus* aos antibacterianos

Décadas após os primeiros pacientes terem sido tratados com antibacterianos, as infecções bacterianas voltaram a ser um problema para a população mundial (SPELLBERG; GILBERT, 2014). A resistência desenvolvida pelos microrganismos frente aos antibióticos pode ser atribuída a diversos fatores, incluindo o uso irracional desses fármacos, ao fluxo rápido e constante de pessoas por diferentes regiões do planeta, o que permite que patógenos tenham acesso à um grande número de hospedeiros, bem como a falta de desenvolvimento de fármacos inovadores (MICHAEL, DOMINEY-HOWES; LABBATE, 2014). Assim, esforços devem ser coordenados para implementar políticas, renovar pesquisas, e buscar medidas para combater a resistência aos antibióticos (VENTOLA, 2015).

A resistência desenvolvida por *S. aureus* frente aos antibacterianos envolve, dentre outros fatores, a aquisição de elementos genéticos móveis por transferência horizontal (JENSEN; LYON, 2009), sendo que estes podem ter evoluído em microrganismos produtores de antibióticos para protegê-los de substâncias antibacterianas (NESME; SIMONET, 2015). Outro fator relacionado a resistência de *S. aureus* aos antibacterianos são mutações que alteram os receptores farmacológicos e o aumento da expressão de bombas de efluxo (FOSTER, 2017).

Em 1959, a meticilina (Figura 2, p. 30), um antibiótico β-lactâmico semissintético resistente à penicilinase (β-lactamase), foi desenvolvida em resposta ao surgimento e disseminação da resistência de microrganismos à penicilina G. No entanto, entre julho e outubro de 1960 foram descritos os primeiros casos de resistência de *S. aureus*, surgindo as cepas MRSA (Methicillin-resistant *Staphylococcus aureus*). Atualmente a meticilina

não é produzida, bem como utilizada clinicamente, mas o MRSA persistiu, podendo adquirir resistência a vários fármacos antibacterianos, tornando a farmacoterapia anti-infecciosa ineficaz (RODVOLD; MCCONEGHY, 2014).

Figura 2. Estrutura da meticilina

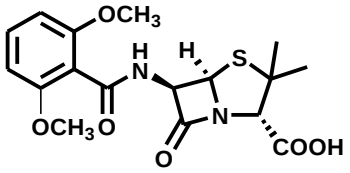

Até o final da década de 1990, os clones de MRSA resistentes à múltiplos fármacos haviam se tornado os agentes mais frequentes das infecções por *S. aureus* (DELEO; CHAMBERS, 2009). Apesar do fato de que atualmente existe uma disponibilidade de vários fármacos antibacterianos estruturalmente diferentes, a terapia mais frequentemente utilizada para o tratamento de infecções por MRSA consistem em glicopeptídeos, principalmente vancomicina (Figura 3, p. 31). No entanto, a partir de 1980, houve um aumento abrupto e continuado da administração de vancomicina, culminando no aumento da frequência de resistência até os dias atuais, resultando no surgimento de cepas VISA (Vancomycin-Intermediate *Staphylococcus aureus*) e VRSA (Vancomycin-resistant *Staphylococcus aureus*) (GARDETE; TOMASZ, 2014).

Assim, desde o final da década de 1980, não se observa descoberta de novos agentes antibacterianos, sendo que o último fármaco liberado para o tratamento de infecções estafilocócicas foi o lipopeptídeo daptomicina, em 1987 (SILVER, 2011). No entanto, na última década, *S. aureus* adquiriu uma elevada relevância clínica, principalmente devido ao aumento no ressurgimento de cepas resistentes e cepas multirresistentes (ZECCONI; SCALI, 2013). Além disso, atualmente, *S. aureus* compõe o grupo de patógenos conhecidos como "ESKAPE" (*Enterococcus faecium*, *Staphylococcus aureus*, *Klebsiella pneumoniae*, *Acinetobacter baumannii*, *Pseudomonas aeruginosa*, and *Enterobacter* species), bactérias Gram-positivas e Gram-negativas que causam numerosas infecções nosocomiais com risco de morte entre os pacientes (RICE, 2010; SANTAJIT; INDRAWATTANA, 2016). Por este motivo, o número crescente de infecções resistentes aos antibacterianos demonstra claramente a necessidade da pesquisa por substâncias capazes de atuar contra esse patógeno.

Figura 3. Estrutura da vancomicina

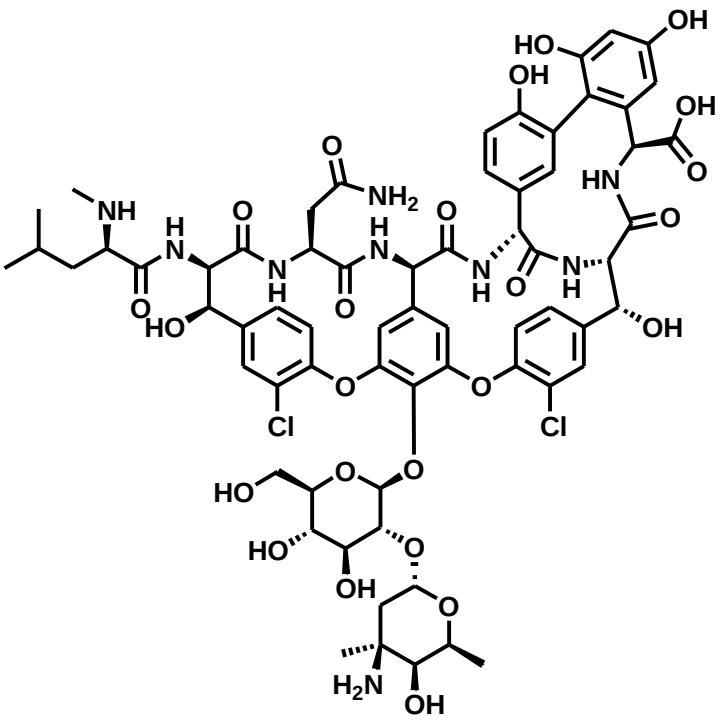

1.4. Produtos naturais como protótipos para fármacos antibacterianos

Os produtos naturais são fontes do desenvolvimento de diversos antibacterianos, atuando como agentes terapêuticos desde de meados do século XX (ROSSITER et al., 2017). Dentre os fármacos antibacterianos aprovados entre 1981 e 2014 pela FDA (Food and Drug Administration) ou organizações similares, mais de 58% eram produtos naturais inalterados ou derivados de produtos naturais, evidenciando a importância dessas substâncias no desenvolvimento de novos agentes antimicrobianos (NEWMAN; CRAGG, 2016).

Um dos produtos naturais mais bem estudados e que apresenta uma ampla variedade de bioatividades é a curcumina (Figura 4, p. 32) substância obtida à partir do extrato seco dos rizomas de *Curcuma longa* (família Zingiberaceae, ordem Zingiberales), vegetal popularmente conhecido como “açafrão-da-índia”, “açafrão-da-terra”, “cúrcuma” ou “turmérico”. Vários estudos atribuem o emprego terapêutico do extrato dos rizomas de *C. longa* ao conjunto de curcuminoides que os constituem: curcumina (60–70%), dimetoxicurcumina (20–27%) e *bis*-dimetoxicurcumina (10–15%), sendo que as

bioatividades são correlacionadas especialmente à curcumina (HEWLINGS; KALMAN, 2017; NELSON et al., 2017).

Figura 4. Estrutura da curcumina

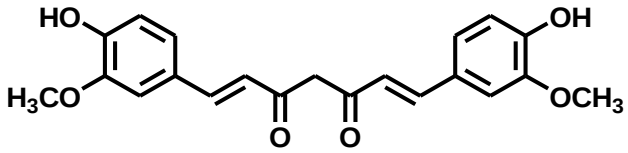

A curcumina foi isolada primeiramente em 1815 e sua estrutura foi determinada em 1910 (HESARI et al., 2018), sendo caracterizada quimicamente por duas subunidades fenílicas, separadas por uma cetona *bis*-α',β'-insaturada, apresentando um esqueleto carbônico $C_6C_7C_6$, ou difenileptanoídico. Desde a sua identificação como componente de um extrato vegetal biologicamente ativo, a curcumina tem sido estudada por diversos pesquisadores, os quais evidenciaram um amplo espectro bioatividades, incluindo: antibacteriana, antifúngica, anti-Parkinson, antioxidante, anti-Alzheimer, anti-HIV e hepatoprotetora (MOGHADAMTOUSI et al., 2014; BRASCH et al., 2017; XU et al., 2018).

Vários estudos ilustram a atividade da curcumina contra *S. aureus* (MOGHADDAM et al., 2009; MUN et al., 2013; WANG et al., 2016; RIBEIRO, 2013; MUN et al., 2014). Dentre estes, Teow and Ali descreveram a atividade sinérgica da curcumina e oito antibacterianos. Este estudo reportou maior interação sinérgica da curcumina com amicacina, gentamicina e ciprofloxacina. Além disso, essas combinações também reduziram consideravelmente a curva de morte de células bacterianas viáveis (TEOW; ALI, 2015). Além das investigações *in* vitro, estudos *in vivo* comprovaram a atividade anti-*S. aureus* da curcumina por diminuir a mortalidade de ratos infectados com MSSA e MRSA (WANG et al., 2016).

No entanto, apesar de demonstrar essas bioatividades, a curcumina apresenta algumas limitações que impedem o seu uso como agente terapêutico, dentre as quais podemos citar: baixa hidrossolubilidade, baixa biodisponibilidade *in vivo* e elevada instabilidade química em condições fisiológicas, sofrendo degradação rápida quando

administrada por via oral (HEWLINGS; KALMAN, 2017). A instabilidade da curcumina vem sendo correlacionada com a subunidade β-dicêtonica (SHETTY et al., 2014), sendo que alguns estudos ilustram que modificações estruturais como a retirada dessa subunidade, e a introdução de diferentes grupos funcionais podem melhorar as propriedades físico-químicas e bioativas da curcumina, fomentando seu possível emprego terapêutico (AWASTHI et al., 2017).

O cinamaldeído (Figura 5, p. 33) é um produto natural obtido das cascas de árvores do gênero *Cinnamomum*, planta perene tropical. *C. aromaticum* e *C. zeylanicum*, são as principais espécies produtoras de cinamaldeído, as quais são popularmente conhecidas como "canela", especiaria amplamente empregada na culinária e medicina popular em nível mundial. Quimicamente, o cinamaldeído, ou 3-fenil-prop-2-enal é um aldeído aromático α,β-insaturado, caracterizado por um esqueleto fenilpropanoídico do tipo C_6C_3. Essa substância apresenta caráter oleoso, volátil e de coloração amarelada (RANASINGHE al., 2013).

Figura 5. Estrutura do cinamaldeído

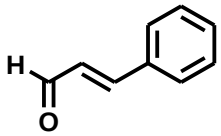

O cinamaldeído apresenta inúmeras bioatividades, incluindo antifúngica, antitumoral e anti-inflamatória (KUMAR; KUMARI, 2019; CHEN et al., 2017). No entanto, a atividade antibacteriana se destaca, sendo que no trabalho de Ferro e colaboradores, o cinamaldeído foi descrito como inibidor dos fatores de virulência de *S. aureus* (FERRO et al., 2016, KUMAR; KUMARI, 2019). No entanto, apesar de apresentar as atividades biológicas mencionadas, o cinamaldeído possui um grupo aldoxila, altamente reativo, sendo que a substituição deste grupo pode aumentar a estabilidade química e sua bioatividade (LOPACHIN; GAVIN, 2014).

Com a finalidade de otimizar as propriedades farmacocinéticas e farmacodinâmicas de protótipos, a hibridação molecular constitui-se em uma das estratégias da Química Medicinal que compreende na união de características estruturais parciais de substâncias bioativas parentais em uma nova estrutura, originando uma

terceira substância (híbrido) que poderá apresentar atividade de uma das substâncias parentais ou conjugar ambas as atividades (VIEGAS-JUNIOR et al., 2007).

Alguns dos híbridos antibacterianos mais bem sucedidos corresponde a uma hibridação entre fluoroquinolonas e oxazolidinonas. As fluoroquinolonas (Figura 6a) são fármacos antibacterianos cujo mecanismo de ação é a inibição do sítio catalítico de topoisomerases bacterianas, enzimas que controlam o estado topológico do DNA e que são, portanto, parte integrante de processos celulares essenciais, como replicação e transcrição. As oxazolidinonas (Figura 6b), por sua vez, são uma classe de antimicrobianos que inibem a etapa de iniciação da biossíntese proteica bacteriana, sendo ativos, principalmente contra patógenos Gram-positivos. Dentre os vários híbridos de fluoroquinolona-oxazolidinona, a substância MCB-3837 (Figura 6c) apresenta atividades antibacterianas superiores às substâncias parentais contra MSSA e MRSA, *Streptococcus pneumoniae*, *Enterococcus faecium* e *Enterococcus faecalis*. Tal substância foi desenvolvida pela Morphochem® e está disponível como um pró-fármaco solúvel em água para regimes de administração intravenosa (KLAHN; BRONSTRUP, 2017).

Figura 6. Estruturas da fluoroquinolona (a), oxazolidinona (b) e do híbrido fluoroquinolona-oxazolidinona MCB-3837 (c)

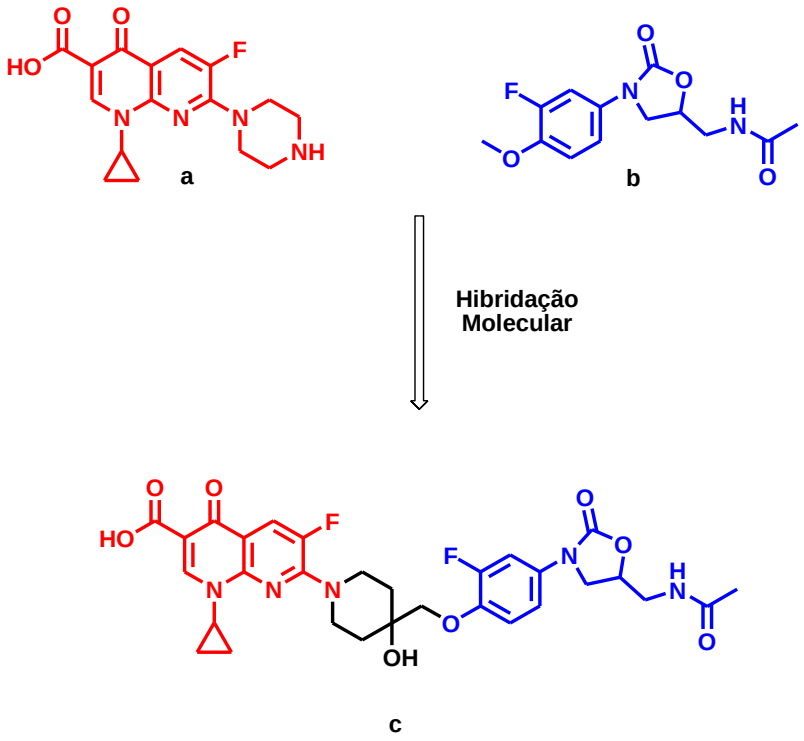

Assim, no presente trabalho, planejou-se duas séries de trinta híbridos de curcumina-cinamaldeído (Figura 7, p. 35). Os híbridos foram planejados à partir da retirada das subunidades β-dicetona e aldoxila da curcumina e cinamaldeído, respectivamente. Reuniu-se o anel guaicol proveniente da curcumina (anel *meta*-metoxilado e *para*-hidroxilado) com a carbonila α,β-insaturada e aromática não-substituída do cinamaldeído, fornecendo híbridos 1,3-difenil-2-propenoicos, comumente chamados de chalconas.

Figura 7. Planejamento dos híbridos curcumina-cinamaldeído

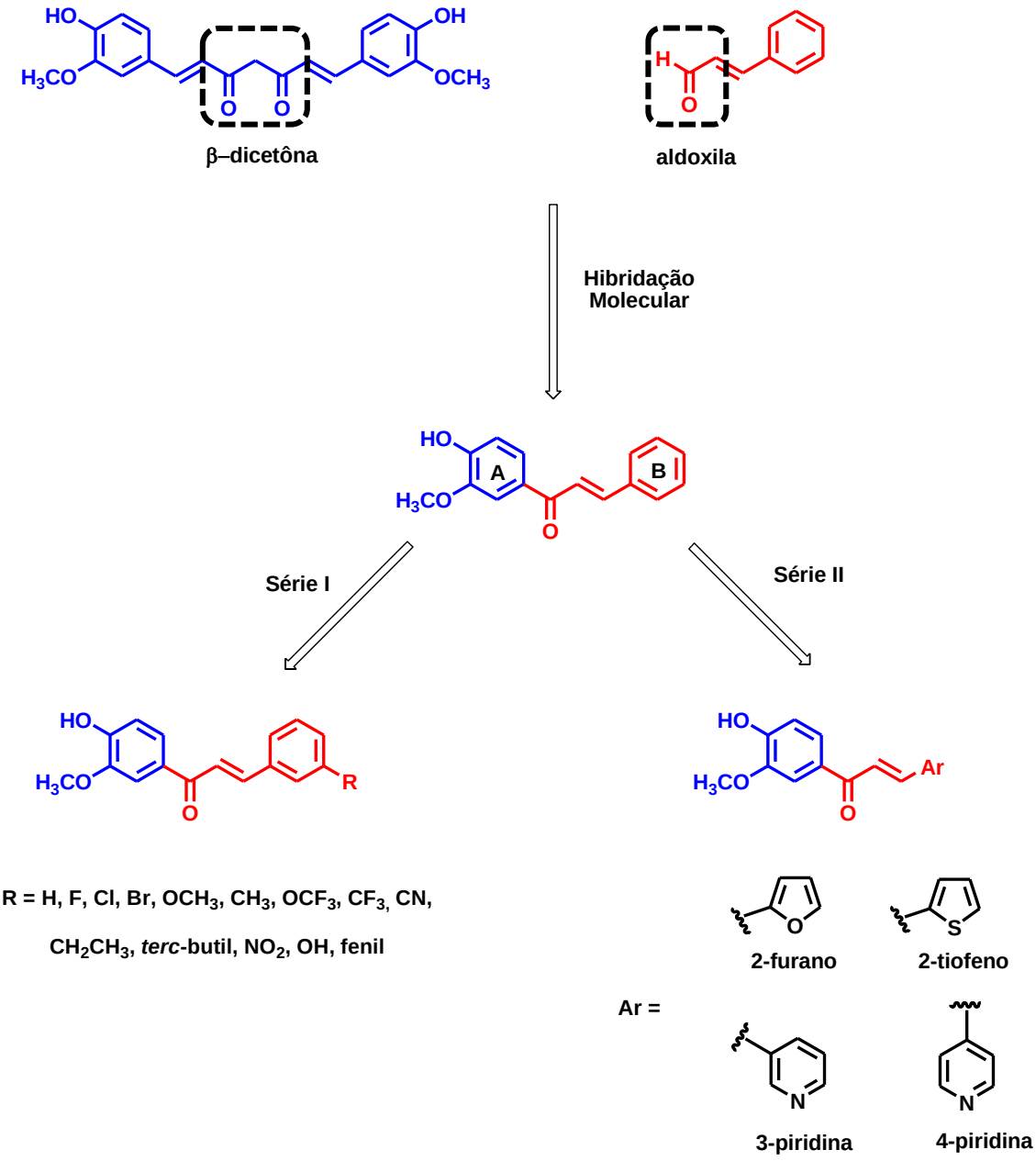

A primeira série de híbrido (série I) foi constituída de híbridos com anel A guaicólico e anel B substituído por átomos e grupos eletrofílicos ou hidrofílicos e doadores ou retiradores de elétrons. A segunda série (série II) foi formada de híbridos com anel A guaiacólico e anel B benzênico substituído por heterociclos (furano, tiofeno e piridina).

2. OBJETIVOS

2.1. Objetivo geral

Sintetizar e avaliar a atividade contra MSSA e MRSA de trinta híbridos chalcônicos curcumina-cinamaldeído.

2.2. Objetivos específicos

A) Síntese, purificação e identificação de trinta híbridos chalcônicos;

B) Avaliação da atividade antibacteriana dos híbridos contra cepas de *Staphylococcus aureus* sensível e resistente à meticilina (MSSA e MRSA);

C) Avaliação da combinação de vancomicina ou meticilina com o híbrido mais ativo contra MSSA e MRSA;

D) Avaliação da atividade inibitória do híbrido mais ativo contra MSSA e MRSA contra a adesão em queratinócitos humanos HaCaT;

E) Avaliação da atividade antibiofilme do híbrido mais ativo e da combinação deste com vancomicina ou meticilina contra biofilmes de MSSA e MRSA;

F) Avaliação do tempo de morte de MSSA e MRSA do híbrido mais ativo;

G) Avaliação da toxicidade do híbrido mais ativo contra MSSA e MRSA, utilizando o invertebrado *Galleria mellonella* como organismo-modelo alternativo;

H) Avaliação da atividade antibacteriana dos híbridos contra outras espécies bacterianas Gram-positivas e Gram-negativas e *Mycobacterium tuberculosis*;

I) Investigação *in silico* das propriedades drug-likeness dos híbridos.

3. REFERÊNCIAS

ARCHER, N. K.; MAZAITIS, M. J.; COSTERTON, J. W.; LEID, J. G.; POWERS, M. E.; SHIRTLIFF, M. E. *Staphylococcus aureus* biofilms: Properties, regulation and roles in human disease. **Virulence**, v. 2, p. 445–459, 2011.

AWASTHI, M.; SINGH, S.; PANDEY, V. P.; DWIVEDI, U. N. Curcumin: Structure-activity relationship towards its role as a versatile multi-targeted therapeutics. **Mini Rev. Org. Chem.**, v. 14, p. 311–332, 2017.

BALASUBRAMANIAN, D.; HARPER, L.; SHOPSIN, B.; TORRES, V. J. *Staphylococcus aureus* pathogenesis in diverse host Environments. **Pathog. Dis.**, v. 75, p. 1–13, 2017.

BOLES, B. R.; HORSWILL, A. R. Agr-mediated dispersal of *Staphylococcus aureus* biofilms. **PLoS Pathog.**, v. 4, p. 1–14, 2008.

BRASCH, J.; FREITAG-WOLF, S.; BECK-JENDROSCHEK, V.; HUBER, M. Inhibition of dermatophytes by photodynamic treatment with curcumin. **Med. Mycol.**, v. 55, p. 754−762, 2017.

BROOKS, J. L.; JEFFERSON, K. K. Staphylococcal biofilms: quest for the magic bullet. **Adv. Appl. Microbiol.**, v. 81, p. 63–87, 2012.

CHEN, B. J.; FU, C. S.; LI, G. H.; WANG, X. N.; LOU, H. X.; REN, D. M.; SHEN, T. Cinnamaldehyde Analogues as Potential Therapeutic Agents. **Mini Rev. Med. Chem.**, v. 17, p. 33–43, 2017.

COSTERTON J. W.; LEWANDOWSKI, Z.; CALDWELL, D. E.; KORBER, D. R.; LAPPIN-SCOTT, H. M. Microbial biofilms. **Annu. Rev. Microbiol.**, v. 49, p. 711–745, 1995.

DAYAN, G. H.; MOHAMED, N.; SCULLY, I. L.; COOPER, D.; BEGIER, E.; EIDEN, J.; JANSEN, K. U.; GURTMAN, A.; ANDERSON, A. S. *Staphylococcus aureus*: the current state of disease, pathophysiology and strategies for prevention. **Expert Rev. Vaccines**, v. 15, p. 1373–1392, 2016.

DELEO, F. R.; CHAMBERS, H. F. Reemergence of antibiotic-resistant *Staphylococcus aureus* in the genomics era. **J. Clin. Invest.**, v. 119, p. 2464–2474, 2009.

DONLAN, R. M.; COSTERTON, J. W. Biofilms: Survival mechanisms of clinically relevant microorganisms. **Clin. Microbiol. Rev.**, v. 15, p. 167–193, 2002.

DUNNE, W. M. Jr. FOCUS Bacterial Adhesion: Seen Any Good Biofilms Lately? **Clin. Microbiol. Rev.**, v. 15, p. 155–166, 2002.

ENANY, S.; ALEXANDER, L. E. C. The Rise of Virulence and Antibiotic Resistance in *Staphylococcus aureus*. 8 Ed., 2017.

FERRO, T. A. F.; ARAÚJO, J. M. M. PINTO, B. L. S.; SANTOS, J. S.; SOUZA, E. B.; SILVA, B. L. R.; COLARES, V. L. P.; NOVAIS, T. M. G.; FILHO, C. M. B.; STRUVE, C.; CALIXTO, J. B.; MONTEIRO-NETO, V.; SILVA, L. C. N.; FERNANDES, E. S. Cinnamaldehyde Inhibits *Staphylococcus aureus* Virulence Factors and Protects against Infection in a *Galleria mellonella* Model. **Front. Microbiol.**, v. 7, p. 1–10, 2016.

FOSTER, T. J.; GEOGHEGAN, J. A.; GANESH, V. K.; HÖÖK, M. Adhesion, invasion and evasion: the many functions of the surface proteins of *Staphylococcus aureus*. **Nat. Rev. Microbiol.**, v. 12, p. 49–62, 2014.

GARDETE, S.; TOMASZ, A. Mechanisms of vancomycin resistance in *Staphylococcus aureus*. **J. Clin. Invest.**, v. 124, p. 2836–2840, 2014.

GIL, C.; SOLANO, C.; BURGUI, S.; LATASA, C.; GARCÍA, B.; TOLEDO-ARANA, A.; LASA, I.; VALLE, J. Biofilm Matrix Exoproteins Induce a Protective Immune Response against *Staphylococcus aureus* Biofilm Infection. **Infect. Immun.**, v. 82, p. 1017–1029, 2014.

HESARI, A.; GHASEMI, F.; SALARINIA, R.; BIGLARI, H.; TABAR, M. H. A.; ABDOLI, V.; MIRZAE, H. Effects of curcumin on NF-κB, AP-1, and Wnt/β-catenin signaling pathway in hepatitis B virus infection. **J. Cell Biochem.**, v. 119 p. 7898–7904, 2018.

HEWLINGS, S. J.; KALMAN, D. S. Curcumin: A review of its' effects on human health. **Foods**, v. 6, p. 1–11, 2017.

JENSEN, S. O.; LYON, B. R. Genetics of antimicrobial resistance in *Staphylococcus aureus*. **Future Microbiol.**, v. 4, p. 565–582, 2009.

KALE, P.; DHAWAN, B. The changing face of community-acquired methicillin-resistant *Staphylococcus aureus*. **Indian J. Med. Microbiol.**, v. 34, p. 275–285, 2016.

KHAN, H. A.; AHMAD, A.; MEHBOOB, R. Nosocomial infections and their control strategies. **Asian Pac. J. Trop. Biomed.**, v. 5, p. 509–514, 2015.

KHAN, H. A.; BAIG, F. K.; MEHBOOB, R. Epidemiology, prevention, control and surveillance. **Asian Pac. J. Trop. Biomed.**, v. 7, p. 478–482, 2017.

KLAHN, P.; BRONSTRUP, M. Bifunctional antimicrobial conjugates and hybrid antimicrobials. **Nat. Prod. Rep.**, v. 34, p. 832–885, 2017

KRISTIAN, S. A.; GOLDA, T.; FERRACIN, F.; CRAMTON, S. E.; NEUMEISTER, B.; PESCHEL, A.; GÖTZ, F.; LANDMANN, R. The ability of biofilm formation does not influence virulence of *Staphylococcus aureus* and host response in a mouse tissue cage infection model. **Microb. Pathog.**, v. 36, p. 237–245, 2004.

KUMAR, S.; KUMARI, R. *Cinnamomum*: review article of essential oil compounds, ethnobotany, antifungal and antibacterial effects. **Open Access J. Sci.**, v. 3, p. 13–16, 2019.

LOPACHIN, R. M.; GAVIN, T. Molecular mechanisms of aldehyde toxicity: a chemical perspective. **Chem. Res. Toxicol.**, v. 27, p. 1081–1091, 2014.

MAGILL, S. S.; EDWARDS, J. R.; BAMBERG, W.; BELDAVS, Z. G.; DUMYATI, G.; KAINER, M. A.; LYNFIELD, R.; MALONEY, M.; MCALLISTER-HOLLOD, L.; NADLE, J.; RAY, S. M.; THOMPSON, D. L.; WILSON, L. E.; FRIDKIN, S. K. Multistate pointprevalence survey of health care-associated infections. **N. Engl. J. Med.**, v. 370, p. 1198–1208, 2014.

MICHAEL, C. A.; DOMINEY-HOWES, D; LABBATE, M. The antimicrobial resistance crisis: causes, consequences, and management. **Front. Public Health**, v. 2, p. 1–8, 2014.

MOGHADAMTOUSI, S.; KADIR, H. A.; HASSANDARVISH, P.; TAJIK, H.; ABUBAKAR, S.; ZANDI, K. A review on antibacterial, antiviral, and antifungal activity of curcumin. **Biomed. Res. Int.**, v. 2014, p. 1−12, 2014.

MOGHADDAM, K. M.; IRANSHAHI, M.; YAZDI, M. C.; SHAHVERDI, A. R. The combination effect of curcumin with different antibiotics against *Staphylococcus aureus*. **Int. J. Green Pharm.**, v. 3, p. 141–143, 2009.

MONTANARO, L.; POGGI, P.; VISAI, L.; RAVAIOLI, S.; CAMPOCCIA, D.; SPEZIALE, P.; ARCIOLA, C. R. Extracellular DNA in biofilms. **Int. J. Artif. Organs**, v. 34, p. 824–831, 2011.

MONTGOMERY, C. P.; DAVID, M. Z.; DAUM, R. S. Host factors that contribute to recurrent staphylococcal skin infection. **Curr. Opin. Infect. Dis.**, v. 28, p. 253–258, 2015.

MUN, S. H.; JOUNG, D. K.; KIM, Y. S.; KANG, O. H.; KIM, S. B.; SEO, Y. S.; KIM, Y. C.; LEE, D. S.; SHIN, D. W.; KWEON, K. T.; KWON, D. Y. Synergistic antibacterial effect of curcumin against methicillin-resistant *Staphylococcus aureus*. **Phytomedicine**, v. 20. p. 714–718, 2013.

MUN, S. H.; KIM, S. B.; KONG, R.; CHOI, J. G.; KIM, Y. C.; SHIN, D. W.; KANG, O. H.; KWON, D. Y. Curcumin reverse methicillin resistance in *Staphylococcus aureus*. **Molecules**, v. 19, p. 18283–18295, 2014.

NEWMAN, D. J.; CRAGG, G. M. Natural Products as Sources of New Drugs from 1981 to 2014. **J. Nat. Prod.**, v. 79, p. 629–661, 2016.

NELSON, K. M.; DAHLIN, J. L.; BISSON, J.; GRAHAM, J.; PAULI, G. F.; WALTERS, M. A. The essential medicinal chemistry of curcumin. **J. Med. Chem.**, v. 60, p. 1620–1637, 2017.

NESME, J.; SIMONET, P. The soil resistome: a critical review on antibiotic resistance origins, ecology and dissemination potential in telluric bacteria. **Environ. Microbiol.**, v. 17, p. 913–930, 2015.

OTTO, M. Staphylococcal infections: mechanisms of biofilm maturation and detachment as critical determinants of pathogenicity. **Annu. Rev. Med.**, v. 64, p. 175–188, 2013.

O'TOOLE. G.; KAPLAN, H. B.; KOLTER, R. Biofilm formation as microbial development. **Annu Rev Microbiol**., v. 54, 49–79, 2000.

PERIASAMY, S.; JOO, H. S.; DUONG, A.C.; BACH, T. H.; TAN, V. Y., CHATTERJEE, S. S.; CHEUNG, G. Y.; OTTO, M. How *Staphylococcus aureus* biofilms develop their characteristic structure. **Proc. Natl. Acad. Sci. USA**, v. 109, p. 1281–1286, 2012.

RANASINGHE, P.; PIGERA, S.; PREMAKUMARA, G. A.; GALAPPATHTHY, P.; CONSTANTINE, G. R.; KATULANDA, P. Medicinal properties of 'true' cinnamon (*Cinnamomum zeylanicum*): a systematic review, **BMC Complement. Altern. Med.**, v. 13, p. 1–10, 2013.

RIBEIRO, A. P. D.; PAVARINA, A. C., L. N.; DOVIGO, L. N.; BRUNETTI, I. L.; BAGNATO, V. S.; VERGANI, C. E.; COSTA, C. A. Phototoxic effect of curcumin on methicillin-resistant *Staphylococcus aureus* and L929 fibroblasts, **Lasers Med. Sci**, v. 28, p. 391–398, 2013.

RICE, L. B. Progress and challenges in implementing the research on ESKAPE pathogens. **Infect. Control Hosp. Epidemiol.**, v. 31, p. S7–S10, 2010.

RODVOLD, K.A.; MCCONEGHY, K.W. Methicillin-resistant *Staphylococcus aureus* therapy: past, present, and future. **Clin. Infect. Dis.**, v. 58, p. S20–S27, 2014.

ROSSITER, S. E.; FLETCHER, M. H. WUEST, W. M. Natural Products as Platforms To Overcome Antibiotic Resistance. **Chem. Rev.**, v. 117, p. 12415–12474, 2017.

SADER, H. S.; MENDES, R. E.; JONES, R. N.; FLAMM, R. K. Antimicrobial susceptibility patterns of community- and hospital-acquired methicillin-resistant *Staphylococcus aureus* from United States Hospitals: results from the AWARE Ceftaroline Surveillance Program (2012–2014). **Diagn. Microbiol. Infect. Dis.**, v. 86, p. 76–79, 2016.

SANTAJIT, S.; INDRAWATTANA, N. Mechanisms of Antimicrobial Resistance in ESKAPE Pathogens, **Biomed. Res. Int.**, v. 2016, p. 1–9, 2016.

SCHERR, T. D.; HEIM, C. E.; MORRISON, J. M.; KIELIAN, T. Hiding in plain sight: interplay between staphylococcal biofilms and host immunity. **Front. Immunol.**, v. 5, p. 1–7, 2014.

SHETTY, D.; KIM, Y. J.; SHIM, H.; SNYDER, J. P. Eliminating the heart from the curcumin molecule: Monocarbonyl curcumin mimics (MACs). **Molecules**, v. 20, p. 249−292, 2014.

SILVER L. L. Challenges of antibacterial discovery. **Clin Microbiol Rev.**, v. 24, p. 71–109, 2011.

SPELLBERG B.; GILBERT, D. N. The future of antibiotics and resistance: a tribute to a career of leadership by John Bartlett. **Clin. Infect. Dis.**, v. 59, p. S71–S75, 2014.

TEOW, S. Y.; ALI, S. A. Synergistic antibacterial activity of Curcumin with antibiotics against *Staphylococcus aureus*. **Pak. J. Pharm. Sci.**, v. 28, p. 2109–2114, 2015.

TONG, S. Y. C.; DAVIS, J. S.; EICHENBERGER, E.; HOLLAND, T. L.; FOWLER, V. G. *Staphylococcus aureus* Infections: Epidemiology, Pathophysiology, Clinical Manifestations, and Management. **Clin. Microbiol. Rev.**, v. 28, p. 603–661, 2015.

VENTOLA, C. L. The Antibiotic Resistance Crisis Part 1: Causes and Threats. **P T**, v. 40, p. 277–283, 2015.

VIEGAS-JUNIOR, C.; DANUELLO, A.; DA SILVA BOLZANI, V.; BARREIRO, E. J.; FRAGA, C. A. Molecular hybridization: a useful tool in the design of new drug prototypes. **Curr. Med. Chem**., v. 14, p. 1829–52, 2007.

VON EIFF, C.; PETERS, G.; BECKER, K. The small colony variant (SCV) concept – the role of staphylococcal SCVs in persistent infections. **Injury**, v. 37, p. S26–S33, 2006.

XU, X. Y.; MENG, X.; LI, S.; GAN, R. Y.; LI, Y.; LI, H. B. Bioactivity, health benefits, and related molecular mechanisms of curcumin: Current progress, challenges, and perspectives. **Nutrients**, v. 10, p. 1–33, 2018.

WANG, J.; ZHOU, X.; LI, W.; DENG, X.; DENG, Y.; NIUB, X. Curcumin protects mice from *Staphylococcus aureus* pneumonia by interfering with the self-assembly process of *α*-hemolysin. **Sci. Rep.**, v. 6, p. 1–12, 2016.

ZECCONI, A.; SCALI, F. *Staphylococcus aureus* virulence factors in evasion from innate immune defenses in human and animal diseases. **Immunol. Lett.**, v. 150, p. 12–22, 2013.

CAPÍTULO II

Antibacterial activity of curcumin-cinnamaldehyde hybrids against MSSA and MRSA planktonic cells and biofilms

Beatriz de C. Marques[a], Mariana B. Santos[a], Isabelle A. T. Kanashiro[a], Mayara A. R. Garcia[a], Gabriela M. Ayusso[a], Josy G. Lazarini[b], Débora L. Campos[c], Fernando R. Pavan[c], Pedro L. Rosalen[b], Janaina C. O. Sardi[b] and Luis O. Regasini[a,]*

[a]*Department of Chemistry and Environmental Sciences, Institute of Biosciences, Humanities and Exact Sciences, São Paulo State University (Unesp), São José do Rio Preto 15054-000, SP, Brazil.*

[b]*Department of Physiological Sciences, Piracicaba Dental School, University of Campinas (Unicamp), Piracicaba 13083-970, SP, Brazil.*

[c]*Department of Biological Sciences, School of Pharmaceutical Sciences (FCFAR), São Paulo State University (UNESP), Araraquara, SP, Brazil.*

*****Address correspondence to this author at the Laboratory of Antibiotics and Chemotherapeutics, IBILCE-Unesp, São José do Rio Preto – 15054-000; Tel.: +55 17 3221-2362. E-mail: luis.regasini@unesp.br.

ABSTRACT

In the present study, thirty hybrids curcumin-cinalmaldehyde were evaluated against methicillin-susceptible and methicillin-resistant *S. aureus* (MSSA and MRSA). In general, molecular hybridization between curcumin and cinnamaldehyde maintained or increased the activity, and the lipophilicity conferred greater activity against *S. aureus*. Hybrid **20** was the most active against MSSA and MRSA, being selected others assays, presenting antibacterial activity similar or superior to the positive controls, when its in combination with vancomycin and methicillin, and its anti-adhesion activity, antibiofilm and time kill of MSSA and MRSA. Toxicity *in G. mellonela* of hybrid **20** was evaluated, killing 50% of the population at 90 mg/kg, after 72 hours of treatment. Hybrids showing activity against *E. faecalis*, *S. epidermidis*, *P. aeruginosa*, *A. baumannii* and *M. tuberculosis*. *In silico* studies for all hybrids indicated good drug-likeness properties. By means of this study, we can prove the antibacterial activity of curcumin-cinnamaldehyde hybrids, stimulating the study of these compounds, in order to search for new agents capable of acting against resistant strains.

Keywords: *Staphylococcus aureus*, curcumin, cinalmaldehyde, molecular hybridization

1. INTRODUCTION

Staphylococcus aureus is a commensal and pathogenic Gram-positive bacteria, which colonizes approximately 30% of the human population [1]. Although colonization is generally not detrimental, this microorganism can break the innate defenses of hosts accessing deeper tissues and causing a variety of surface and systemic infections [2]. In healthy individuals, *S. aureus* often causes infections, such as impetigo, folliculitis and cutaneous abscesses. In addition, severe infections include pyomyositis, necrotizing fasciitis [1] and necrotizing pneumonia [3,4]. Biofilm is a set of cells that are attached to a substrate, interface, or one another, dispersed in a polymer matrix, exhibiting different phenotypes in planktonic cells, as well as gene expression and protein production. Although biofilm formation is not a prerequisite for persistent infection, it occurs in most cases, requiring more specific pharmacotherapy by drug association [5].

Since the end of the 1980's, there is a disability in the discovery of innovative antibacterial agents, being that the last drug released fot the Staphylococcal infections treatment was daptomycin, in 1987 [6]. However, in the last decade, *S. aureus* has presented a high clinical relevance, mainly due to the increase in the resurgence of drug-resistant strains and multidrug-resistant strains [7], and to make up the group of pathogens known as ESKAPE, which includes Gram-positive and Gram-negative species that cause numerous nosocomial infections with risk of death among sick individuals [8,9], which inhibits research by substances capable of acting against this pathogen.

Curcumin (Figure 1a), is a compound from *Curcuma longa* rhizomes formed by two guaicol rings separated by a *bis*-α',β'-unsaturated ketone, responsible for presenting numerous bioactivities, including anti-*S. aureus* activity. Mun and co-authors showed the anti-*S. aureus* activity of curcumin, presented Minimal Inhibitory Concentrations (MIC) ranged from 125 to 250 μg/mL against 10 strains of *S. aureus* [10]. Despite antibacterial

activity, curcumin has low water solubility, low bioavailability and high instability under physiological conditions [11], being that the curcumin instability has been correlated with the β-dicetyl subunit [12]. Awasthi and co-authors have shown that removal of the β-diketone in its skeleton can improve the physico-chemical and bioactive properties [13]. An example of this is the work of Mourão and collaborators that described antibacterial anti-*S. aureus* activity of curcumin, in which a monocarbonyl group replaced β-diketone subunit [14]. Cinnamaldehyde (Figure 1b), is an α,β-unsaturated aromatic aldehyde from tree barks of the genus *Cinnamomum* [15,16]. Among the numerous bioavailabilities attributed to cinnamaldehyde, we highlight the antibacterial activity [17], including the inhibition of virulence factors of *S. aureus* [18]. However, cinnamaldehyde presents aldoxyl group, undesirable functionality due to its high reactivity, and its replacement of increase its bioactivity [19]. Polaquini and co-authors compared anti-*S. aureus* activity of cinnamaldehyde analogs without aldoxyl group and cinnamaldehyde, described increase in anti-*S. aureus* at 6 times in these analogues [20].

We decided used curcumin and cinnamaldehyde for desing of molecular hybridization hybrids [21]. Hybridization as designed by using guaicol ring and phenyl-α,β-unsaturated ketone of curcumin and cinnamaldehyde, respectively. Furthermore, undesirable β-diketone and aldoxyl was removed furnishing 1,3-diphenylprop-2-en-1-one (or chalcone) framework (Figure 2). These hybrids were evaluated for their antibacterial activity against methicillin-sensitive and methicillin-resistant *S. aureus*, MSSA and MRSA respectively. The most active hybrid against MSSA and MRSA (**20**) was evaluated for its anti-*S. aureus* activity when combined with vancomycin or methicillin. Additionally, selected hybrid was evaluated for its inhibitory activity against the adhesion of MSSA and MRSA in human keratinocytes HaCaT. MSSA and MRSA antibiofilm activity of **20** combined with vancomycin or methicillin, as well as its

interference in the time kill of MSSA and MRSA. Toxicity of selected hybrid was determined using the *Galleria mellonella* invertebrate. Finally, *in silico* investigation was performed to predict drug-likeness properties of all hybrids.

2. RESULTS AND DISCUSSION

2.1. Chemistry

The aldol condensation reactions of Claisen-Schmidt led to thirty curcumin-cinnamaldehyde hybrids **1**–**30**, which were purified by sílica gel column, using mixturs of hexane and ethyl acetate as mobile phase, with yields of 6–96% (Figure 3) [22]. Among these **2, 3, 12, 13, 16–18, 20, 21, and 27–29** are new chemical entites [23].

Curcumin-cinnamaldehyde hybrids were identified by analysis of their ^{1}H and ^{13}C NMR spectra. Interpretation of the ^{1}H NMR spectra allowed to confirm enone bridge in approximately in δ_H 7.60 and 7.80 ppm, with coupling constants (*J*) of 15.8 Hz, which were attributed to double bonds with *E* configuration. ^{13}C NMR spectra exhibited signal typical of α,β-unsaturated carbonyls (δc ≈ 189 ppm).

Hybrids also were analyzed by High Performance Liquid Chromatography (HPLC-PAD) to furnish UV-Vis spectrum and purity of compounds. UV-Vis spectra demonstrated values of $\lambda_{max} \approx 350$ nm, which is related to the conjugation of the B ring with the enone bridge. Purity of the curcumin-cinnamaldehyde hybrids was obtained from area peaks at λ_{max} of each analite chromatograms. Their *n*-octanol-water partition coefficients (Log $P_{o/w}$) were also determined by using of retention time.

Detailed spectral analysis and chromatograms were presented in the supplementary material.

2.2. Biological Activity

2.2.1. Antibacterial activity of curcumin-cinnamaldehyde hybrids against MSSA and MRSA

Anti-*S. aureus* activity from of curcumin-cinnamaldehyde hybrids was expressed as Minimal Inhibitory Concentration (MIC) and Minimal Bactericidal Concentration (MBC) values against MSSA and MRSA, using microdilution method (Table 1) [24].

Comparison of anti-*S. aureus* activity of curcumin and cinnamaldehyde (parent compounds) and their hybrid (**1**) suggested molecular hybridization was responsible to increase of anti-*S. aureus* activity, since curcumin and cinnamaldehyde presented MIC and MBC ≥ 62.5 μg/mL for MSSA and MRSA, whereas **1** presented MIC and MBC values of 31.25 and 62.5 μg/mL. These results ilustrate molecular hybridization, in which the union of structural characteristics of distinct bioactive compounds into a new structure, giving rise to a compound which may exhibit activity of one of the parent compounds or combine both activities [21].

Hybrids with the highest antibacterial potency presented MIC and MBC values equal to or lower than 15.6 μg/mL and 31.2 μg/mL, respectively. These hybrids substituted by 2-fluor (**2**), 4-trifluoromethoxyl (**10**), 4-isopropyl (**19**) and 4-*terc*-butyl (**20**) on ring B. Thus, MIC and MBC results suggested the addition of lipophilic substituents on the ring B incresead antibacterial activity, since it promoted superior activity than when compared to unsubstituted (**1**).

In addition, the increase of lipophilicity conferred higher anti-*S. aureus* potency, altering the MIC value of 31.25 μg/mL for **1**, 15.6 μg/mL for **19**, to 7.8 μg/mL for **20**, against MSSA and 31.25 μg/mL for **1**, 7.8 μg/mL for **19**, and 3.9 μg/mL for **20** for MRSA. Similarly, Pignatello and coauthors described a group of coumpounds whose antibacterial

activity increases with increasing lipophilicity, which may be justified by the greater permeation of lipophilic compouds by the phospholipid biomembranes [25].

The electronic parameter had low effect on anti-*S.aureus* activity, since bioactive hybrids replaced with 2-fluor (**2**) and 4-trifluoromethyl (**10**) presented an electron-withdrawing effect, while 4-isopropyl (**19**) and 4-*terc*-butyl (**20**) presented an electron-donating effect. Hybrid **20** showed the most pronounced antibacterial activity against MSSA (MIC = 7.8 μg/mL) and MRSA (MIC = 3.9 μg/mL), and was selected for subsequent bioassays.

2.2.2. Effects of combination of vancomycin or methicillin with hybrid 20 against MSSA and MRSA

Mun and coauthors described that the association between curcumin and oxacillin, ampicillin, ciprofloxacin and norfloxacin decrease MIC against MRSA, suggesting that the combination of antibacterial compounds with drugs may increase anti-*S. aureus* activity [26]. Thus, we evaluated the combination of hybrid **20** with vancomycin or methicillin in their MIC values (Table 2), as the objective of optimizing the antibacterial activity of the most active curcumin-cinnamaldehyde hybrid against MSSA and MRSA.

Our results suggested that associations between **20** and vancomycin or methicillin decreased MIC values against two strains. For MSSA, MIC of **20** decreased from 7.8 μg/mL to 1.95 μg/mL for both combinations, whereas for MRSA, MIC of **20** decreased from 3.9 μg/mL to 0.97 μg/mL after its associated with vancomycin and from 3.9 μg/mL to 1.95 μg/mL after its association with methicillin.

Similarly, Gaur and collaborators described the synergistic activity of five chalcones (curcumin-cinnamaldehyde hybrids) with norfloxacin, in which the combination was able to significantly reduce norfloxacin MIC values to 16 times. The

results further indicated that in Swiss albino mice systemically infected with MRSA, the combination was able to significantly decrease the systemic bacterial load in blood, liver, kidney, lung and spleen when compared to the use of the two compounds alone [27].

2.2.3. Inhibitors effects of hybrid 20 on adhesion of *S. aureus* onto human keratinocytes

Staphylococcal adhesion onto surfaces is a first event that occurs in infection and biofilm formation, involving a wide variety of proteins that mediate bacteria-host interation. Thus, a compound that acts to prevent bacterial adhesion may be of clinical interest [28].

Before evaluating the inhibitory activity of **20** against MSSA and MRSA adhesion, we evaluated its cytotoxicity against HaCaT cell line. This experiment was carried out in order to eliminate the possibility of that lower *S. aureus* adhesion to cells due to the toxicity that **20** against the cell line. As shown in Figure 4, **20** at 1/2 MIC concentration, for both MSSA (3.9 µg/mL) and MRSA (1.95 µg/mL), presented a percentage of cell viability of 92%. Thus, 1/2 MIC value is the concentration with low HaCaT toxicity.

Inhibitory effects of **20** on adhesion of MSSA and MRSA onto HaCaT were investigated. As shown in Figure 5, treatment with hybrid at 1/2 MIC decreased adherence of MSSA and MRSA from 1 to 3 hours, when compared to treated with negative control. Inhibitory effects were very similar during the experimental period for MSSA and MRSA. It is observed that, compared to negative control, **20** was able to reduce bacterial adhesion similarly to vancomycin, for both strains. In addition, it was found that over time, bacterial adhesion remained stable in the treated cells. Such results suggest that **20**, treated employed at a 1/2 MIC values affects the adhesion mechanism of *S. aureus* onto

epithelial cells. These results suggest that **20** may be antibacterial compound with action in the first step of infection and establishment of biofilm formation [29].

2.2.4. Antibiofilm activity of hybrid 20

Transition from the planktonic cells to biofilm cells makes it difficult to treat an infection, since when dispersed in a extracelular matrix are considerably less susceptible to the action of antibacterial compounds, escaping from the host's defenses and becoming tolerant to high concentrations of antimicrobials [30]. Infections associated with biofilm represent about 80% of nosocomial infections, and *S. aureus* is one of the main species involved in this context [31].

Thus, in order to evaluate the antibacterial action of **20** against the formation and survival of MSSA and MRSA biofilms, a quantitative assay was performed to determine the CFU/mL after treatment with **20** at concentrations of MIC and 10 × MIC. Results were presented in Figures 6 and 7.

In general, against MSSA and MRSA, **20** decrease the survival of biofilms, when compared to the negative control, with better results at the concentration of 10 × MIC values, presenting antibiofilm activity similar or higher than vancomycin and methicillin at the same concentrations. In addition, it can be said that all types of treatment (**20**, vancomycin or methicillin) were more effective in the biofilm formation, than in the mature biofilm, evidencing the greater difficulty of acting in a community, adhering and well-established [32].

For MSSA biofilm formation, comparison of **20**, vancomycin and methicillin indicated a similar reduction in CFU/mL among treatments with **20** (MIC) and methicillin (MIC), and among **20** (10 × MIC), vancomycin (MIC and 10 × MIC) and methicillin (10 × MIC). For MRSA biofilm formation, similar reduction in CFU/mL was identified

among **20** (MIC) and methicillin (MIC), and among **20** (10 × MIC) and vancomycin (10 × MIC). In addition, we identify a reduction of 10 $\log_{10}$ in CFU/mL between **20** (10 × MIC) and negative control, whereas for MRSA biofilm formation was identify a reduction of 7 log10 in CFU / mL between **20** (10 × MIC) and negative control. These results indicate the similarity in antibiofilm activity among **20** and antibacterial drugs.

On the other hand, for MSSA mature biofilm, **20** (10 × MIC) presented smaller values of CFU/mL, with higher antibiofilm activity than vancomycin and methicillin. For MRSA mature biofilm, we identify similar antibiofilm activity among **20**, vancomycin and methicillin at MIC values, and **20** (10 × MIC) presented similar reduction than methicillin (10 × MIC).

Among the possible factors that could justify the difference in the activity of **20** against MSSA and MRSA biofilms, we can mention the work of Pozzi and coauthors who reported that MSSA biofilm formation occurs mainly through the biossynthesis of intercellular polysaccharide adhesin (PIA), whereas in MRSA biofilm formation is related to adhesion of fibronectin binding protein (fnbB) [33]. Thus, other experiments must be performed in order to evidence the performance of **20** against PIA and fnbB.

Finally, Scanning Electron Microscopy (SEM) analysis were performed to visually assess the effects of **20** on the structure and integrity of the MSSA and MRSA biofilm mature (Figure 8). Hybrid **20** altered the three-dimensional structure of MSSA and MRSA biofilm mature, showing progressive reduction with the increased concentration tested. Thus, SEM photomicrographs illustrate the reduction of MSSA and MRSA biofilms treated with **20**, corroborating the results of the quantitative analyzes presented in Figures 6 and 7.

2.2.5. Effects of combination of vancomycin or methicillin with hybrid 20 against MSSA and MRSA biofilm

Due to the resistance of the biofilm cells to most antibacterial drugs is necessary to search for new strategies that affect or eradicate the biofilm cells [34]. We evaluated the activity of **20** against formation and mature biofilm of MSSA and MRSA when combined with vancomycin or methicillin at MIC and 10 × MIC values (Figures 9 and 10), in order to potentiate the antibiofilm effects of these compounds.

Our results indicated that for MSSA biofilm formation, the combination between **20** and vancomycin, and between **20** and methicillin at their respective MIC and 10 × MIC values, decreased significantly similar to the quantification of CFU/mL when compared with negative control. Against MRSA biofilm formation, the combination of **20** and vancomycin and **20** and methicillin at 10×MIC values showed the lowest number of CFU/mL .

In relation to MSSA mature biofilm, a considerable decrease in the number of CFU/mL were also observed at MIC of both combinations. However, with emphasis on the combination between **20** and vancomycin, and between **20** and methicillin at 10×MIC. For MRSA mature combination at 10 × MIC between **20** and vancomycin, and between **20** and methicillin showed the lowest number of CFU/mL.

When compared to MSSA and MRSA biofilms treated with **20**, vancomycin or methicillin alone, the combination between **20** and vancomycin, or between **20** and methicillin at MIC and 10 × MIC were similar or incresead the antibiofilm activity. These results suggested that the association between antibacterial drugs may result in greater bioactivity, including in a biofilm [35].

2.2.6. Effect of hybrid 20 on MSSA and MRSA time kill

We also investigated effects of **20** against MSSA and MRSA after 2, 4, 8 and 12 hours of exposure at concentrations of MIC and 10 × MIC, in order to evaluate the influence of **20** on MSSA and MRSA time kill, since the ability to kill a microorganism is one of the fundamental aspects in the elucidation of its antibacterial potential [36]. Results are shown in Figure 11.

Against MSSA, **20** at MIC reduced the number of viable cells after 2 hours, keeping that number until the end of 12 hours. Similarly, **20** at 10 × MIC value reduced the number of viable cells after 2 hours. However, it reduced the number over time until it achieved stability in the number of viable cells after 8 hours of treatment, exhibiting antibacterial activity superior to vancomycin in two concentrations tested (MIC and 10 × MIC values).

Against MRSA, **20** at MIC reduced the number of viable cells in 2 hours, keeping that number until the end of 12 hours. At 10 × MIC, the number of viable cells was reduced slightly after 8 hours of treatment, when the number of viable cells gradually increased until the end of the experiment.

In addition, when we compared the negative control with the treatments of **20** to MIC and 10 × MIC after 12 hours, our results indicate a decrease > 4 $\log_{10}$ CFU/mL, being that for Rolston and co-authors a decrease ≥ 3 log10 in UFC/mL indicates the bactericidal activity of a compound [37].

2.2.7. Toxicity of hybrid 20 against *Galleria mellonella*

After *in vitro* identification of a substance with antibacterial activity, evaluations to determine its toxicity in eukaryotes are indicated, aiming to investigate possible adverse effects in humans. Often, toxicity is assessed in a mammalian model, including

mice and rats. However, these experiments occur for long periods, are expensive, and require complex ethical considerations [38, 39].

In this context, *Galleria mellonella*, is an insect of Lepidoptera order, belonging to the Family Pyrilidae [40]. Their larvae are popularly known as wax worm and has been used as alternative animal model. Compared with the use of conventional mammalian models, *G. mellonella* larvae are more economically viable and easier to grow, and do not require complex laboratory structure. In addition, the use of *G. mellonella* does not require the approval of animal use ethics committees and their short shelf-life makes them ideal for rapid studies [41].

In vivo toxicity of **20** was evaluated using *G. mellonella*, being that the Figure 12 shows *G. mellonella* survival when treated with different doses of **20**. At 10 to 60 mg/kg the toxicity of **20** was low, since it was killed only 10% of larvae at 60 mg/kg. However, **20** at 90 mg/kg had toxic effects against 50% of the larvae, after 72 hours of treatment. DMSO was used as a vehicle and did not show statistically significant toxicity ($P>0.05$).

Acute toxicity results in *G. mellonella* suggested that **20** does not exhibit significant toxic effects *in vivo* when tested at concentrations two hundred times greater than those used for its antibacterial activity against planktonic cells and on biofilms. These results stimulate the continuation of toxicity studies of **20** in other animal models.

2.2.8. Activity of hybrids curcumin-cinnamaldehyde against others Gram-positive and Gram-negative species and *Mycobacterium tuberculosis*

In order to understand the spectrum of hybrids synthesized, we also evaluated their antibacterial activity against *E. faecalis, S. epidermidis, A. baumannii, E. coli* and *P. aeruginosa* by the microdilution method [24], as well as their antimycobacterial activity

against *M. tuberculosis*, performed according to Palomino and collaborators [42]. Results are shown in Table 3.

Against the Gram-positive species (*E. faecalis* and *S. epidermidis*) and Gram-negative *P. aeruginosa*, hybrids showed MIC and MBC values similar to those presented against MSSA and MRSA. Among thirty compounds tested against *E. faecalis* and *S. epidermidis*, the most potent presented MIC values equal to or lower than 15.6 μg/mL and MBC values equal to or lower than 31.2 μg/mL. Moreover, lipophilic hybrids (including **20**) demonstrated potent antibacterial activity, which may be justified by the greater ease of permeation by phospholipid biomembranes [25].

Against Gram-negative *E. coli*, the MIC and MBC values presented for hybrids were greater than 62.5 μg/mL. Gram-negative specie *A. baumannii* was the most susceptible to panel of hybrids, presenting the lowest MIC and MBC values. Among compounds, fourteen had MIC values below 15.6 μg/mL and MBC values lower than 31.2 μg/mL, indicating potent anti-*A. baumannii* activity.

Against *M. tuberculosis*, fifteen hybrids presented MIC values below 10 μg/mL, while curcumin and cinnamaldehyde presented values higher than 25.0 and 200.0 μg/mL, respectively. In addition, compounds substituted by electron-withdrawing atoms and groups were more activity when compared to those substituted by electron-donating groups. Also, lipophilic groups increases the antimycobacterial activity of hybrids in an expressive way, with emphasis on compound **8**, which presented higher antimycobacterial activity, with a MIC value of 0.7 μg/mL. These results may be justified by the fact that the mycobacterial cell wall is rich in lipids, mainly mycolic acids and lipophilic compounds are more able to penetrate through *M. tuberculosis* cell [43].

2.3. *In silico* drug-likeness predictions of hybrids 1–30

The interest in researching the drug-likeness properties of bioactive compounds is one of the strategies to select the best drug candidates from a library, including lipophilicity determined by logarithm of compound partition coefficient between *n*-octanol and water ($\log P_{o/w}$), molecular mass (MW), number of hydrogen donors (HBD) and number of hydrogen acceptors (HBA), that may aid in the conduct of the next experiments of a candidate for the drug [44].

In this context, Lipinski and co-authors established five drug-likeness rules to predict the absorption of candidates to orally administered drugs: $\log P_{o/w} \leq 5.00$, MW ≤ 500.00 Da, HBD ≤ 5.00, HBA ≤ 10 and the fifth rule was the permission to violate one of the previous rules. For these authors, substances that violate more than one of these rules may imply in pharmacokinetic problems of drug candidates [45]. All curcumin-cinnamaldehyde hybrids presented $\log P \leq 4.97$, MW ≤ 333.18 Da, HBD = 2 and HBA ≤ 6. Like Lipinski and co-authors, Veber and collaborators have suggested two drug-likeness properties: HBA + HBD ≤ 12 and Number of Routable Bonds (NROBT) ≤ 10 [46]. All hybrids exhibited HBA + HBD ≤ 4 and NROBT ≤ 6. Therefore, according to the Lipinski' and Veber' filters, hybrids did not violate their rules, corroborating the good drug-likeness properties (Table 4).

Human Intestinal Absorption (HIA) is one of the most important pharmacokinetic properties that should be studied for the planning and development of new oral medicines [47]. Yee and co-authors classified the intestinal absorption of compounds according to % HIA values, and a compound is poorly absorbed if it presents % HIA ≤ 20%, moderately absorbed if it presents 20% > HIA < 70% and well absorbed if present 70% > HIA ≤ 100% [48]. All hybrids showed % HIA ≥ 93% (Table 4), and were then considered to be well absorbed by the intestine if administered orally.

Evaluation of the compound permeation through the blood-brain barrier (BBB) is a pharmacokinetic property that can be investigated before proceeding with the development of a drug candidate, since this barrier is a self-defense mechanism that controls the passage of compounds from blood to the brain [49]. Thus, the potential of compounds that permeate BBB should be evaluated, mainly when brain is site of infectium, as meningitis caused by *S. aureus* [1], *P. aeruginosa* [50] and *M. tuberculosis* [51]. Brito-Sánchez and collaborators defined that a compound presents high permeability when it presents BBB ≥ 0 and poor permeability when BBB is < 0 [52]. All hybrids presented values of BBB between 0.03 and 3.46 (Table 4), indicating good absorption in the central nervous system, and the most active substance against *S. aureus* (hybrid **20**) is the one with the highest BBB value (3.46), further instigating the research in this substance that can act in staphylococcal meningitis, as well as in other infections of *S. aureus*.

3. CONCLUSIONS

Our study demonstrated that molecular hybridization between curcumin and cinnamaldehyde maintained or increased the activity of hybrids, with lipophilicity conferring greater activity against *S. aureus*. Hybrid **20** was the most active against MSSA and MRSA, being selected for evaluation of its combination with antibiotics, and its anti-adhesion activity, antibiofilm and time kill of MSSA and MRSA, presenting antibacterial activity similar or superior to the positive controls used. Toxicity *in G. mellonela* of hybrid **20** was evaluated, killing 50% of the population at 90 mg/kg, after 72 hours of treatment. Hybrids also showing activity against *E. faecalis*, *S. epidermidis*, *P. aeruginosa*, *A. baumannii* and *M. tuberculosis*. In relation to *in silico* studies, hybrids did not violate the rules established by Lipinski and Veber, and presented a high % HIA and

BBB values, indicating good drug-likeness properties. By means of this study, we can prove the antibacterial activity of curcumin-cinnamaldehyde hybrids, stimulating the study of these compounds, in order to search for new agents capable of acting against resistant strains.

4. EXPERIMENTAL

4.1. Chemistry

Curcumin (≥94%) and cinnamaldehyde (99%) were purchased from Merck®. Curcumin-cinnamaldehyde hybrids of this study were synthesized by Claisen-Schmidt aldol condensation reactions according to the methodology described by Santos and collaborators [22]. For this, 5 mmol of acetovanilone (Merck®) and 5 mmol of the respective aryl aldehydes (Merck®) were solubilised in 10 mL of ethanol and 20 mL of sodium ethoxide (800 mg of sodium hydroxide in 20 mL of ethanol). Reactions were maintained under magnetic stirring at room temperature and monitored by thin-layer chromatography (TLC). Reaction medium was poured onto ice from deionized water and acidified at pH 2.0 with hydrochloric acid. Precipitated crude products were filtered and dried at room temperature. Water-soluble crude products were submitted to liquid-liquid partition with ethyl acetate.

All crude products were purified over silica gel column, using mixtures of hexane and ethyl acetate as mobile phase. Details of the spectroscopy data analyses are provided in the supplementary material.

4.2. Biology

4.2.1. Bacterial strains and culture conditions

Strains of *Staphylococcus epidermidis* (ATCC® 12228), *Enterococcus faecalis* (ATCC® 29212), Methicillin-sensitive *Staphylococcus aureus* (ATCC® 25923), Methicillin-resistant *Staphylococcus aureus* (ATCC® 33591), *Escherichia coli* (ATCC® 43895), *Pseudomonas aeruginosa* (ATCC® 27853), and *Acinetobacter baumannii* (ATCC® 19606), were obtained from Fiocruz (Fundação Oswaldo Cruz, Rio de Janeiro, Brazil). All strains were stocked at –20 ° C, and subcultured on Brain Heart Infusion (BHI) agar. For experiments, was a single colony was inoculated and incubated at 37 ° C for 24 hours.

Strain of *M. tuberculosis* H37Rv (ATCC 27294) were purchased from ATCC®, being cultivated in Middlebrook 7H9 medium (Difco®) enriched with 10% OADC (oleic acid, albumin, dextrose and catalase).

4.2.2. Antibacterial activity of curcumin-cinamaldehyde hibrids 1–30

Antibacterial activity of curcumin, cinnamaldehyde and curcumin-cinnamaldehyde hybrids was expressed in terms of the Minimum Inhibitory Concentration (MIC), which is defined as the lowest concentration able to inhibit bacterial growth. Assays against Gram-negative and Gram-positive species were performed according to the M07-A10 of the Clinical and Laboratory Standards Institute (CLSI), with minor modifications [24].

Compounds were solubilized in DMSO in concentrations ranging from 0.48 to 62.5 μg/mL. For the MIC determination, sensitivity tests were performed according to the microdilution in method using Mueller-Hinton culture medium in a final volume of 200

μL. Vancomycin (Merck®), methicillin (Merck®) and gentamicin (Merck®) were used as reference antibacterial drugs.

The strains were subcultured onto BHI agar at 37 ° C for 24 hours. Inoculum was prepared in sterile 0.9% saline in dispersions of 2.5 to 5.0 × 10^8 CFU/mL. Inoculum absorbance was confirmed by (Spectrophotometer Unico 1100RS). Inoculum were suspended in Mueller-Hinton culture medium at 2.5 and 5.0 × 10^5 CFU/mL and distributed into 96-well plates (Kasvi®) by volume of 100 μL. Sterility control of the culture medium was employed in the first row with the addition of 200 μL of Mueller-Hinton. Plates were incubated at 37 °C for 24 hours. Subsequently, MIC was measured by visual reading.

In order to analyze letal effect of curcumin-cinnamaldehyde hybrids we also mensured the Minimum Bactericidal Concentration (MBC). After reading the result of MIC values, each concentration of the 96-well microplate (Merck®) was transferred to TSA agar plate (Kasvi®). Plates were incubated at 37 °C for 24 hours.

4.2.3. Antimycobacterial activity of curcumin-cinamaldehyde hibrids 1–30

Antimycobacterial activity of compounds was determined by broth microdilution method, performed according to Palomino and collaborators, with minor modifications [42].

Compounds were solubilized in DMSO and diluted in growth medium in concentrations raging from 0.09 to 25.0 μg/mL. Mycobacterial inoculum was incubated on the shaker at 37 ° C 120 rpm for seven days until reaching a turbidity of 1.0 on the McFarland scale. Mycobacterial suspension was adjusted to 3.0 × 10^5 colony forming units per ml (CFU/mL) and 100 μL of inoculum was added to each well of a 96 well plate (Kasvi®) along with 100 μL of the solution of compound. The plate was incubated for

seven days at 37 °C with 5% CO_2. After that time, 30 μL of resazurin (Merck®) solubilized in sterile water was added. After 24 hours, well fluorescence was read using the Cytation 3 equipment (Biotek®) with excitation and emission filters at wavelengths of 530 and 590 nm, respectively. Isoniazid was used as a reference antitubercular drug.

4.2.4. Effects of combination of vancomycin or methicillin with hybrid 20 against MSSA and MRSA

In order to determine the antibacterial activity of **20** against *S. aureus* MSSA and MRSA when compared with vancomycin and methicillin, the hybrid 20 at MIC value was evaluated when it was combined with the vancomycin (Merck®) or methicillin (Meck®) at MIC values. For this, microdilution method was used, as decribed by Miladi and co-authors, with minor modifications [53].

Hybrid **20** and drugs of this assay were solubilized in DMSO: **20** in concentrations ranging from 0.48 to 62.5 μg/mL, vancomycin at 0.5 μg/mL (MIC for MSSA and MRSA) and methicillin at 0.5 μg/mL (MIC for MSSA) and 2.0 μg/mL (MIC for MRSA). Inocula were performed according to the M07-A10 of the Clinical and Laboratory Standards Institute (CLSI), with minor modifications [24]. Sterility control of the culture medium was used in the first row with the addition of 200 μL of Mueller-Hinton medium. Plates were incubated at 37 °C for 24 hours. Subsequently, MIC of **20** in combination with MIC values of vancomycin and methicillin was measured by visual reading.

4.2.5. Inhibitors effects of hybrid 20 on adhesion of *S. aureus* onto human keratinocytes

Anti-adhesion activity assay was performed in order to evaluate the ability of *S. aureus* to adhere to human keratinocytes (HaCaT) after treatment with **20** at 1/2 MIC

value, according to Sardi and co-authors [29]. This concentration was selected as it ensures that bacterial growth and survival are not affected by effect antimicrobial of compound. For this, HaCaT cell line were obtained from the Bank of Cells of Rio de Janeiro (RJ, Brazil), and maintained in Dulbecco's medium (DMEM) (Gibco®) supplemented with 10 % fetal bovine serum (Gibco®), 100 μg streptomycin sulfate, 100 U penicillin mL/L and 200 mM L-glutamine at 37 ºC under 5 % CO_2.

Cell toxicity assay was performed in order to verify whether in the time period of the adhesion assay (3 hours), the cells would show toxicity to the hybrid **20**. HaCaT (1.0×10^5 cells/well) was seeded into a 96-well plate (Kasvi®) and incubated for 48 hours. Supernatants were removed and substituted with 100 μL of DMEM with compounds at 30 μL, at 1/2 MIC. Wells containing only cells and culture medium were used as negative control (100% of cell viability). After 3 hours, supernatants were removed and 100 μL a solution of 3-(4,5-dimethylthiazol-2-yl)-2,5-diphenyltetrazolium bromide (MTT) (Merck®) was added to each well and the plate was incubated for another 3 hours at 37 °C, until the reading absorbance was measured at 470 nm.

Adhesion curve at 1, 2 and 3 hours was plotted to determine the initial time of bacterial adhesion to the HaCaT cells. The assay was performed using 96-well plates (Kasvi®) containing 1.0×10^5 cells per well. Before formation of monolayers of cells in the wells, aliquots of 200 μL bacterial inoculum of MSSA and MRSA (5.0×10^3 CFU/mL) were added to each well. Plates were incubated at 37 ºC and 5 % of CO_2 for the 1, 2 and 3 hours. After each incubation time, the cells were washed three times with sterile saline 0,9% and then trypsinized. Aliquots of 100 μL were plated for quantification of CFU measurement onto TSB (Tryptic Soy Broth) plates and incubated at 37 ºC for 24 hours. Percentage of inhibition of adhesion was calculated based on the final number of adhered bacteria in relation to an untreated group, indicating 100 % bacterial adhesion.

4.2.6. Antibiofilm of S. aureus activity of hybrid 20

Evaluation of the antibiofilm activity of hybrid **20** was carried out by three tests, including its effects on biofilm formation, mature biofilm and on tridimensional structure of biofilm of MSSA and MRSA, according to the protocols described by Sardi and co-authors [29].

4.2.6.1. Effects of 20 on biofilm formation and mature biofilm

MSSA and MRSA biofilm were formed in 96-well microtiter plates (Kasvi®). 100µL of a cell suspension at 1.0×10^8 CFU/mL of MSSA and MRSA was added to a 96-well microplate. Plates were incubated at 37 ° C for 2 hours (biofilm formation) and 24 hours (mature biofilm), allowing cell adhesion. Sterile saline 0,9% as added to each well to remove planktonic cells, and biofilms were treated with hybrid **20** at MIC and 10 × MIC values for 24 hours at 37 °C.

After incubation, biofilms were washed to remove the planktonic killed cells, desorbed and resuspended from the bottom of the wells. 50 µL volume containing the cell suspension from each well was aspirated and transferred to an eppendorf tube containing 450 µL of sterile saline 0,9%. Ten serial dilutions were performed and 10 µL of each suspension was pipetted into TSA (Tryptic Soy Agar) plates. The survival percentage of CFU/mL was determined by the survival of untreated MSSA and MRSA biofilms after 24 hours at 37 °C. Vancomycin (Sigma-Aldrich®) and methicillin (Sigma-Aldrich®) was used as the reference antibacterial drugs.

4.2.6.2. Effects of hybrid 20 on tridimensional structure of MSSA and MRSA biofilm

In order to evaluate the effect of hybrid **20** on the structure and integrity of the MSSA and MRSA biofilms, Scanning Electron Microscopy (SEM) was performed,

according to Sardi and collaborators [25]. First, the biofilms were cultured for 24 hours at 37 °C on glass slides in tissue culture treated chambers (Corning BD Falcon®), washed three times with sterile saline 0.9% and then treated at MIC and 10 × MIC values of hybrid **20**. Untreated biofilm was used as negative control. After 24 hours, the samples were washed with sterile saline 0.9% and maintained in 2.5% glutaraldehyde / PBS (v / v, pH 7.4) solution for 2 hours at room temperature. The slides were dehydrated gradually with ethanol (50 to 100%) for 5 minutes, coated with 40 mA gold customize (BAL-TEC SCD 050®), after dying, observed in a scanning microwave microscope (Jeon JSM 5600LV).

4.2.7. Effects of combination of hybrid 20 with vancomicina and methicillin against MSSA and MRSA biofilm

In this assay, the activity of the **20** against the formation and mature biofilm of MSSA and MRSA was evaluated in combination with vancomycin or methicillin at MIC and 10×MIC values. These experiments were performed as protocols described by Sardi and co-authors [29].

4.2.8. Effect of hybrid 20 on MSSA and MRSA time kill

Time kill assay was performed in order to verify the time of **20** needed to promote death of MSSA and MRSA, following methodology described by Graziano and collaborators, with minor modifications [54]. In ten tubes, 40 mL TSB (Kasvi®) culture medium, 40 μl of MSSA and MRSA 1.0×10^8 cells/mL were added. In tubes 1 and 2, 100 μL of **20** was added at MIC concentration, while in tubes 3 and 4 100 μL of **20** at 10 × MIC value was added. In tubes 5 and 6, 100 μL of vancomycin was added at MIC value,

while in tubes 7 and 8 100 μL of vancomycin 10 × MIC was added. Tubes 9 and 10 were considered negative controls of untreated MSSA and MRSA cells, respectively.

The tubes were incubated at 37 °C and thereafter at 0, 2, 4, 8 and 12 hours, 50 μL of the contents were removed and diluted in sterile saline 0.9% at ratio 1:1 for subsequent serial dilution and TSA (Kasvi®) agar plating. The survival percentage of CFU/mL was determined according to the survival of MSSA and MRSA without prior treatment with **20** or vancomycin after 24 hours at 37 °C.

4.2.9. Toxicity of hybrid 20 against *Galleria mellonella*

Toxicity of **20** was evaluated against *G. mellonella* larvae, as described by Megaw and collaborators [55]. A set of 60 healthy larvae with weight between 200 and 300 mg were randomly selected six groups. The individuals were kept on ice for 20 minutes and had their prolegs were cleaned with 70% ethanol. 10 μL of **20** at different doses: 10 mg/kg, 30 mg/kg, 60 mg/kg, and 90 mg/kg, DMSO 1% and saline (0.9%) were injected into the larvae hemocoel via the last left proleg using a Hamilton syringe (Hamilton, Reno, NV®). Larvae were maintained at 37 ºC and their survival monitored at each 12 hours for 72 hours. Larvae unable to move when touched and showing high levels of melanization were considered dead.

4.2.10. Statistical analysis

All experiments were performed using three replicates per group and in three independent experiments. Data were analyzed by using GraphPad version 5.00 (San Diego, CA, USA). Biofilm results were analyzed by one-way analysis of variance (ANOVA) with Tukey's multiple comparison test, against a significance level of 5 %. For the *in vivo* toxicity assay with *G. mellonella*, Kaplan-Meier killing curves were

plotted on GraphPad Prism 5.0 and estimations of differences in survival were compared using the Log-rank test.

4.3. *In silico* drug-likeness properties predictions 1–30

In silico studies were performed to predict drug-likeness properties of all hybrids. For this, we used the Molinspiration [56] and PreADMET [57] toolkits, analyzing: molecular weight (MW), number of hydrogen bonding donors (HBD), number of hydrogen bond acceptors (HBA), number (NROTB) in order to categorize hybrids in the Lipinski' and Veber' rules. Percentage of intestinal absorption (HIA) and the capacity for penetration into the blood-brain barrier (BBB) of all hybrids were calculated to indicate their pharmacokinetics properties [47, 58].

ACKNOWLEDGMENTS

BCM gratefully acknowledges financial support from the São Paulo State Research Foundation (FAPESP) (2014/18330-0, 2018/15083-2 and 2017/09245-7), the Coordination for the Improvement of Higher Education Personnel (CAPES) (Financing Code 001) and the National Research Council (CNPq) (471129/2013-5, 306251/2016-7, 429322/2018-6) and National Institute of Science na Technology – Biodiversity and Natural Products (INCT - BioNat). Also, we would like to thank the Multiuser Center of Biomolecular Innovation (FAPESP 2009/53989-4) for the use of Bruker Avance III 9.397 T (400 MHz) and 14.095 T (600 MHz) spectrometers and the Laboratory-II of Nuclear Magnetic Resonance for the use of Bruker Fourier (300 MHz) spectrometer.

REFERENCES

[1] S. Y. C. Tong, J. S. Davis, E. Eichenberger, T. L. Holland, V. G. Fowler, *Staphylococcus aureus* Infections: Epidemiology, Pathophysiology, Clinical Manifestations and Management, Clin. Microbiol. Rev., 28 (2015) 603–661.

[2] D. Balasubramanian, L. Harper, B. Shopsin, V. J. Torres, *Staphylococcus aureus* pathogenesis in diverse host Environments, Pathog. Dis., 75 (2017) 1–13.

[3] H. S. Sader, R. E. Mendes, R. N. Jones, R. K. Flamm, Antimicrobial susceptibility patterns of community- and hospital-acquired methicillin-resistant *Staphylococcus aureus* from United States Hospitals: results from the AWARE Ceftaroline Surveillance Program (2012-2014), Diagn. Microbiol. Infect. Dis., 86 (2016) 76–79.

[4] P. Kale, B. Dhawan, The changing face of community-acquired methicillin-resistant *Staphylococcus aureus*, Indian J. Med. Microbiol., 34 (2016) 275–285.

[5] S. A. Kristian, T. Golda, F. Ferracin, S. E. Cramton, B. Neumeister, A. Peschel, F. Götz, R. Landmann, The ability of biofilm formation does not influence virulence of *Staphylococcus aureus* and host response in a mouse tissue cage infection model, Microb. Pathogenesis, 36 (2014) 237–245.

[6] L. L. Silver, Challenges of antibacterial discovery. Clin. Microbiol. Rev., 24 (2011) 71–109.

[7] A. Zecconi, F. Scali, *Staphylococcus aureus* virulence factors in evasion from innate immune defenses in human and animal diseases, Immunol. Lett., 150 (2013) 12–22.

[8] L. B. Rice, Progress and challenges in implementing the research on ESKAPE pathogens, Infect. Control Hosp. Epidemiol., 31 (2010) S7–S10.

[9] S. Santajit, N. Indrawattana, Mechanisms of Antimicrobial Resistance in ESKAPE Pathogens, Biomed. Res. Int., 2016 (2016) 1–9.

[10] Mun, S. H.; Kim, S. B.; Kong, R.; Choi, J. G.; Kim, Y. C.; Shin, D. W.; Kang, O. H.; Kwon, D. Y. Curcumin reverse methicillin resistance in *Staphylococcus aureus*. **Molecules**, v. 19, p. 18283–18295, 2014.

[11] X. Y. Xu, X. Meng, S. Li, R. Y. Gan, Y. Li, H. B. Li, Bioactivity, health benefits, and related molecular mechanisms of curcumin: Current progress, challenges, and perspectives, Nutrients, 10 (2018) 1–33.

[12] Shetty, D.; Kim, Y. J.; Shim, H.; Snyder, J. P. Eliminating the heart from the curcumin molecule: Monocarbonyl curcumin mimics (MACs). Molecules, v. 20, p. 249−292, 2014.

[13] M. Awasthi, S. Singh, V. P. Pandey, U. N. Dwivedi, Curcumin: Structure-activity relationship towards its role as a versatile multi-targeted therapeutics. Mini Rev. Org. Chem., 14 (2017) 311–332.

[14] L. G. Mourão, C. R. Polaquini, M. Kopacz, G. S. Torrezan, G. M. Ayusso, G. Dilarri, L. B. Cavalca, A. Zielinska, D. Scheffers, L. O. Regasini, H. Ferreira, A simplified curcumin targets the membrane of *Bacillus subtilis*, Microbiologyopen, 8 (2018) 1–12.

[15] P. Ranasinghe, S. Pigera, G. A. Premakumara, P. Galappaththy, G. R. Constantine, P. Katulanda, Medicinal properties of 'true' cinnamon (*Cinnamomum zeylanicum*): a systematic review, BMC Complement. Altern. Med., 13 (2013) 1–10.

[16] S. Kumar, R. Kumari, *Cinnamomum*: review article of essential oil compounds, ethnobotany, antifungal and antibacterial effects, Open Access J Sci., 3 (2019) 13–16.

[17] C. Shi, X. Zhang, X. Zhao, R. Meng, Z. Liu, X. Chen, N. Guo, Synergistic interactions of nisin in combination with cinnamaldehyde against *Staphylococcus aureus* in pasteurized milk. Food Control, 71 (2017) 10–16.

[18] T. A. F. Ferro, J. M. M. Araújo, B. L. S. Pinto, J. S. Santos, E. B. Souza, B L. R. Silva, V. L. P. Colares, T. M. G. Novais, C. M. B. Filho, C. Struve, J. B. Calixto, V. Monteiro-Neto, L. C. N. Silva, E. S. Fernandes, Cinnamaldehyde Inhibits *Staphylococcus aureus* Virulence Factors and Protects against Infection in a *Galleria mellonella* Model, Front Microbiol., 7 (2016) 1–10.

[19] R. M. Lopachin, T. Gavin. Molecular mechanisms of aldehyde toxicity: a chemical perspective. Chem. Res. Toxicol., 27, (2014) 1081–1091.

[20] C. R. Polaquini, G. S. Torrezan, V. R. Santos, A. C. Nazaré, D. L. Campos, L. A. Almeida, I. C. Silva, H. Ferreira, F. R. Pavan, C. Duque, L. O. Regasini Antibacterial

and Antitubercular Activities of Cinnamylideneacetophenones, Molecules, 22 (2017) 1–12.

[21] Viegas-Junior, C.; Danuello, A.; Da Silva Bolzani, V.; Barreiro, E. J.; Fraga, C. A. Molecular hybridization: a useful tool in the design of new drug prototypes. Curr. Med. Chem., 14 (2007) 1829–52.

[22] M. B. Santos, V. C. Pinhanelli, M. A. R. Garcia, G. Silva, S. J. Baek, S. C. França, A. L. Fachin, M. Marins, L. O. Regasini, Antiproliferative and pro-apoptotic activities of 2'- and 4'- aminochalcones against tumor canine cells, Eur. J. Med. Chem., 138 (2017) 884–889.

[23] SciFinder. Available in: < https://scifinder.cas.org/> Access in: 10 mai 2019.

[24] CLSI. Methods for Dilution Antimicrobial Susceptibility Tests for Bacteria That Grow Aerobically; Approved Standard–Tenth Edition.; CLSI Document M07-A10. Wayne, P.A: Clinical Laboratory Standards Institute; 2015.

[25] R. Pignatello, T. Musumeci, L. Basile, C. Carbone, and G. Puglisi, Biomembrane models and drug-biomembrane interaction studies: Involvement in drug design and development, J. Pharm. Bioallied Sci., 3 (2011) 4–14.

[26] S. H. MUN, S. B. KIM, R. KONG, J. G. CHOI, Y. C. KIM, D. W. SHIN, O. H. KANG, D. Y. KWON, Curcumin reverse methicillin resistance in *Staphylococcus aureus*, Molecules, 19 (2014) 18283–18295.

[27] GAUR, R., GUPTA, V.K., PAL, A., DAROKAR, M.P., BHAKUNI, R.S., KUMARC, B. *In vitro* and *in vivo* synergistic interaction of substituted chalcone derivatives with norfloxacin against methicillin resistant *Staphylococcus aureus*, RSC Adv., 5, (2015) 5830–5845.

[28] C. Heilmann, Adhesion Mechanisms of Staphylococci, Adv. Exp. Med. Biol., 715 (2011) 105–123.

[29] J. C. O. Sardi, C. R. Polaquini, I. A. Freires, L. C. C. Galvão, J. G. Lazarini, G. S. Torrezan, L. O. Regasini, P. L. Rosalen, Antibacterial activity of diacetylcurcumin

against *Staphylococcus aureus* results in decreased biofilm and cellular adhesion, J. Med. Microbiol., 66 (2017) 816–824.

[30] M. Bhattacharya, D. J. Wozniak, P. Stoodley, L. Hall-Stoodley, Prevention and treatment of *Staphylococcus aureus* biofilms. Expert Rev. Ant. Infect. Ther., 13 (2015) 1499–1516.

[31] U. Römling, C. Balsalobre, Biofilm infections, their resilience to therapy and innovative treatment strategies, J. Intern. Med., 272 (2012) 541–561.

[32] C. Gil, C. Solano, S. Burgui, C. Latasa, B. García, A. Toledo-Arana, I. Lasa, J. Valle, Biofilm Matrix Exoproteins Induce a Protective Immune Response against *Staphylococcus aureus* Biofilm Infection, Infect. Immun., 82 (2014) 1017–1029.

[33] C. Pozzi, E. M. Waters, J. K. Rudkin, C. R. Schaeffer, A. J. Lohan, P. Tong, B. J. Loftus, G. B. Pier, P.D. Fey, R. C. Massey, J. P. Gara, Methicillin resistance alters the biofilm phenotype and attenuates virulence in *Staphylococcus aureus* device-associated infections, PLoS Pathog., 8 (2012) 1–15.

[34] C. R. Belanger, S. C. Mansour, D. Pletzer, R. E. W. Hancock, Alternative strategies for the study and treatment of clinical bacterial biofilms, Emerg. Top. Life Sci., 1 (2017) 41–53.

[35] E. Akbari-Ayezloy, N. Hosseini-Jazani, S. Yousefi, N. Habibi, Eradication of methicillin resistant *S. aureus* biofilm by the combined use of fosfomycin and β-chloro-L-alanine. Iran J. Microbiol., 9 (2017) 1–10.

[36] M. Balouiri, M. Sadiki, S. K. Ibnsouda, Methods for *in vitro* evaluating antimicrobial activity: A review. J. Pharmaceut. Anal., 6 (2016) 71–79.

[37] K. V. Rolston, W. Wang, L. Nesher, J. R. Smith, M. J. Rybak, R. A. Prince, Time-kill determination of the Bactericidal activity of Telavancin and Vancomycin against clinical Methicillin-resistant *Staphylococcus aureus* isolates from Cancer Patients, Diagn. Microbiol. Infect. Dis., 87 (2017) 338–342.

[38] C. J. Y. Tsai, J. M. S. Loh, T. Proft, *Galleria mellonella* infection models for the study of bacterial diseases and for antimicrobial drug testing, Virulence, 7 (2016) 214–229.

[39] A. P. Desbois, P. J. Coote, Wax moth larva (*Galleria mellonella*): an *in vivo* model for assessing the efficacy of antistaphylococcal agentes, J. Antimicrob. Chemoth., 66 (2011) 1785–1790.

[40] M. Scoble, Classification of the Lepidoptera, Oxford University Press, 1995.

[41] N. Ramarao, C. Nielsen-Leroux, D. Lereclus, The insect *Galleria mellonella* as a powerful infection model to investigate bacterial pathogenesis, J. Vis. Exp., 11 (2012) 1–7.

[42] J. C. Palomino, A. Martin, M. Camacho, H. Guerra, J. Swings, F. Portaels, Resazurin Microtiter Assay Plate: Simple and inexpensive method for detection of drug resistance in *Mycobacterium tuberculosis*, Antimicrob. Agents Chemother., 46 (2002) 2720–2722.

[43] A. Koch, V. Mizrahi, *Mycobacterium tuberculosis*, Trends Microbiol., 26 (2018) 555–556.

[44] S. Mignani, J. Rodrigues, H. Tomas, R. Jalal, P. P. Singh, J. P. Majoral, R. A.Vishwakarma, Present drug-likeness filters in medicinal chemistry during the hit and lead optimization process: how far can they be simplified?, Drug Discov. Today, 23 (2018) 605–615.

[45] C. A. Lipinski, Lead-and drug-like compounds: the rule-of-five revolution, Drug Discov. Today Technol., 1 (2004) 337–341.

[46] D. F. Veber, S. R. Johnson, H. Y. Cheng, B. R. Smith, K. W. Ward, K. D. Kopple, Molecular properties that influence the oral bioavailability of drug candidates, J. Med. Chem., 45 (2002) 2615–2623.

[47] H. E. Selick, A. P. Beresford, M. H. Tarbit, The emerging importance of predictive ADME simulation in drug discovery, Drug. Discov. Today, 7 (2002) 109–116.

[48] S. Yee, In vitro permeability across Caco-2 cells (colonic) can predict in vivo (small intestinal) absorption in man – fact or myth, Pharm. Res., 14 (1997) 763–766.

[49] C. Saraiva, C. Praça, R. Ferreira, T. Santos, L. Ferreira, L. Bernardino, Nanoparticle-mediated brain drug delivery: Overcoming blood–brain barrier to treat neurodegenerative diseases, J. Control. Release, 235 (2016) 34–47.

[50] S. Pai, L. Bedford, R. Ruramayi, S. H. Aliyu, J. Sule, D. Maslin, D. A. Enoch, *Pseudomonas aeruginosa* meningitis/ventriculitis in a UK tertiary referral hospital. QJM, 109 (2016) 85–89.

[51] L. M. van Leeuwen, M. Boot, C. Kuijl, D. I. Picavet, G. van Stempvoort, S. M. A. van der Pol, H. E. Vries, N. N. van der Wel, M. van der Kuip, A. M. van Furth, A. M. van der Sar, W. Bitter, Mycobacteria employ two different mechanisms to cross the blood–brain barrier, Cell. Microbiol., 20 (2018) 1–17.

[52] Y. Brito-Sanchez, Y. Marrero-Ponce, S. J. Barigye, I. Yaber-Goenaga, C. M. Perez, H. Le-Thi-Thu, A. Cherkasov, Towards better BBB passage prediction using an extensive and curated data set, Mol. Inform., 34 (2015) 308–330.

[53] H. Miladi, T. Zmantar, B. Kouidhi, Y. M. A. Al Qurashi, A. Bakhrouf, Y. Chaabouni, K. Mahdouani, K. Chaieb, Synergistic effect of eugenol, carvacrol, thymol, p-cymene and g-terpinene on inhibition of drug resistance and biofilm formation of oral bacteria, Microb. Pathog., 112 (2017) 156–163.

[54] T. S. Graziano, M. C. Cuzzullin, G. C. Franco, H. O. Schwartz-Filho, E. D. Andrade, F. C. Groppo, K. Cogo-Müller, Statins and Antimicrobial Effects: Simvastatin as a Potential Drug against *Staphylococcus aureus* Biofilm, 10 (2015) 1–17.

[55] J. Megaw, T. P. Thompson, R. A. Lafferty, B. F. Gilmore, *Galleria mellonella* as a novel *in vivo* model for assessment of the toxicity of 1-alkyl-3-methylimidazolium chloride ionic liquids, Chemosphere, 139 (2015) 197–201.

[56] Molinspiration Cheminformatics. Available in: <https://www.molinspiration.com/cgi-bin/properties> Access in: 8 mai 2019.

[57] PreADMET. Available in: <https://preadmet.bmdrc.kr/adme/> Access in: 8 mai 2019.

[58] N. Polkam, V. R. Ramaswamy, P. Rayam, T. R. Allaka, H. S. Anantaraju, S. Dharmarajan, Y. Perumal, D. Gandamalla, N. R. Yellu, S. Balasubramanian, J. S. Anireddy, Synthesis, molecular properties prediction and anticancer, antioxidant evaluation of new edaravone derivatives, Bioorg. Med. Chem. Lett., 26 (2016) 2562–2568.

Figure 1. Structure of curcumin (a). Structure of cinnamaldehyde (b)

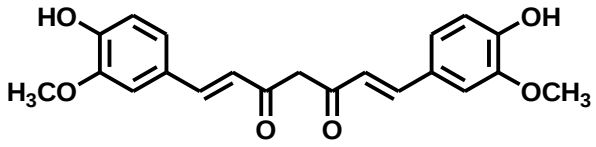

a

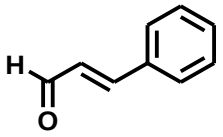

b

Figure 2. Desing of hybrids **1–30** from curcumin and cinnamaldehyde as parent compound

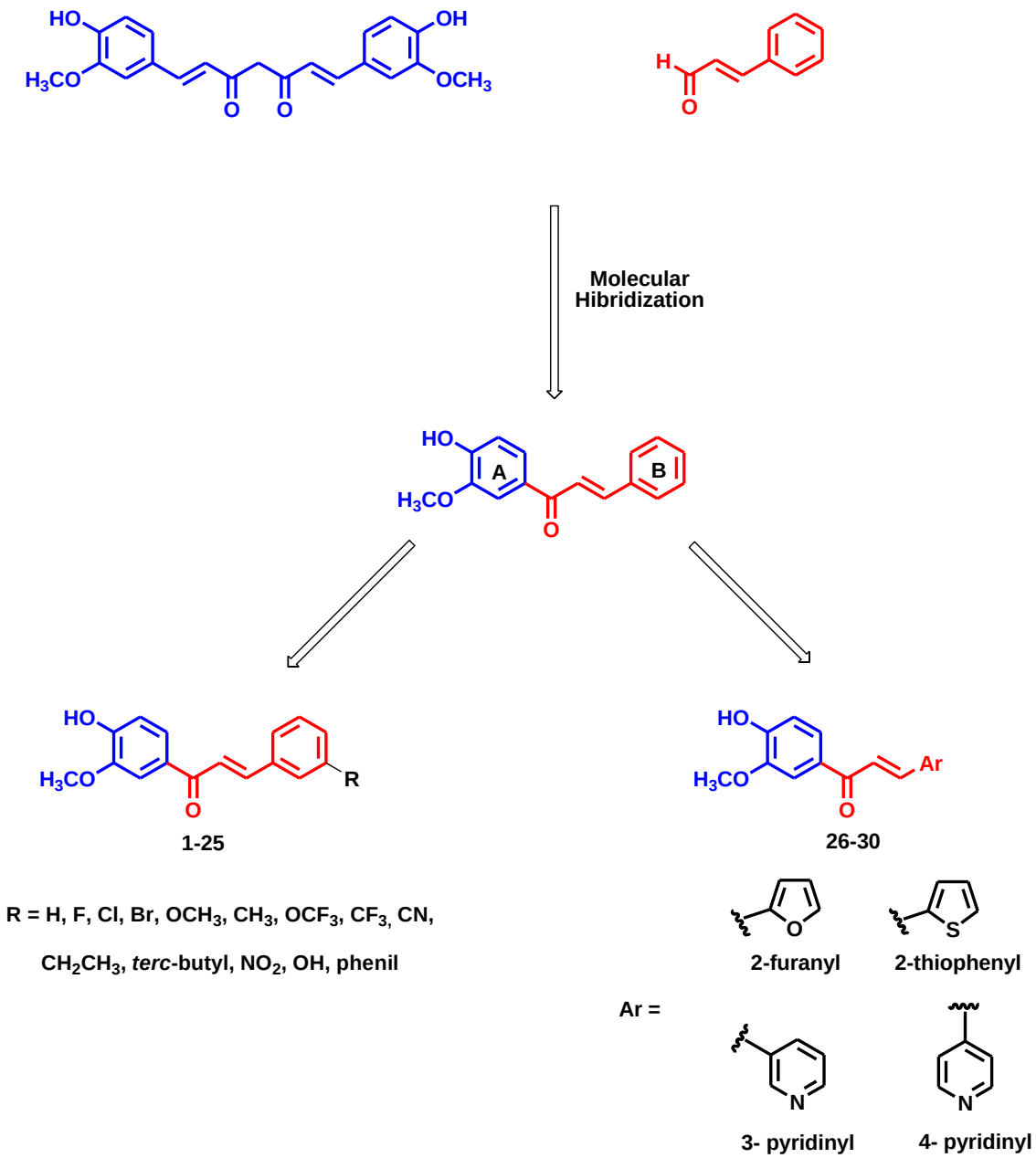

Figure 3. Synthesis of hybrids curcumin- cinnamaldehyde **1–30**

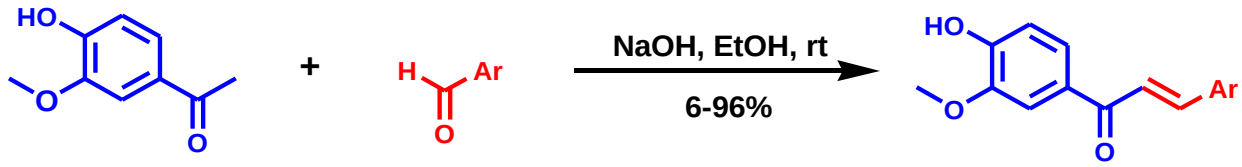

Figure 4. HaCaT viability (in %) treated with **20** at 3.9 µg/mL for MSSA and 1.95 µg/mL for MRSA

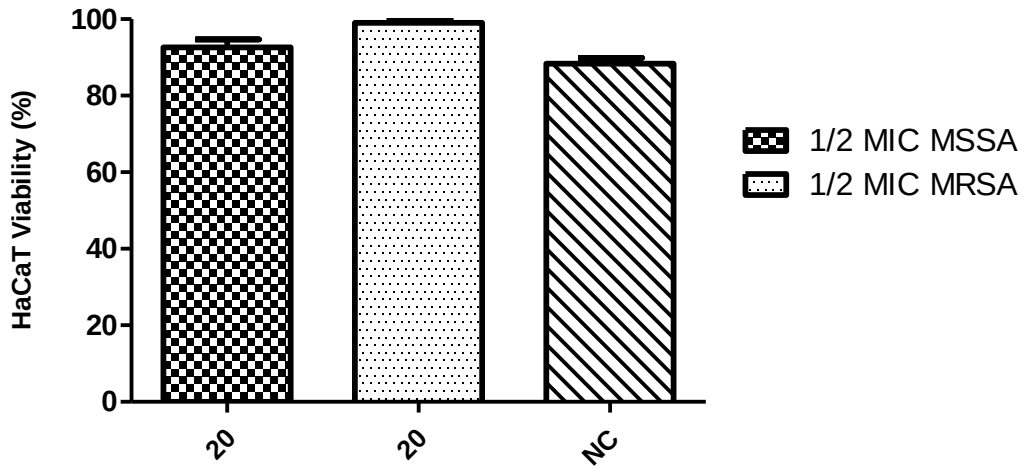

NC = negative control

Figure 5. Percentage of inhibitory effects (mean±SD) of hybrid **20** onto adhesion of MSSA (A) and MRSA (B) to human keratinocytes. Different letters indicate $P<0.0001$

A

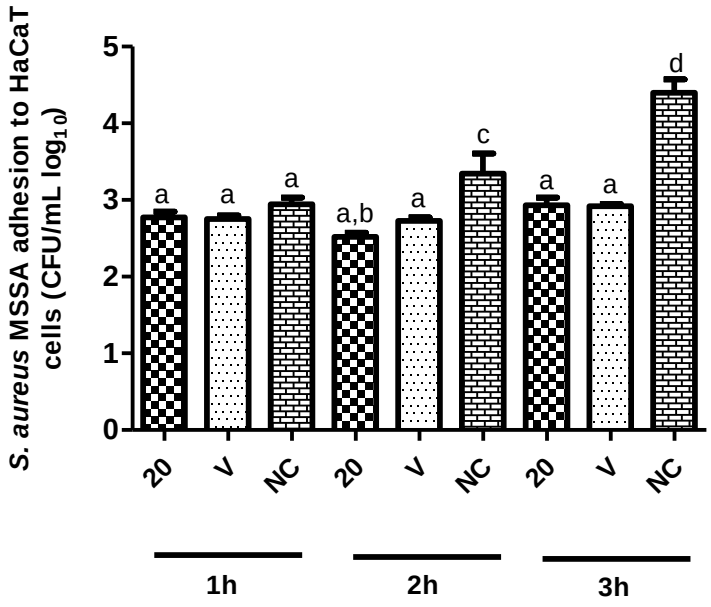

V = vancomicyn; NC = negative control

B

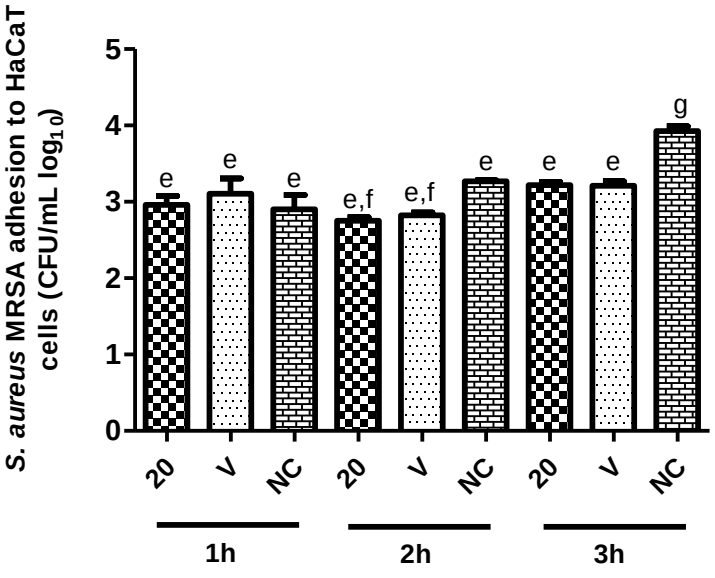

V = vancomicyn; NC = negative control

Figure 6. Quantitative analysis (determination of CFU/mL) of the inhibitory effects (mean±SD) of hybrid **20**, vancomycin and methicillin on MSSA (A) and MRSA (B) biofilme formation. Different letters indicate P<0.0001

A

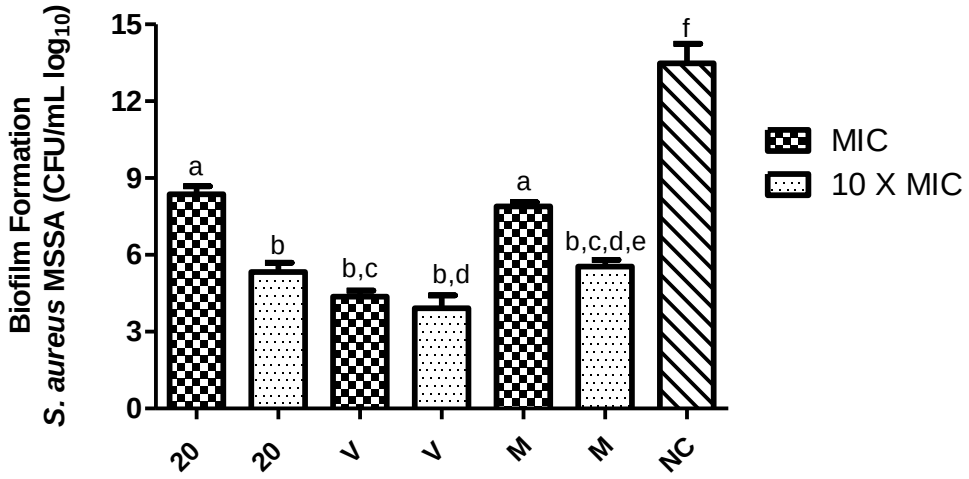

V = vancomycin; M = methicillin; NC = negative control

B

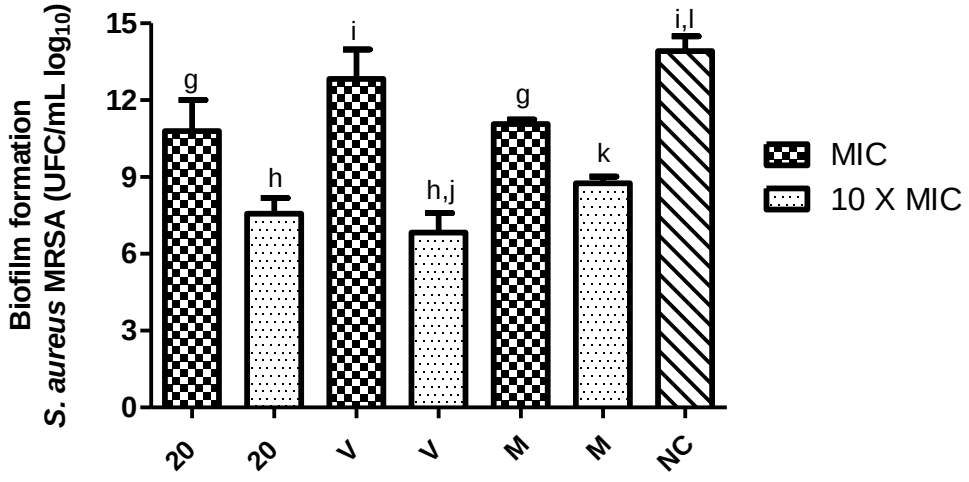

V = vancomycin; M = methicillin; NC = negative control

Figure 7. Quantitative analysis (determination of CFU/mL) of the inhibitory effects (mean±SD) of hybrid **20**, vancomycin and methicillin on MSSA (A) and MRSA (B) mature biofilm. Different letters indicate P<0.0001

A

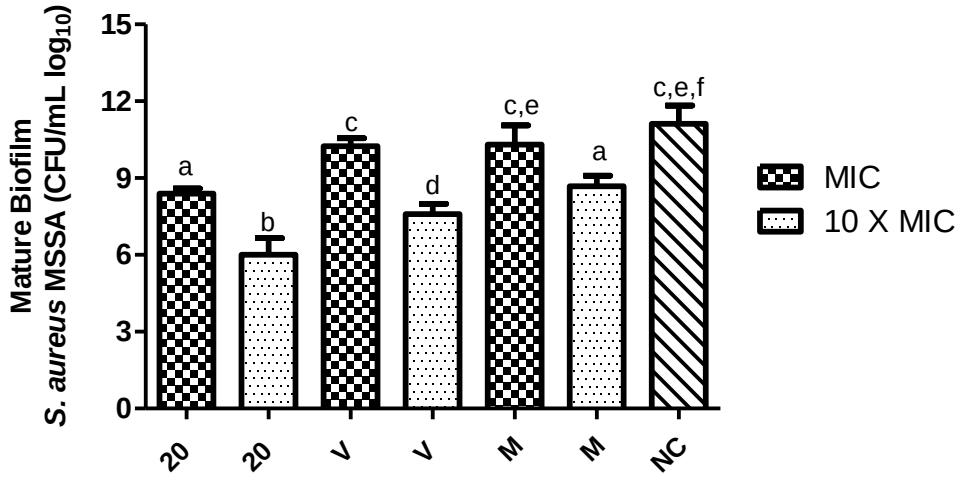

V = vancomycin; M = methicillin; NC = negative control

B

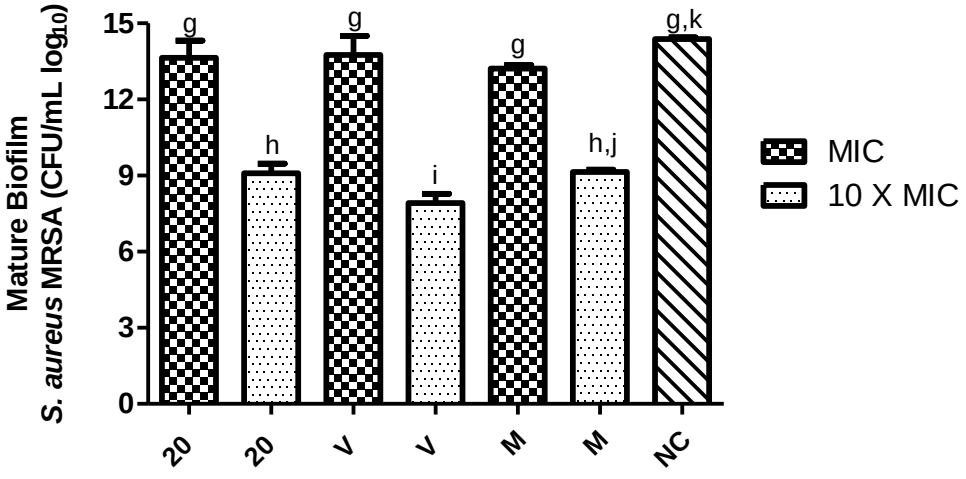

V = vancomycin; M = methicillin; NC = negative control

Figura 8. SEM photomicrographs (×5000) showing MSSA and MRSA biofilm cells after treatment with hybrid **20**

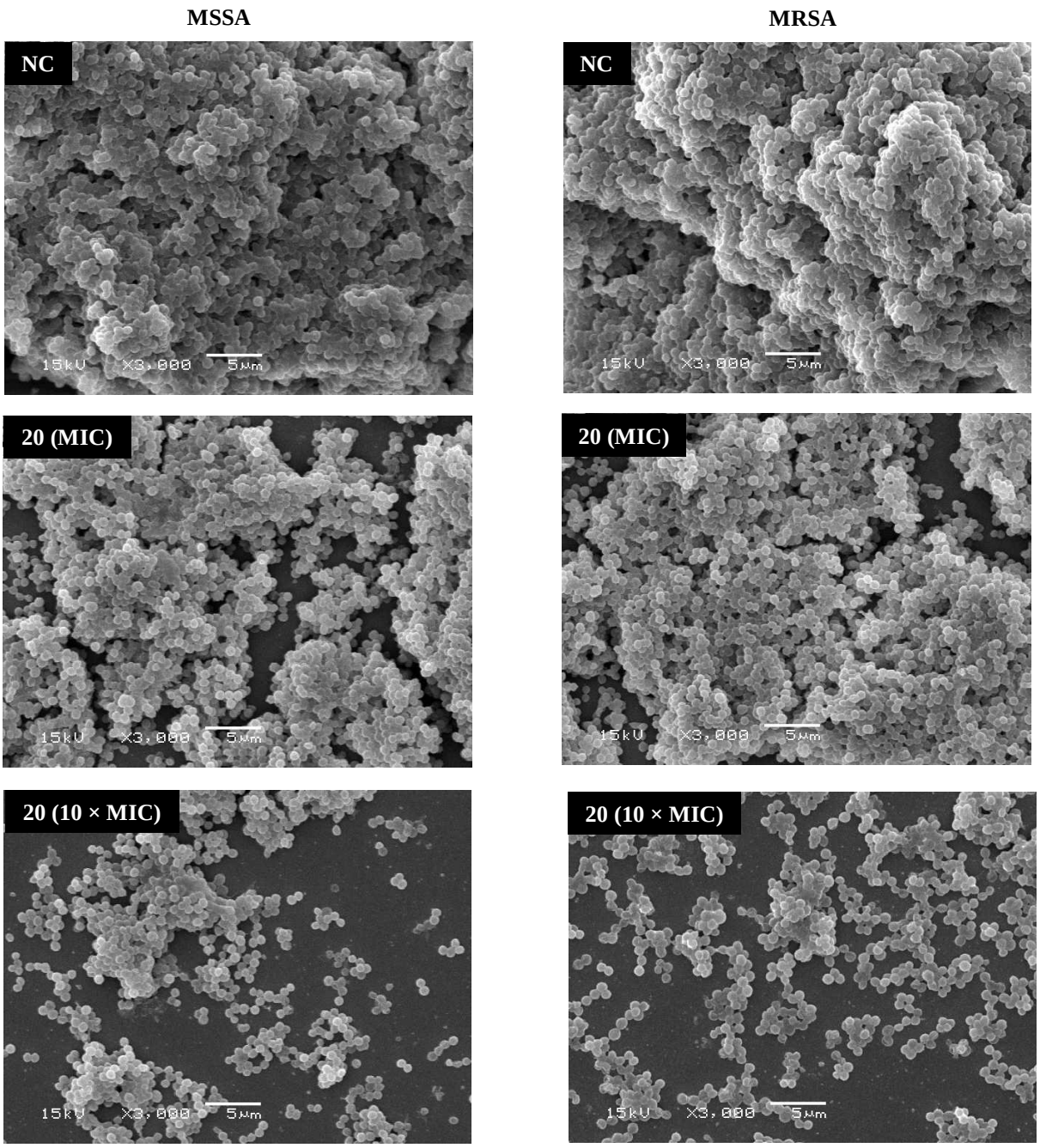

NC = negative control

Figure 9. Quantitative analysis (determination of CFU/mL) of the inhibitory effects (mean±SD) of hybrid **20** combined with vancomycin and methicillin on MSSA (A) and MRSA (B) biofilme formation. Different letters indicate P<0.0001

A

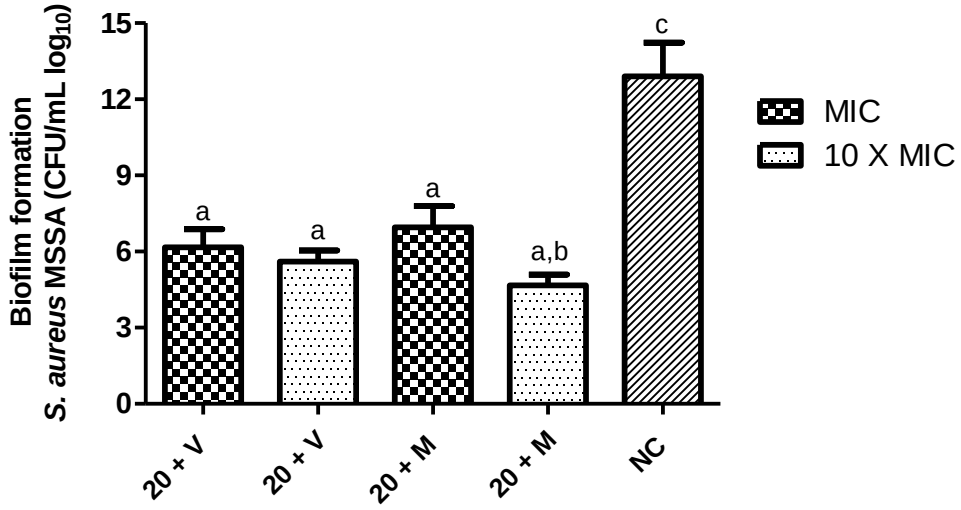

V= vancomycin; M = methicillin; NC = negative control

B

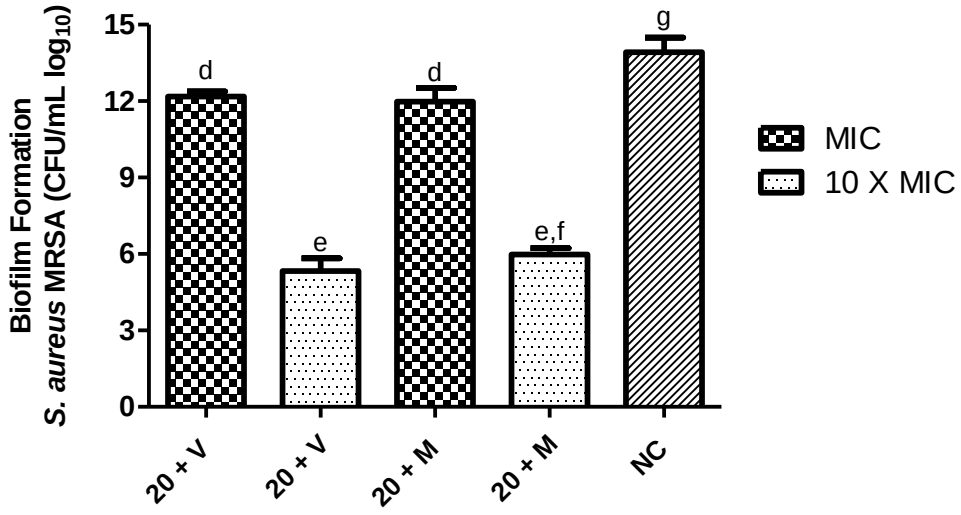

V= vancomycin; M = methicillin; NC = negative control

Figure 10. Quantitative analysis (determination of CFU/mL) of the inhibitory effects (mean±SD) of hybrid **20** combined with vancomycin and methicillin on MSSA (A) and MRSA (B) mature biofilme. Different letters indicate P<0.0001

A

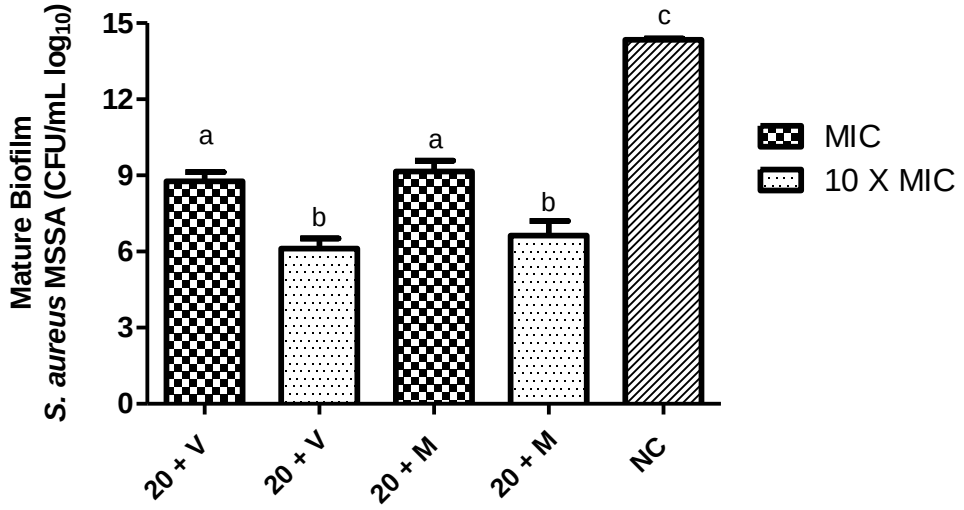

V= vancomycin; M = methicillin; NC = negative control

B

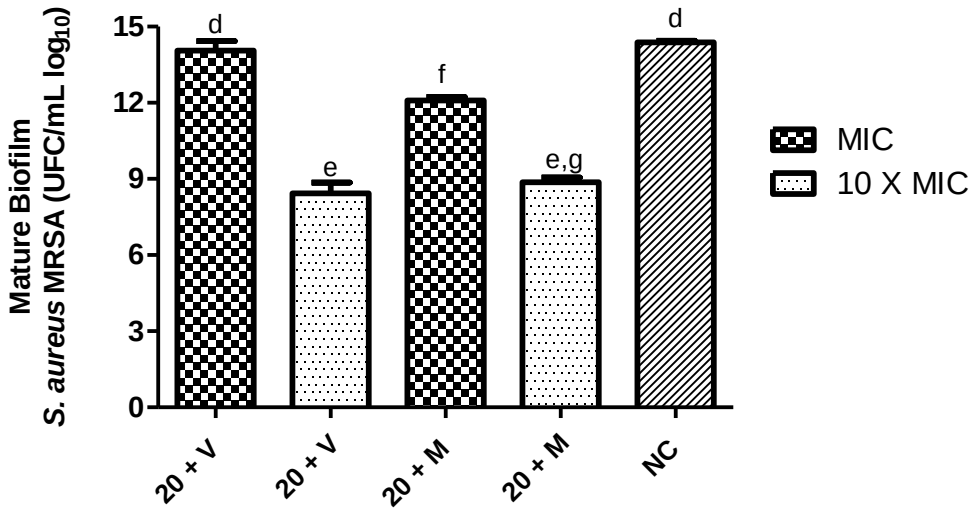

V= vancomycin; M = methicillin; NC = negative control

Figure 11. Effect of hybrid **20** and vancomycin on cell viability of MSSA (A) and MRSA (B) during 12 hours exposure

A

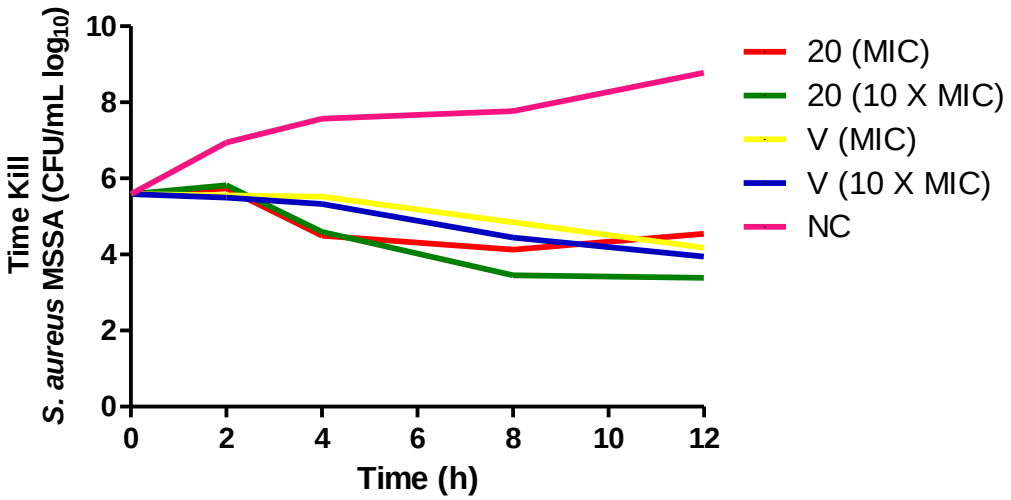

NC = negative control

B

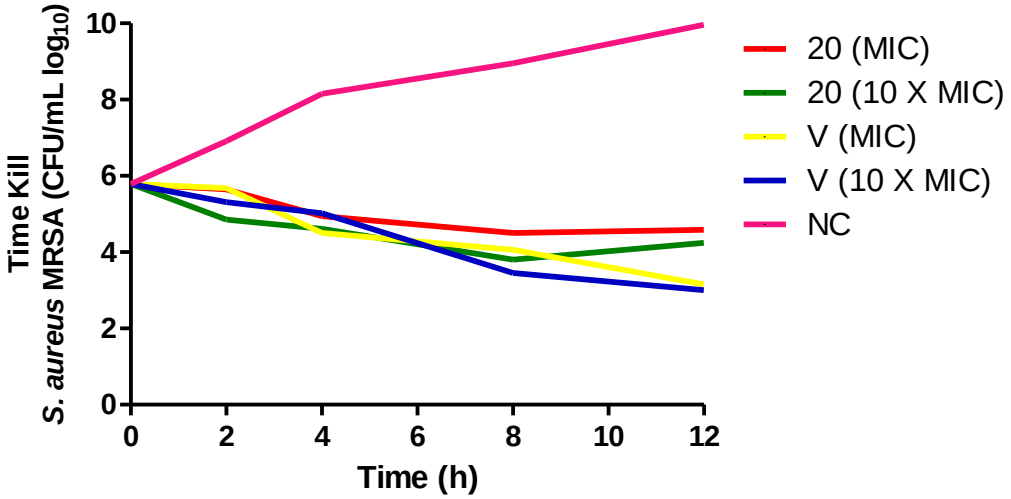

NC = negative control

Figure 12. Percentage of *Galleria mellonella* survival after treatment with hybrid **20** for 72 hours

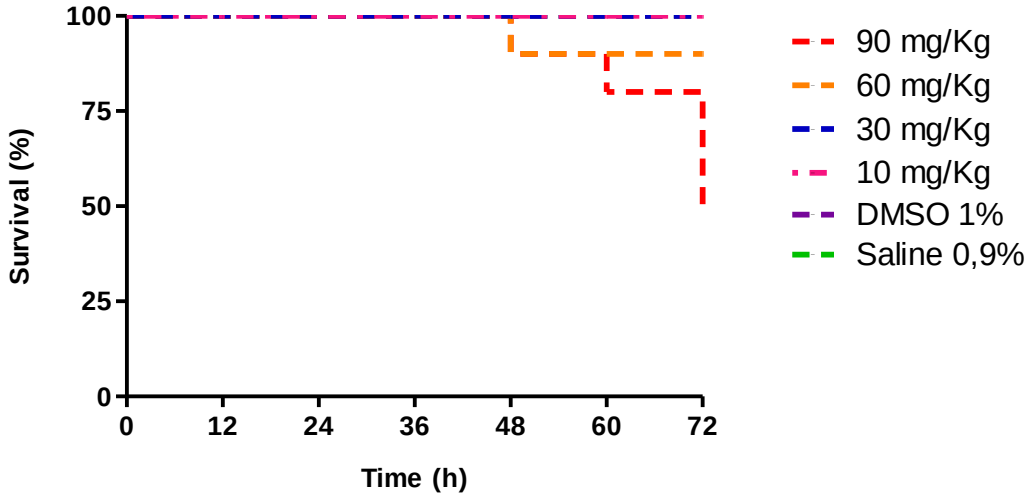

Table 1. Antibacterial activity of hybrids curcumin-cinnamaldehyde against MSSA and MRSA

Entry	Ar	*S. aureus* MSSA MIC/ MBC (μg/mL)	*S. aureus* MRSA MIC/ MBC (μg/mL)	Entry	Ar	*S. aureus* MSSA MIC/ MBC (μg/mL)	*S. aureus* MRSA MIC/ MBC (μg/mL)
Curcumin	-	*/*	*/*	**17**	3-methylphenyl	*/*	31.2/ 62.5
Cinnamaldehyde	-	*/*	*/*	**18**	4-methylphenyl	62.5/ *	31.2/ 62.5
1	phenyl	31.25/ 62.5	31.25/ 62.5	**19**	4-isopropylphenyl	15.6/ 31.2	7.8/ 15.6
2	2-fluorphenyl	15.6/ 31.2	15.6/ 31.2	**20**	4-*terc*-butylphenyl	7.8/ 15.6	3.9/ 7.8
3	3-fluorphenyl	*/*	*/*	**21**	2-methoxyphenyl	*/*	62.5/ *
4	4-fluorphenyl	*/*	*/*	**22**	3-methoxyphenyl	*/*	62.5/ *
5	4-chlorophenyl	*/*	*/*	**23**	4-methoxyphenyl	*/*	*/*
6	4-chlorophenyl	*/*	*/*	**24**	3-hydroxyphenyl	62.5/ > 62.5	31,2/ 62,5
7	3,4-dichlorophenyl	*/*	*/*	**25**	4-hydroxyphenyl	*/*	*/*
8	3-bromophenyl	*/*	*/*	**26**	2-furanyl	*/*	*/*
9	4-bromophenyl	*/*	*/*	**27**	2-thiophenyl	*/*	*/*
10	4-trifluoromethoxylphenyl	15.6/ 31.2	7.8/ 15.6	**28**	3- pyridinyl	*/*	62.5/*
11	4-trifluoromethylphenyl	*/*	*/*	**29**	4- pyridinyl	*/*	*/*
12	4-cyanophenyl	*/*	*/*	**30**	1,4-biphenyl	*/*	*/*
13	3-nitrophenyl	*/*	*/*	**vancomycin**	-	0.5	0.5
14	4-nitrophenyl	*/*	*/*	**meticillin**	-	0.5	2.0
15	4-*N*, *N*-dimethylaminophenyl	*/*	*/*	**gentamycin**	-	-	-
16	2-methylphenyl	31.2/ 62.5	62.5/ *	**isoniazid**	-	-	-

* = MIC and/or MBC ≥ 62.5 μg/mL

Table 2. Minimum Inhibitory Concentration (MIC) of **20** with and without combination with vancomycin (V) MIC and methicillin (M) MIC

Microorganism	**20**	**20 + MIC of V**	**20 + MIC of M**
MSSA	7.8	1.95	1.95
MRSA	3.9	0.97	1.95

MSSA = Methicilin-sensitive *Staphylococcus aureus*; MRSA = Methicilin-*resistant Staphylococcus aureus*; V = vancomycin; M = methicillin

Table 3. Antibacterial activity of hybrids curcumin-cinnamaldehyde against Gram-positive and Gram-negative species

Entry	Ar	*E. faecalis* MIC/ MBC (μg/mL)	*S. epidermidis* MIC/ MBC (μg/mL)	*A. baumannii* MIC/ MBC (μg/mL)	*E. coli* MIC/ MBC (μg/mL)	*P. aeruginosa* MIC/ MBC (μg/mL)	*M. tuberculosis* *MIC* (μg/mL)
Curcumin	-	*/*	*/*	31.25/ 62.5	*/*	*/*	> 25.0
Cinnamaldehyde	-	*/*	*/*	62.5/ *	*/*	*/*	> 100
1	phenyl	*/*	31.25/ 62.5	31.25/ 62.5	*/*	*/*	16.7 ± 1.3
2	2-fluorphenyl	*/*	*/*	15.6/ 31.25	*/*	31.25/ 62.5	3.9 ± 0.8
3	3-fluorphenyl	*/*	*/*	*/*	*/*	*/*	1.4 ± 1.0
4	4-fluorphenyl	*/*	*/*	15.6/ 31.25	*/*	*/*	19.8 ± 0.6
5	4-chlorophenyl	*/*	*/*	7.8/15.6	*/*	*/*	4.2 ± 1.6
6	4-chlorophenyl	*/*	*/*	7.8/ 15.6	*/*	*/*	12.7 ± 0.9
7	3,4-dichlorophenyl	*/*	*/*	31.25/ 62.5	*/*	*/*	9.0 ± 0.3
8	3-bromophenyl	*/*	*/*	7.8/ 15.6	*/*	*/*	0.7 ± 0.3
9	4-bromophenyl	*/*	*/*	*/*	*/*	*/*	> 100
10	4-trifluoromethoxylphenyl	*/*	*/*	3.9/ 7.8	*/*	*/*	3.7 ± 2.0
11	4-trifluoromethylphenyl	*/*	*/*	*/*	*/*	*/*	> 100
12	4-cyanophenyl	*/*	*/*	*/*	*/*	*/*	4.6 ± 2.3
13	3-nitrophenyl	*/*	*/*	*/*	*/*	*/*	2.0 ± 0.7
14	4-nitrophenyl	*/*	*/*	*/*	*/*	*/*	6.6 ± 1.4
15	4-*N*, *N*-dimethylaminophenyl	*/*	*/*	62.5/ *	*/*	*/*	22.4 ± 1.0
16	2-methylphenyl	*/*	*/*	15.6/ 31.25	*/*	*/*	4.9 ± 1.4
17	3-methylphenyl	*/*	*/*	7.8/ 15.6	*/*	*/*	5.8 ± 2.8
18	4-methylphenyl	*/*	*/*	15.6/ 31.25	*/*	*/*	> 100
19	4-isopropylphenyl	15.6/ 31.25	7.8/ 15.6	7.8/ 15.6	*/*	7.8/ 15.6	21.9 ± 0.4
20	4-*terc*-butylphenyl	7.8/ 15.6	7.8/ 15.6	3.9/ 7.8	*/*	3.9/ 7.8	17.0 ± 0.2
21	2-methoxyphenyl	*/*	*/*	31.25/ 62.5	*/*	*/*	4.8 ± 0.9

Continuation of Table 3

22	3-methoxyphenyl	*/*	*/*	15.6/ 31.25	*/*	*/*	5.0 ± 0.9
23	4-methoxyphenyl	*/*	*/*	31.25/ 62.5	*/*	*/*	> 100
24	3-hydroxyphenyl	*/*	*/*	31.25/ 62.5	*/*	*/*	1.6 ± 0.2
25	4-hydroxyphenyl	*/*	*/*	62.5/ *	*/*	*/*	> 100
26	2-furanyl	*/*	*/*	62.5/ *	*/*	*/*	> 100
27	2-thiophenyl	*/*	62,5/ > 62,5	31.25/ 62.5	*/*	*/*	> 100
28	3- pyridinyl	*/*	*/*	15.6/ 31.25	*/*	*/*	10.8 ± 0.8
29	4- pyridinyl	62,5/ *	*/*	15.6/ 31.25	*/*	*/*	2.7 ± 0.4
30	1,4-biphenyl	*/*	*/*	*/*	*/*	*/*	19.7 ± 9.1
vancomycin	-	2/-	2/-	-	-	-	-
meticillin	-	-	-	-	-	-	-
gentamycin	-	-	-	1/-	0.25/-	0.5/-	-
isoniazid	-	-	-	-	-	-	0.04

* = MIC and/or MBC ≥ 62.5 μg/mL

Table 4. *In silico* Drug-likeness Predictions of hybrids curcumin-cinnamaldehyde

Hybrid	Ar	log $P_{o/w}$	MW (Da)	HBD	HBA	Lipinsk's Violations	HBD + HBA	NROBT	Veber's Violations	HIA (%)	BBB
1	phenyl	2.96	254.28	1	3	0	4	4	0	95	0.55
2	2-fluorphenyl	3.01	272.27	1	3	0	4	4	0	95	0.70
3	3-fluorphenyl	3.27	272.27	1	3	0	4	4	0	95	0.65
4	4-fluorphenyl	2.99	272.27	1	3	0	4	4	0	95	0.77
5	3-chlorophenyl	3.92	288.73	1	3	0	4	4	0	96	1.36
6	4-chlorophenyl	3.72	288.73	1	3	0	4	4	0	96	1.51
7	3,4-dichlorophenyl	4.74	323.17	1	3	0	4	4	0	96	3.33
8	3-bromophenyl	4.10	333.18	1	3	0	4	4	0	96	1.54
9	4-bromophenyl	3.89	333.18	1	3	0	4	4	0	96	1.70
10	4-trifluoromethoxylphenyl	4.17	333.28	1	4	0	5	6	0	96	3.67
11	4-trifluoromethylphenyl	3.84	322.28	1	3	0	4	5	0	96	2.02
12	4-cyanophenyl	2.27	279.29	1	6	0	7	4	0	96	0.03
13	3-nitrophenyl	3.02	299.28	1	6	0	7	5	0	90	0.2
14	4-nitrophenyl	2.88	299.28	1	6	0	7	5	0	94	0.01
15	4-*N*, *N*-dimethylaminophenyl	3.26	297.35	1	4	0	5	5	0	96	0.46
16	2-methylphenyl	3.66	268.31	1	3	0	4	4	0	96	1.18
17	3-methylphenyl	3.77	268.31	1	3	0	4	4	0	96	1.16
18	4-methylphenyl	3.57	268.31	1	3	0	4	4	0	96	1.08
19	4-isopropylphenyl	4.57	296.37	1	3	0	4	5	0	96	2.77
20	4-*terc*-butylphenyl	4.97	310.39	1	3	0	4	5	0	96	3.46
21	2-methoxyphenyl	3.14	284.31	1	4	0	5	5	0	96	0.17
22	3-methoxyphenyl	3.23	284.31	1	4	0	5	5	0	96	0.13
23	4-methoxyphenyl	3.06	284.31	1	4	0	5	5	0	96	0.16

Continuation of Table 4

24	3-hydroxyphenyl	2.04	270.28	2	4	0	6	4	0	93	0.54
25	4-hydroxyphenyl	1.70	270.28	2	4	0	6	4	0	93	0.48
26	2-furanyl	2.37	224.24	1	3	0	4	4	0	96	0.05
27	2-thiophenyl	2.85	260.31	1	3	0	4	4	0	96	0.02
28	3- pyridinyl	1.76	255.27	1	4	0	5	4	0	96	0.03
29	4- pyridinyl	0.82	255.27	1	4	0	5	4	0	96	0.02
30	1,4-biphenyl	4.74	330.38	1	3	0	4	5	0	96	1.76

log Po/w = logarithm of compound partition coefficient between n-octanol and water; MW = molecular weight, HBD = number of hydrogen bond donors; HBA = number of hydrogen bond acceptors; NROTB = number of routable bonds, TPSA = topological polar surface area; HIA = percentage of human intestinal absorption; BBB = blood-brain barrier penetration

SUPPLEMENTARY MATERIAL

Antibacterial activity of curcumin-cinnamaldehyde hybrids against MSSA and MRSA planktonic cells and biofilms

Beatriz de C. Marques[a], Mariana B. Santos[a], Isabelle A. T. Kanashiro[a], Mayara A. R. Garcia[a], Gabriela M. Ayusso[a], Josy G. Lazarini[b], Débora L. Campos[c], Fernando R. Pavan[c], Pedro L. Rosalen[b], Janaina C. O. Sardi[b] and Luis O. Regasini[a,]*

[a]Department of Chemistry and Environmental Sciences, Institute of Biosciences, Humanities and Exact Sciences, São Paulo State University (Unesp), São José do Rio Preto 15054-000, SP, Brazil;

[b]Department of Physiological Sciences, Piracicaba Dental School, University of Campinas (Unicamp), Piracicaba 13083-970, SP, Brazil.

[c]Department of Biological Sciences, School of Pharmaceutical Sciences (FCFAR), São Paulo State University (UNESP), Araraquara, SP, Brazil.

*****Address correspondence to this author at the Laboratory of Antibiotics and Chemotherapeutics, IBILCE-Unesp, São José do Rio Preto – 15054-000; Tel.: +55 17 3221-2362. E-mail: luis.regasini@unesp.br.

1. SPECTROSCOPY DATA ANALYSES

Melting points of all compounds were determined on a capillary point apparatus with a digital thermometer. UV-Vis spectrum and purity of compounds were recorded on HPLC-PAD analyses, using MeOH:H_2O (3:1) as mobile phase. Purity of hybrids were measured through band area values, which ranged from 86 to 100%. Melting points ranged from 82 to 195 ºC. UV-Vis spectra indicated values of $\lambda_{max} \sim 350$ nm.

^{1}H NMR and ^{13}C NMR spectra were recorded on a Bruker Avance III 14.1 T (600 MHz), Bruker Avance III 9.4 T (400 MHz) and Bruker Fourier 7.1 T (300 MHz) spectrometers. Compounds were solubilized in deuterated chloroform ($CDCl_3$) or hexadeuterate dimethylsulfoxide (DMSO-d_6). Chemical shifts (δ) and coupling constants (J) were expressed in ppm and Hz, respectively. Multiplicities were reported as singlet (s), doublet (d), doublet of doublet (dd), doublet of doublet of doublets (ddd) and multiplet (m). ^{1}H NMR spectra presented a pair of doublets with J typical of hydrogens linked to carbon-carbon double bonds with *trans* configuration ($J \approx 16$ Hz). ^{13}C NMR spectra exhibited signals of α,β-unsaturated ketones ($\delta \approx 189$ ppm). The simultaneous presence of these signals in the NMR spectra confirmed the formation of enone bridge in the structure of designed compounds.

According to Scifinder [1] database, hybrids **2, 3, 12, 13, 16–18, 20, 21, and 27–29** were identified as new chemical entities.

Caracterization data of hybrids curcumin-cinnamaldehyde

1.1. (*E*)-1-(4-hydroxy-3-methoxyphenyl) -3-phenyl-2-propen-1-one (**1**): **Molecular mass:** 254.28 Da. **Purity:** 92.3%. **Yield:** 68%. **Melting point:** 57–59 °C. **UV-Vis:** λ_{max} 311 nm. **^{1}H NMR (400 MHz; CDCl$_3$):** 7.83 (d; 15.6; H-β), 7.67 (m; H-2, H-3, H-5 and H-6), 7.57 (d; 15.6; H-α), 7.44 (m; H-4, H-2' and H-6'), 7.02 (d; 8.0; H-5'), 6.21 (s; 4'-OH), 4.00 (s; 3'-OCH$_3$). **^{13}C NMR (100 MHz; CDCl$_3$):** 188.6 (C-β'), 150.4 (C-3'), 146.9 (C-4'), 144.0 (C-β), 135.1 (C-1), 131.0 (C-1'), 130.4 (C-4), 128.9 (C-3 and C-5), 128.4 (C-2 and C-6), 123.8 (C-5'), 123.7 (C-6'), 121.7 (C- α), 110.5 (C-2'), 56.1 (3'-OCH3).

1.2. (*E*)-1-(4-hydroxy-3-methoxyphenyl)-3-(2-fluorophenyl)-2-propen-1-one (**2**): **Molecular mass:** 272.27 Da. **Purity:** 92.5%. **Yield:** 67%. **Melting point:** 127–129 °C. **UV-Vis:** λ_{max} 328 nm. **^{1}H NMR (600 MHz; DMSO-*d*$_6$):** 8.11 (dd; 7.9 and 1.4; H-6), 7.94 (d; 15.5; H-β), 7.87 (d; 15.5; H-α), 7.76 (dd,; 8.3 and 2.0; H-6'), 7.71 (dd; 8.0 and 1.0; H-3), 7.59 (d; 2.0; H-2'), 7.47 (dd; 7.5 and 7.5; H-5), 7.37 (ddd; 7.9, 7.9 and 1.6; H-4), 6.92 (d; 8.3; H-5') and 3.85 (s; 3'-OCH$_3$). **^{13}C NMR (150 MHz; CDCl$_3$):** 187.4 (C-β'), 162.9 (d, $J_{C,F}$ = 243.5; C-2), 152.6 (C-3'), 148.3 (C-4'), 141.7 (C-β), 138.0 (C-1'), 131.3 (C-4), 129.8 (C-6), 125.9 (C-5), 124.4 (C-6'), 123.9 (C-1), 117.5 (C-α), 115.5 (C-5), 115.0 (d, $J_{C,F}$ = 21,9; C-3), 112.2 (C-2'), 56.2 (3'-OCH$_3$).

1.3. (*E*)-1-(4-hydroxy-3-methoxyphenyl)-3-(fluorophenyl)-2-propen-1-one (**3**): **Molecular mass:** 272.27 Da. **Purity:** 86.8%. **Yield:** 37%. **Melting point:** 119**–**121 °C. **UV-Vis:** λ_{max} 325 nm. **^{1}H NMR (300 MHz; DMSO-*d*$_6$):** 10.11 (s; 4'-OH), 7.99 (d; 15.5; H-β), 7.88 – 7.85 (m; H-2), 7.82 (dd; 8.3 and 2.0; H-6'), 7.67 (d; 15.5; H-α), 7.66 (d; 6.5; H-6), 7.62 (d; 2.0; H-2'), 7.49 (ddd; 8.4, 6.5 and 3.5; H-5), 7.27 (ddd; 8.4, 8.3 and 2.0; H-4), 6.92 (d; 8.3; H-5') and 3.87 (s; 3'-OCH$_3$). **^{13}C NMR (150 MHz; CDCl$_3$):** 187.4 (C-β'), 162.9 (d, $J_{C,F}$ = 243.5; C-3), 152.6 (C-3'), 148.3 (C-4'), 141.7 (C-β), 138.0 (C-1), 131.3 (d, $J_{C,F}$ = 8.4; C-5), 129.8 (C-1'), 125.9 (C-6'), 124.4 (C-6), 123.9 (C-α), 117.4 (d, $J_{C,F}$ = 21.4; C-4), 115.5 (C-5), 115.0 (d, $J_{C,F}$ = 21.4; C-2), 112.2 (C-2'), 56.2 (3'-OCH$_3$).

1.4. (*E*)-1-(4-hydroxy-3-methoxyphenyl)-3-(fluorophenyl)-2-propen-1-one (**4**): **Molecular mass:** 272.27 Da. **Purity:** 98.1%. **Yield:** 29%. **Melting point:** 143–145 °C. **UV-Vis:** λ_{max} 321 nm. **^{1}H NMR (400 MHz; DMSO-*d*$_6$):** 7.95 (dd; 8.9 and 5,6; H-2 and H-6), 7.88 (d; 15.6; H-β), 7.79 (dd; 8.4; H-6'), 7.68 (d; 15.6; H-α), 7.61 (d; 2.0; H-2'), 7.29 (dd; 8.9 and 8.9; H-3 and H-5), 6.92 (d; 8.4; H-5') and 3.87 (s; 3'-OCH_3). **^{13}C NMR (150 MHz; DMSO-*d*$_6$):** 187.5 (C-β'), 163.7 (d, J_{CF} = 248.5; C-4), 152.4 (C-3'), 148.3 (C-4'), 141.9 (C-β), 132.0 (C-1'), 131.5 (d, $J_{C,F}$ = 8.5; C-2 and C-6), 129.9 (C-1), 124.2 (C-6'), 122.4 (C-α), 116.3 (d, $J_{C,F}$ = 21.6; C-3 and C-5), 115.5 (C-5'), 112. 1 (C-2'), 56.2 (3'-OCH_3).

1.5. (E)-1-(4-hydroxy-3-methoxyphenyl)-3-(3-chlorophenyl)-2-propen-1-one (**5**): **Molecular mass:** 288.73 Da. **Purity:** 100.0%. **Yield:** 32%. **Melting point:** 137–139 °C. **UV-Vis:** λ_{max} 340 nm. **^{1}H NMR (300 MHz; DMSO-*d*$_6$):** 10.11 (s; 4'-OH), 8.05 (d; 7.1; H-6), 8.01 (d; 15.9; H-β), 7.84 (dd; 8.4, and 2.1; H-6'), 7.81 (dd; 4.1 and 1.5; H-2), 7.65 (d; 15.9; H-α), 7.62 (d; 2.1; H-2'), 7.50 – 7.45 (m; H-4 and H-5), 6.91 (d; 8.4; H-5') and 3.87 (s; 3'-OCH_3). **^{13}C NMR (150 MHz; DMSO-*d*$_6$):** 187.3 (C-β'), 152.6 (C-3'), 148.2 (C-4'), 141.4 (C-β), 137.6 (C-1), 134.2 (C-3), 131.1 (C-1'), 130.3 (C-5), 129.7 (C-4), 128.3 (C-2), 128.2 (C-6), 124.4 (C-6'), 124.0 (C-α), 115.4 (C-5'), 112.17 (C-2') and 56.2 (3'-OCH_3).

1.6. (*E*)-1-(4-hydroxy-3-methoxyphenyl)-3-(4-chlorophenyl)-2-propen-1-one (**6**): **Molecular mass:** 288.73 Da. **Purity:** 97.8%. **Yield:** 33%. **Melting point:** 145–147 °C. **UV-Vis:** λ_{max} 315 nm. **^{1}H NMR (400 MHz; CDCl$_3$):** 7.77 (d; 15.6; H-β), 7.67 (d; 1.9; H-2'), 7.67 – 7.64 (m; H-6'), 7.60 (d; 8.5; H-2 and H-6), 7.54 (d; 15.6; H-α), 7.41 (dd; 8.5; H-3 and H-5), 7.02 (d; 8.5; H-5') and 4.01 (s; 3'OCH_3). **^{13}C NMR (150 MHz; DMSO-*d*$_6$):** 187.3 (C-β'), 152.5 (C-3'), 148.2 (C-4'), 141.7 (C-β), 135.2 (C-4), 134.3 (C-1), 130.9 (C-3 and C-5), 129.7 (C-1'), 129.3 (C-2 and C-6), 124.3 (C-6'), 123.2 (C-α), 115.4 (C-5'), 112.0 (C-2') and 56.1 (3'OCH_3).

1.7. (*E*)-1-(4-hydroxy-3-methoxyphenyl)-3-(3,4-dichlorophenyl)-2-propen-1-one (**7**): **Molecular mass:** 323.17 Da. **Purity:** 100.0%. **Yield:** 14%. **Melting point:** 152–154 °C.

UV-Vis: λ_{max} 326 nm. **^{1}H NMR (600 MHz; DMSO-*d*$_6$):** 8.28 (d; 2.0; H-2), 8.04 (d; 15.6; H-β), 7.88 (dd; 8.3 and 2.0; H-6'), 7.85 (dd; 8.4; 2.0; H-6), 7.72 (d; 8.4; H-5), 7.66 (d; 15.6; H-α), 7.62 (d; 2.0; H-2'), 6.92 (d; 8.3; H-5') and 3.88 (s; 3'OCH_3). **^{13}C NMR (150 MHz; DMSO-*d*$_6$):** 187.2 (C-β'), 152.6 (C-3'), 148.3 (C-4'), 140.38 (C-β), 136.30 (C-1), 132.8 (C-3), 132.2 (C-4), 131.4 (C-1), 130.5 (C-5), 129.7 (C-2), 129.4 (C-6), 124.6 (C-6'), 124.5 (C-α), 115.4 (C-5'), 112.1 (C-2') and 56.2 (3'OCH_3).

1.8. (*E*)-1-(4-hydroxy-3-methoxyphenyl)-3-(3-bromophenyl)-2-propen-1-one (**8**): **Molecular mass:** 333.18 Da. **Purity:** 100.0%. **Yield:** 66%. **Melting point:** 94–96 °C [4]. **UV-Vis:** λ_{max} 337 nm. **^{1}H NMR (300 MHz; DMSO-*d*$_6$):** 8.19 (dd; 1.5 and 1.5; H-2), 8.00 (d; 15.5; H-β), 7.85 (d; 7.9; H-4), 7.84 (dd; 8.4 and 2.1; H-6'), 7.64 (d; 15.5; H-α), 7.62 (d; 2.1; H-2'), 7.62 (d; 8.4; H-6), 7.40 (dd; 7.9 and 8.4; H-5), 6.92 (d; 8.4; H-5') and 3.87 (s; 3'-OCH_3). **^{13}C NMR (150 MHz; DMSO-*d*$_6$):** 187.3 (C-β'), 152.6 (C- 3'), 148.3 (C-4'), 141.4 (C-β), 137.9 (C-1), 133.2 (C-1'), 131.3 (C-5), 131.1 (C-4), 129.74 (C-2), 128.5 (C-6), 124.5 (C-6'), 124.0 (C-3), 122.8 (C-α), 115.4 (C-5') and 112.1 (C-2) and 56.2 (3'-OCH_3).

1.9. (*E*)-1-(4-hydroxy-3-methoxyphenyl)-3-(4-bromophenyl)-2-propen-1-one (**9**): **Molecular mass:** 333.18 Da. **Purity:** 98.2%. **Yield:** 6%. **Melting point:** 160–162 °C. **UV-Vis:** λ_{max} 329 nm. **^{1}H NMR (400 MHz; DMSO-*d*$_6$):** 7.95 (d; 15.5; H-β), 7.83 (d; 8.5; H-3 and H-5), 7.79 (dd; 8.4 and 2.0; H-6'), 7.64 (d; 15.5; H-α), 7.65 (d; 8.5; H-2 and H-6), 7.61 (d; 2.0; H-2'), 6.92 (d; 8.4; H-5') and 3.87 (s; 3'OCH_3). **^{13}C NMR (150 MHz; DMSO-*d*$_6$):** 187.3 (C-β'), 152.5 (C-3'), 148.2 (C-4'), 141.8 (C-β), 134.6 (C-1), 132.2 (C-3 and C-5), 131.1 (C-1'), 129.7 (C-2 and C-6), 124.3 (C-6'), 123.2 (C-4), 121.1 (C-α), 115.4 (C-5'), 112.0 (C-2') and 56.1 (3'-OCH_3).

1.10. (*E*)-1-(4-hydroxy-3-methoxyphenyl)-3-(4-trifluoromethoxyphenyl)-2-propen-1-one (**10**): **Molecular mass:** 338.28 Da. **Purity:** 100.0%. **Yield:** 19%. **Melting point:** 123–125 °C. **UV-Vis:** λ_{max} 326 nm. **^{1}H NMR (400 MHz; DMSO-*d*$_6$):** 8.03 (d; 8.6; H-2 and H-6), 7.97 (d; 15.6; H-β), 7.81 (dd; 8.3 and 2.0; H-6'), 7.71 (d; 15.6; H-α), 7.63 (d; 2.0; H-2'), 7.45 (d; 8.6; H-3 and H-5), 6.93 (d; 8.3; H-5') and 3.88 (s; 3'-OCH_3). **^{13}C NMR**

(150 MHz; DMSO-*d*$_6$): 187.3 (C-β'), 152.8 (C-4), 149.8 (C-3'), 148.3 (C-4'), 141.3 (C-β), 134.8 (C-1), 131.1 (C-2,C-6 and 4-OCF_3), 129.7 (C-1'), 124.4 (C-6'), 123.8 (C-α), 121.7 (C-3 and C-5), 120.5 (d, $J_{C,F}$ = 256.8; OCF_3), 115.5 (C-5'), 112.1 (C-2') and 56.2 (3'-OCH_3).

1.11. (*E*)-1-(4-hydroxy-3-methoxyphenyl)-3-(4-trifluoromethylphenyl)-2-propen-1-one (**11**): **Molecular mass:** 322.28 Da. **Purity:** 94.9%. **Yield:** 19%. **Melting point:** 86–88 °C. **UV-Vis:** λ_{max} 341 nm. **^{1}H NMR (400 MHz; DMSO-*d*$_6$):** 8.11 (d; 8.0; H-3 and H-5), 8.07 (d; 15.7; H-β), 7.83 (dd; 8.4 and 2.0; H-6'), 7.81 (d; 8.0; H-2 and H-6), 7.74 (d; 15.7; H-α), 7.64 (d; 2.0; H-2'), 6.93 (d; 8.4; H-5') and 3.89 (s; 3'OCH_3). **^{13}C NMR (150 MHz; DMSO-*d*$_6$):** 187.4 (C-β'), 160.3 (C-3'), 152.1 (C-4'), 148.1 (C-β), 143.6 (C-1), 131.3 (C-2 and C-6), 130.2 (C-1'), 126.5 (C-4), 123.8 (C-6'), 118.9 (C-α), 116.2 (C-3 and C-5), 115.4 (C-5'), 112.0 (C-2'), 56.1 (3'-OCH_3).

1.12. (*E*)-1-(4-hydroxy-3-methoxyphenyl)-3-(4-cyanophenyl)-2-propen-1-one (**12**): **Molecular mass:** 279.29 Da. **Purity:** 87.9%. **Yield:** 14%. **Melting point:** 113–115 °C. **UV-Vis:** λ_{max} 304 nm. **NMR (600 MHz; DMSO-*d*$_6$):** 8.10 (d; 15.6; H-β), 8.10 (d; 8.4; H-2 and H-6), 7.93 (d; 8.4; H-3 and H-5), 7.84 (dd; 8.3 and 2.0; H-6'), 7.73 (d; 15.6; H-α), 7.63 (d; 2.0; H-2'), 6.93 (d; 8.3; H-5') and 3.88 (s; 3'OCH_3). **^{13}C NMR (150 MHz; DMSO-*d*$_6$):** 187.4 (C-β'), 161.6 (C-3'), 152.2 (C-4'), 148.2 (C-β), 143.1 (C-1), 131.1 (C-3 and C-5), 130.1 (C-1'), 127.9 (C-4), 123.9 (C-6'), 119.9 (C-α), 115.4 (C-5'), 114.8 (C-2 and C-6), 112.0 (C-2'), 56.1 (3'-OCH_3).

1.13. (*E*)-1-(4-hydroxy-3-methoxyphenyl)-3-(3-nitrophenyl)-2-propen-1-one (**13**): **Molecular mass:** 299.28 Da. **Purity:** 100.0%. **Yield:** 40%. **Melting point:** 184–186 °C. **UV-Vis:** λ_{max} 343 nm. **^{1}H NMR (600 MHz; DMSO-*d*$_6$):** 8.74 (s; H-2), 8.34 (d; 7.8; H-4), 8.26 (dd; 8.0 and 1.7; H-6), 8.14 (d; 15.6; H-β), 7.88 (dd; 8.3 and 1.9; H-6'), 7.79 (d; 15.6; H-α), 7.74 (dd; 8.0 and 7.8; H-5), 7.63 (d; 1.9; H-2'), 6.92 (d; 8.3; H-5') and 3.87 (s; 3'-OCH_3). **^{13}C NMR (150 MHz; DMSO-*d*$_6$):** 187.2 (C-β'), 153.3 (C-3'), 148.9 (C-4'), 148.4 (C-3), 140.5 (C-β), 137.3 (C-1), 135.4 (C-6), 130.8 (C-1'), 129.3 (C-5), 125.4 (C-6'), 124.8 (C-α), 124.8 (C-2), 123.4 (C-4), 115.5 (C-5'), 112.1 (C-2') and 56.2 (3'-OCH_3).

1.14. (*E*)-1-(4-hydroxy-3-methoxyphenyl)-3-(4-nitrophenyl)-2-propen-1-one (**14**): **Molecular mass:** 299.28 Da. **Purity:** 100.0%. **Yield:** 96%. **Melting point:** 196–198 °C. **UV-Vis:** λ_{max} 315 nm. **^{1}H NMR (600 MHz; DMSO-*d*$_6$):** 8.10 (d; 15.6; H-β), 8.27 (d; 8.7; H-3 and H-5), 8.14 (d; 8.7; H-2 and H-6), 7.83 (dd; 8.4 and 2.0; H-6'), 7.75 (d; 15.6; H-α), 7.62 (d; 2.0; H-2'), 6.93 (d; 8.4; H-5') and 3.88 (s; 3'OCH$_3$). **^{13}C NMR (150 MHz; DMSO-*d*$_6$):** 192.7 (C-β'), 161.7 (C-4), 157.9 (C-3'), 143.3 (C-4'), 133.2 (C-β), 130.9 (C-2 and C-6), 129.8 (C-1), 129.6 (C-1'), 127.6 (C-6'), 125.2 (C-α), 120.9 (C-5'), 114.9 (C-3 and C-5), 112.8 (C-2') and 56.2 (3'-OCH$_3$).

1.15. (*E*)-1-(4-hydroxy-3-methoxyphenyl)-3-(4-*N*,*N*-dimethylaminophenyl)-2-propen-1-one (**15**): **Molecular mass:** 297.35 Da. **Purity:** 99.1%. **Yield:** 96%. **Melting point:** 120–122 °C. **UV-Vis:** λ_{max} 424 nm. **^{1}H NMR (400 MHz; DMSO-*d*$_6$):** 7.70 (d; 9.0; H-2 and H-6), 6.76 (d; 9.0; H-3 and H-5), 7.73 (dd; 8.3 and 2.0; H-6'), 7.63 (s; H-α and H-β), 7.60 (d; 2.0; H-2'), 6.90 (d; 8.3; H-5'), 3.87 (s; 3'OCH$_3$) and 3,01 (s; -N(CH$_3$)$_2$). **^{13}C NMR (150 MHz; DMSO-*d*$_6$):** 187.2 (C-β'), 152.2 (C-3'), 151.8 (C-4'), 148.1 (C-β), 144.3 (C-1), 131.0 (C-2 and C-6), 130.6 (C-1'), 123.6 (C-4), 122.7 (C-6'), 116.6 (C-α), 115.4 (C-5'), 112.2 (C-3 and C-5), 111.9 (C-2'), 56.1 (3'-OCH$_3$).

1.16. (*E*)-1-(4-hydroxy-3-methoxyphenyl)-3-*o*-tolil-2-propen-1-one (**16**): **Molecular mass:** 268.31 Da. **Purity:** 89.9%. **Yield:** 50%. **Melting point:** 117–119 °C. **UV-Vis:** λ_{max} 333 nm. **^{1}H NMR (300 MHz; DMSO-*d*$_6$):** 10.08 (s; 4'-OH), 7.98 (m; H-6), 7.93 (d; 15.4; H-β), 7.80 (d; 15.4; H-α), 7.78 (dd; 8.3 and 2.0; H-6'), 7.62 (d; 2.0; H-2'), 7.36 – 7.20 (m; H-3, H-4 and H-5), 6.91 (d; 8.3; H-5'), 3.87 (s; 3'-OCH$_3$) and 2.43 (s, 2-CH$_3$). **^{13}C NMR (150 MHz; DMSO-*d*$_6$):** 187.6 (C-β'), 152.42 (C-3'), 148.24 (C- 4'), 140.23 (C-β), 138.2 (C-1), 134.0 (C-2), 131.2 (C-1'), 130.5 (C-3), 129.9 (C-4), 127.2 (C-6), 126.8 (C-5), 124.1 (C-6'), 123.5 (C-α), 115.5 (C-5'), 112.1 (C-2'), 56.1 (3'-OCH$_3$) and 19.8 (2-CH$_3$).

1.17. (*E*)-1-(4-hydroxy-3-methoxyphenyl)-3-*m*-tolil-2-propen-1-one (**17**): **Molecular mass:** 268.31 Da. **Purity:** 100.0%. **Yield:** 46%. **Melting point:** 111–113 °C. **UV-Vis:** λ_{max} 329 nm. **^{1}H NMR (300 MHz; DMSO-*d*$_6$):** 10.08 (s; 4'-OH), 7.90 (d; 15.1; H-β), 7.80 (dd; 8.3 and 2.0; H-6'), 7.68 (d; 15.1; H-α), 7.68 – 7.62 (m; H-2 and H-6), 7.61 (d; 2.0;

H-2'), 7.34 (dd; 7.6 and 7.5; H-5), 7.25 (d; 7.5; H-4), 6.91 (d; 8.3; H-5'), 3.87 (s; 3'-OCH_3) and 2.36 (s; 3-CH_3). **^{13}C NMR (150 MHz; DMSO-*d*$_6$):** 187.5 (C-β'), 152.4 (C-3'), 148.2 (C- 4'), 143.3 (C-β), 138.5 (C-1), 135.2 (C-3), 131.51 (C-1'), 129.9 (C-5), 129.5 (C-4), 129.2 (C-2), 126.6 (C-6'), 124.22 (C-6), 122.3 (C-α), 115.4 (C-5'), 112.1 (C-2'), 56.1 (3'-OCH_3) and 21.3 (3-CH_3).

1.18. (*E*)-1-(4-hydroxy-3-methoxyphenyl)-3-*p*-tolil-2-propen-1-one (**18**): **Molecular mass:** 253.27 Da. **Purity:** 93.6%. **Yield:** 24%. **Melting point:** 140–142 °C. **UV-Vis:** λ_{max} 335 nm. **^{1}H NMR (400 MHz; DMSO-*d*$_6$):** 7.86 (d; 15.6; H-β) 7.76 (d; 8.1; H-2 and H-6), 7.27 (d; 8.1; H-3 and H-5), 7.77 (dd; 8.4 and 2.0; H-6'), 7.66 (d; 15.6; H-α), 7.61 (d; 2.0; H-2'), 6.91 (d; 8.4; H-5'), 3.87 (s; 3'OCH_3) and 2.35 (s; 4-CH_3). **^{13}C NMR (150 MHz; DMSO-*d*$_6$):** 187.5 (C-β'), 152.3 (C-3'), 148.2 (C-4'), 143.2 (C-β), 140.8 (C-1), 132.6 (C-1'), 129.9 (C-3 , C-4 and C-5), 129.2 (C-2 and C-6), 124.1 (C-6'), 121.4 (C-α), 115.4 (C-5'), 112.1 (C-2'), 56.2 (3'-OCH_3), 21.5 (4-CH_3).

1.19. (*E*)-1-(4-hydroxy-3-methoxyphenyl)-3-(4-propan-2-ylphenyl)-2-propen-1-one (**19**): **Molecular mass:** 296.36 Da. **Purity:** 92.7%. **Yield:** 15%. **Melting point:** 81–83 °C. **UV-Vis:** λ_{max} 341 nm. **^{1}H NMR (600 MHz; DMSO-*d*$_6$):** 7.88 (d; 15.5; H-β), 7.80 (d; 8.2; H-2 and H-6), 7.79 (dd; 8.0 and 2.2; H-6'), 7.33 (d; 8.2; H-3 and H-5), 7.61 (d; 2.2; H-2'), 7.67 (d; 15.5; H-α), 6.92 (d; 8.0; H-5'), 3.88 (s; 3'OCH_3), 2.94 (m; -CH) and 1.23 (d; -$(CH_3)_2$). **^{13}C NMR (150 MHz; $CDCl_3$):** 187.6 (C-β'), 152.3 (C-3'), 151.6 (C-4'), 148.2 (C-4), 143.3 (C-β), 133.1 (C-1'), 129.9 (C-1), 129.4 (C-2 and C-6), 127.3 (C-3 and C-5), 124.1 (C-6'), 121.5 (C-α), 115.4 (C-5'), 112.0 (C-2'), 56.1 (3'-OCH_3), 33.8 (4-$C(CH_3)_2$), 24.1 ($(CH_3)_2$).

1.20. (*E*)-1-(4-hydroxy-3-methoxyphenyl)-3-(4-*terc*-butyl)-2-propen-1-one (**20**): **Molecular mass:** 310.39 Da. **Purity:** 99.3%. **Yield:** 29%. **Melting point:** 90–92 °C. **UV-Vis:** λ_{max} 342 nm. **^{1}H NMR (600 MHz; DMSO-*d*$_6$):** 7.87 (d; 15.5; H-β), 7.80 (d; 8.4; H-2 and H-6), 7.80 – 7.77 (m; H-6'), 7.67 (d; 15.5; H-α), 7.61 (d; 2.0; H-2'), 7.47 (d; 8.2; H-3 and H-5), 6.92 (d; 8,3; H-5'), 3.87 (s; 3'OCH_3) and 1.31 (s; -$(CH_3)_3$). **^{13}C NMR (100 MHz; $CDCl_3$):** 187.6 (C-β'), 153.7 (C-3'), 152.3 (C-4'), 148.2 (C-4), 143.1 (C-β), 132.7

(C-1'), 129.9 (C-1), 129.1 (C-2 and C-6), 126.2 (C-3 and C-5), 124.1 (C-6'), 121.7 (C-α), 115.4 (C-5'), 112.0 (C-2'), 56.1 (3'-OCH_3), 35.1 (4-$C(CH_3)_3$), 31.4 ($(CH_3)_3$).

1.21. (*E*)-1-(4-hydroxy-3-methoxyphenyl)-3-(2-methoxyphenyl)-2-propen-1-one (**21**): **Molecular mass:** 284.31 Da. **Purity:** 100.0%. **Yield:** 39%. **Melting point:** 119–121 °C. **UV-Vis:** λ_{max} 359 nm. **^{1}H NMR (300 MHz; DMSO-*d*$_6$):** 10.06 (s; 4'-OH), 8.01 (d; 15.7; H-β), 7.96 (m; H-6), 7.86 (d; 15.7; H-α), 7.75 (dd; 8.3 and 2.0; H-6'), 7.60 (d; 2.0; H-2'), 7.43 (ddd; 8.0, 7.7 and 1.6; H-4), 7.10 (d; 8.0; H-3), 7.02 (dd; 7.7 and 7.5; H-5), 6.91 (d; 8.3; H-5'), 3.89 (s; 2-OCH_3) and 3.87 (s; 3'-OCH_3). **^{13}C NMR (150 MHz; DMSO-*d*$_6$):** 187.6 (C-β'), 158.6 (C-1), 152.3 (C- 3'), 148.2 (C-4'), 137.6 (C-β), 132.4 (C-1'), 130.0 (C-4), 128.7 (C-6), 124.0 (C-5'), 123.6 (C-α), 122.3 (C-5), 121.1 (C-5'), 115.4 (C-2'), 112.2 (C-1), 112.0 (C-2), 56.1 (2-OCH_3) and 56.1 (3'-OCH_3).

1.22. (*E*)-1-(4-hydroxy-3-methoxyphenyl)-3-(3-methoxyphenyl)-2-propen-1-one (**22**): **Molecular mass:** 284.31 Da. **Purity:** 100.0%. **Yield:** 40%. **Melting point:** 109°C. **UV-Vis:** λ_{max} 329 nm. **^{1}H NMR (300 MHz; DMSO-*d*$_6$):** 10.08 (s; 4'-OH), 7.93 (d; 15.6; H-β), 7.81 (dd; 8.3 and 2.0; H-6'), 7.65 (d; 15.6; H-α), 7.61 (d; 2.0; H-2'), 7.46 – 7.42 (m; H-2 and H-6), 7.36 (dd; 8.0 and 7.8; H-5), 7.01 (ddd; 8.0, 2.4 and 1.0; H-4), 6.91 (d; 8.3; H-5'), 3.87 (s; 3'-OCH_3) and 3.82 (s; 3-OCH_3). **^{13}C NMR (150 MHz; DMSO-*d*$_6$):** 187.5 (C-β'), 160.11 (C-3), 152.45 (C- 3'), 148.2 (C-4'), 140.1 (C-β), 136.7 (C-1), 130.3 (C-1'), 129.9 (C-5), 124.3 (C-6'), 122.8 (C-α), 121.9 (C-6), 116.7 (C-6'), 115.4 (C-2'), 113.9 (C-4), 112.1 (C-2), 56.1 (3'-OCH_3) and 55.7 (3-OCH_3).

1.23. (*E*)-1-(4-hydroxy-3-methoxyphenyl)-3-(4-methoxyphenyl)-2-propen-1-one (**23**): **Molecular mass:** 284.31 Da. **Purity:** 100.0%. **Yield:** 23%. **Melting point:** 121–123°C. **UV-Vis:** λ_{max} 350 nm. **^{1}H NMR (400 MHz; DMSO-*d*$_6$):** 7.84 (d; 8.8; H-2 and H-6), 7.79 (d; 15.5; H-β), 7.77 (dd; 8.3 and 2.0; H-6'), 7.67 (d; 15.5; H-α), 7.62 (d; 2.0; H-2'), 7.02 (d; 8.8; H-3 and H-5), 6.92 (d; 8.3; H-5'), 3.88 (s; 4-OCH_3) and 3.82 (s; 3'OCH_3). **^{13}C NMR (150 MHz; $CDCl_3$):** 187.5 (C-β'), 161.6 (C-3'), 152.2 (C-4'), 148.2 (C-4), 143.1 (C-β), 131.1 (C-2 and C-6), 130.2 (C-1'), 128.0 (C-1), 123.9 (C-6'), 120.0 (C-α), 115.4 (C-5'), 114.8 (C-3 and C-5), 112.1 (C-2'), 56.2 (3'-OCH_3), 55.8 (4-OCH_3).

1.24. (*E*)-1-(4-hydroxy-3-methoxyphenyl)-3-(3-hydroxyphenyl)-2-propen-1-one (**24**): **Molecular mass:** 270.28 Da. **Purity:** 100.0%. **Yield:** 18%. **Melting point:** 74–76 °C. **UV-Vis:** λ_{max} 334 nm. **^{1}H NMR (600 MHz; DMSO-*d*$_6$):** 7.83 (d; 15.5; H-β), 7.78 (dd; 8.3 and 2.0; H-6'), 7.61 (d; 2.0; H-2'), 7.59 (d; 15.5; H-α), 7.30 (d; 7.7; H-6), 7.25 (dd; 7.8 and 7.8; H-5), 7.22 (dd; 1.8 and 1.8; H-2), 6.92 (d; 8.3; H-5'), 6.87 (ddd; 7.9, 2.5 and 0.9; H-4) and 3.88 (s; 3'OCH$_3$). **^{13}C NMR (150 MHz; CDCl$_3$):** 187.6 (C-β'), 158.2 (C-3), 152.4 (C-3'), 148.2 (C-4'), 143.4 (C-β), 136.6 (C-1), 130.3 (C-1'), 129.9 (C-5), 124.1 (C-6'), 122.4 (C-α), 120.2 (C-6), 117.9 (C-5'), 115.6 (C-2'), 115.5 (C-4), 112.1 (C-2), 56.2 (3'-OCH$_3$).

1.25. (*E*)-1-(4-hydroxy-3-methoxyphenyl)-3-(4-hydroxyphenyl)-2-propen-1-one (**25**): **Molecular mass:** 270.28 Da. **Purity:** 100.0%. **Yield:** 8%. **Melting point:** 194–196 °C. **UV-Vis:** λ_{max} 354 nm. **^{1}H NMR (600 MHz; DMSO-*d*$_6$):** 10.00 (sl; 4'-OH),7.75 (dd; 8.3 and 2.0; H-6'), 7.73 (d; 8.6; H-2 and H-6), 7.72 (d; 15.4;H-β), 7.63 (d; 15.4; H-α), 7.61 (d; 2.0; H-2'), 6.91 (d; 8.3; H-5'), 6.84 (d; 8.2; H-3 and H-5) and 3.87 (s; 3'OCH$_3$). **^{13}C NMR (150 MHz; CDCl$_3$):** 187.4 (C-β'), 160.3 (C-3'), 152.1 (C-4'), 148.2 (C-4), 143.6 (C-β), 131.3 (C-2 and C-6), 130.2 (C-1'), 126.5 (C-1), 123.8 (C-6'), 118.9 (C-α), 116.2 (C-3 and C-5), 115.4 (C-5'), 112.0 (C-2'), 56.1 (3'-OCH$_3$).

1.26. (*E*)-1-(4-hydroxy-3-methoxyphenyl)-3-(2-furanyl)-2-propen-1-one (**26**): **Molecular mass:** 244.24 Da. **Purity:** 100.0%. **Yield:** 10%. **Melting point:** 87–89 °C. **UV-Vis:** λ_{max} 326 nm. **^{1}H NMR (400 MHz; DMSO-*d*$_6$):** 7.88 (d; 1.6; H-2'), 7.70 (dd; 8.4 and 1.6; H-6'), 7.67 (dd; 8.3 and 2.1; H-5), 7.56 (d; 15,4; H-β), 7.55 (d; 2.0; H-2), 7.51 (d; 15.4; H-α), 7.06 (dd; 3.4 and 0.5; H-3), 6.67 (dd; 1.8; H-4), 6.91 (d; 8.4; H-5') and 3.86 (s; 3'OCH$_3$). **^{13}C NMR (100 MHz; CDCl$_3$):** 186.9 (C-β'), 152.5 (C-3'), 151.8 (C-1), 148.3 (C-4'), 146.3 (C-4), 129.8 (C-β), 129.7 (C-1'), 123.9 (C-α), 119.2 (C-6'), 116.8 (C-5'), 115.5 (C-2'), 113.5 (C-3), 111.8 (C-2), 56.0 (3'-OCH$_3$).

1.27. (*E*)-1-(4-hydroxy-3-methoxyphenyl)-3-(2-thiophenyl)-2-propen-1-one (**27**): **Molecular mass:** 260.31 Da. **Purity:** 100.0%. **Yield:** 8%. **Melting point:** 93–95 °C. **UV-Vis:** λ_{max} 353 nm. **^{1}H NMR (400 MHz; DMSO-*d*$_6$):** 7.85 (d; 15.3; H-β), 7.74 (dd; 4.2

and 0.8; H-3), 7.70 (dd; 8.4 and 2.0; H-6'), 7.65 (d; 3.5; H-5), 7.56 (d; 2.0; H-2'), 7.56 (d; 15.3; H-α), 7.18 (dd; 5.0 and 3.6; H-4), 6.91 (d; 8.4; H-5') and 3.86 (s; 3'OCH_3). **^{13}C NMR (150 MHz; $CDCl_3$):** 186.9 (C-β'), 152.7 (C-3'), 148.4 (C-1), 140.4 (C-4'), 135.9 (C-4), 132.8 (C-β), 130.4 (C-1'), 129.6 (C-α), 129.1 (C-6'), 124.1 (C-5'), 120.9 (C-2'), 115.5 (C-3), 111.8 (C-2), 56.1 (3'-OCH_3).

1.28. (*E*)-1-(4-hydroxy-3-methoxyphenyl)-3-(3-pyridinyl)-2-propen-1-one (**28**): **Molecular mass:** 255.27 Da. **Purity:** 100.0%. **Yield:** 12%. **Melting point:** 171–173 °C. **UV-Vis:** λ_{max} 311 nm. **^{1}H NMR (400 MHz; DMSO-d_6):** 8.67 (dd; 4.7 and 1.3; H-2), 8.14 (d; 15.3;H-β), 7.89 (dd; 4.7 and 1.3; H-4 and H-6), 7.72 (dd; 8.4 and 2.0; H-6'), 7.66 (d; 15.4; H-α), 7.58 (d; 2.0; H-2'), 7.43 (dd; 8.9 and 4.7; H-5), 6.93 (d; 8.4; H-5') and 3.87 (s; 3'OCH_3). **^{13}C NMR (150 MHz; $CDCl_3$):** 187.6 (C-β'), 153.5 (C-3'), 152.9 (C-4'), 150.5 (C-2), 148.4 (C-4), 142.3 (C-β), 137.6 (C-6), 129.5 (C-6'), 125.6 (C-1), 125.2 (C-1'), 125.1 (C-α), 124.4 (C-5), 115.6 (C-5'), 111.8 (C-2'), 56.1 (3'-OCH_3).

1.29. (*E*)-1-(4-hydroxy-3-methoxyphenyl)-3-(4-pyridinyl)-2-propen-1-one (**29**): **Molecular mass:** 255.27 Da. **Purity:** 100.0%. **Yield:** 42%. **Melting point:** 151–153 °C. **UV-Vis:** λ_{max} 353 nm. **^{1}H NMR (300 MHz; DMSO-d_6):** 8.95 (d; 6.5; H-2 and H-6), 8.45 (d; 6.5; H-3 and H-5), 8.41 (d; 15.6; H-β), 7.89 (dd; 8.4 and 2.0; H-6'), 7.77 (d; 15.6; H-α), 7.63 (d; 2.0; H-2'), 6.98 (d; 8.4; H-5') and 3.87 (s; 3'-OCH_3). **^{13}C NMR (150 MHz; DMSO-d_6):** 186.9 (C-β'), 153.4 (C-3'), 150.6 (C-4'), 148.5 (C-β), 143.6 (C-3 and C-5), 137.6 (C-1), 131.7 (C-1'), 129.1 (C-α), 125.6 (C-2 and C-6), 125.1 (C-6'), 115.6 (C-5'), 112.2 (C-2'), 56.3 (3'-OCH_3).

1.30. (*E*)-1-(4-hydroxy-3-methoxyphenyl)-3-(1,1-biphenyl-4-il)-2-propen-1-one (**30**): **Molecular mass:** 330.38 Da. **Purity:** 94.9%. **Yield:** 6%. **Melting point:** 191–193 °C. **UV-Vis:** λ_{max} 352 nm. **^{1}H NMR (600 MHz; DMSO-d_6):** 8.00 (d; 15.3;H-β), 7.99 (d; 8.5; H-3 and H-5), 7.83 (dd; 8.3 and 2.0; H-6'), 7.78 (d; 8.5; H-2 and H-6), 7.76 (dd; 8.0 and 1.2; H-2'' and H-6''), 7.75 (d; 15.3; H-α), 7.65 (d; 2.0; H-2'), 7.51 (dd; 8.0 and 8.0; H-3 and H-5), 7.43 – 7.40 (m; H-4''), 6.93 (d; 8.3; H-5') and 3.89 (s; 3'OCH_3). **^{13}C NMR (150 MHz; DMSO-d_6):** 187.5 (C-β'), 152.4 (C-3'), 148.3 (C-4'), 142.7 (C-β), 142.3 (C-

1), 139.8 (C-1'), 134.5 (C-6'), 130.0 (C-4), 129.9 (C-3''' and C-5'''), 129.5 (C-2''' and C-6'''), 128.4 (C-5''), 127.5 (C-3 and C-5), 127.2 (C-2 and C-6), 124.2 (C-6'), 122.5 (C-α), 115.5 (C-5'), 112.1 (C-2') and 56.2 (3'-OCH_3).

REFERENCES

[1] SciFinder. Available in: < https://scifinder.cas.org/> Access in: 10 mai 2019.

Figure S1. i) ^{1}H NMR spectrum of **hybrid 1** (400 MHz; $CDCl_3$)

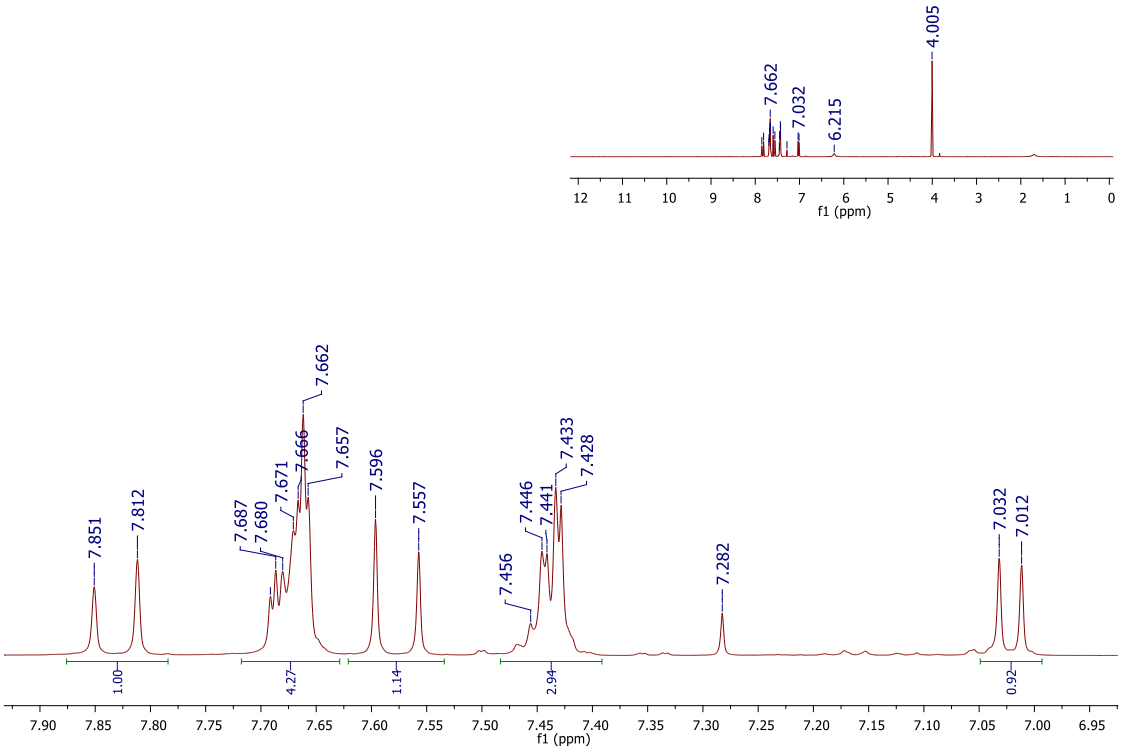

Figure S1. ii) ^{13}C NMR spectrum of **hybrid 1** (100 MHz; $CDCl_3$)

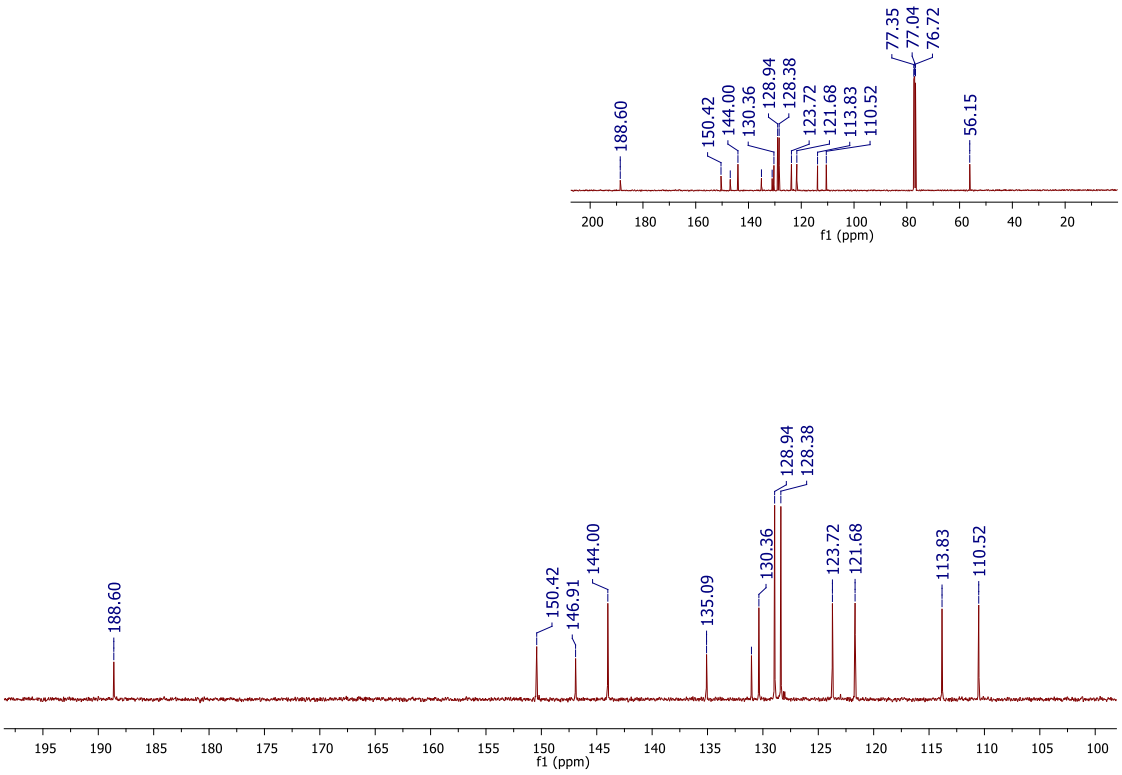

Figure S1. iii) UV-Vis spectrum of **hybrid 1** (MeOH/H_2O (3:1))

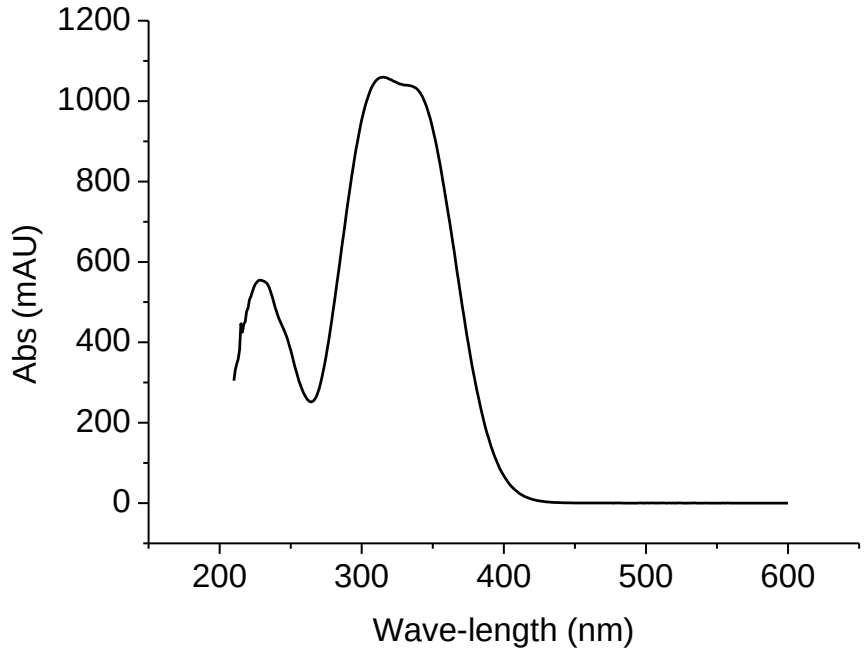

Figure S1. iv) HPLC chromatogram of **hybrid 1** (MeOH/H_2O (3:1))

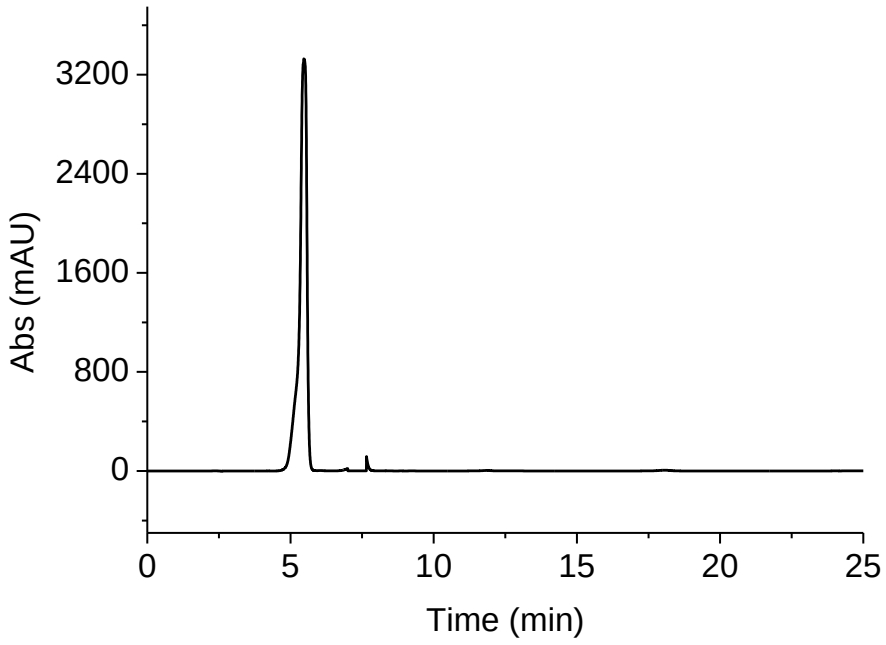

Figure S2. i) ^{1}H NMR spectrum of **hybrid 2** (600 MHz; DMSO-d_6)

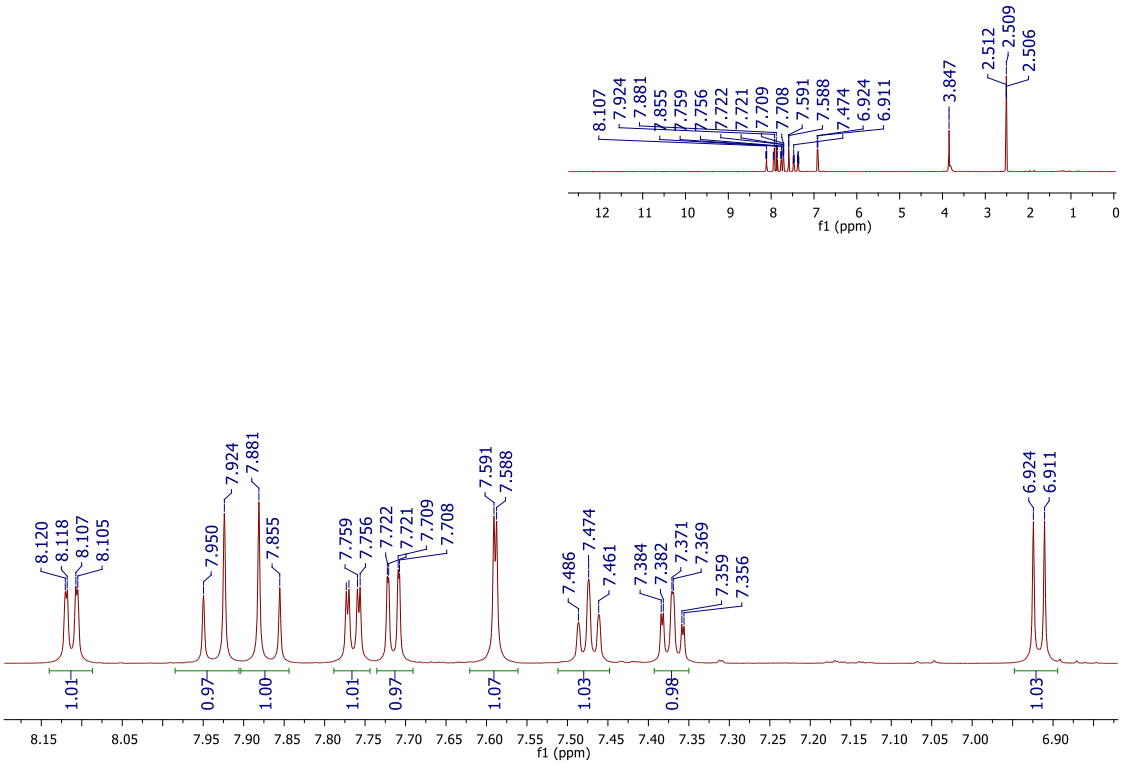

Figure S2. ii) ^{13}C NMR spectrum of **hybrid 2** (150 MHz; DMSO-d_6)

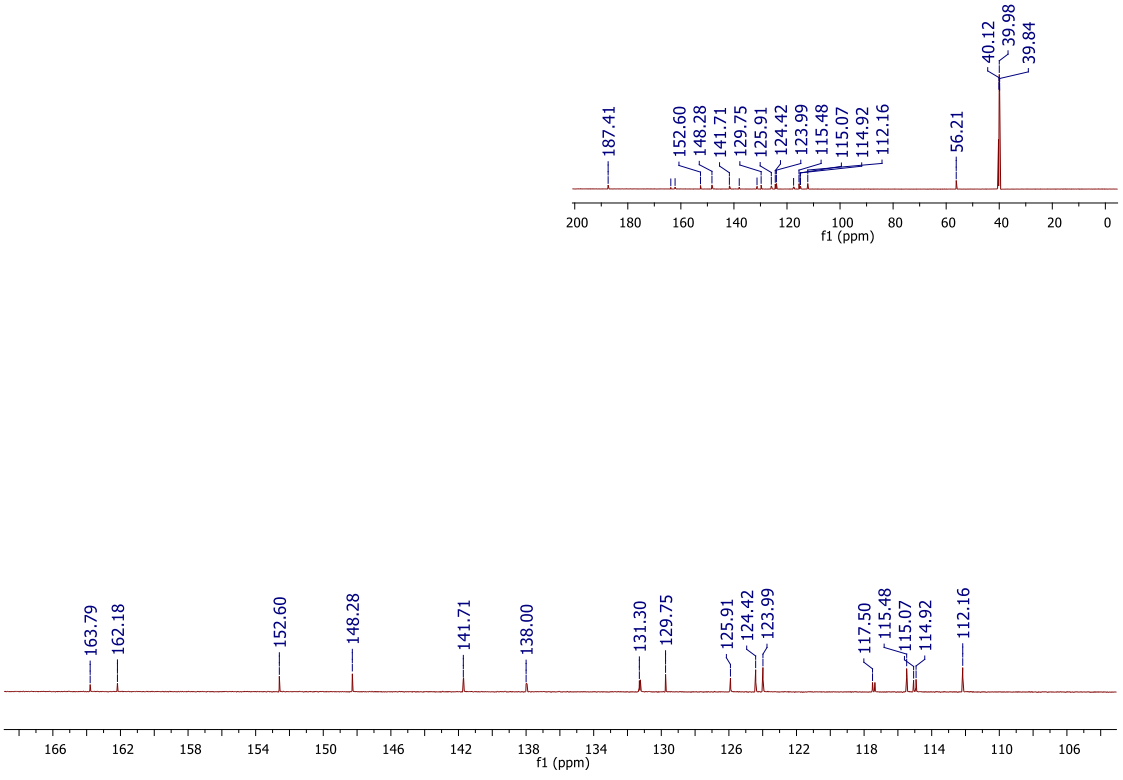

Figure S2. iii) UV-Vis spectrum of **hybrid 2** (MeOH/H_2O (3:1))

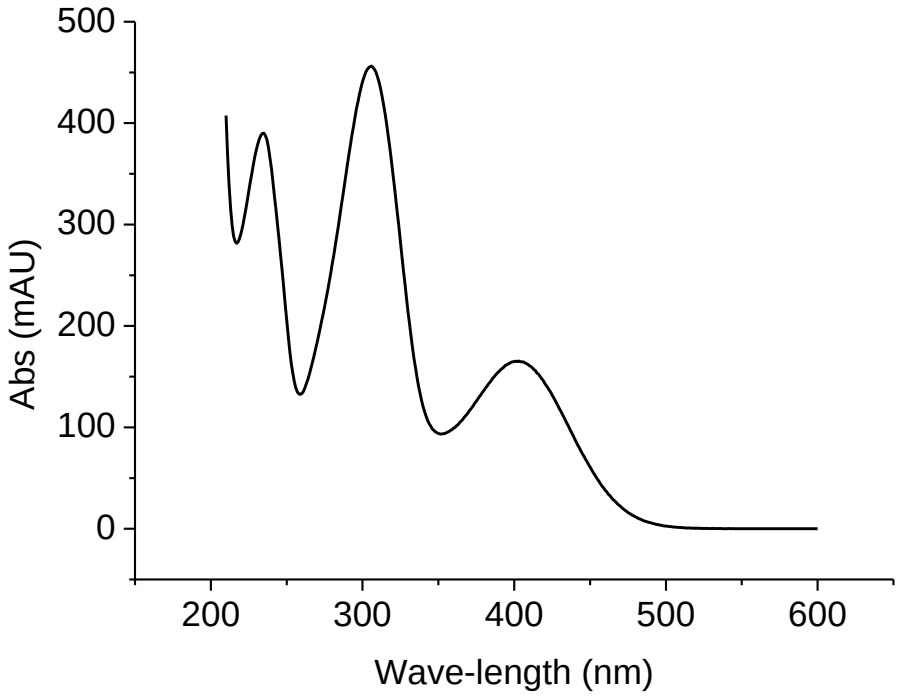

Figure S2. iv) HPLC chromatogram of **hybrid 2** (MeOH/H_2O (3:1))

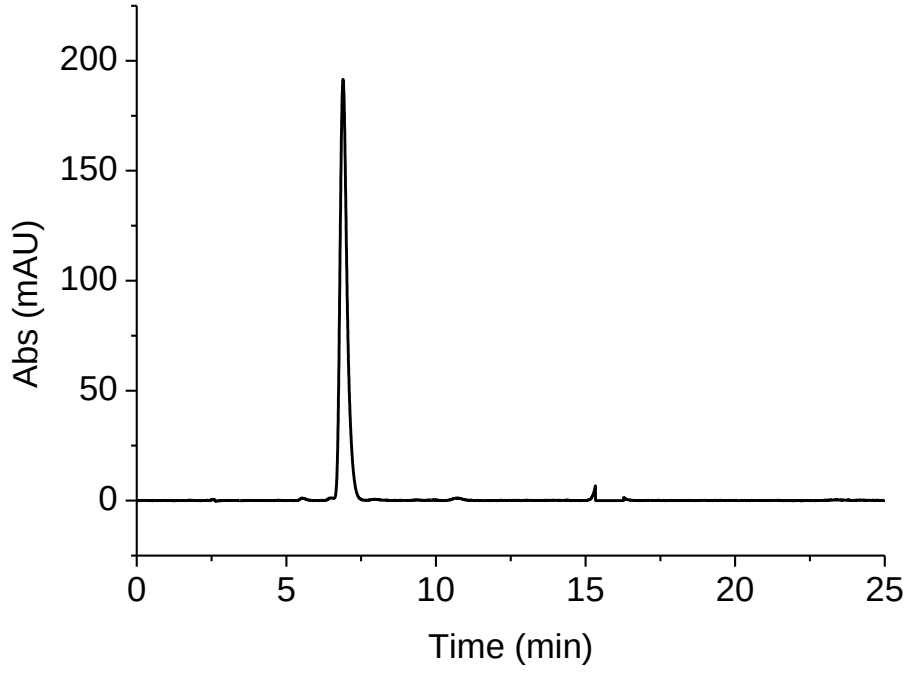

Figure S3. i) ^{1}H NMR spectrum of **hybrid 3** (300 MHz; DMSO-d_6)

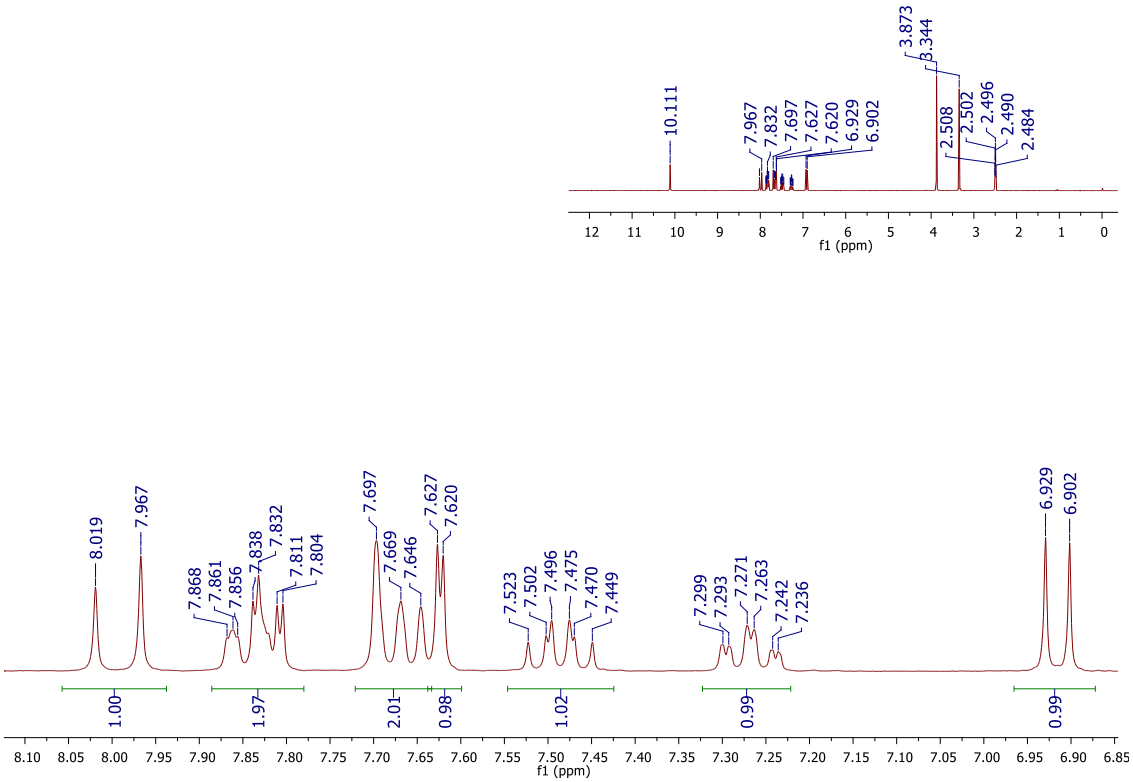

Figure S3. ii) ^{13}C NMR spectrum of **hybrid 3** (150 MHz; DMSO-d_6)

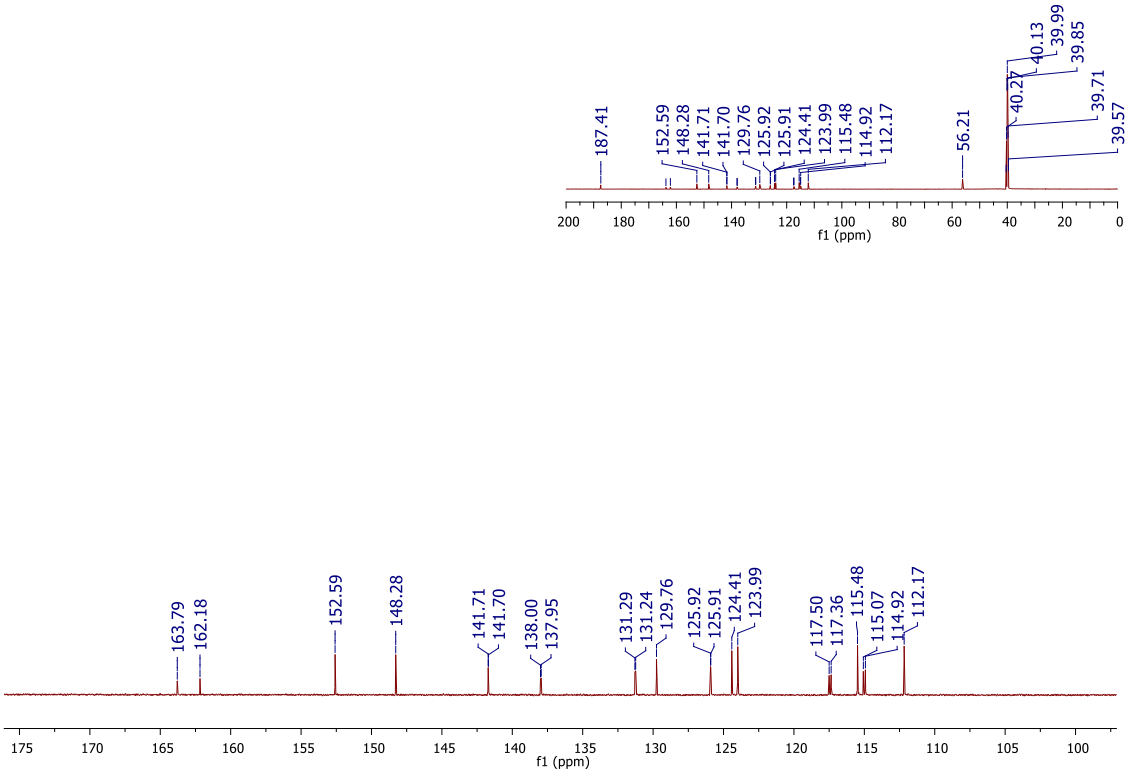

Figure S3. iii) UV-Vis spectrum of **hybrid 3** (MeOH/H_2O (3:1))

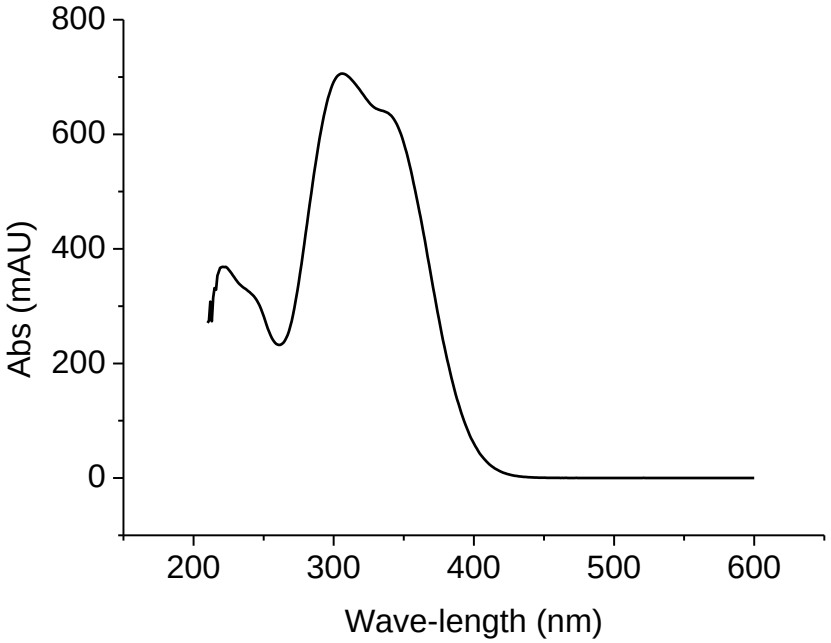

Figure S3. iv) HPLC chromatogram of **hybrid 3** (MeOH/H_2O (3:1))

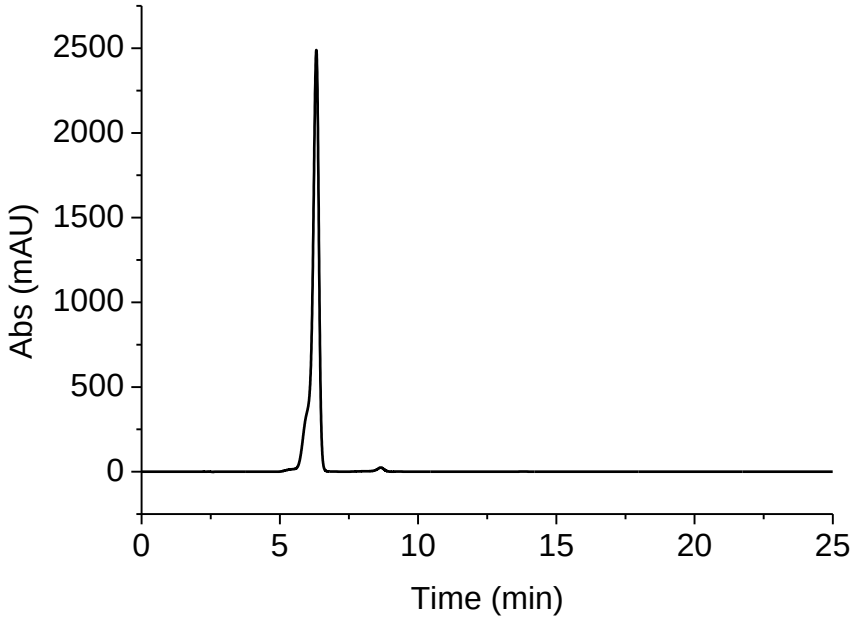

Figure S4. i) ^{1}H NMR spectrum of **hybrid 4** (400 MHz; DMSO-d_6)

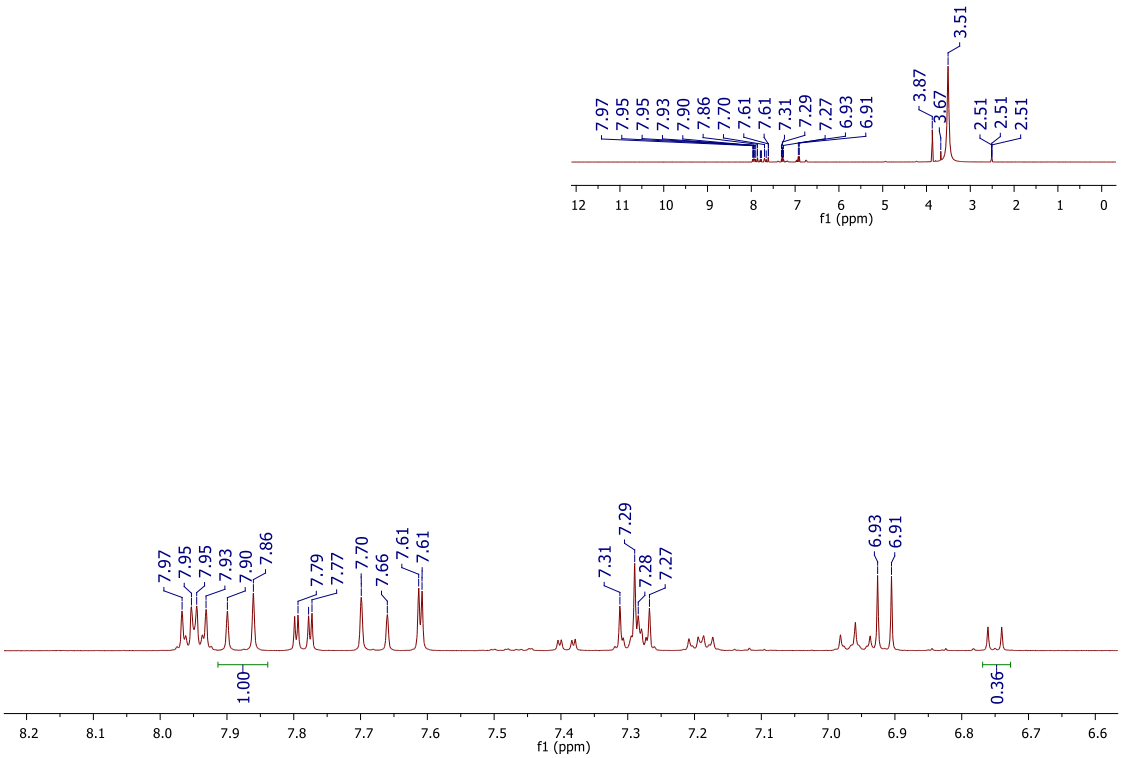

Figure S4. ii) ^{13}C NMR spectrum of **hybrid 4** (150 MHz; DMSO-d_6)

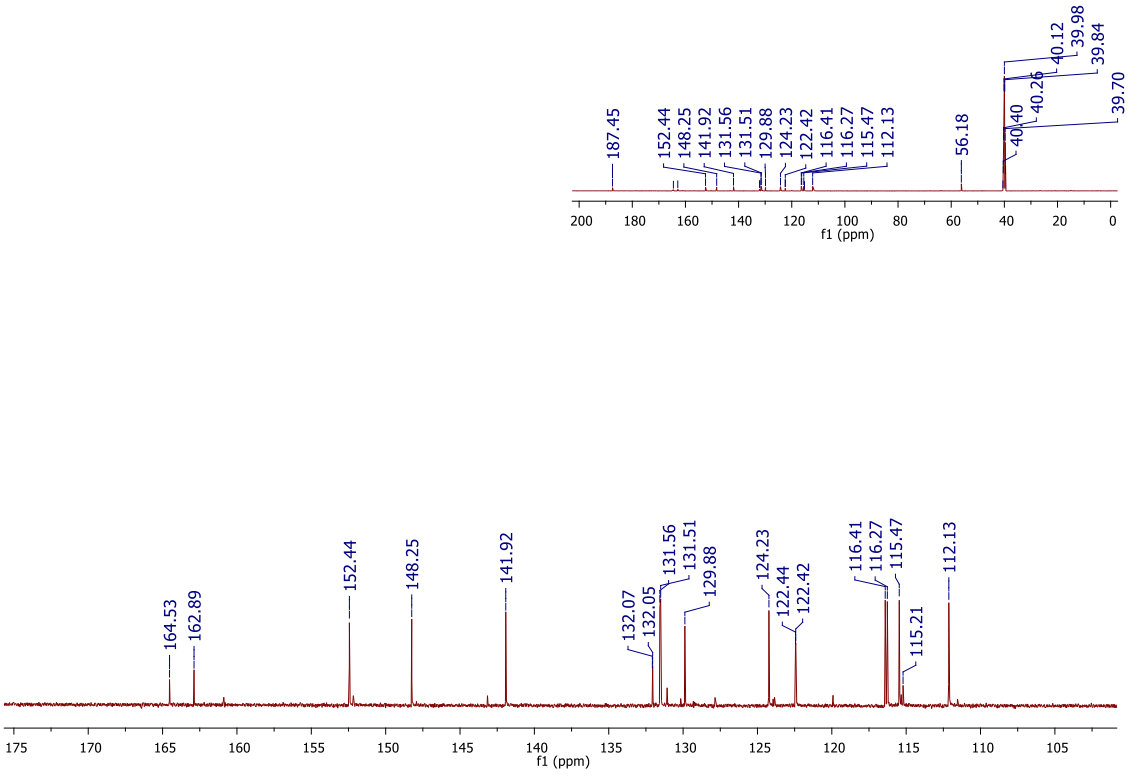

Figure S4. iii) UV-Vis spectrum of **hybrid 4** (MeOH/H_2O (3:1))

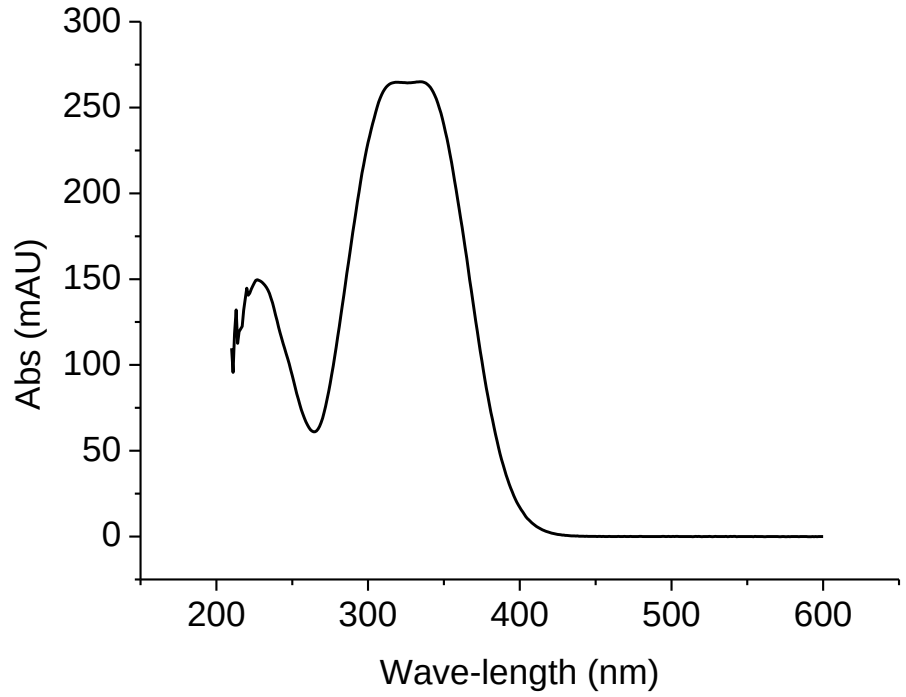

Figure S4. iv) HPLC chromatogram of **hybrid 4** (MeOH/H_2O (3:1))

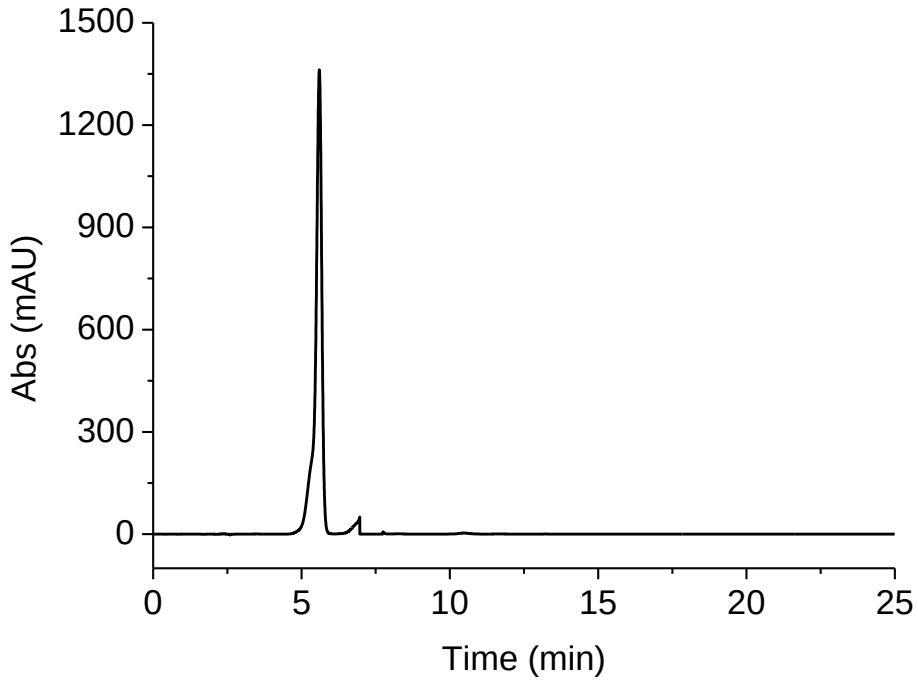

Figure S5. i) ^{1}H NMR spectrum of **hybrid 5** (300 MHz; DMSO-d_6)

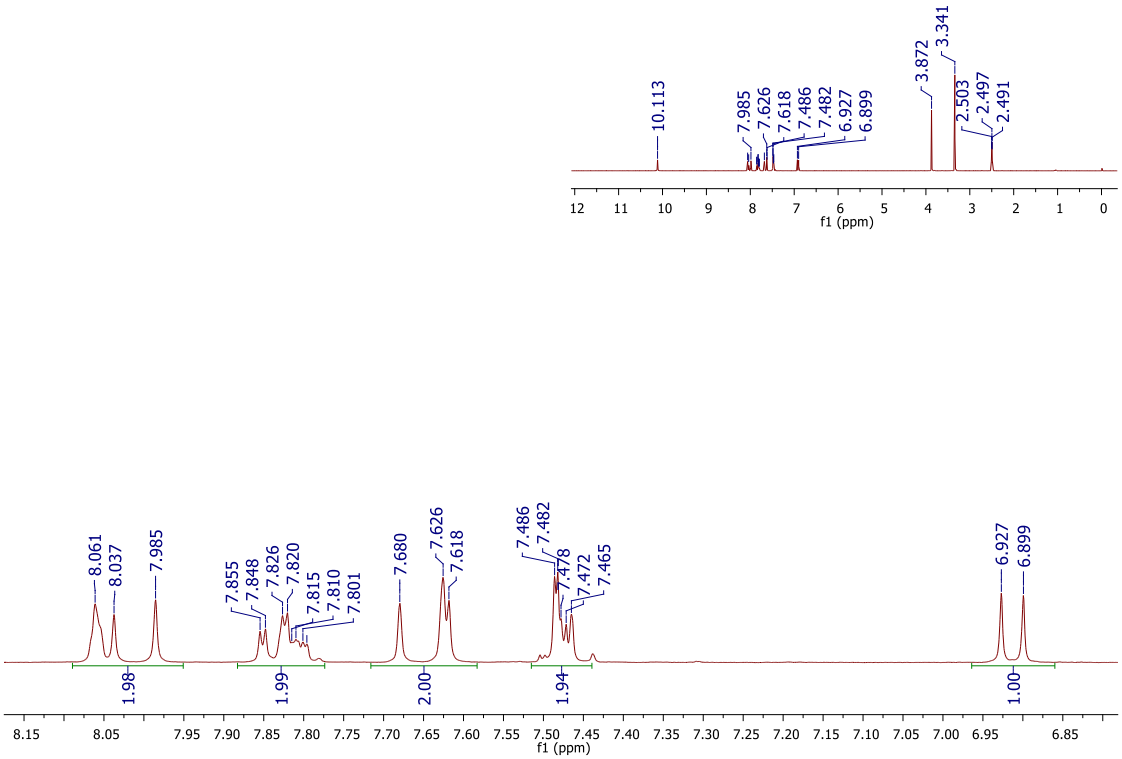

Figure S5. ii) ^{13}C NMR spectrum of **hybrid 5** (150 MHz; DMSO-d_6)

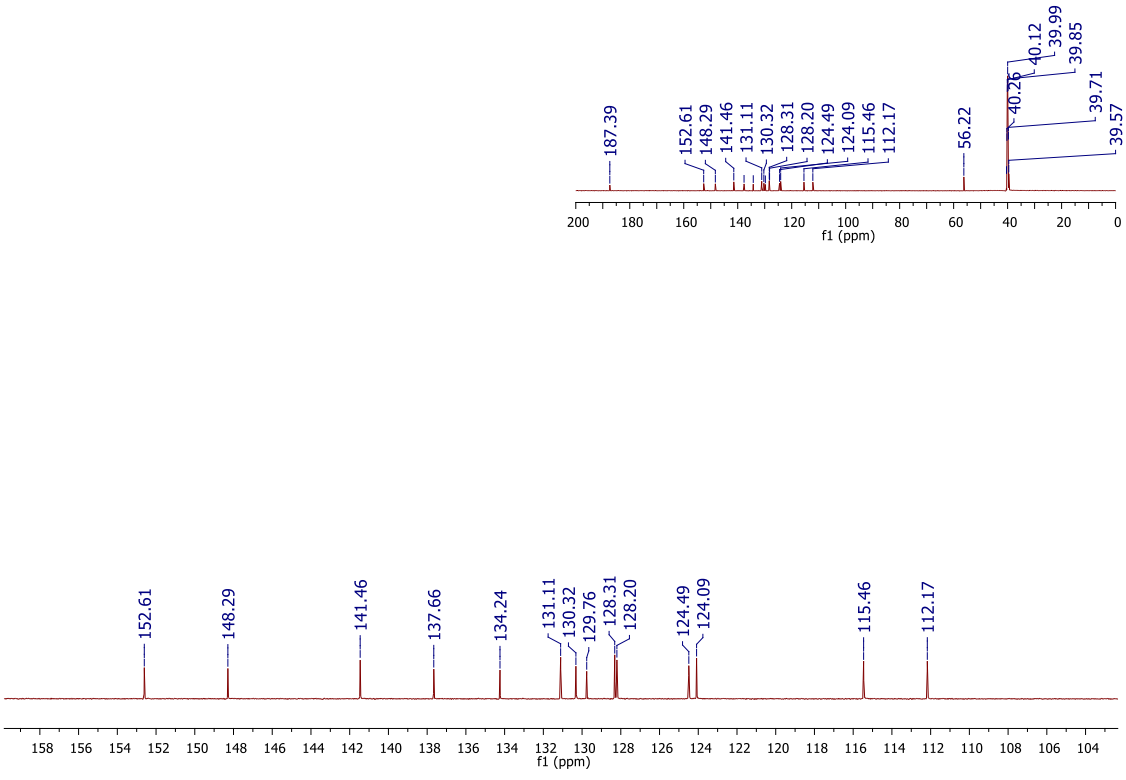

Figure S5. iii) UV-Vis spectrum of **hybrid 5** (MeOH/H_2O (3:1))

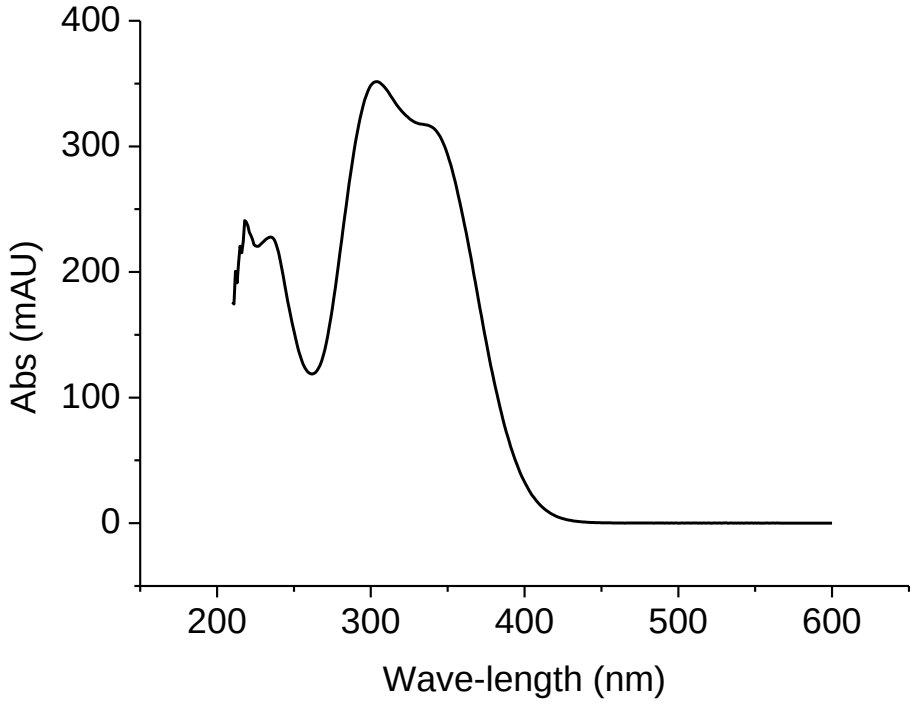

Figure S5. iv) HPLC chromatogram of **hybrid 5** (MeOH/H_2O (3:1))

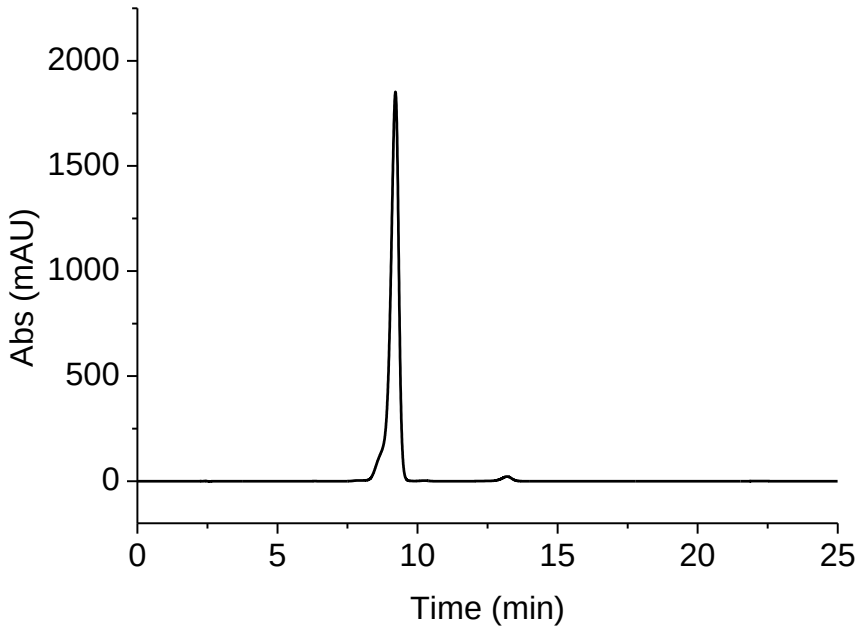

Figure S6. i) ^{1}H NMR spectrum of **hybrid 6** (400 MHz; DMSO-d_6)

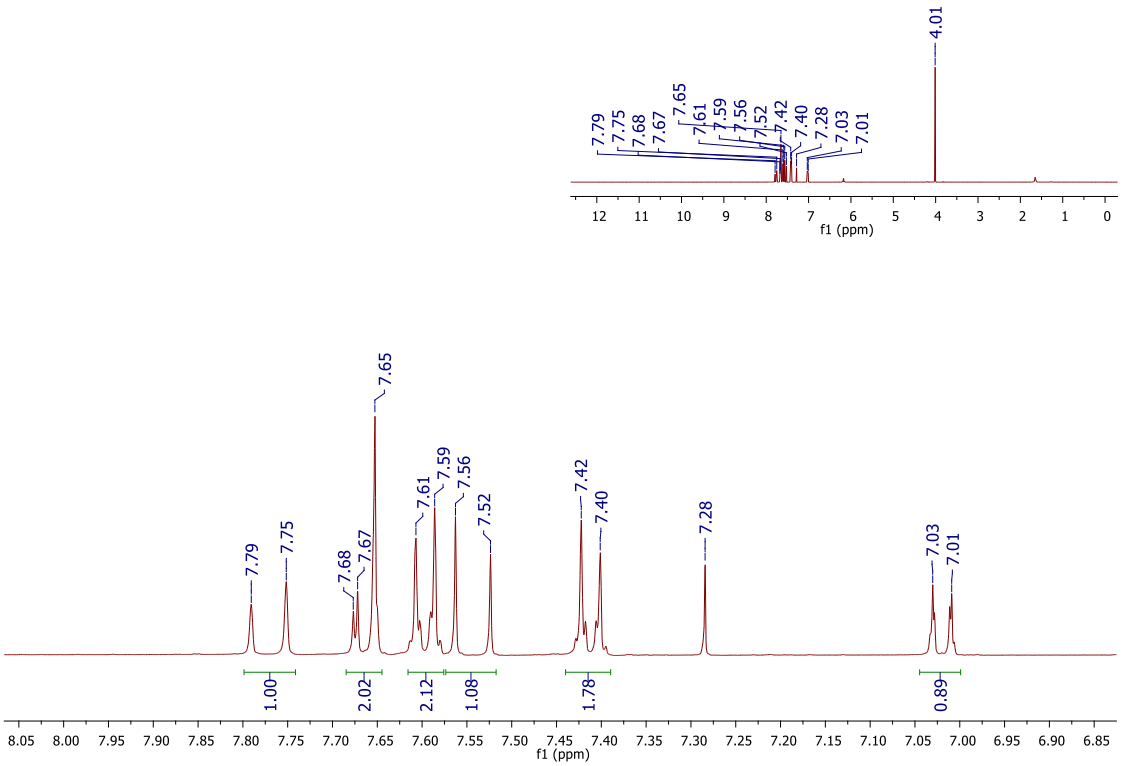

Figure S6. ii) ^{13}C NMR spectrum of **hybrid 6** (150 MHz; DMSO-d_6)

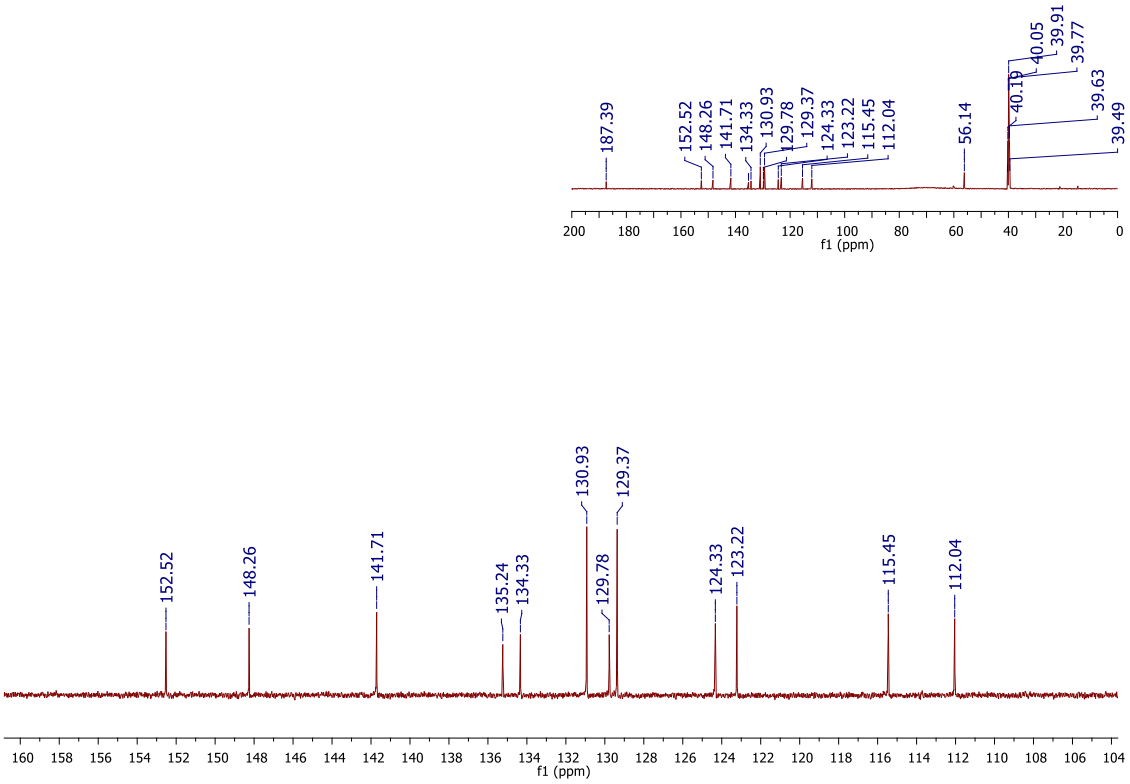

Figure S6. iii) UV-Vis spectrum of **hybrid 6** (MeOH/H_2O (3:1))

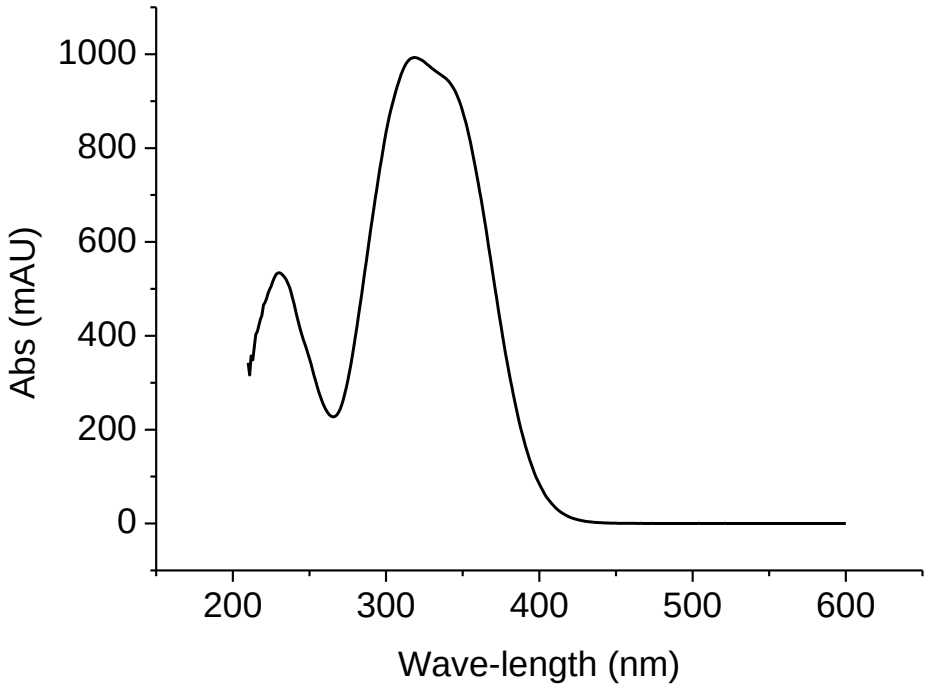

Figure S6. iv) HPLC chromatogram of **hybrid 6** (MeOH/H_2O (3:1))

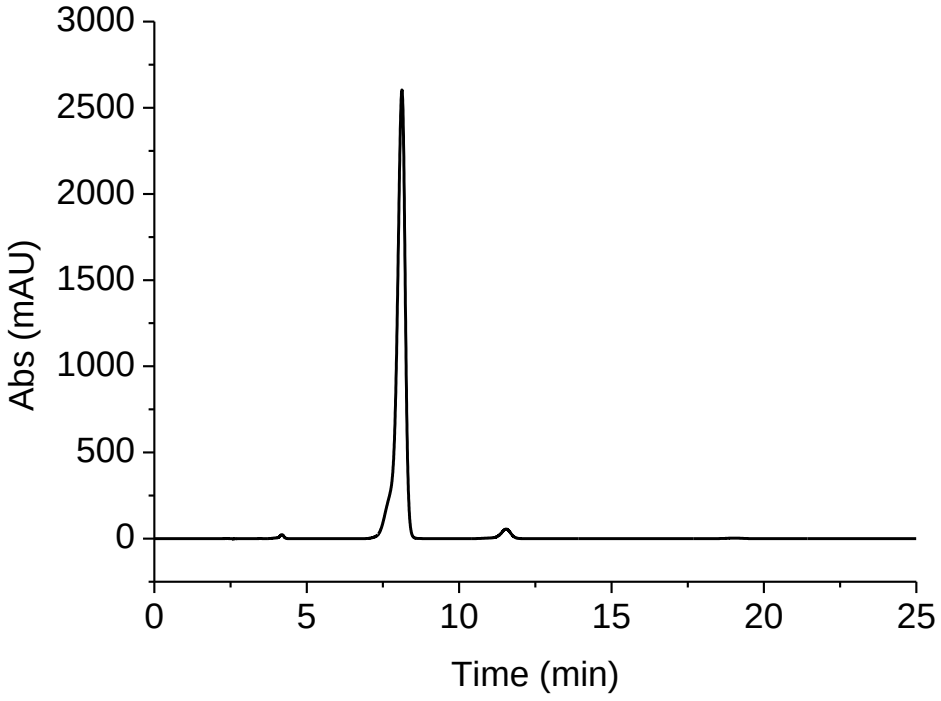

Figure S7. i) ^{1}H NMR spectrum of **hybrid 7** (600 MHz; DMSO-d_6)

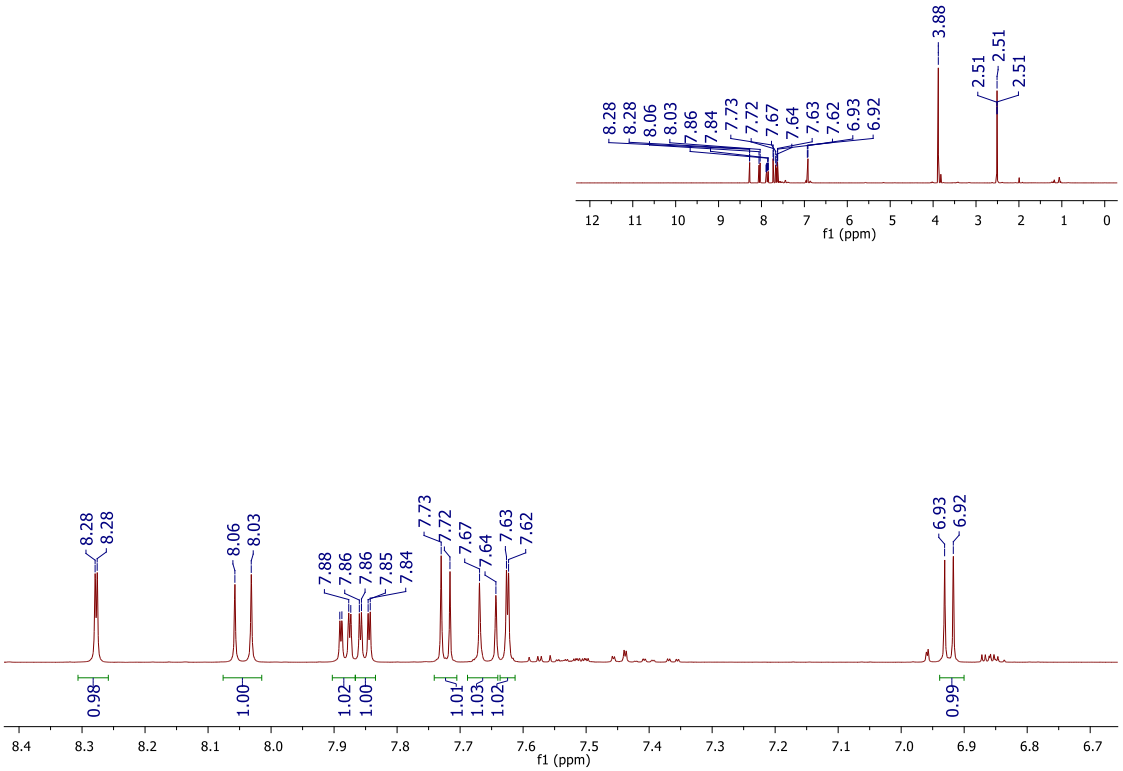

Figure S7. ii) ^{13}C NMR spectrum of **hybrid 7** (150 MHz; DMSO-d_6)

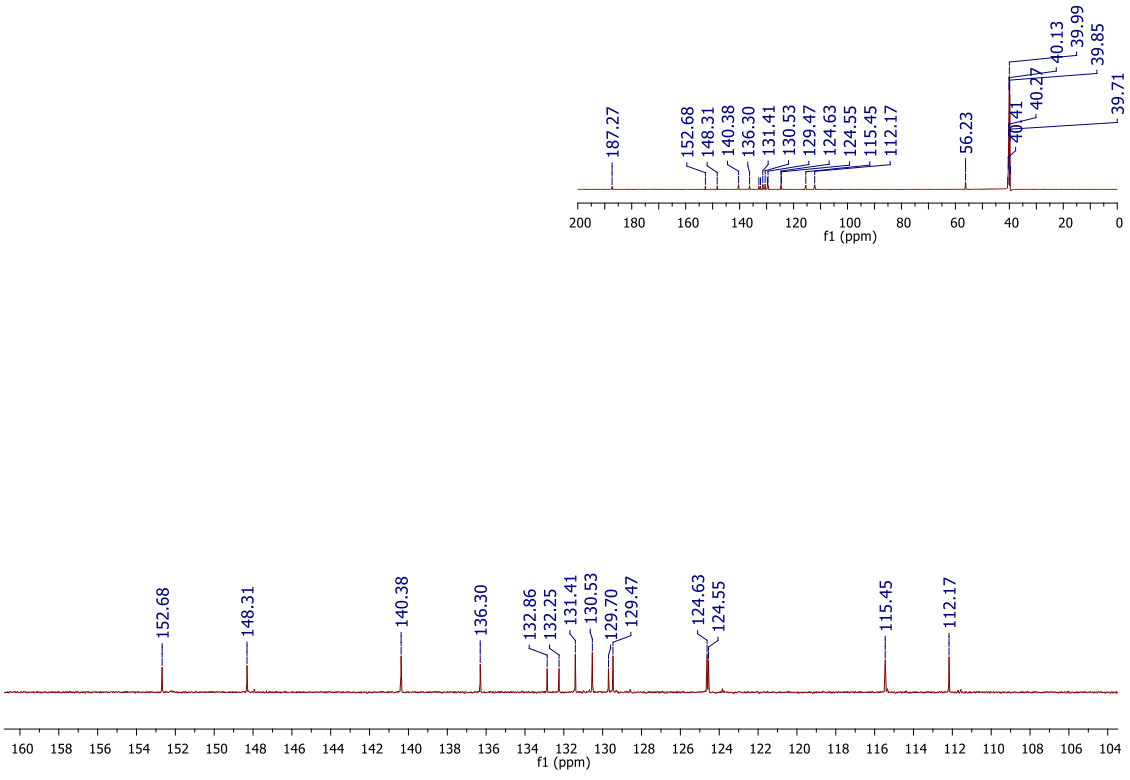

Figure S7. iii) UV-Vis spectrum of **hybrid 7** (MeOH/H_2O (3:1))

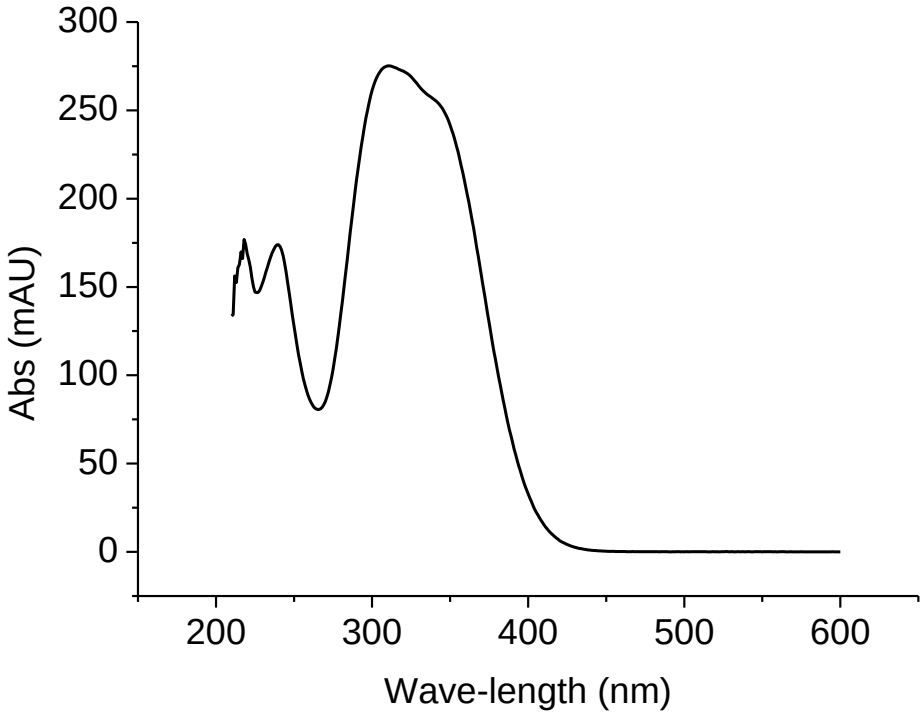

Figure S7. iv) HPLC chromatogram of **hybrid 7** (MeOH/H_2O (3:1))

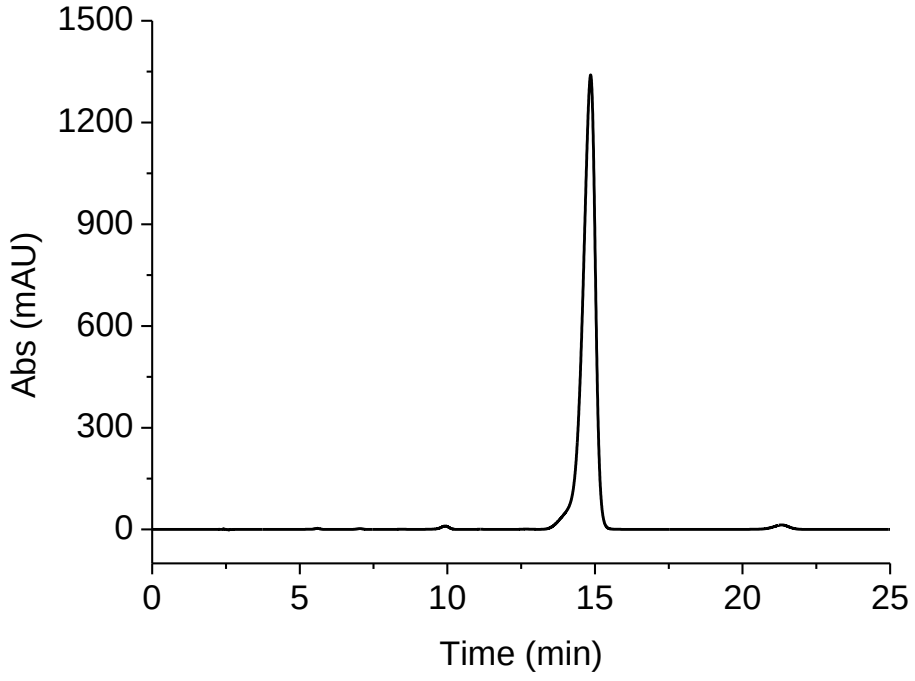

Figure S8. i) ^{1}H NMR spectrum of **hybrid 8** (300 MHz; DMSO-d_6)

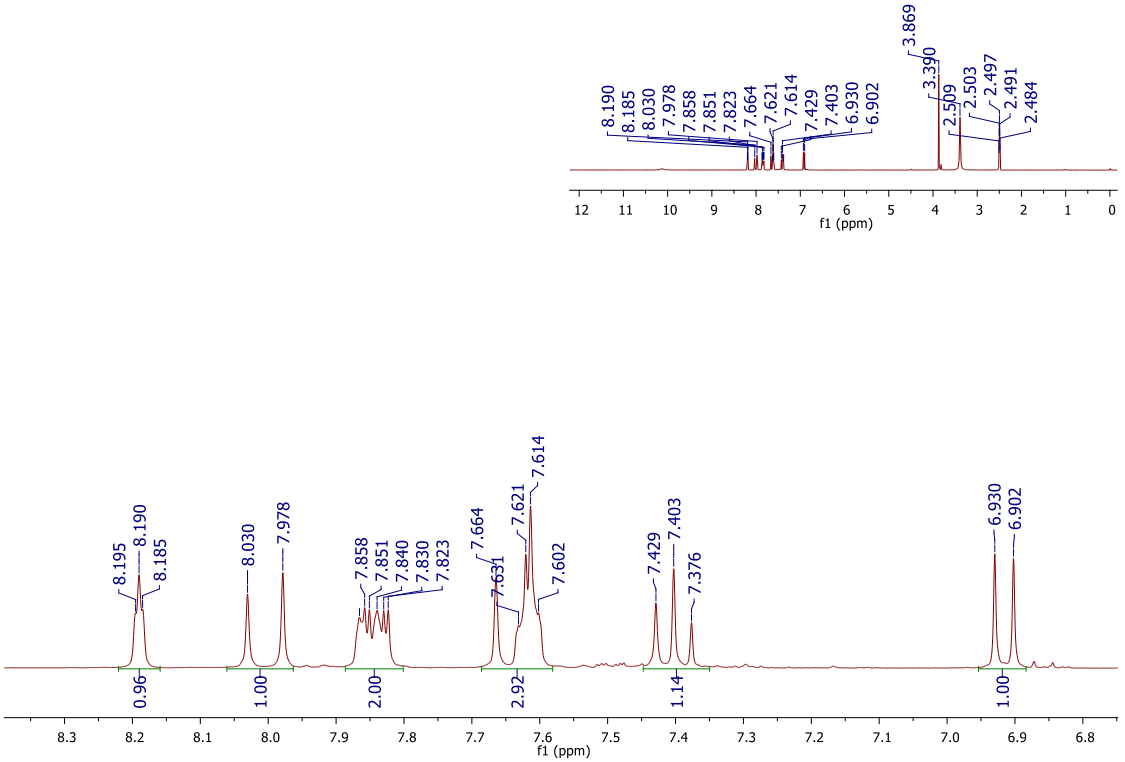

Figure S8. ii) ^{13}C NMR spectrum of **hybrid 8** (150 MHz; DMSO-d_6)

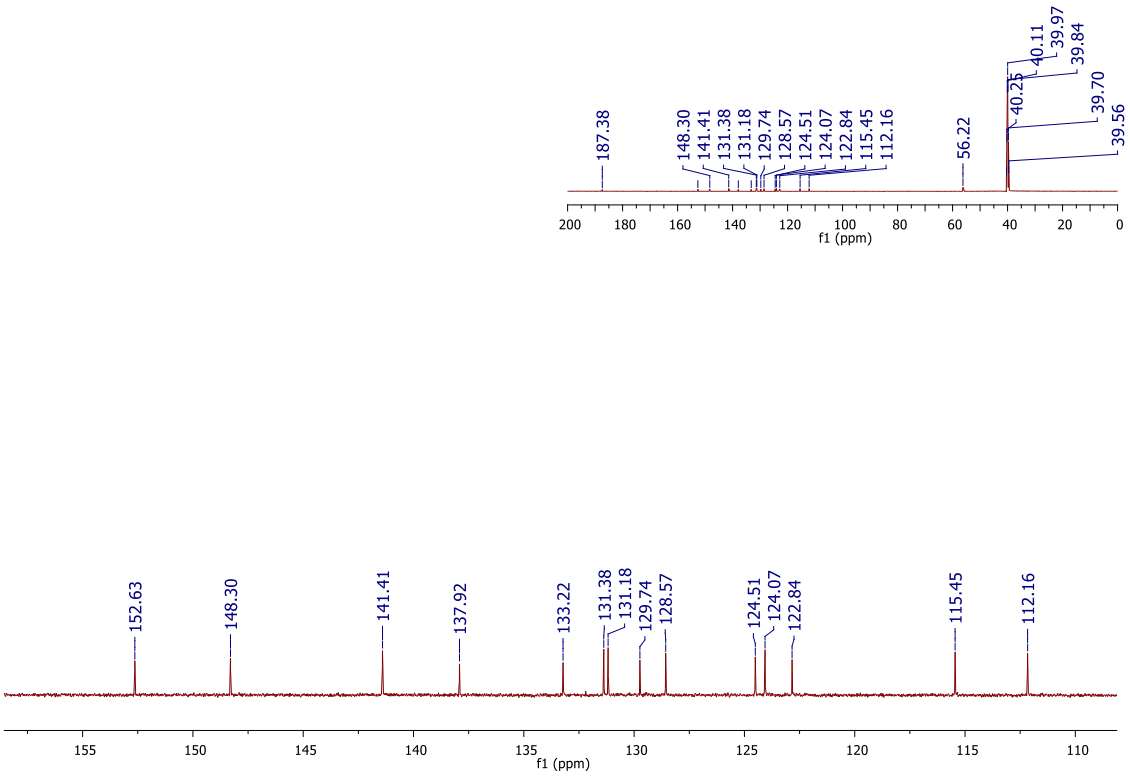

Figure S8. iii) UV-Vis spectrum of **hybrid 8** (MeOH/H_2O (3:1))

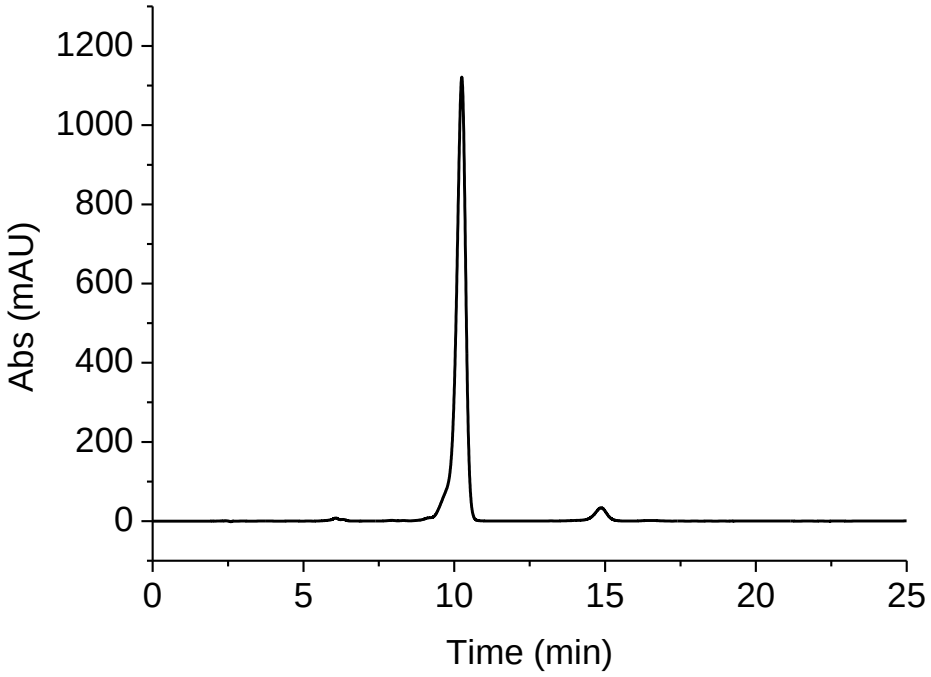

Figure S8. iv) HPLC chromatogram of **hybrid 8** (MeOH/H_2O (3:1))

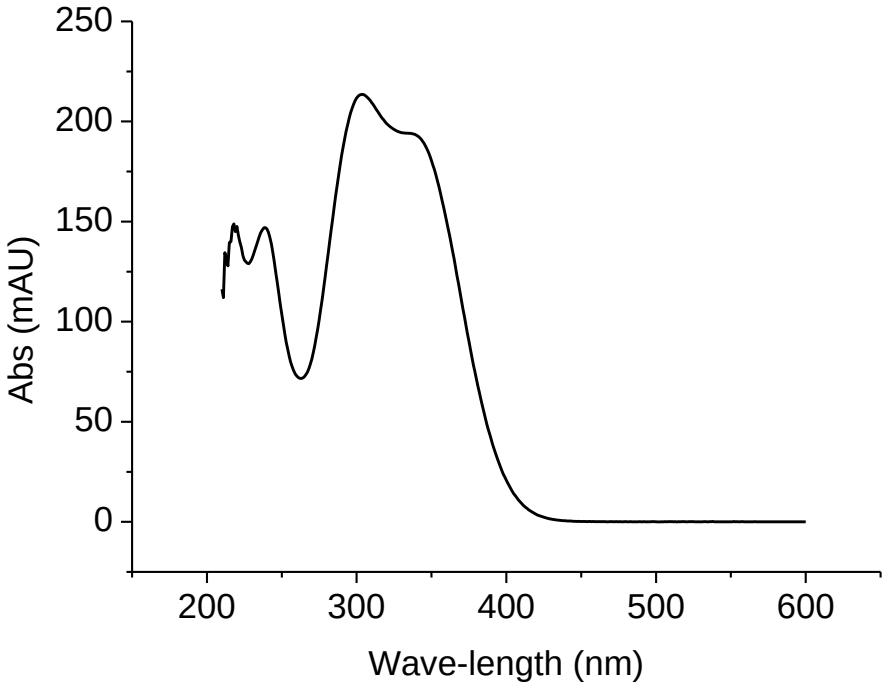

Figure S9. i) ^{1}H NMR spectrum of **hybrid 9** (400 MHz; DMSO-d_6)

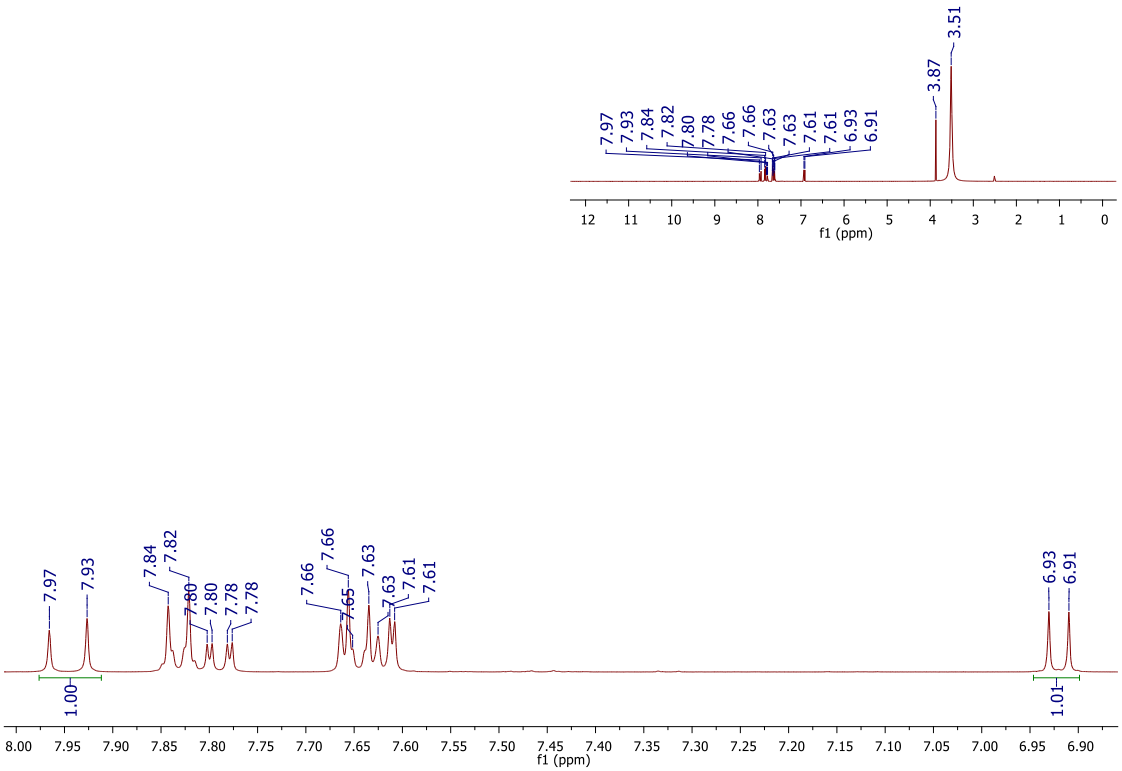

Figure S9. ii) ^{13}C NMR spectrum of **hybrid 9** (150 MHz; DMSO-d_6)

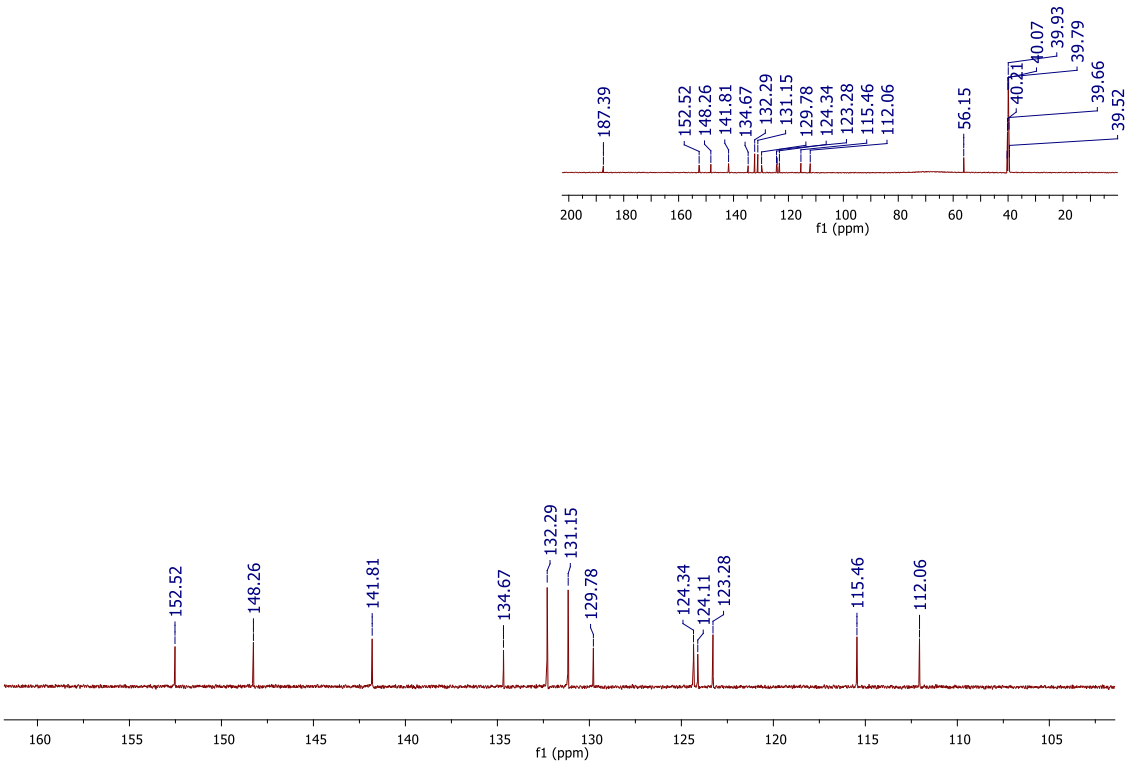

Figure S9. iii) UV-Vis spectrum of **hybrid 9** (MeOH/H_2O (3:1))

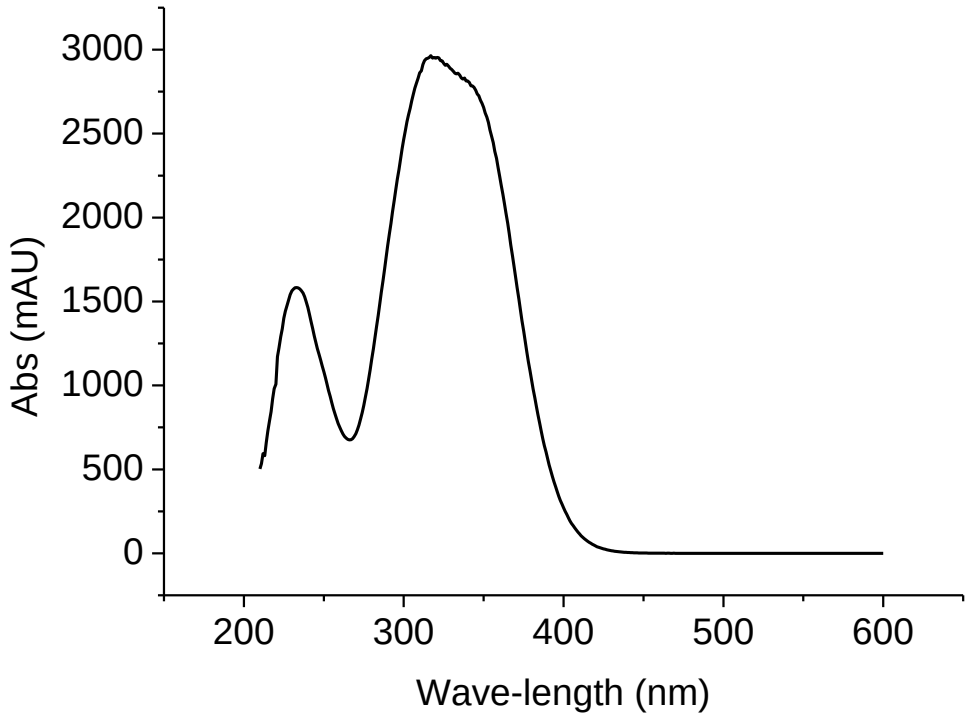

Figure S9. iv) HPLC chromatogram of **hybrid 9** (MeOH/H_2O (3:1))

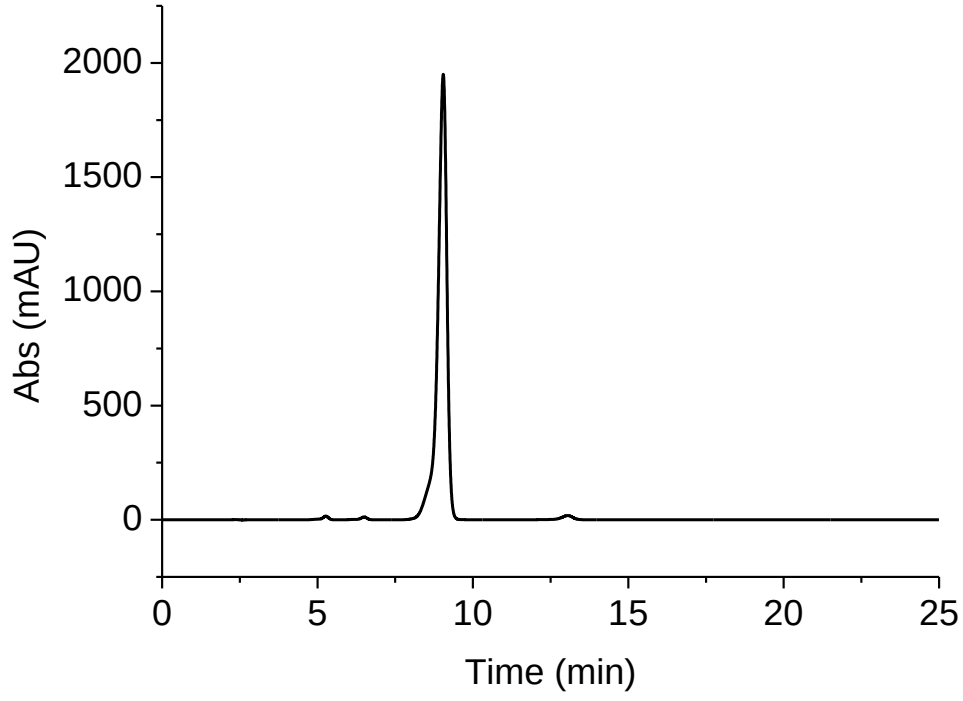

Figure S10. i) ^{1}H NMR spectrum of **hybrid 10** (600 MHz; DMSO-d_6)

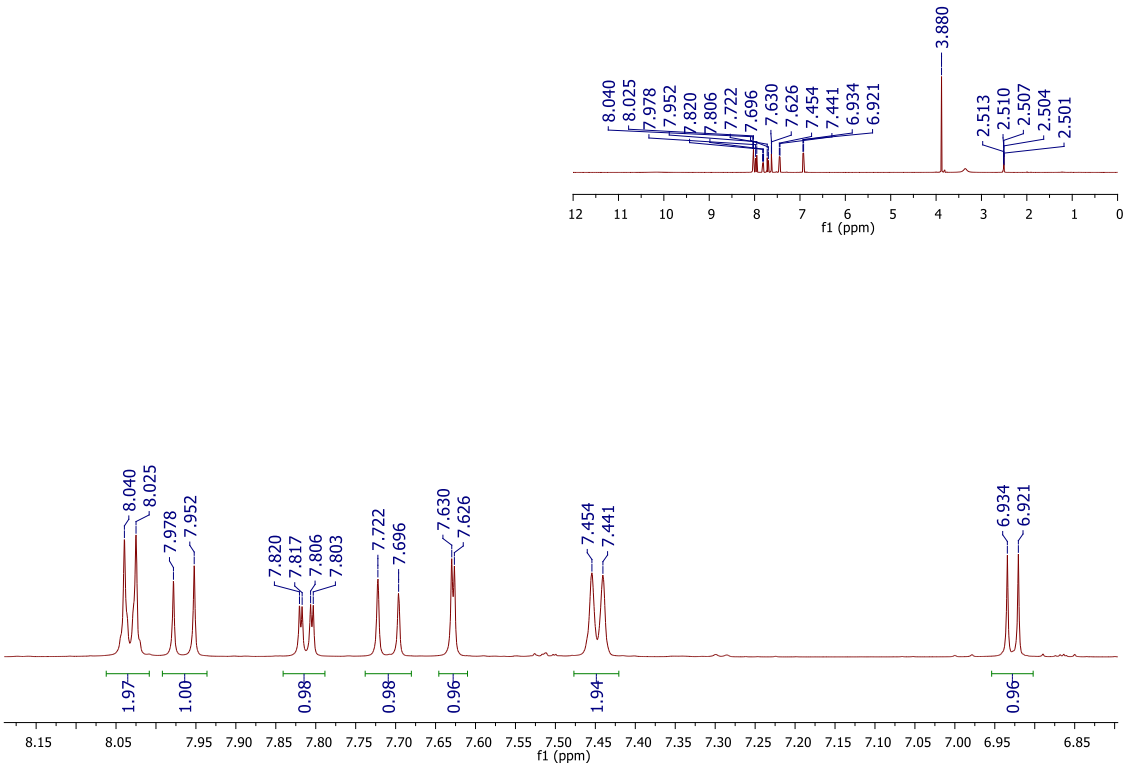

Figure S10. ii) ^{13}C NMR spectrum of **hybrid 10** (150 MHz; DMSO-d_6)

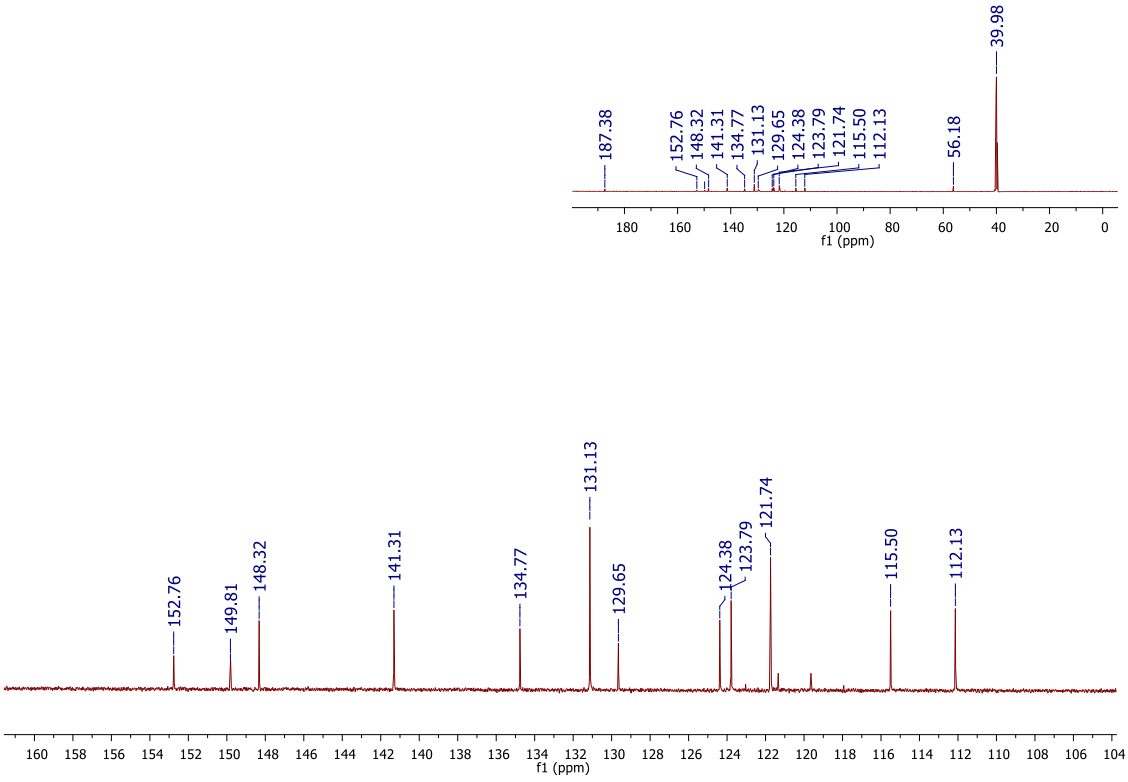

Figure S10. iii) UV-Vis spectrum of **hybrid 10** (MeOH/H_2O (3:1))

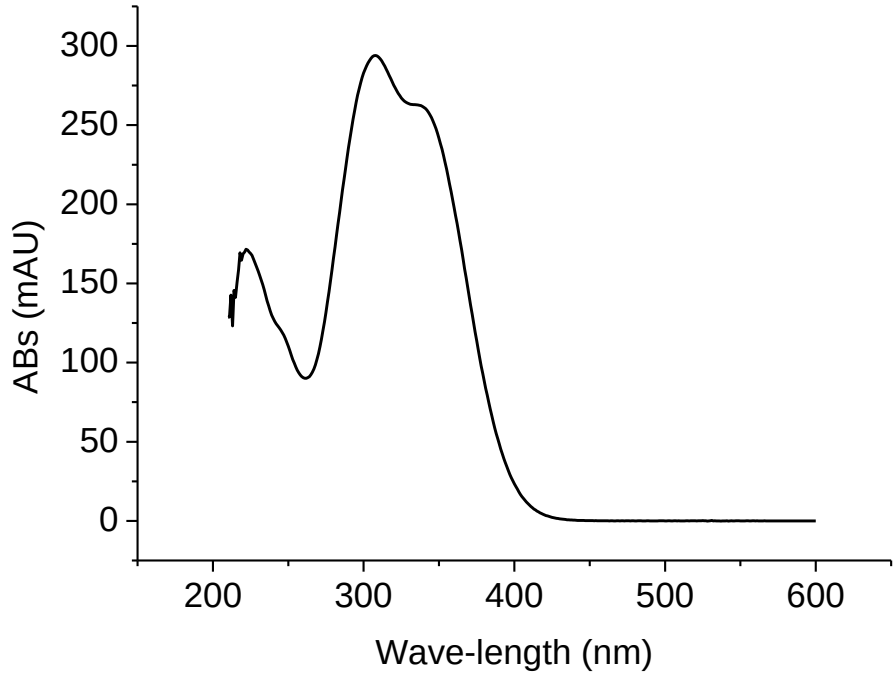

Figure S10. iv) HPLC chromatogram of **hybrid 10** (MeOH/H_2O (3:1))

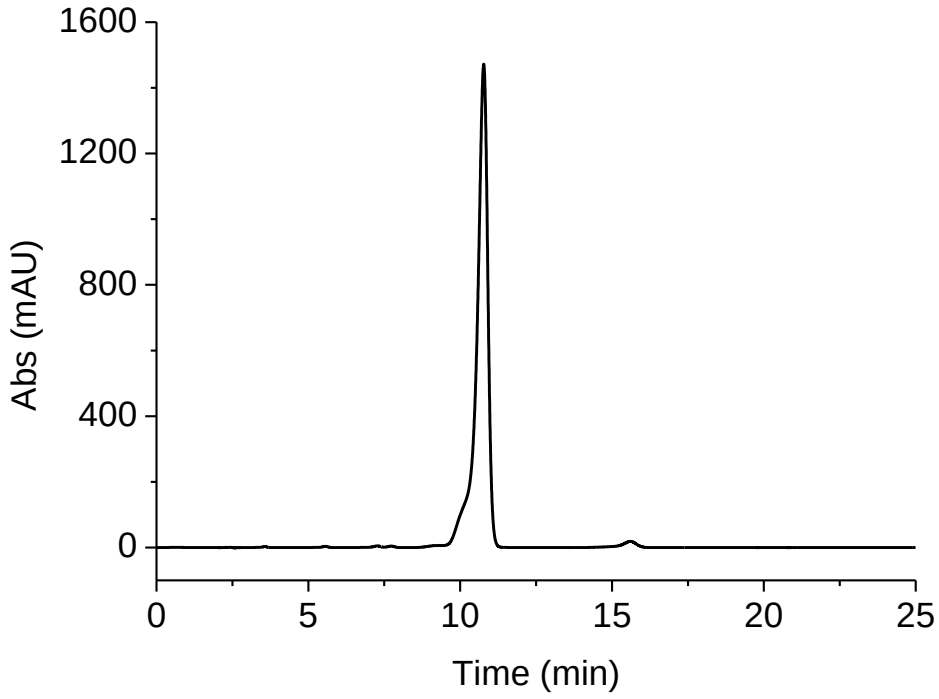

Figure S11. i) ^{1}H NMR spectrum of **hybrid 11** (400 MHz; DMSO-d_6)

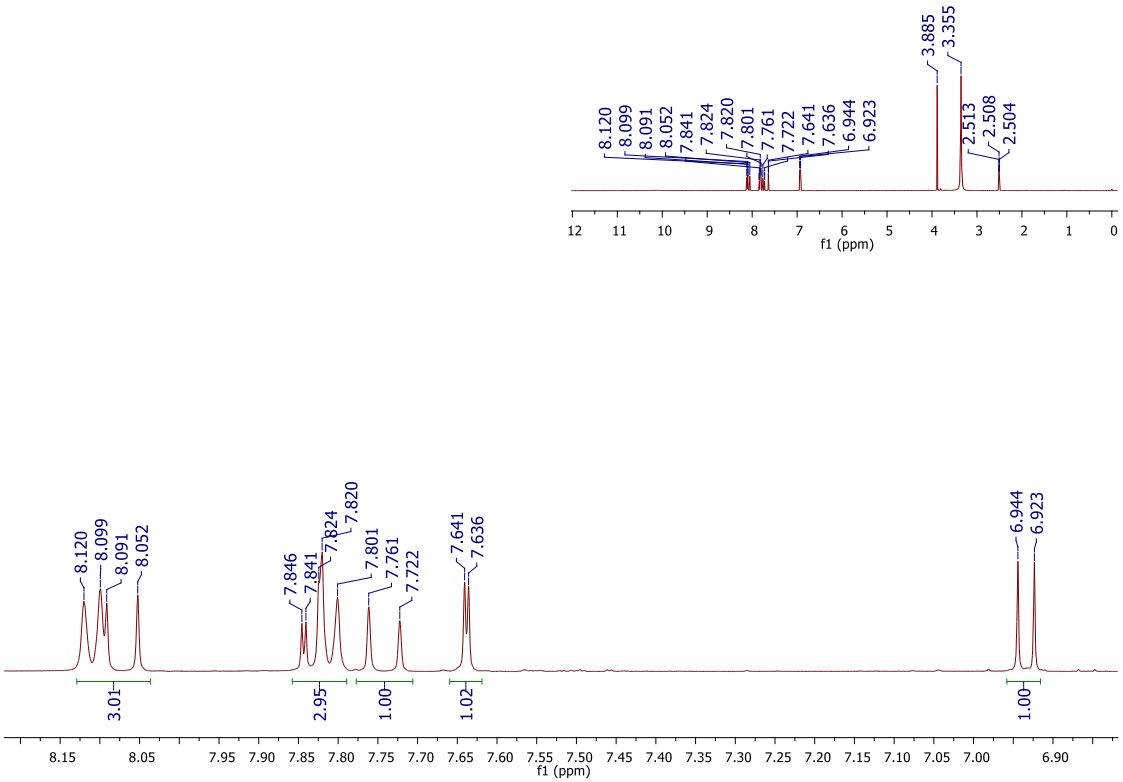

Figure S11. ii) ^{13}C NMR spectrum of **hybrid 11** (150 MHz; DMSO-d_6)

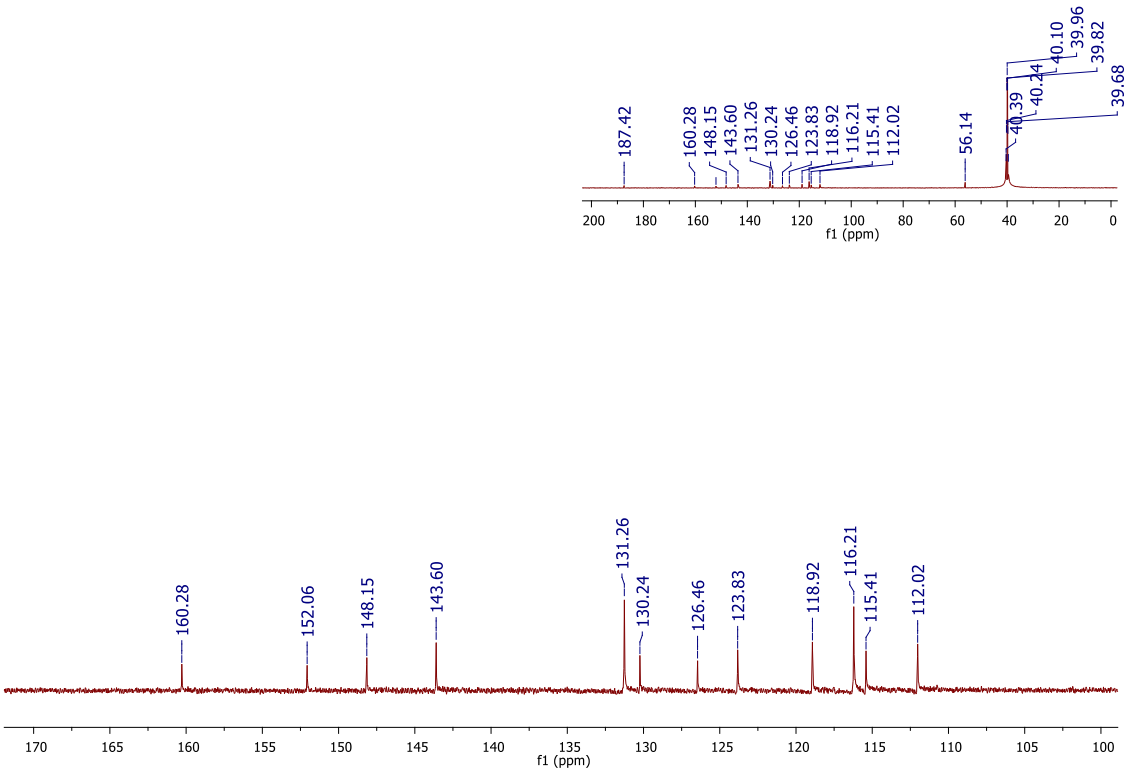

Figure S11. iii) UV-Vis spectrum of **hybrid 11** (MeOH/H_2O (3:1))

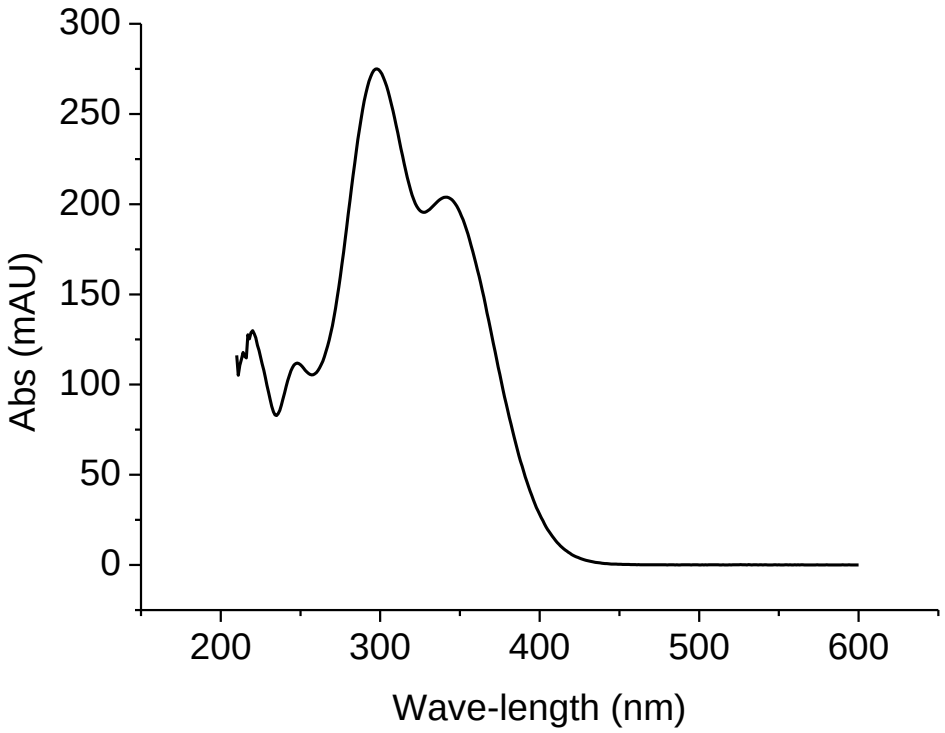

Figure S11. iv) HPLC chromatogram of **hybrid 11** (MeOH/H_2O (3:1))

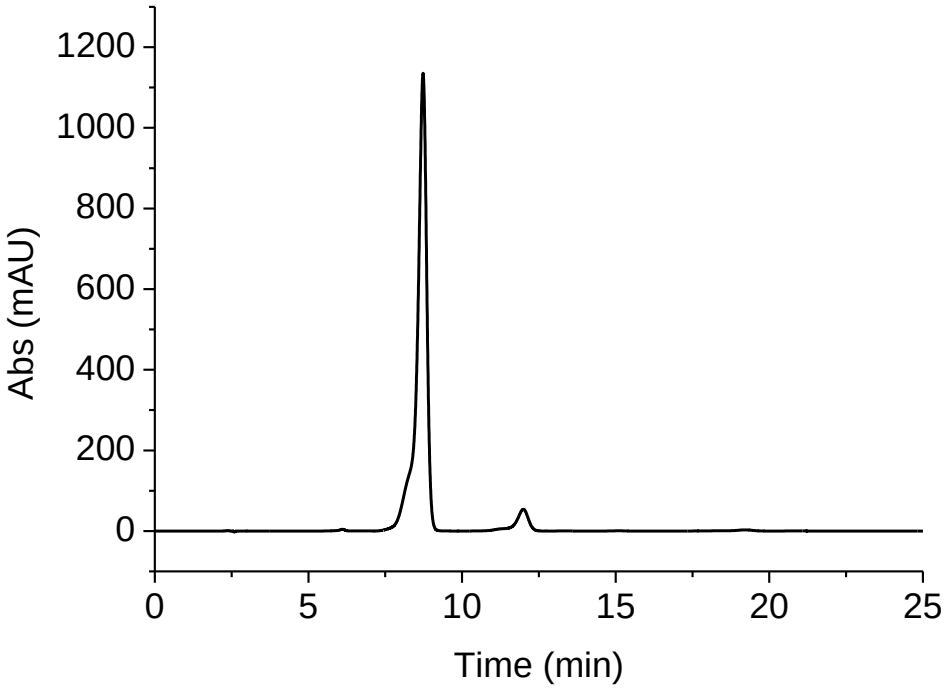

Figure S12. i) ^{1}H NMR spectrum of **hybrid 12** (600 MHz; DMSO-d_6)

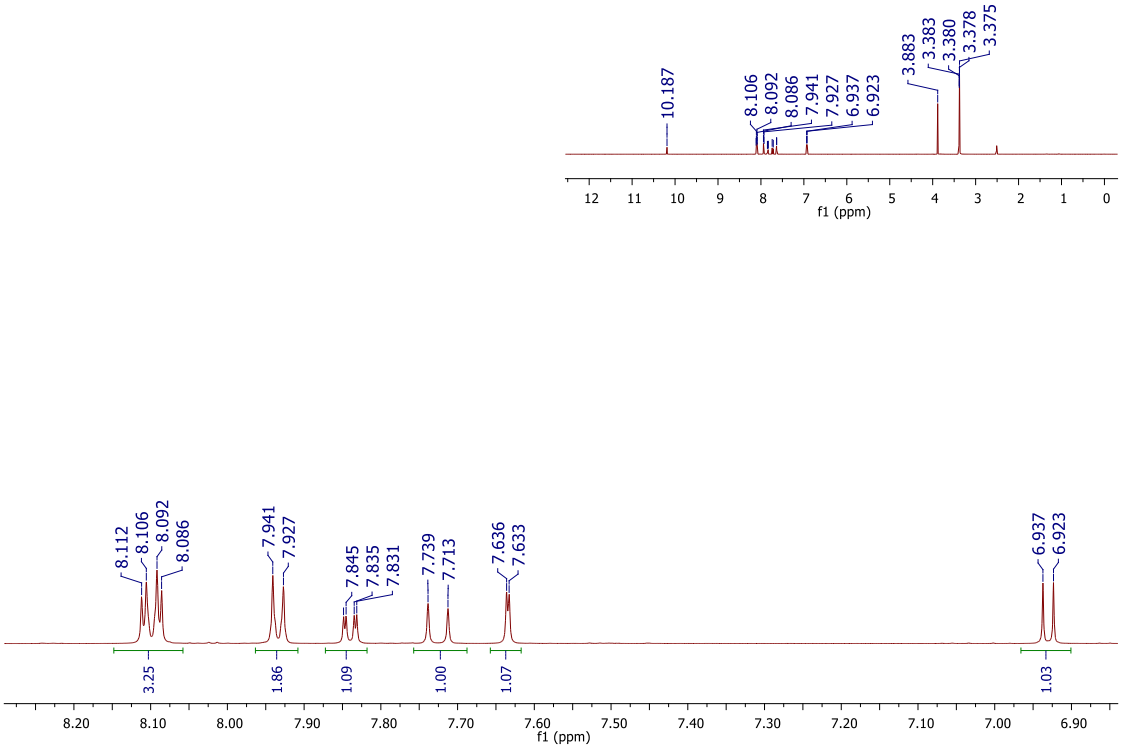

Figure S12. ii) ^{13}C NMR spectrum of **hybrid 12** (150 MHz; DMSO-d_6)

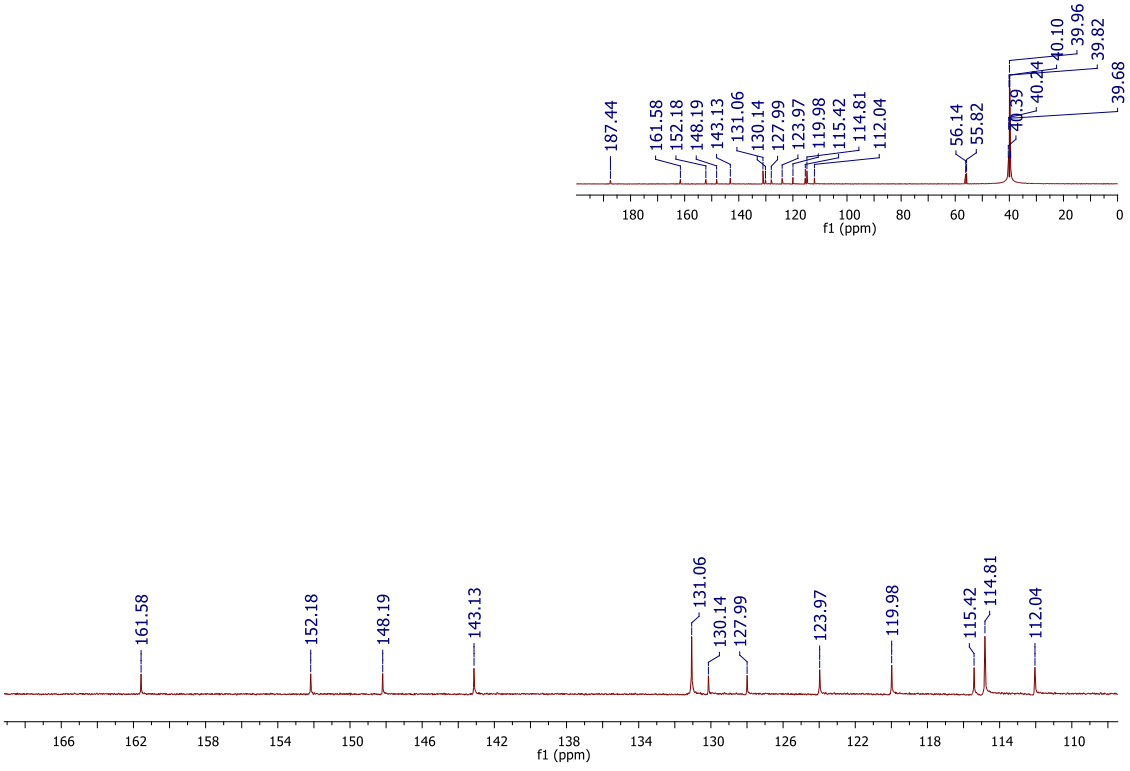

Figure S12. iii) UV-Vis spectrum of **hybrid 12** (MeOH/H_2O (3:1))

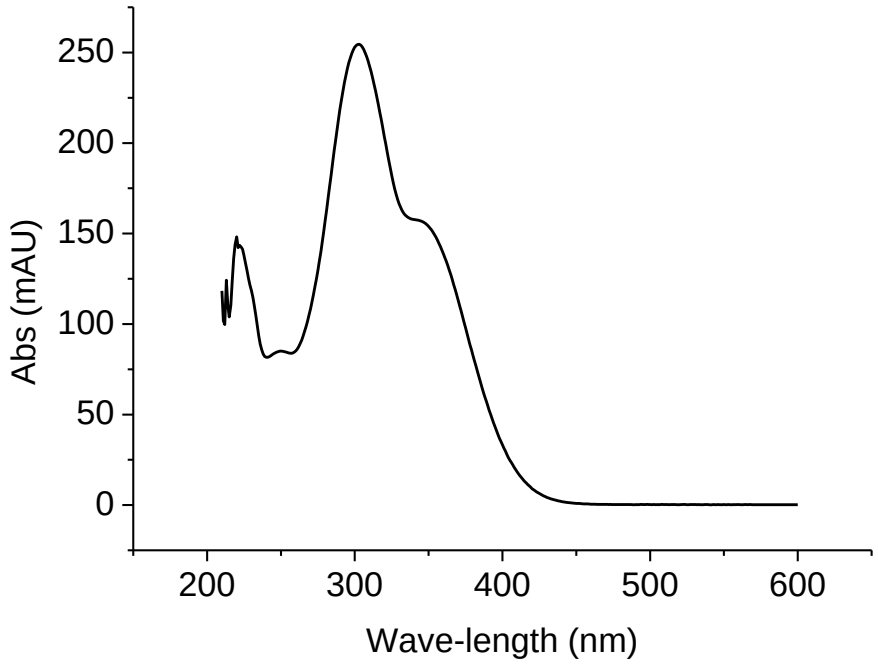

Figure S12. iv) HPLC chromatogram of **hybrid 12** (MeOH/H_2O (3:1))

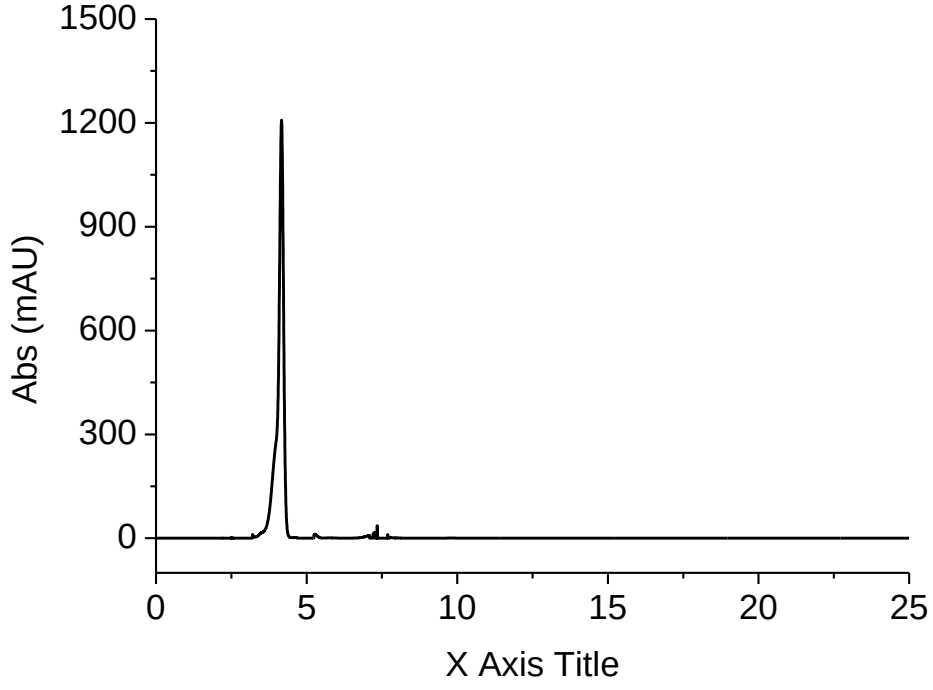

Figure S13. i) ^{1}H NMR spectrum of **hybrid 13** (600 MHz; DMSO-d_6)

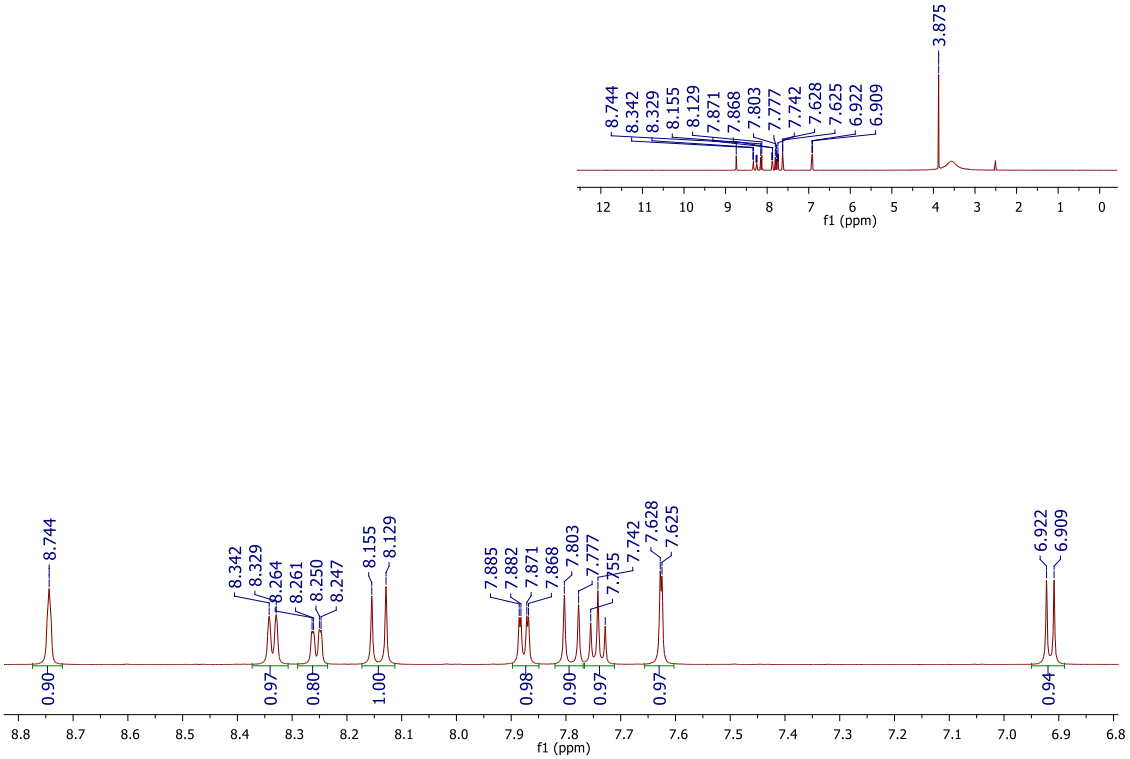

Figure S13. ii) ^{13}C NMR spectrum of **hybrid 13** (150 MHz; DMSO-d_6)

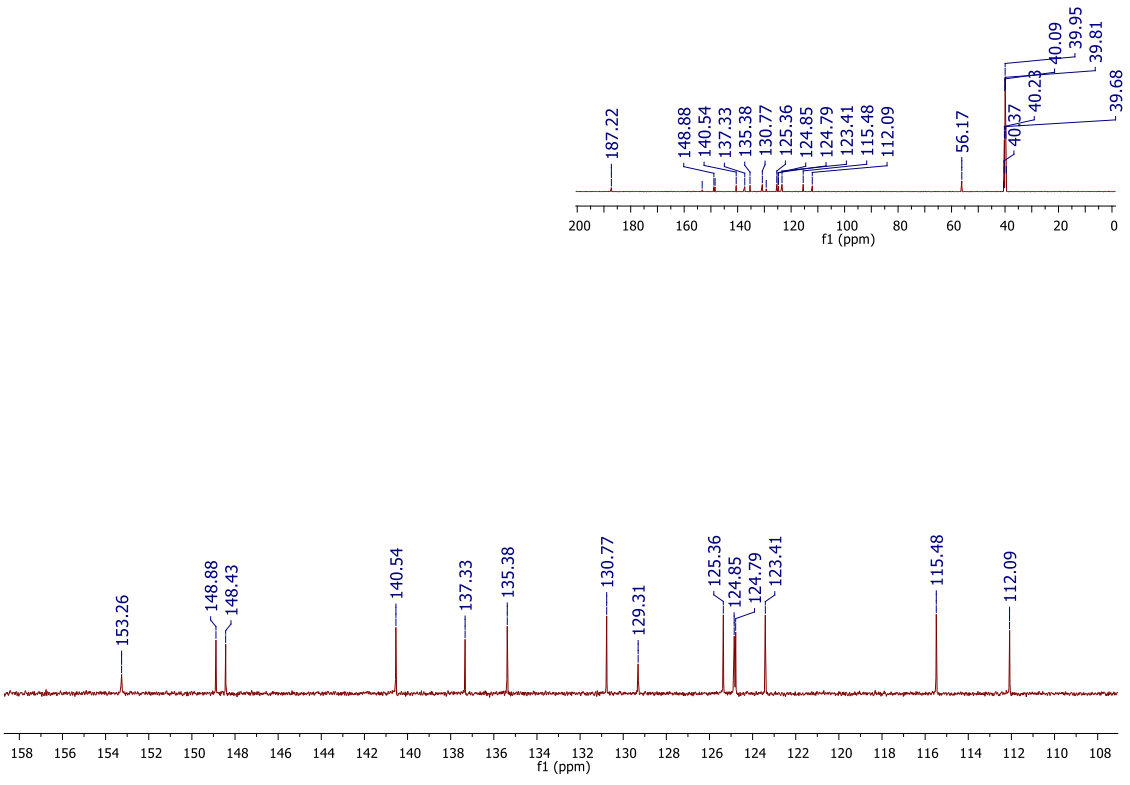

Figure S13. iii) UV-Vis spectrum of **hybrid 13** (MeOH/H_2O (3:1))

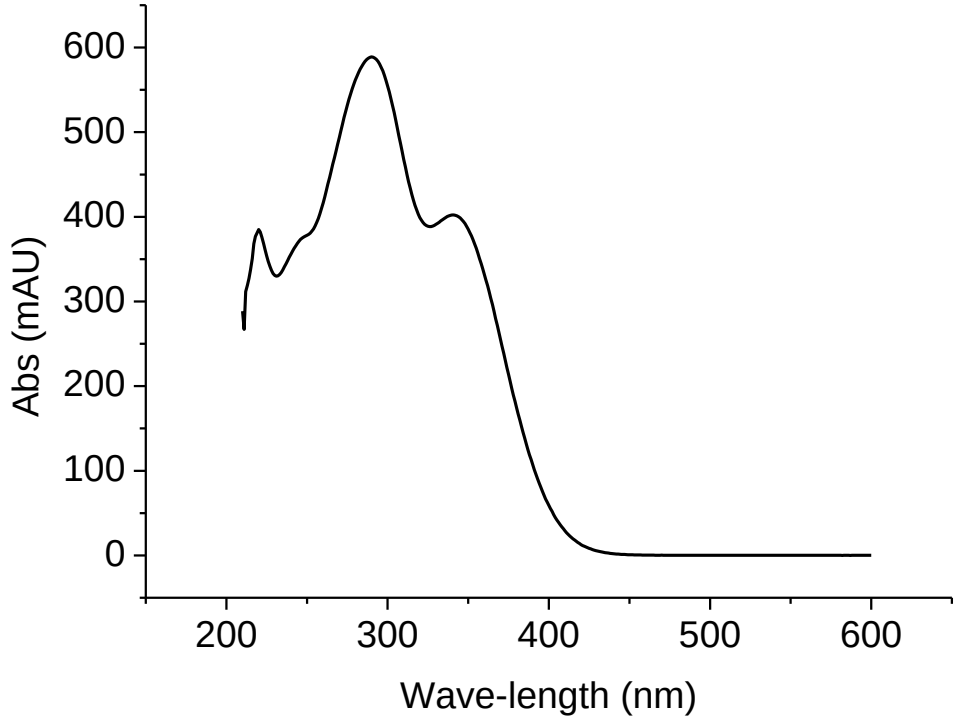

Figure S13. iv) HPLC chromatogram of **hybrid 13** (MeOH/H_2O (3:1))

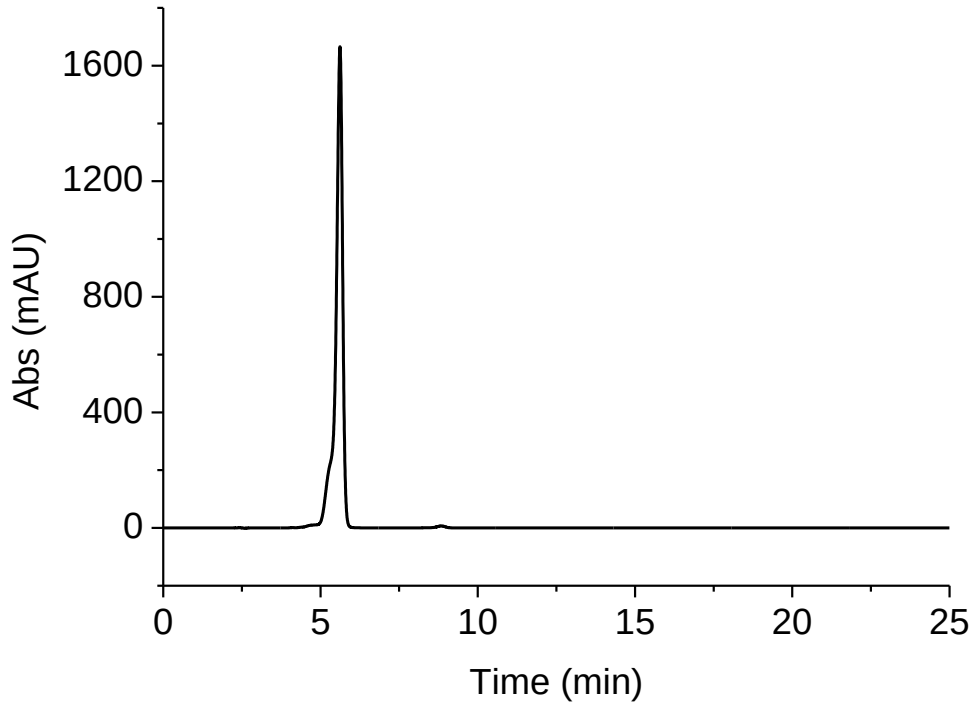

Figure S14. i) ^{1}H NMR spectrum of **hybrid 14** (400 MHz; DMSO-d_6)

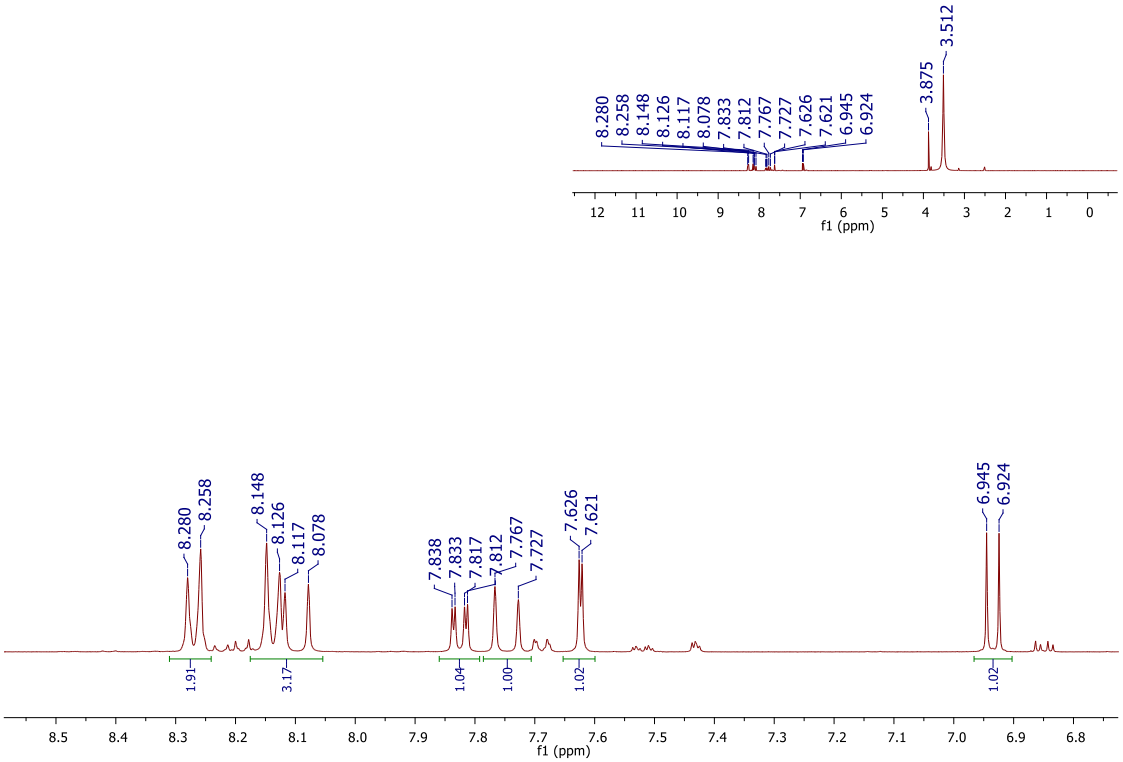

Figure S14. ii) ^{13}C NMR spectrum of **hybrid 14** (150 MHz; DMSO-d_6)

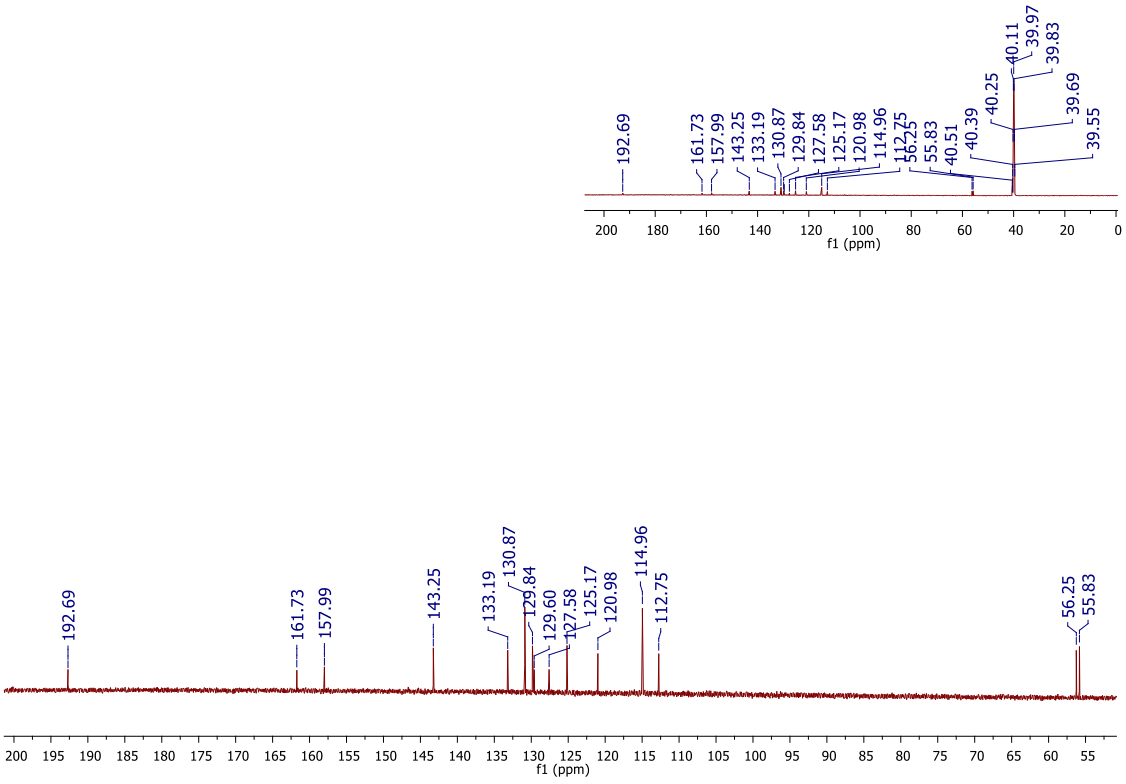

Figure S14. iii) UV-Vis spectrum of **hybrid 14** (MeOH/H_2O (3:1))

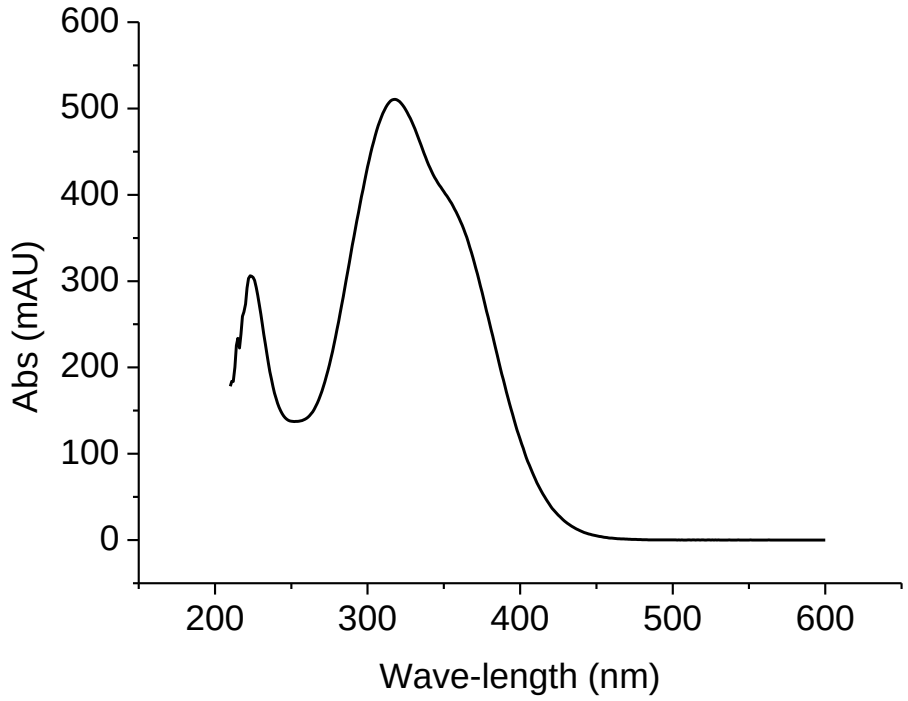

Figure S14. iv) HPLC chromatogram of **hybrid 14** (MeOH/H_2O (3:1))

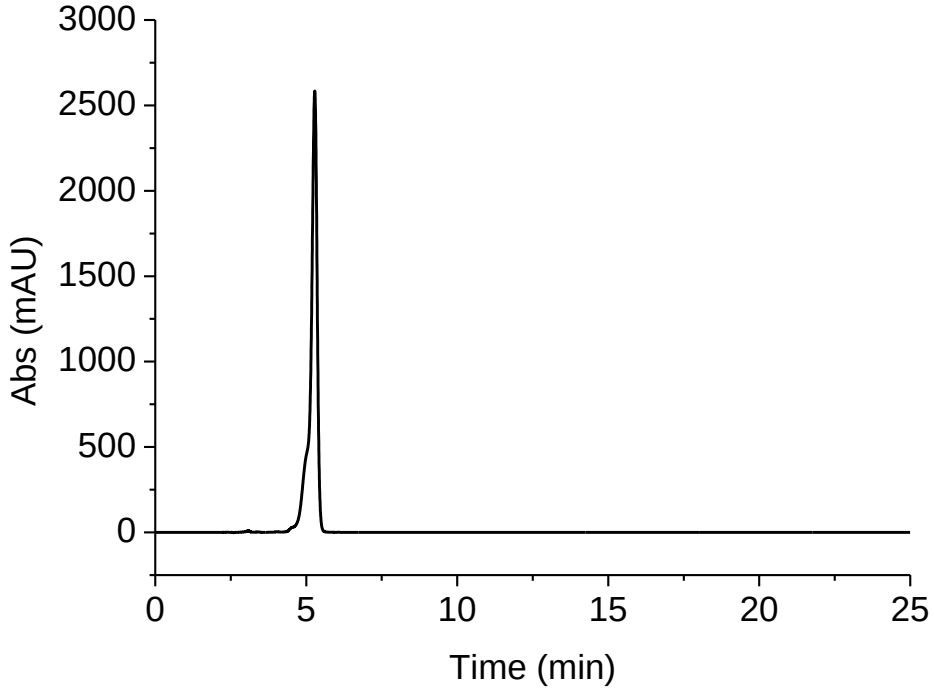

Figure S15. i) ^{1}H NMR spectrum of **hybrid 15** (400 MHz; DMSO-d_6)

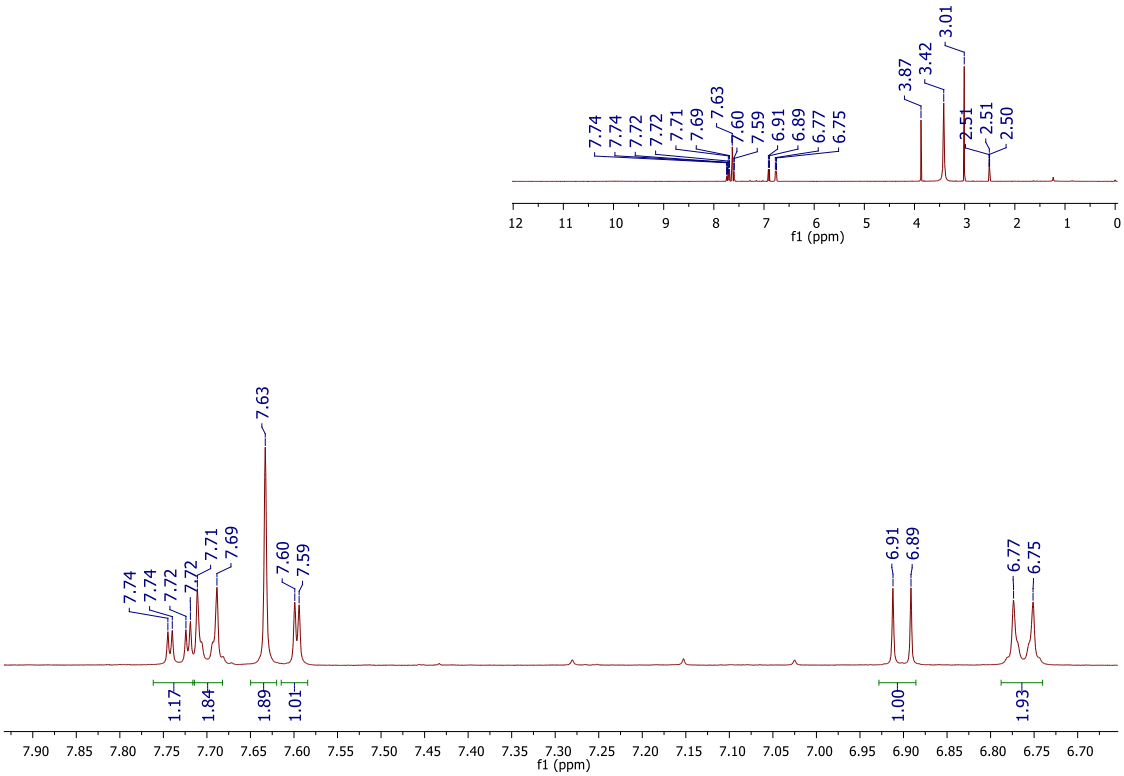

Figure S15. ii) ^{13}C NMR spectrum of **hybrid 15** (150 MHz; DMSO-d_6)

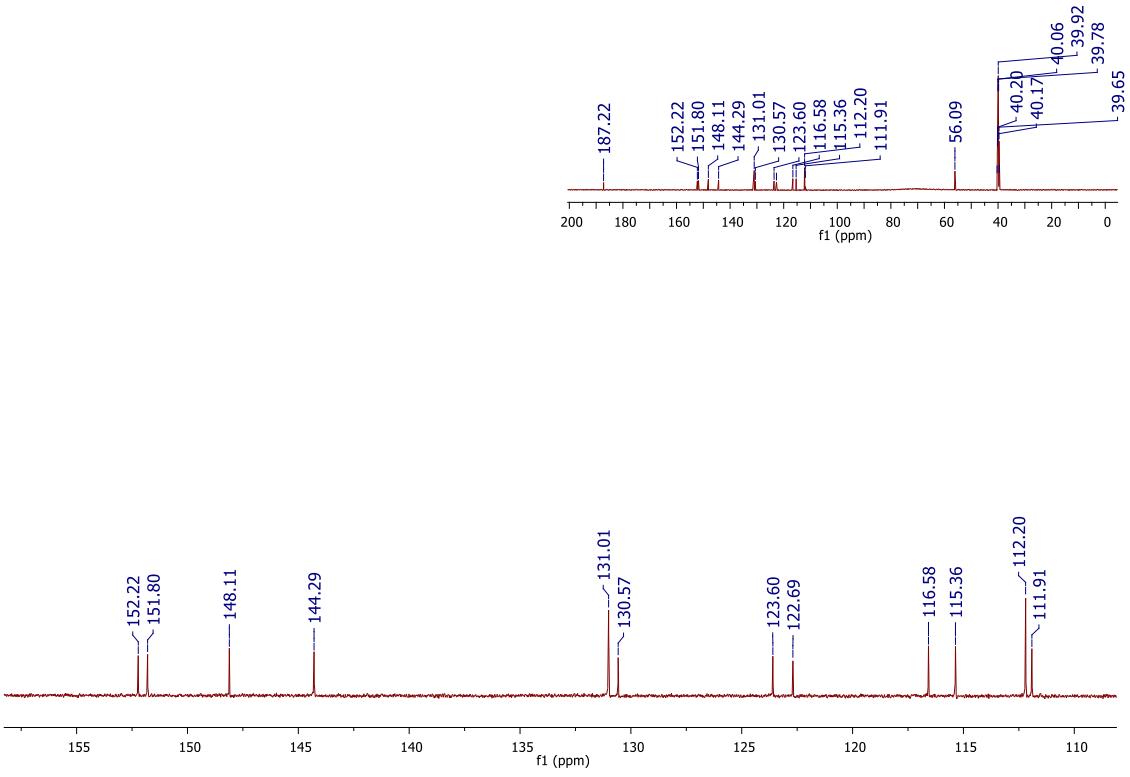

Figure S15. iii) UV-Vis spectrum of **hybrid 15** (MeOH/H_2O (3:1))

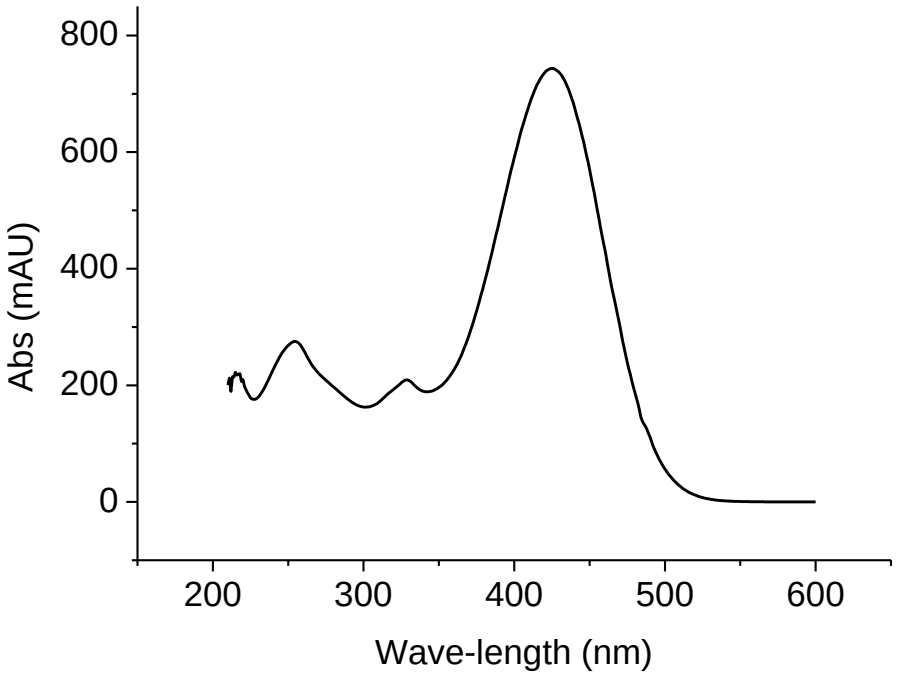

Figure S15. iv) HPLC chromatogram of **hybrid 15** (MeOH/H_2O (3:1))

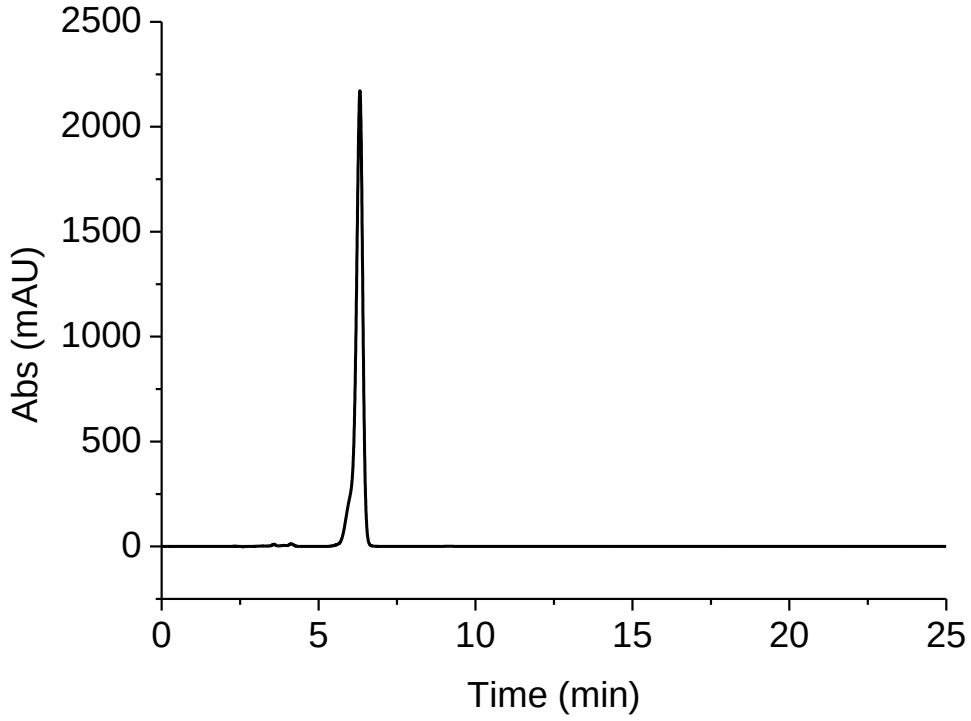

Figure S16. i) ^{1}H NMR spectrum of **hybrid 16** (300 MHz; DMSO-d_6)

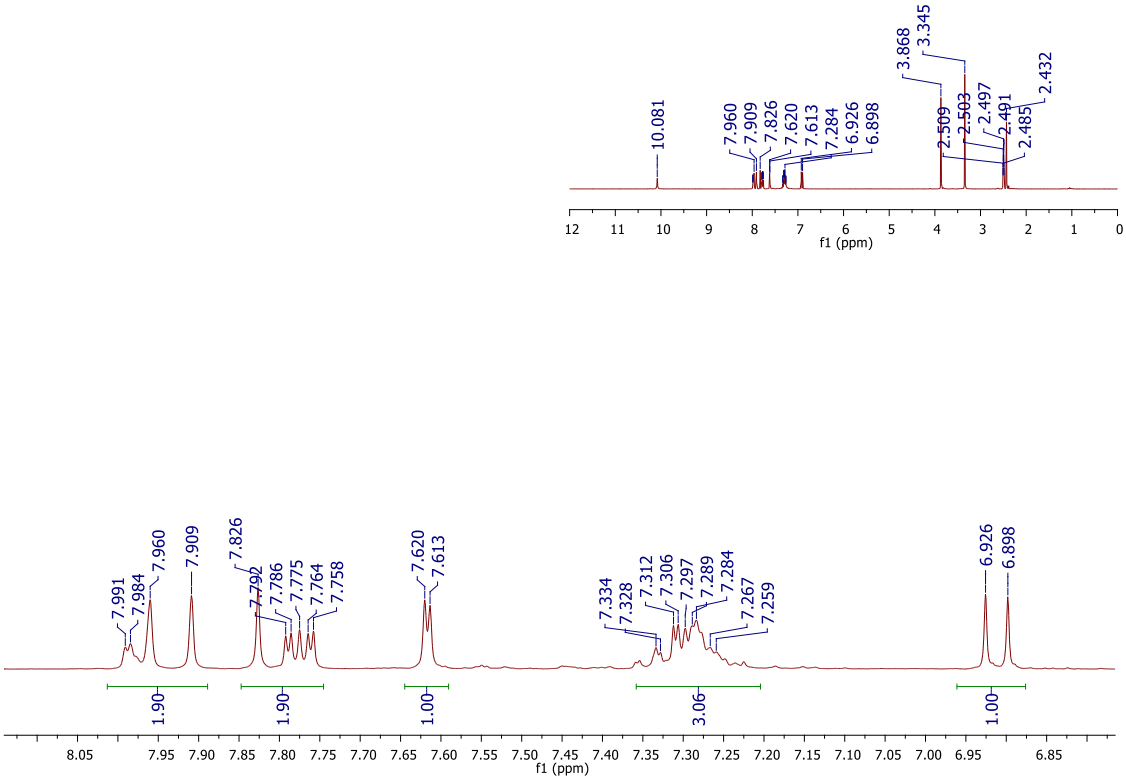

Figure S16. ii) ^{13}C NMR spectrum of **hybrid 16** (150 MHz; DMSO-d_6)

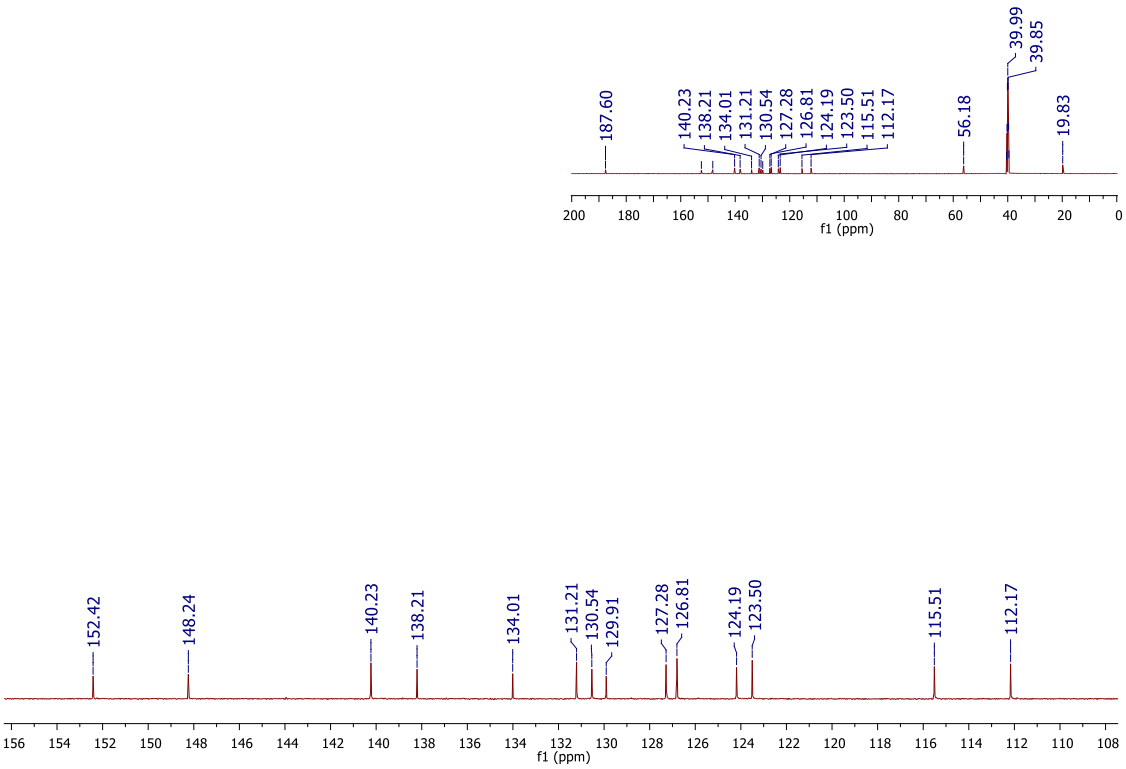

Figure S16. iii) UV-Vis spectrum of **hybrid 16** (MeOH/H_2O (3:1))

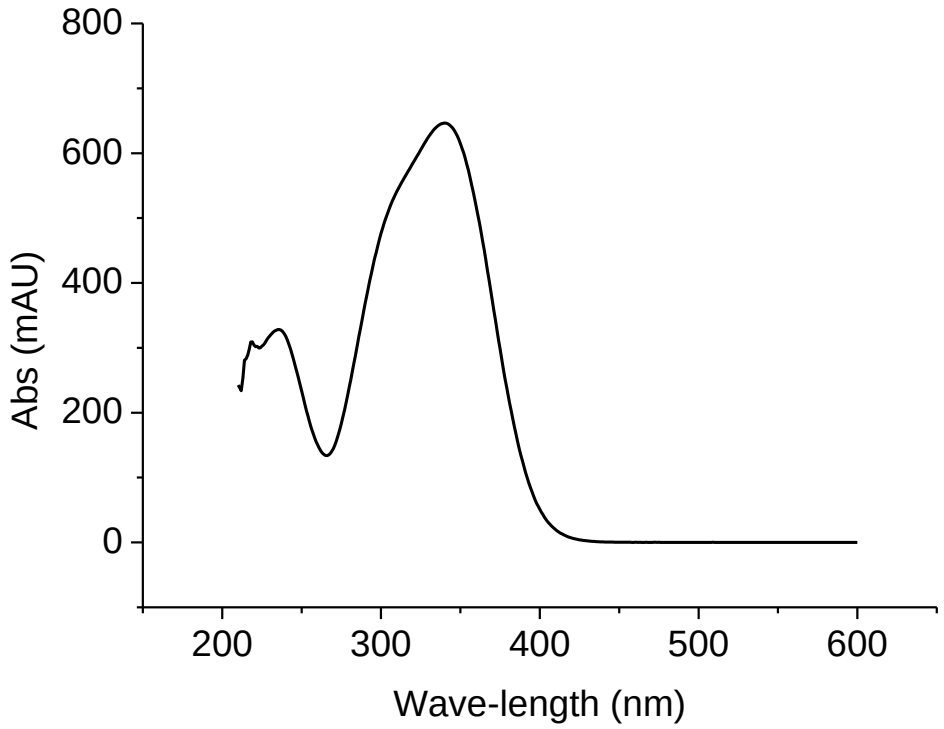

Figure S16. iv) HPLC chromatogram of **hybrid 16** (MeOH/H_2O (3:1))

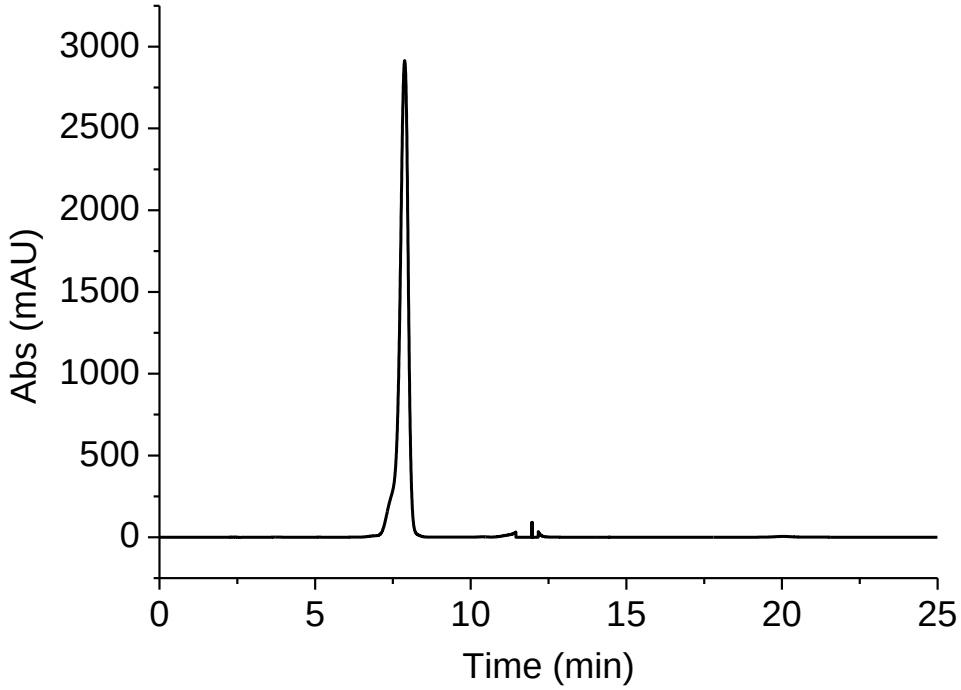

Figure S17. i) ^{1}H NMR spectrum of **hybrid 17** (300 MHz; DMSO-d_6)

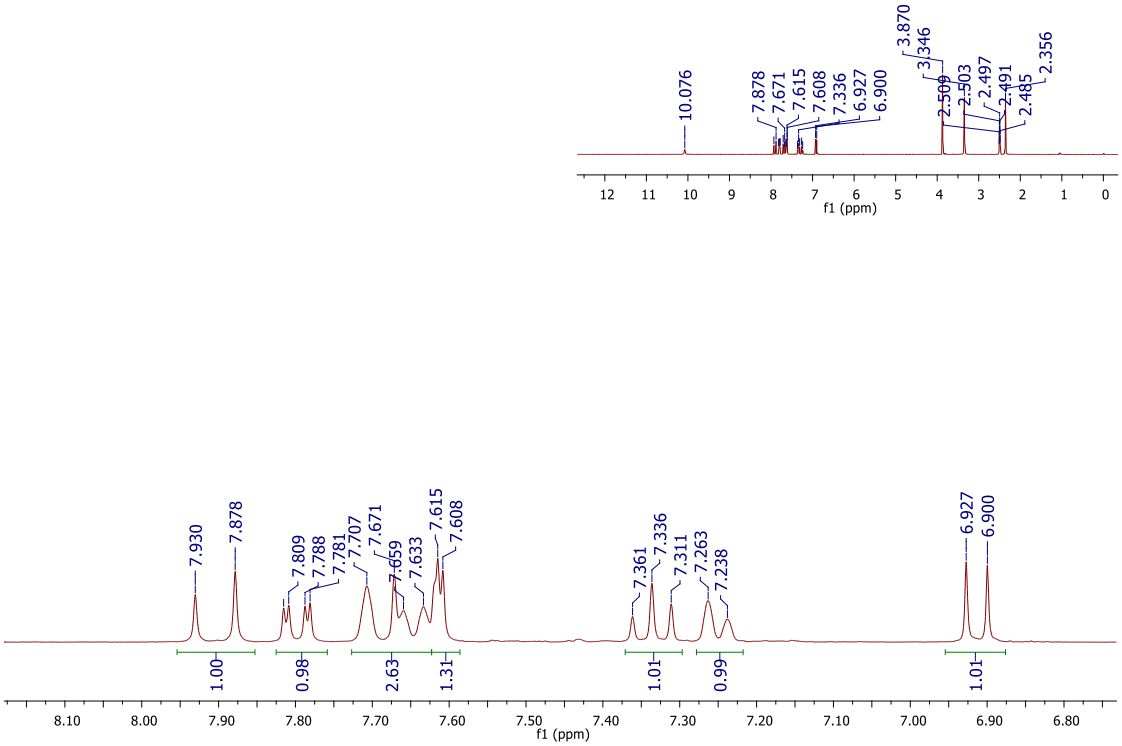

Figure S17. ii) ^{13}C NMR spectrum of **hybrid 17** (150 MHz; DMSO-d_6)

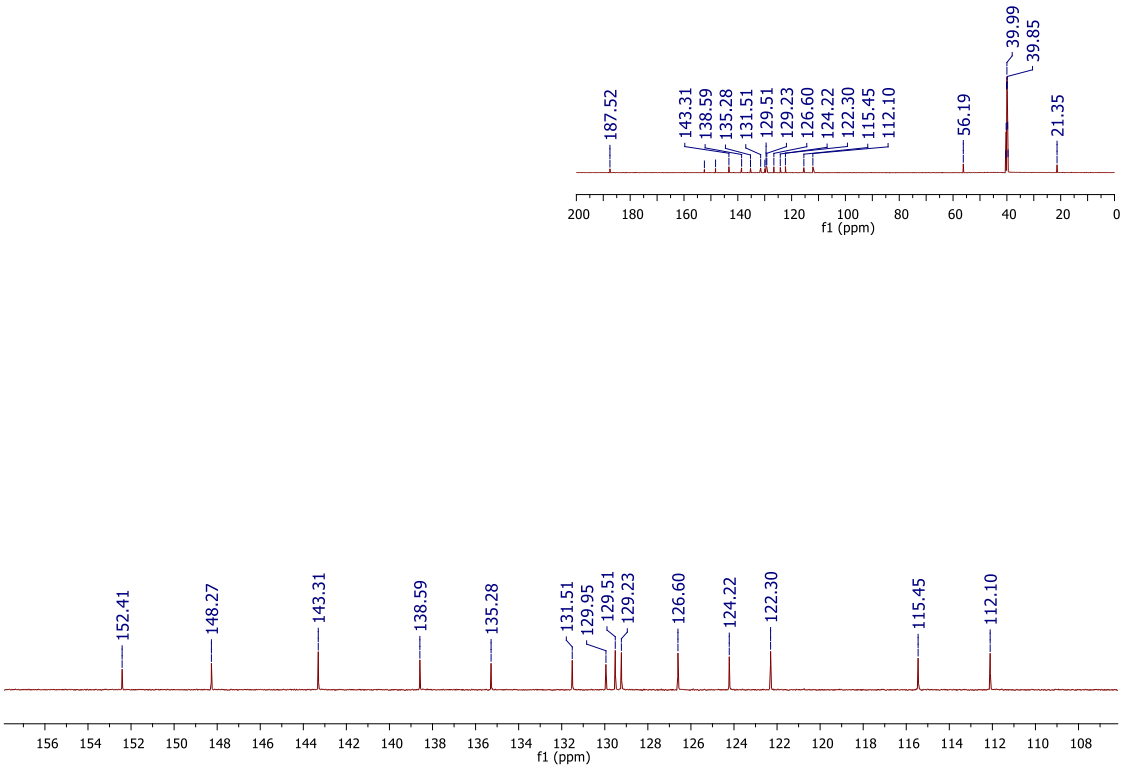

Figure S17. iii) UV-Vis spectrum of **hybrid 17** (MeOH/H_2O (3:1))

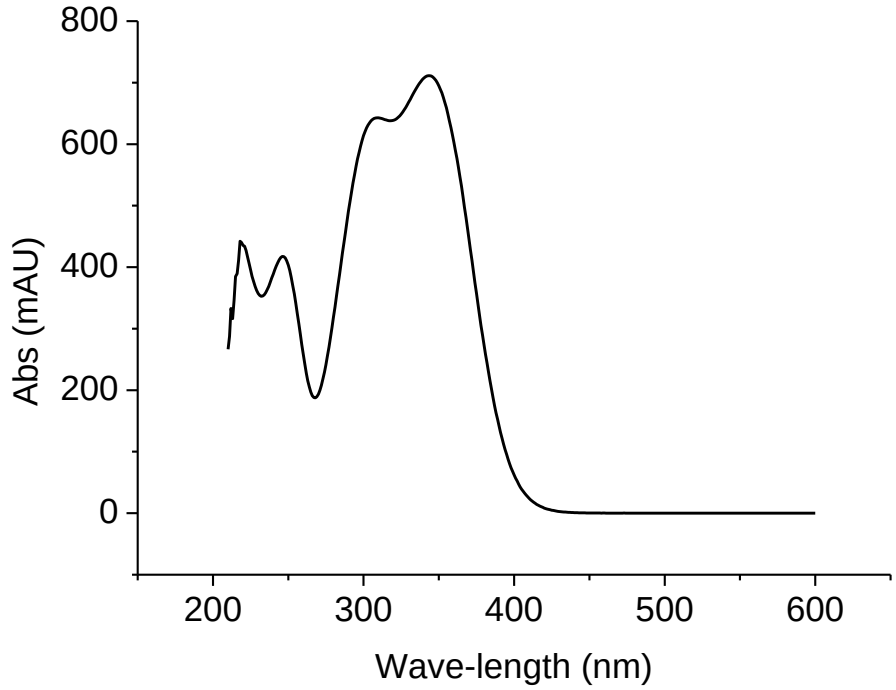

Figure S17. iv) HPLC chromatogram of **hybrid 17** (MeOH/H_2O (3:1))

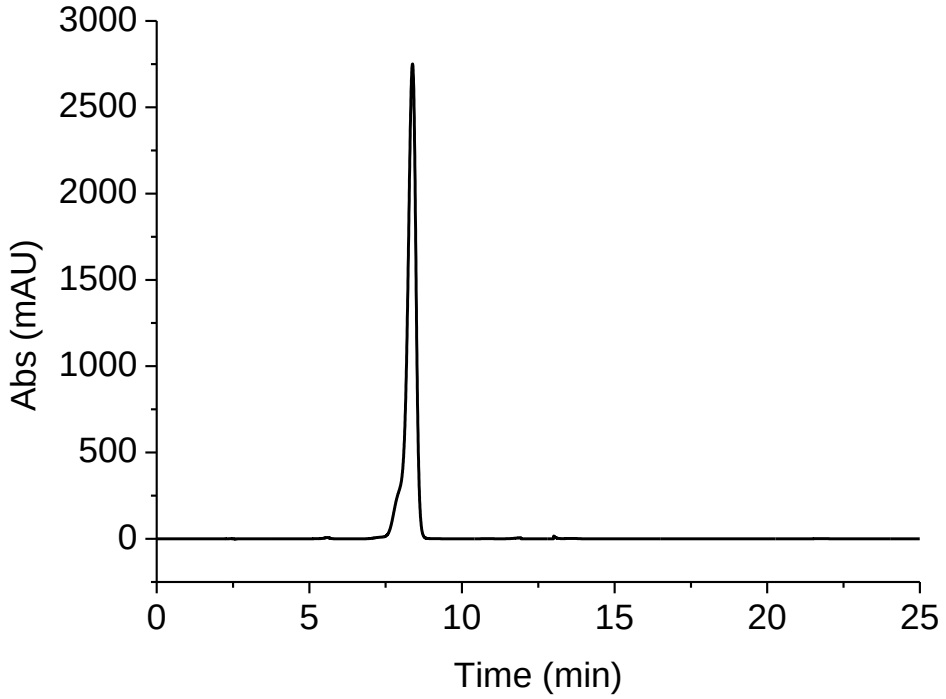

Figure S18. i) ^{1}H NMR spectrum of **hybrid 18** (400 MHz; DMSO-d_6)

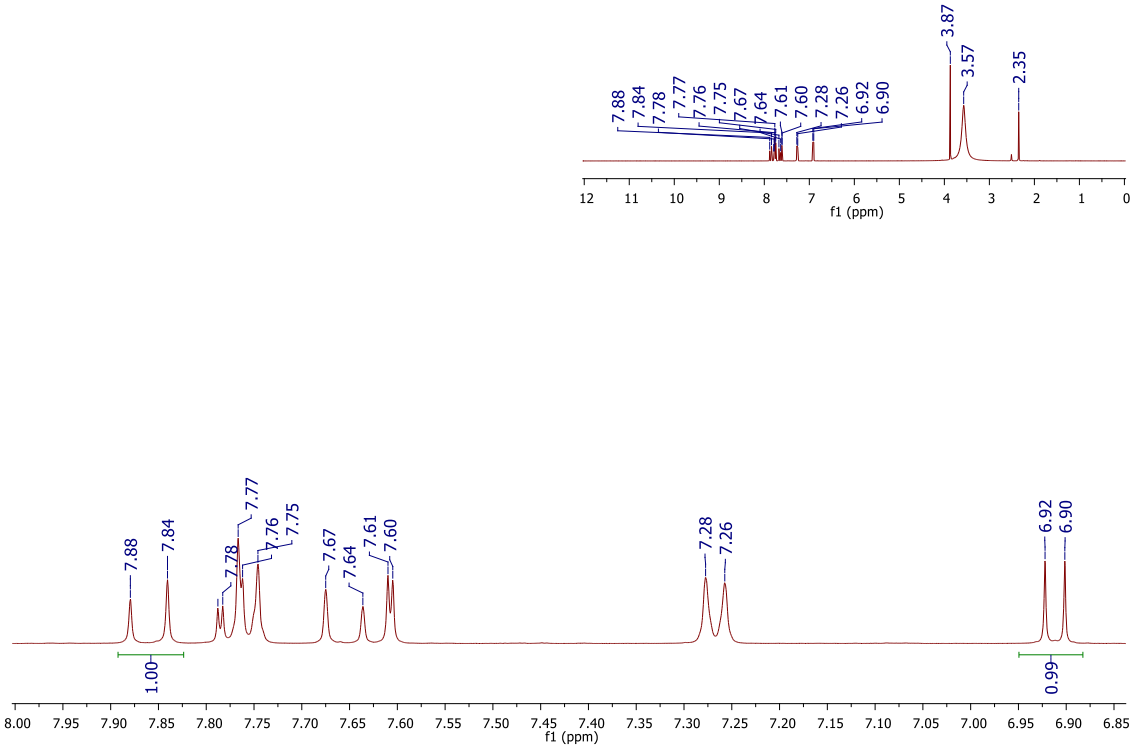

Figure S18. ii) ^{13}C NMR spectrum of **hybrid 18** (150 MHz; DMSO-d_6)

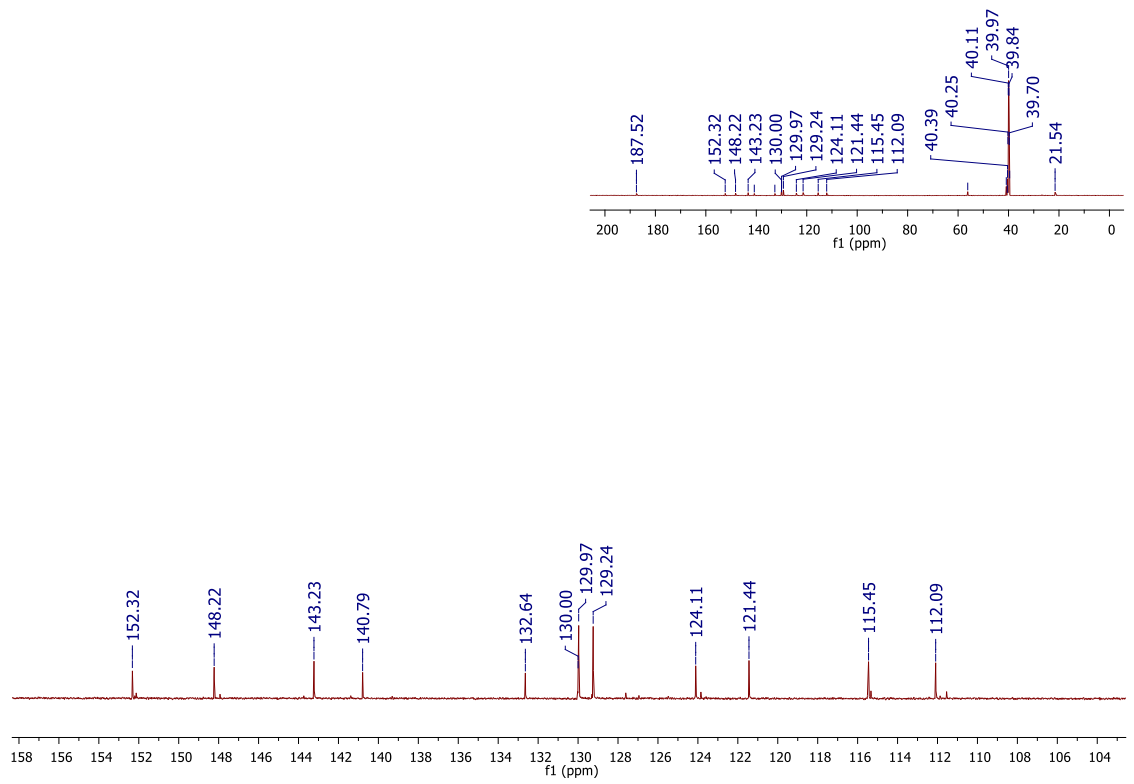

Figure S18. iii) UV-Vis spectrum of **hybrid 18** (MeOH/H_2O (3:1))

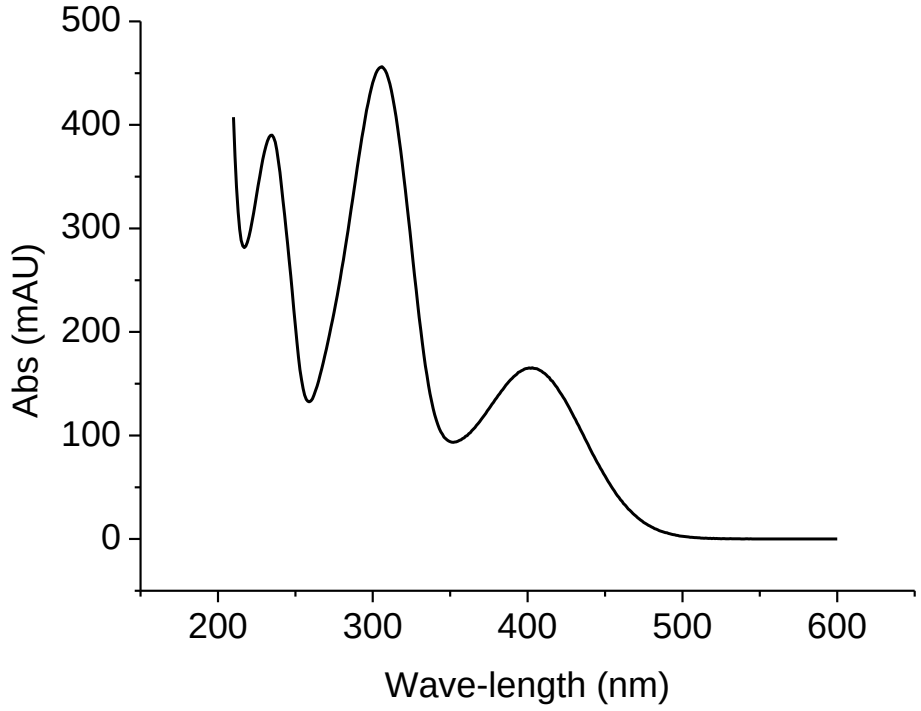

Figure S18. iv) HPLC chromatogram of **hybrid 18** (MeOH/H_2O (3:1))

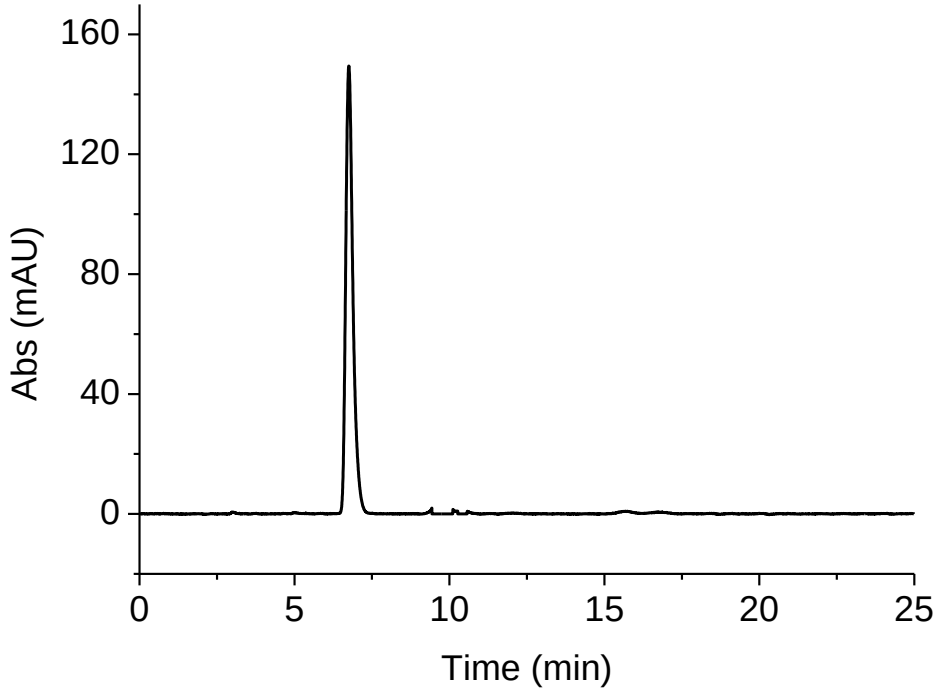

Figure S19. i) ^{1}H NMR spectrum of **hybrid 19** (600 MHz; DMSO-d_6)

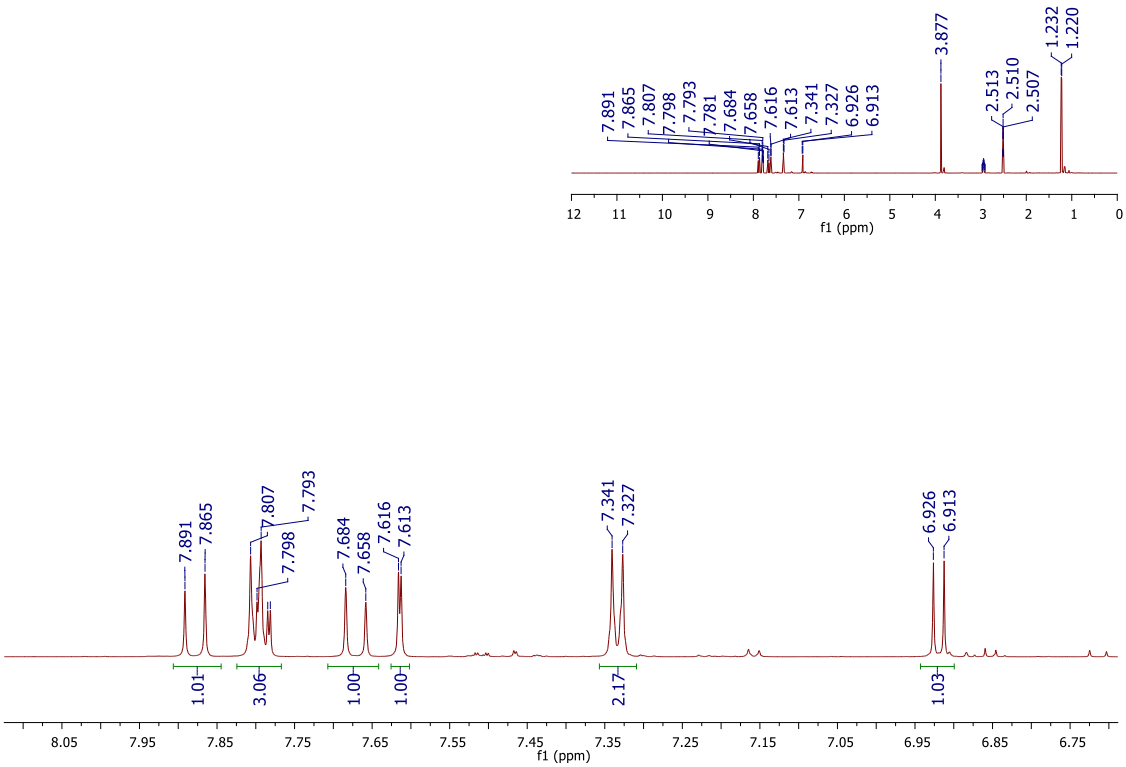

Figure S19. ii) ^{13}C NMR spectrum of **hybrid 19** (150 MHz; DMSO-d_6)

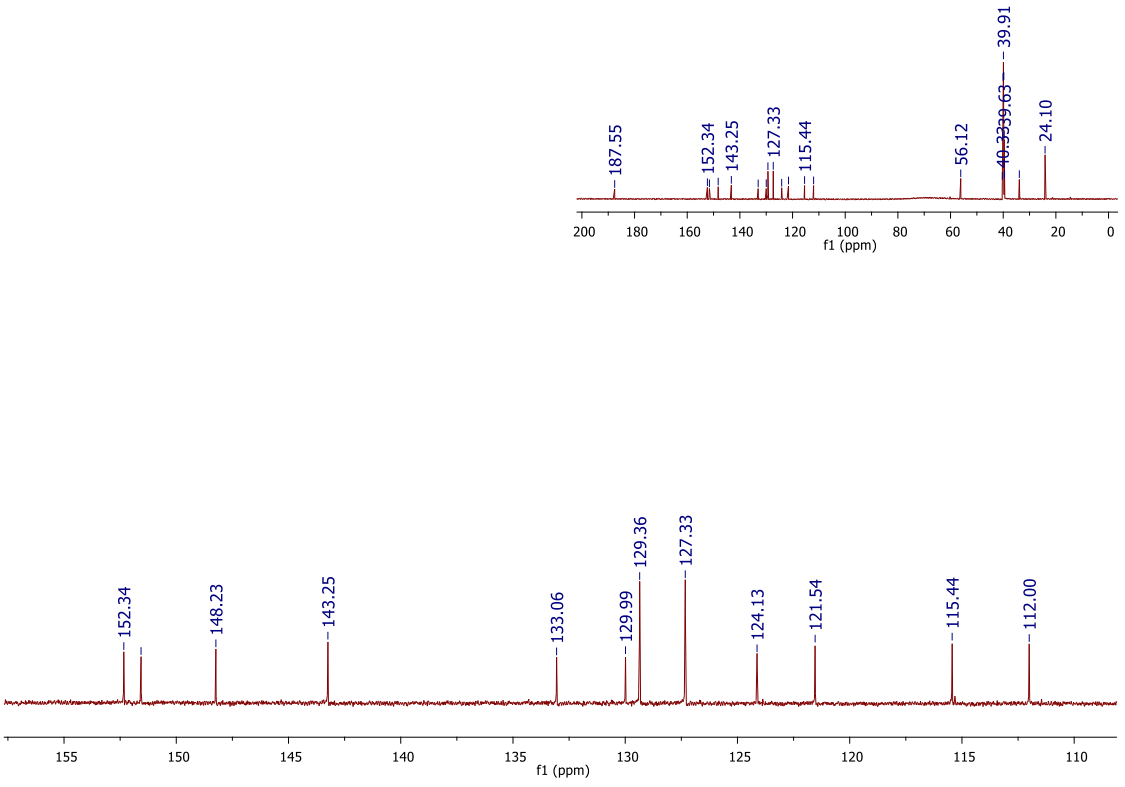

Figure S19. iii) UV-Vis spectrum of **hybrid 19** (MeOH/H_2O (3:1))

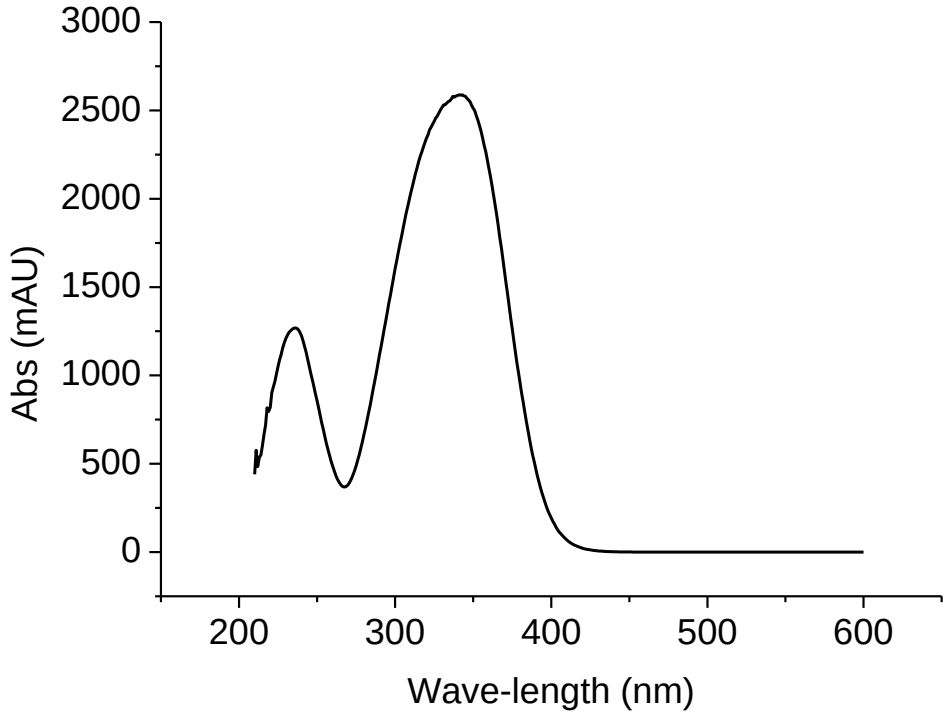

Figure S19. iv) HPLC chromatogram of **hybrid 19** (MeOH/H_2O (3:1))

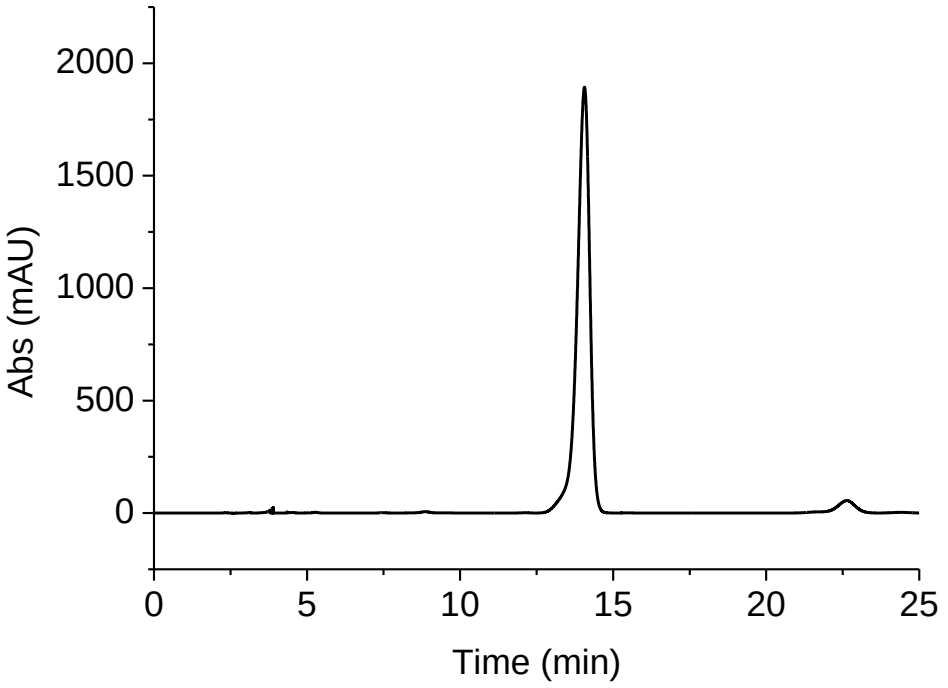

Figure S20. i) ^{1}H NMR spectrum of **hybrid 20** (600 MHz; DMSO-d_6)

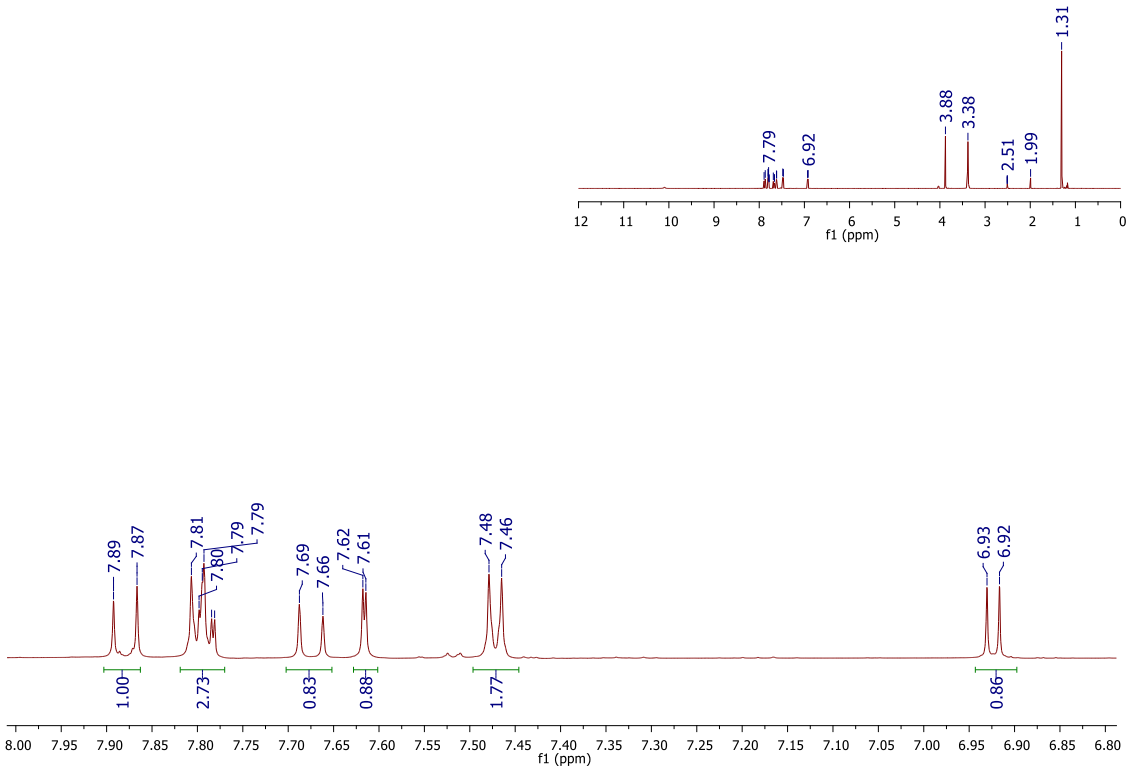

Figure S20. ii) ^{13}C NMR spectrum of **hybrid 20** (100 MHz; DMSO-d_6)

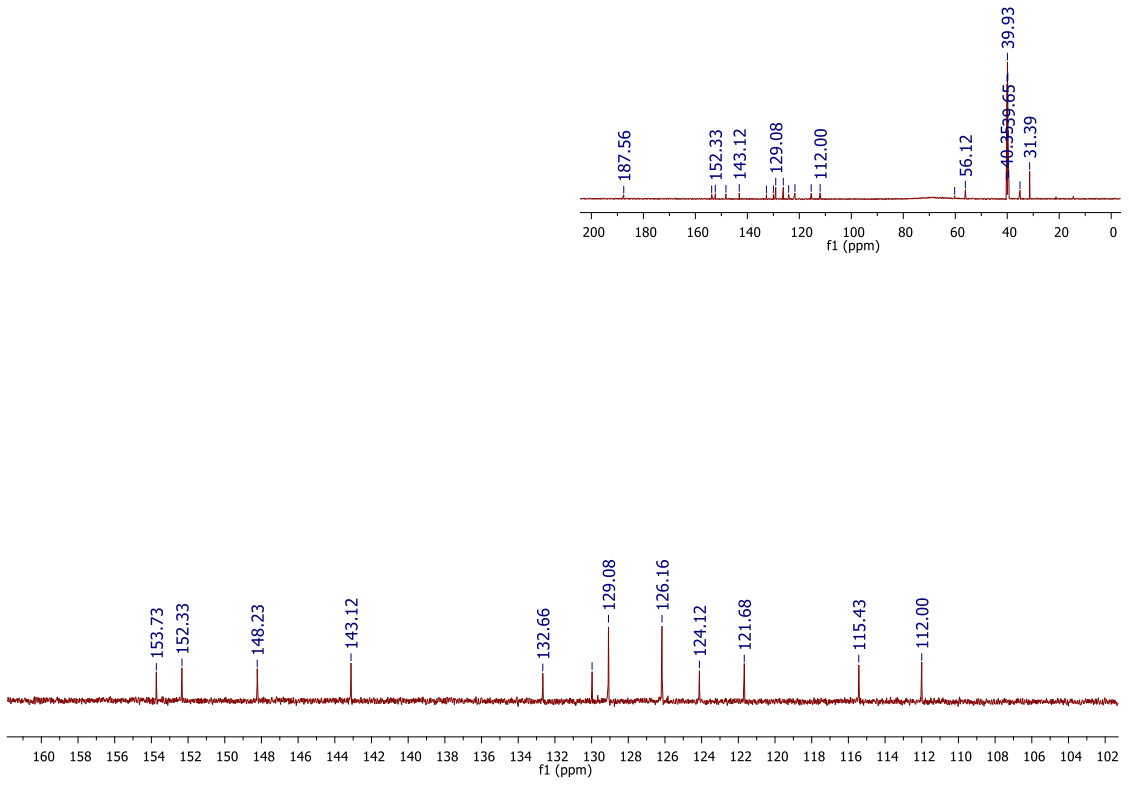

Figure S20. iii) UV-Vis spectrum of **hybrid 20** (MeOH/H_2O (3:1))

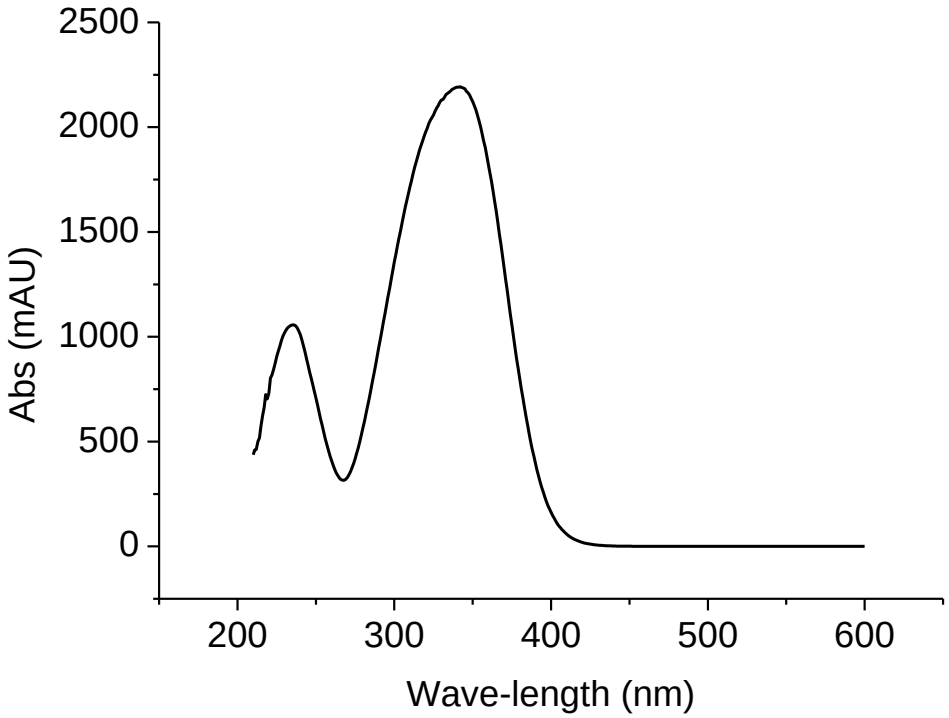

Figure S20. iv) HPLC chromatogram of **hybrid 20** (MeOH/H_2O (3:1))

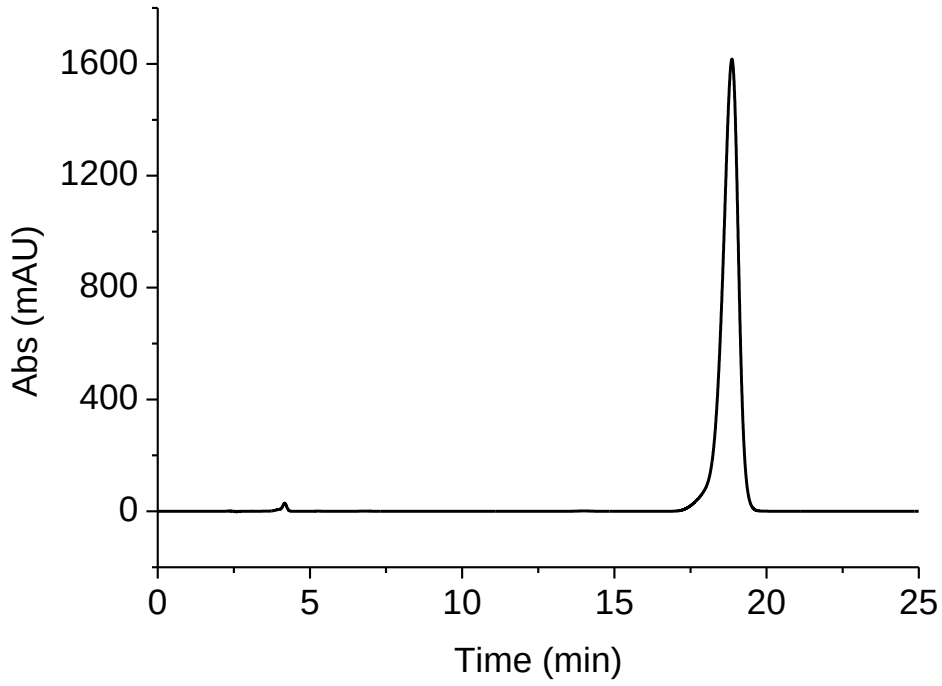

Figure S21. i) ^{1}H NMR spectrum of **hybrid 21** (300 MHz; DMSO-d_6)

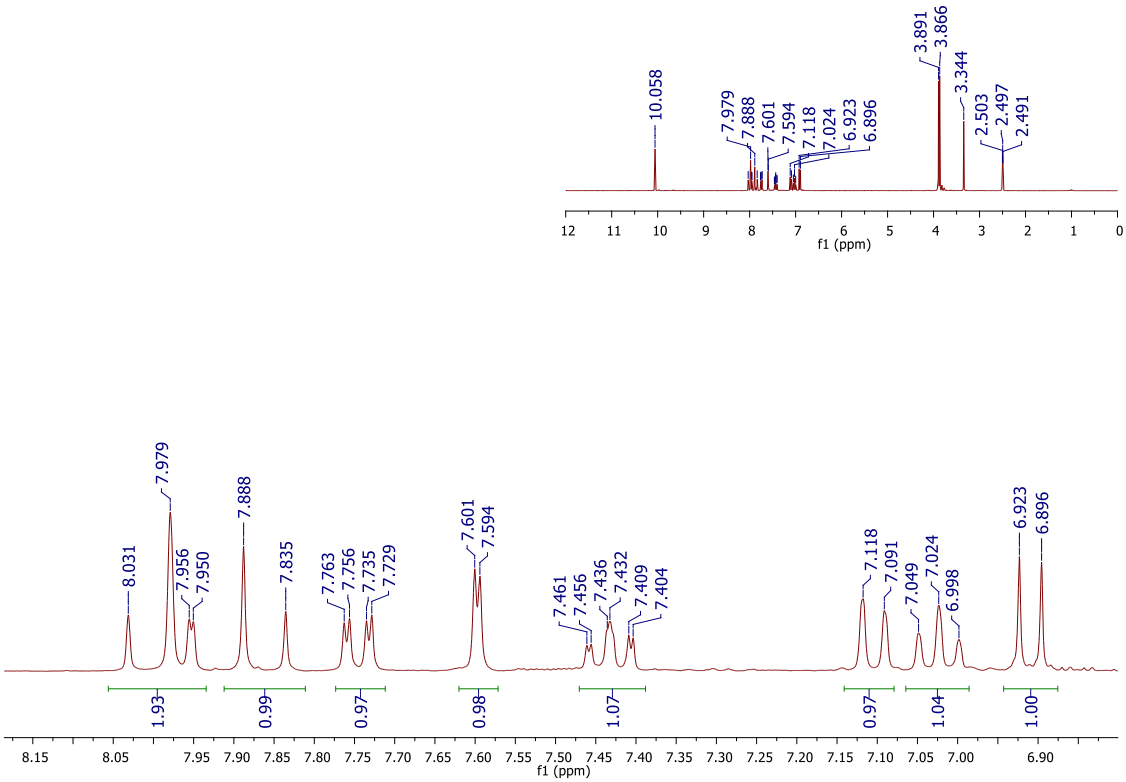

Figure S21. ii) ^{13}C NMR spectrum of **hybrid 21** (150 MHz; DMSO-d_6)

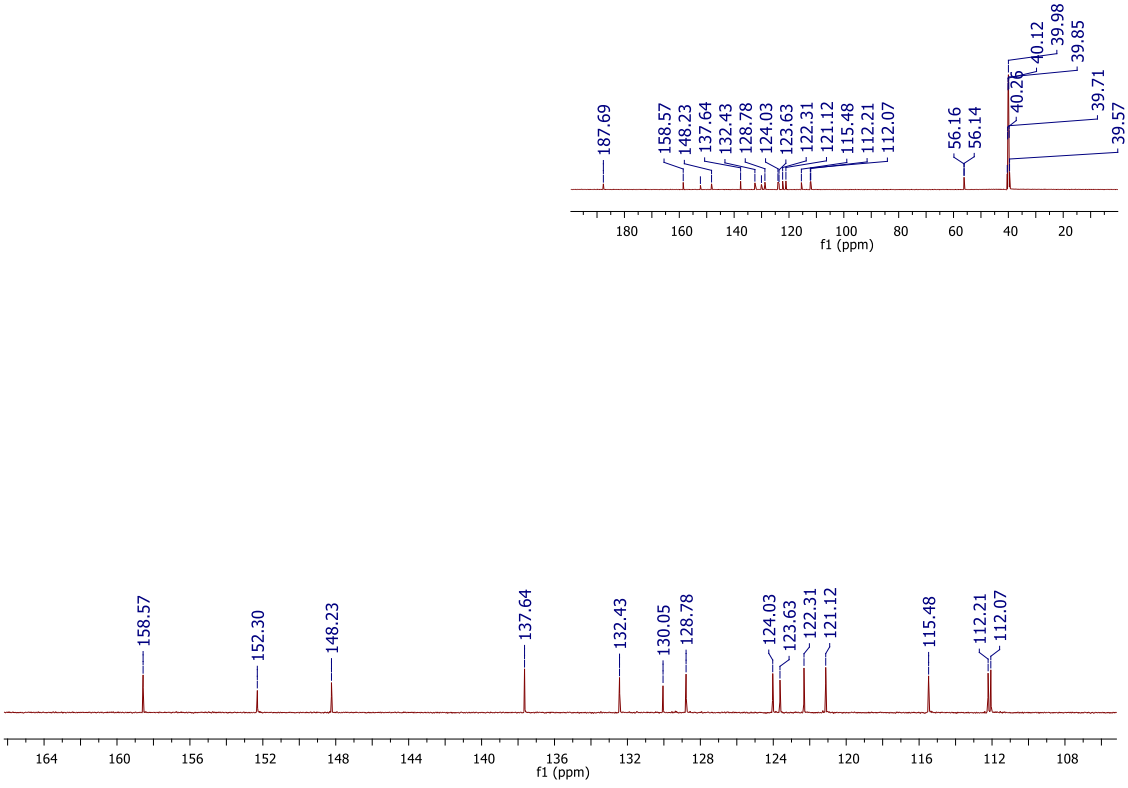

Figure S21. iii) UV-Vis spectrum of **hybrid 21** (MeOH/H_2O (3:1))

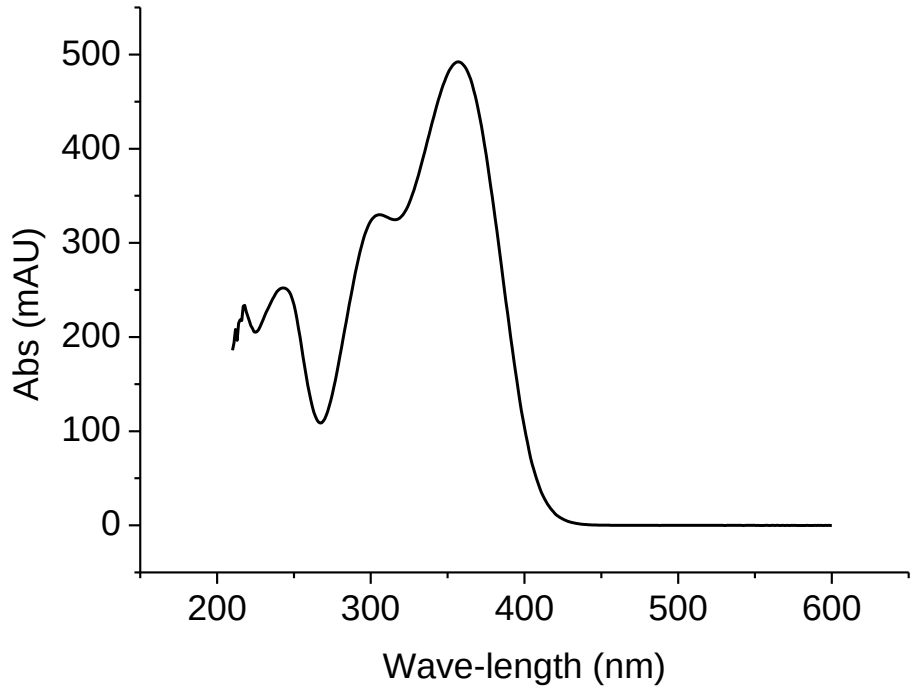

Figure S21. iv) HPLC chromatogram of **hybrid 21** (MeOH/H_2O (3:1))

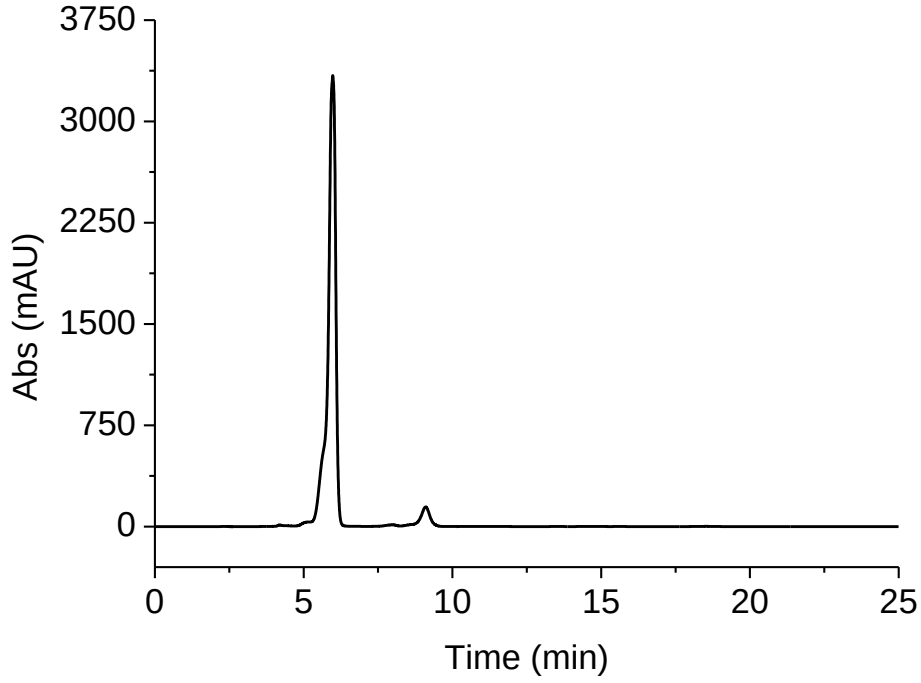

Figure S22. i) ^{1}H NMR spectrum of **hybrid 22** (300 MHz; DMSO-d_6)

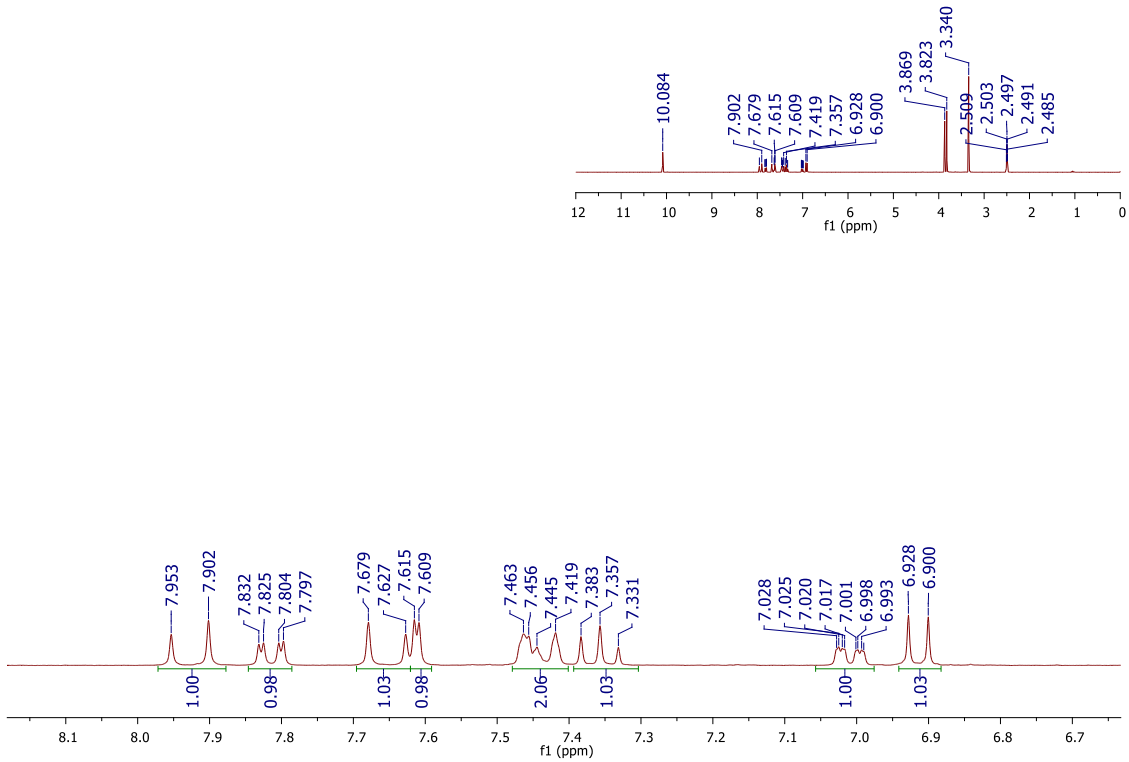

Figure S22. ii) ^{13}C NMR spectrum of **hybrid 22** (150 MHz; DMSO-d_6)

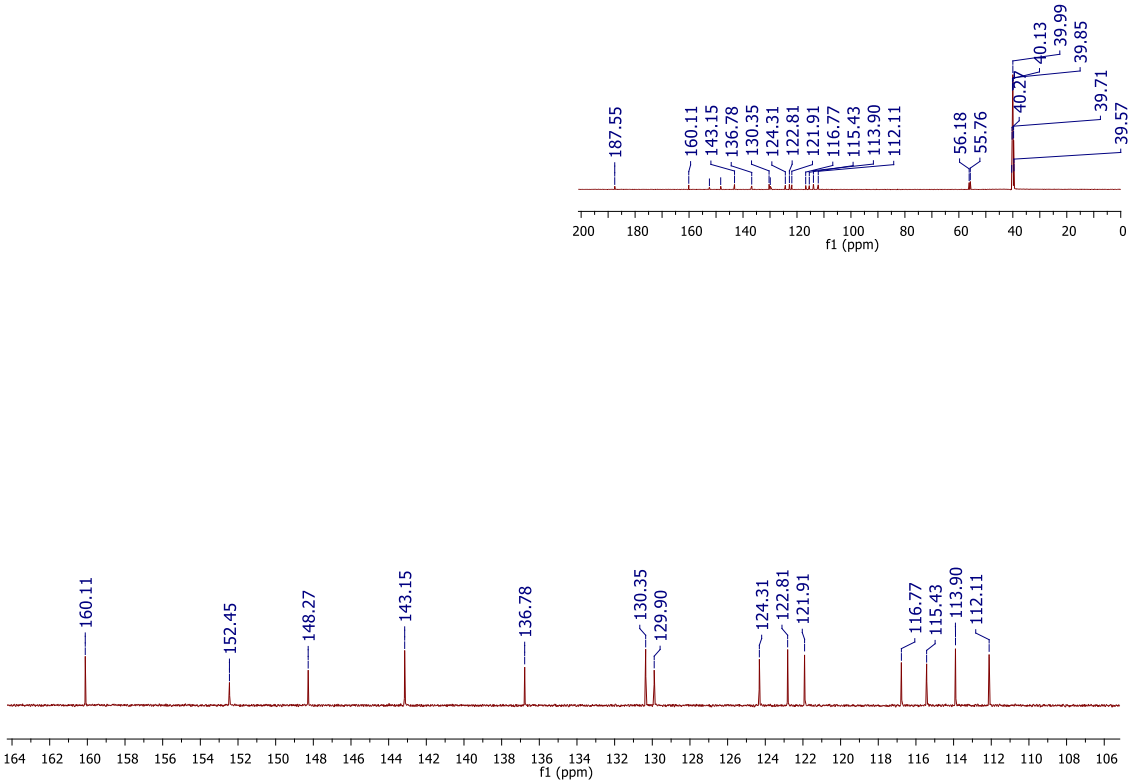

Figure S22. iii) UV-Vis spectrum of **hybrid 22** (MeOH/H_2O (3:1))

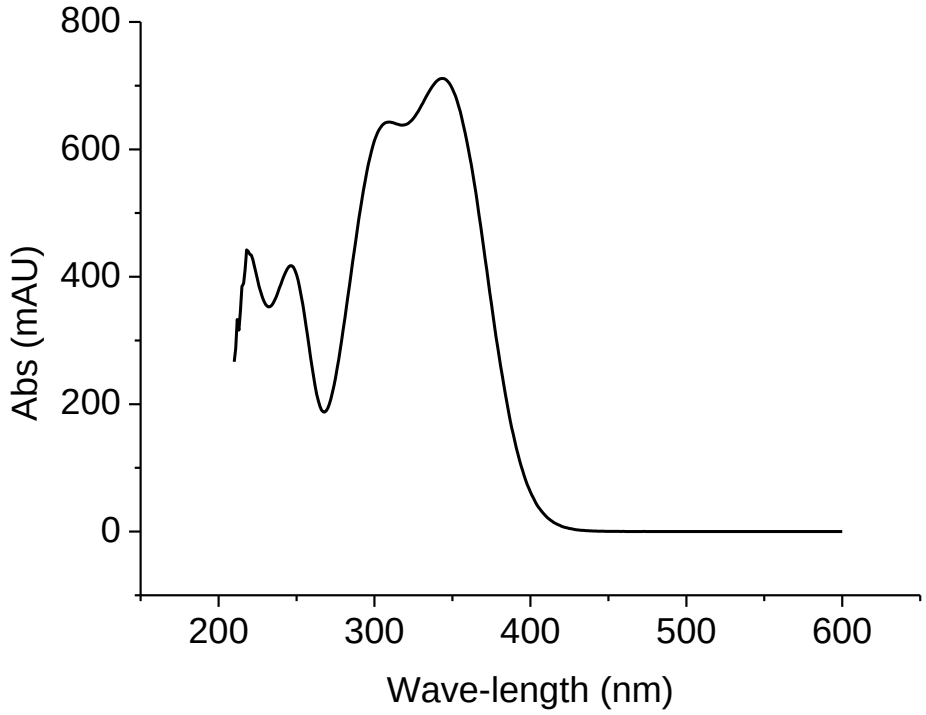

Figure S22. iv) HPLC chromatogram of **hybrid 22** (MeOH/H_2O (3:1))

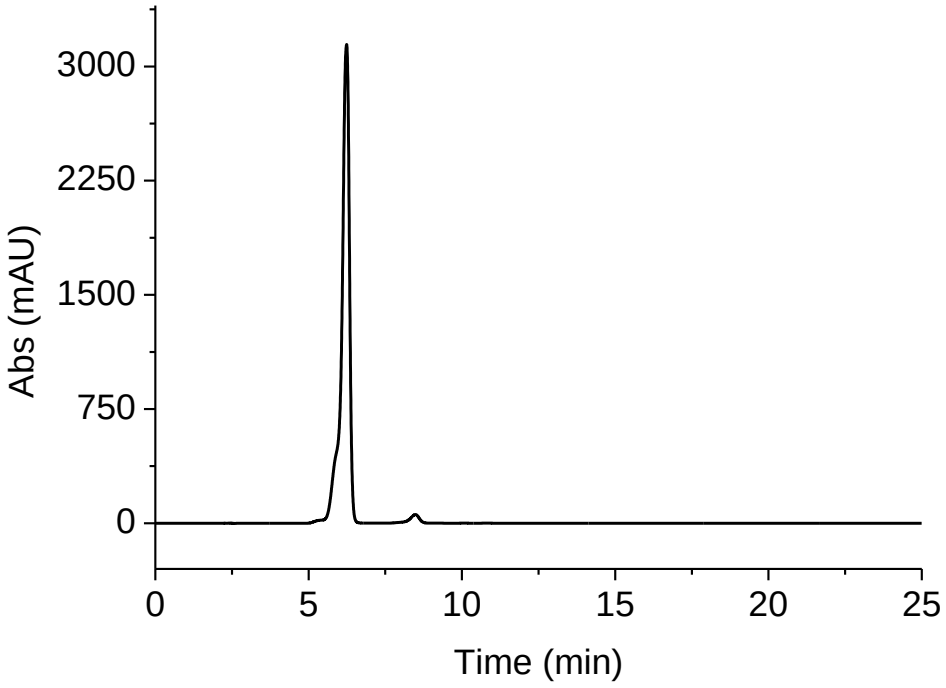

Figure S23. i) ^{1}H NMR spectrum of **hybrid 23** (400 MHz; DMSO-d_6)

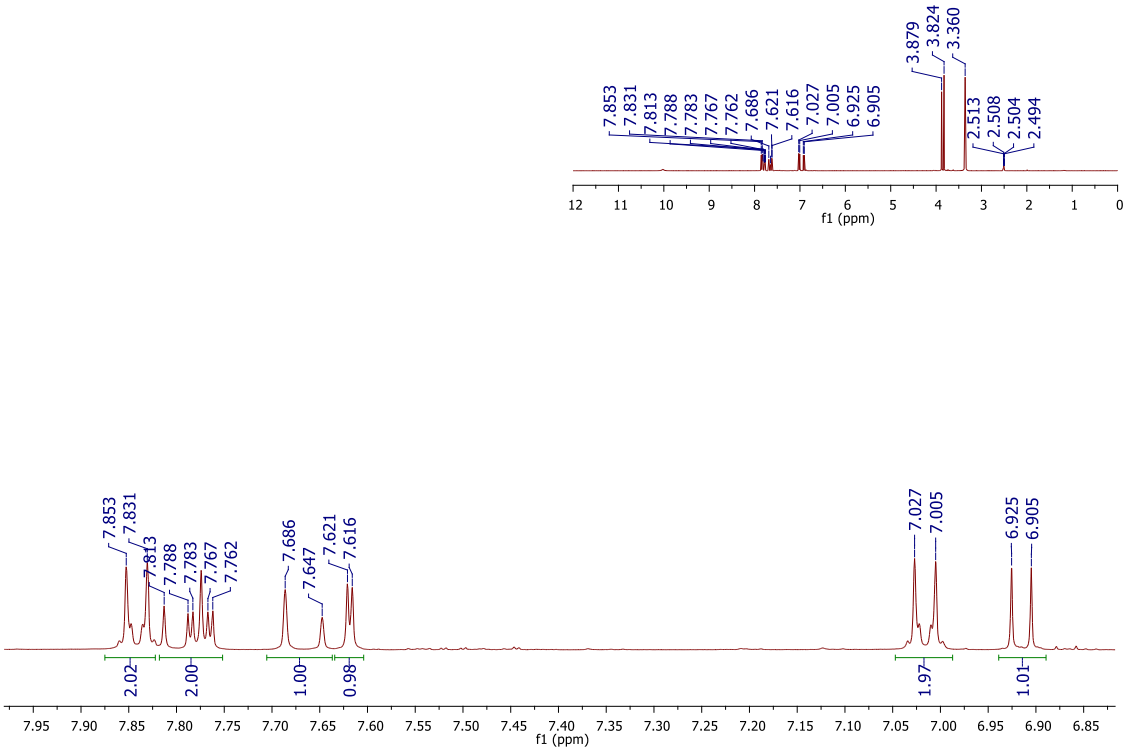

Figure S23. ii) ^{13}C NMR spectrum of **hybrid 23** (150 MHz; DMSO-d_6)

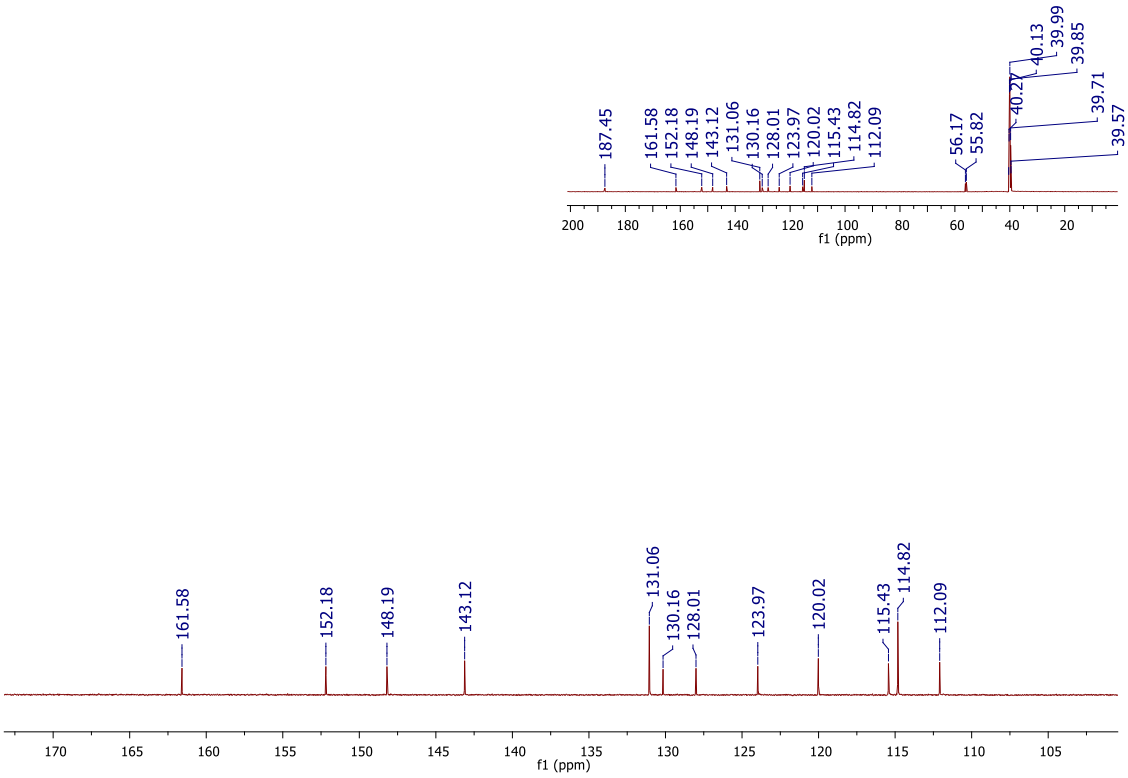

Figure S23. iii) UV-Vis spectrum of **hybrid 23** (MeOH/H_2O (3:1))

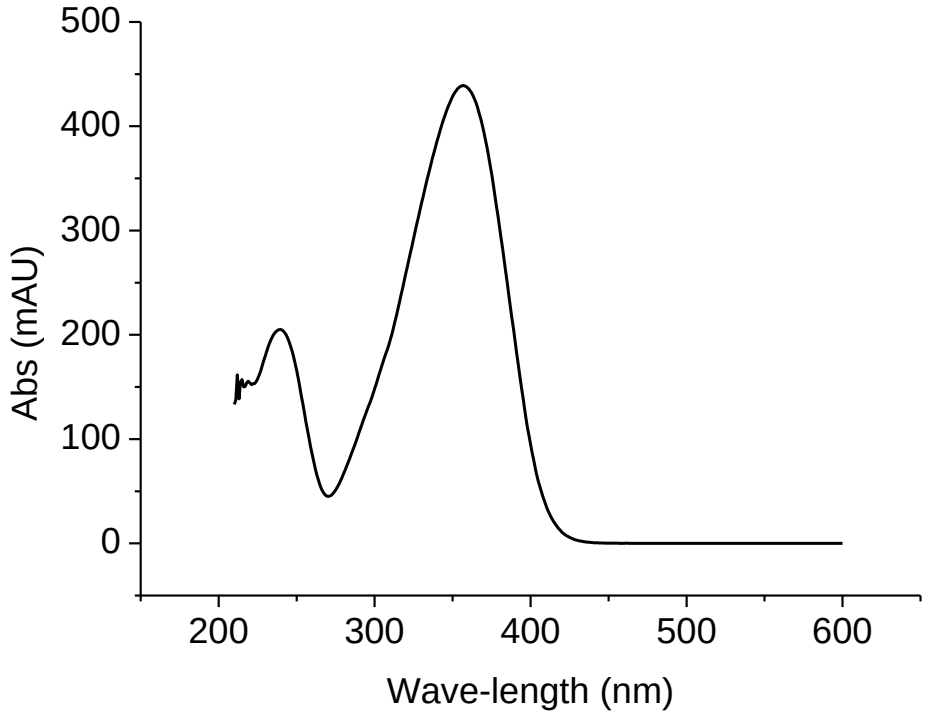

Figure S23. iv) HPLC chromatogram of **hybrid 23** (MeOH/H_2O (3:1))

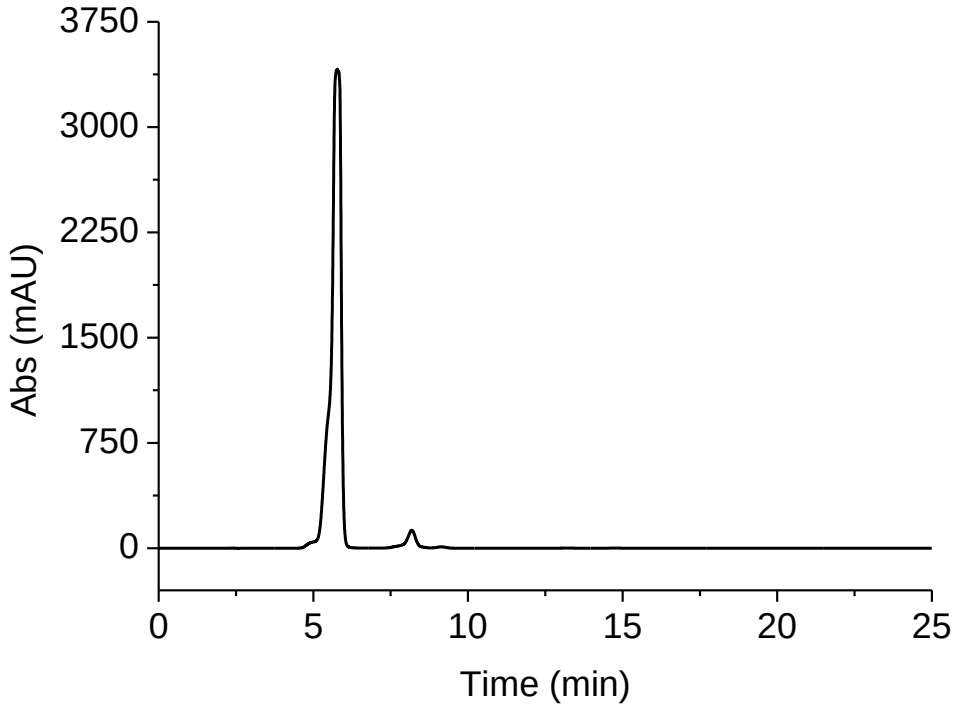

Figure S24. i) ^{1}H NMR spectrum of **hybrid 24** (600 MHz; DMSO-d_6)

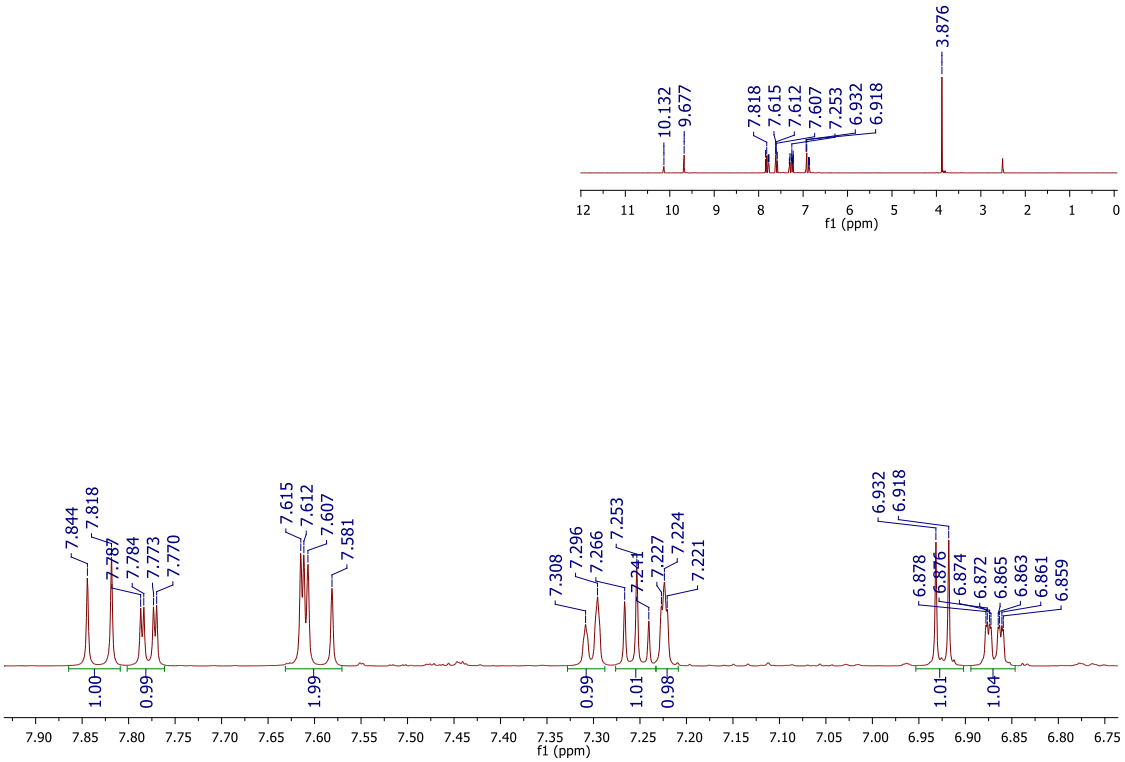

Figure S24. ii) ^{13}C NMR spectrum of **hybrid 24** (150 MHz; DMSO-d_6)

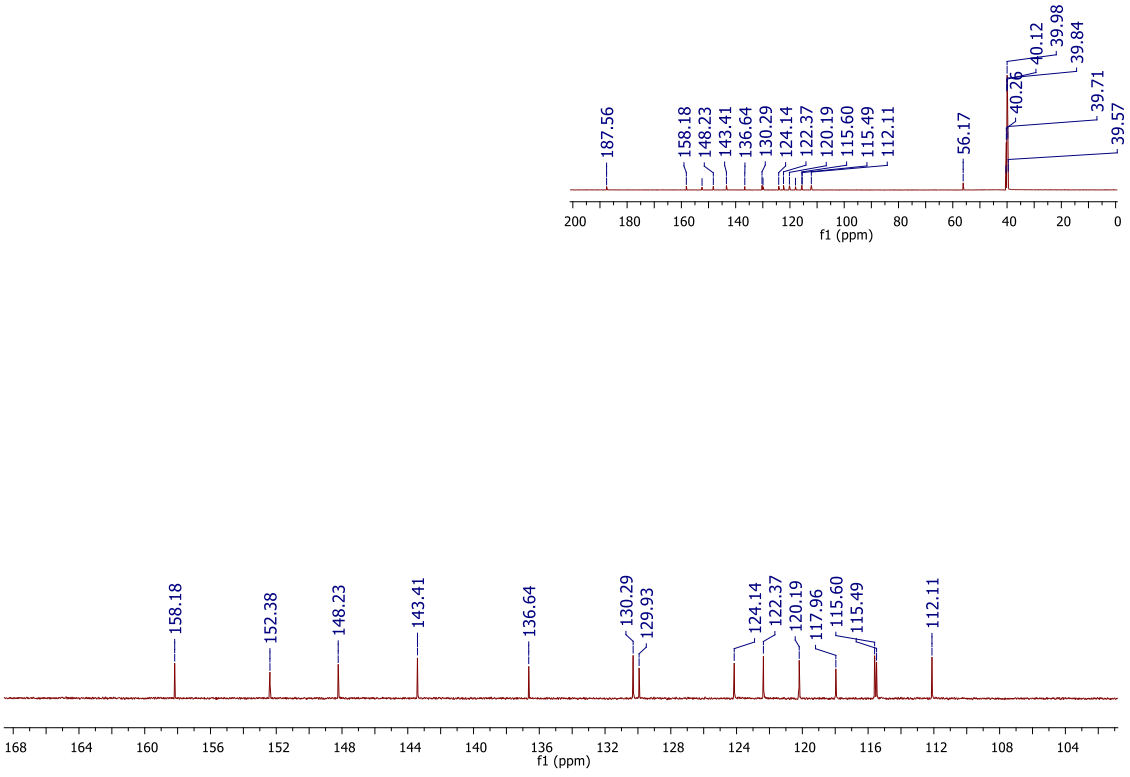

Figure S24. iii) UV-Vis spectrum of **hybrid 24** (MeOH/H_2O (3:1))

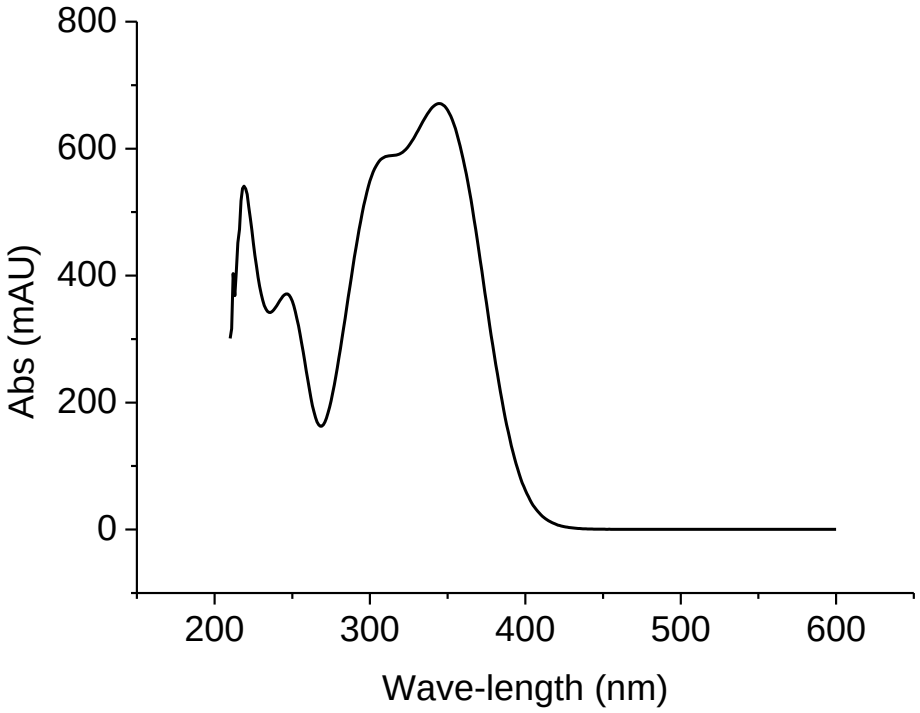

Figure S24. iv) HPLC chromatogram of **hybrid 24** (MeOH/H_2O (3:1))

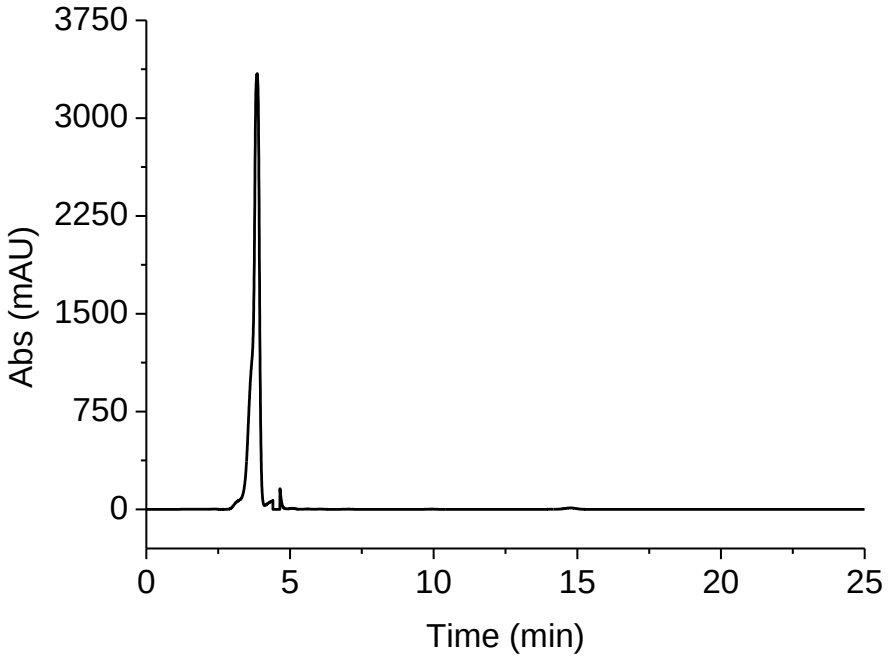

Figure S25. i) ^{1}H NMR spectrum of **hybrid 25** (600 MHz; DMSO-d_6)

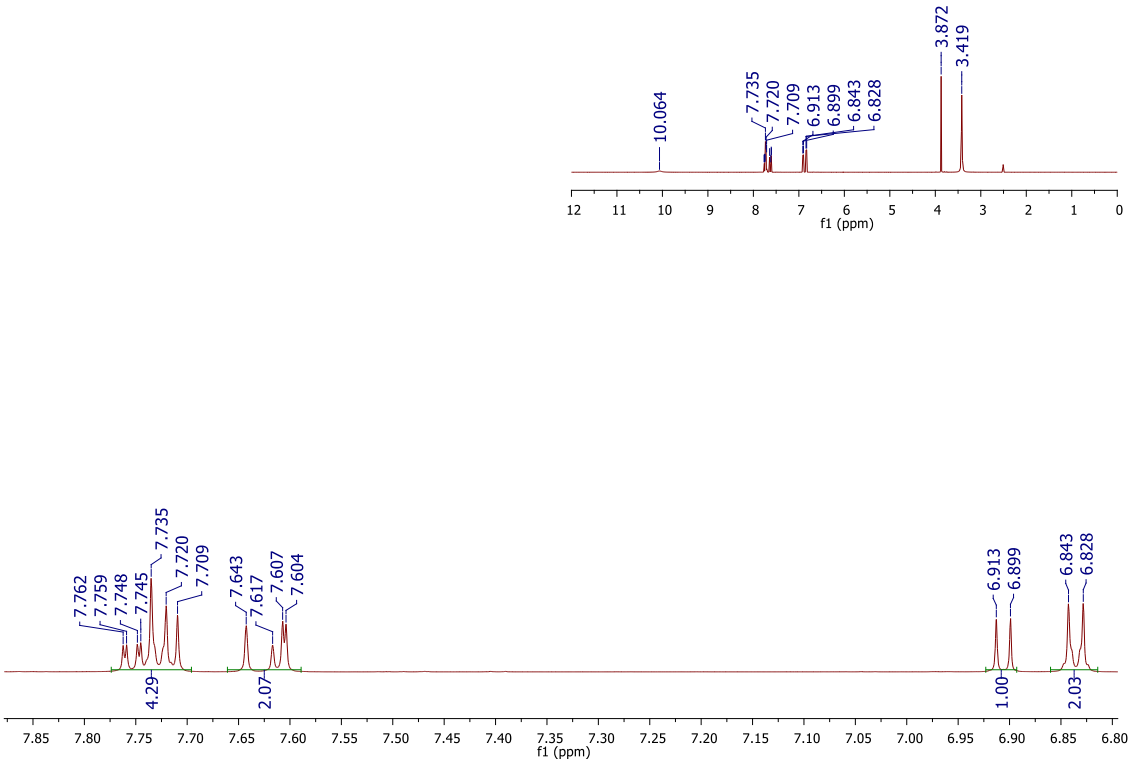

Figure S25. ii) ^{13}C NMR spectrum of **hybrid 25** (150 MHz; DMSO-d_6)

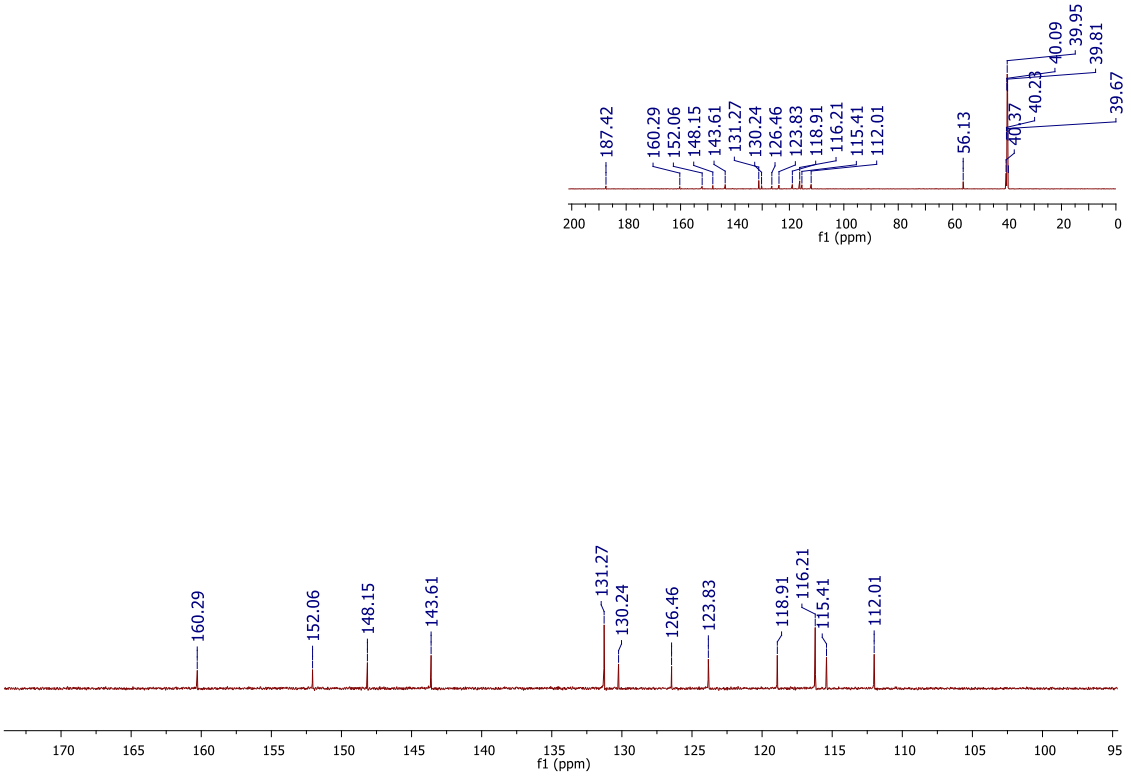

Figure S25. iii) UV-Vis spectrum of **hybrid 25** (MeOH/H_2O (3:1))

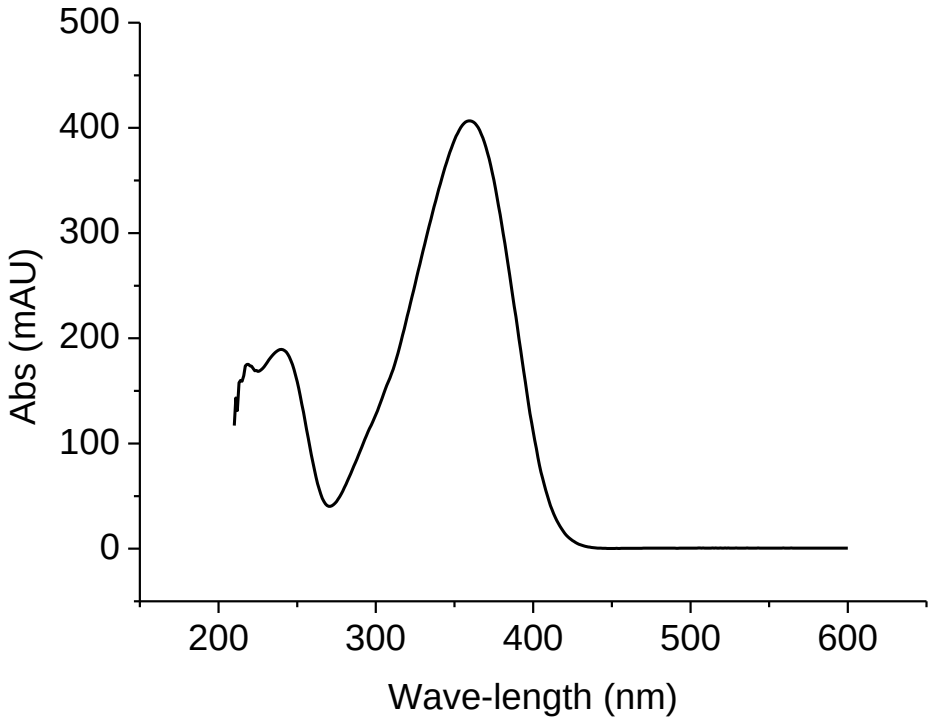

Figure S25. iv) HPLC chromatogram of **hybrid 25** (MeOH/H_2O (3:1))

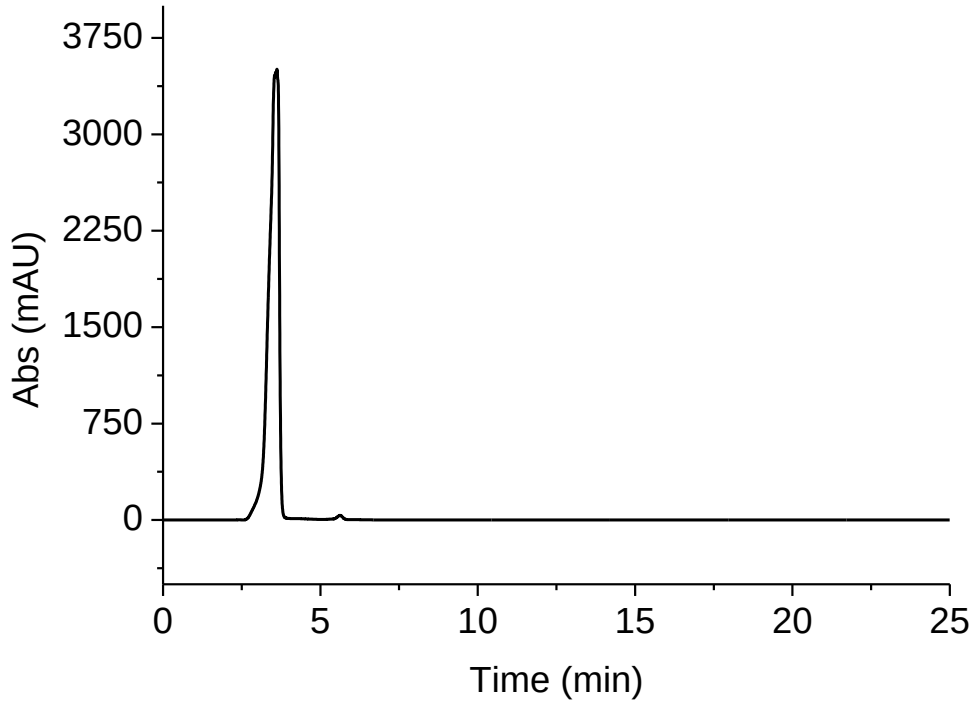

Figure S26. i) ^{1}H NMR spectrum of **hybrid 26** (400 MHz; DMSO-d_6)

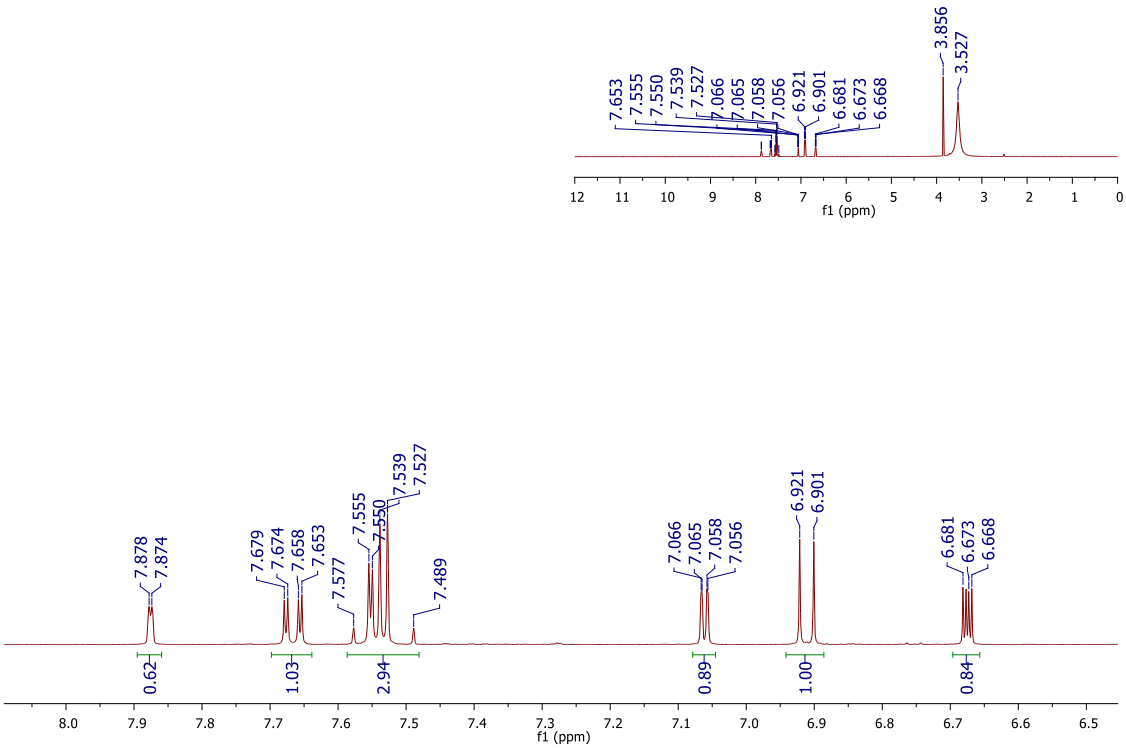

Figure S26. ii) ^{13}C NMR spectrum of **hybrid 26** (150 MHz; DMSO-d_6)

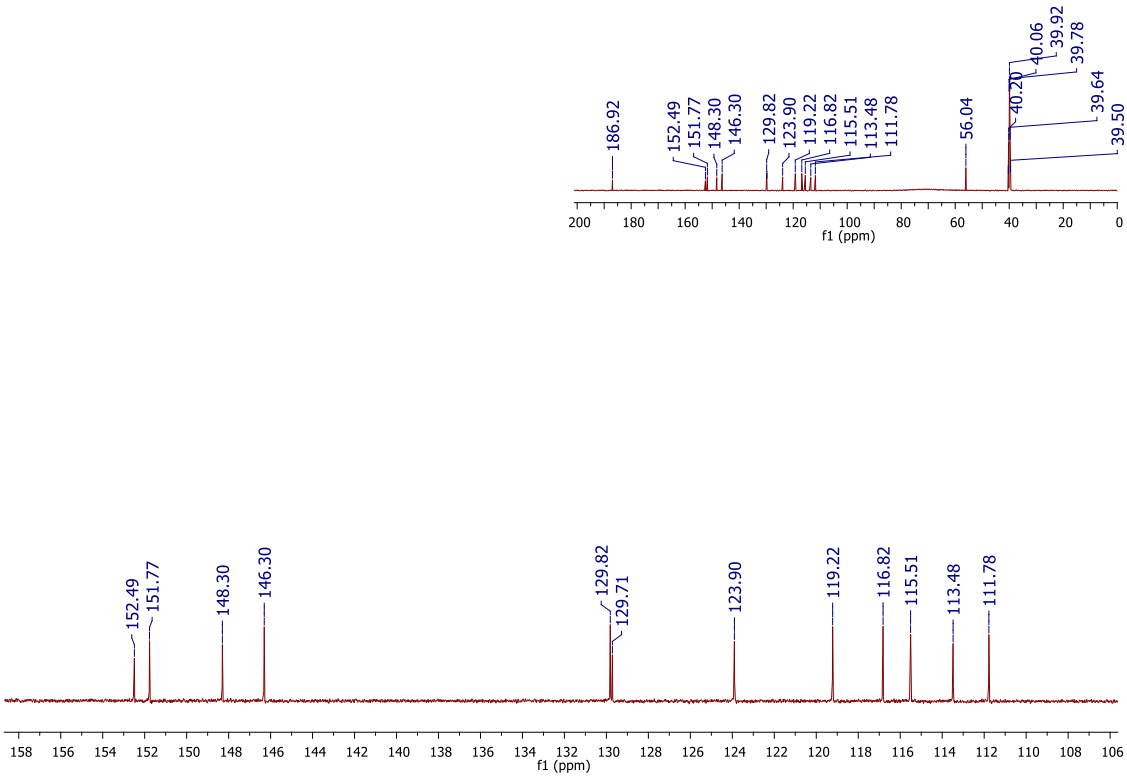

Figure S26. iii) UV-Vis spectrum of **hybrid 26** (MeOH/H_2O (3:1))

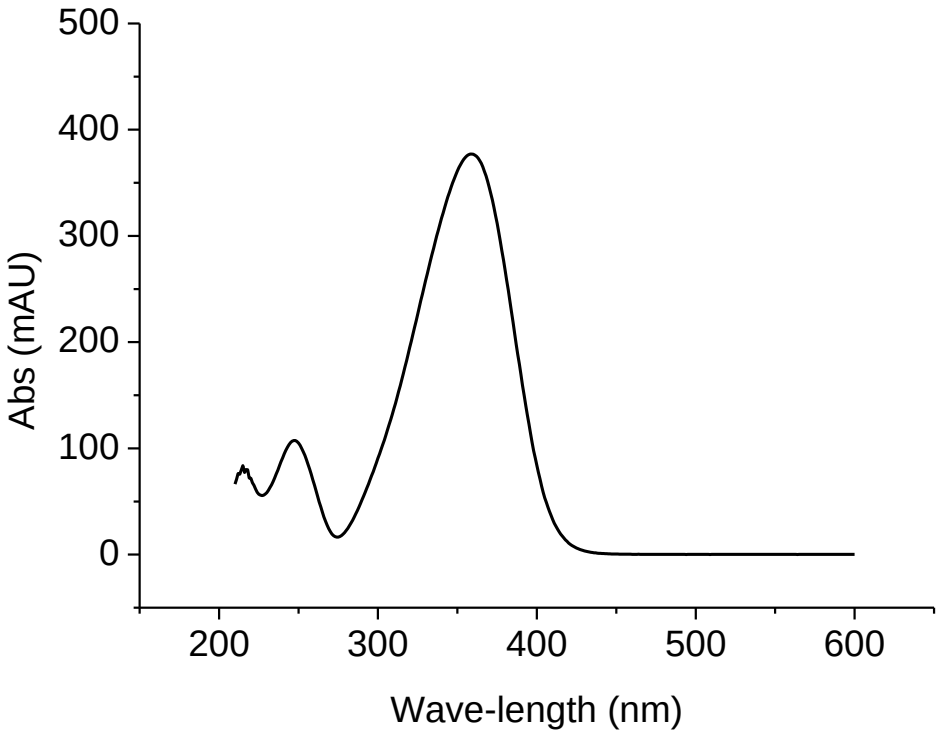

Figure S26. iv) HPLC chromatogram of **hybrid 26** (MeOH/H_2O (3:1))

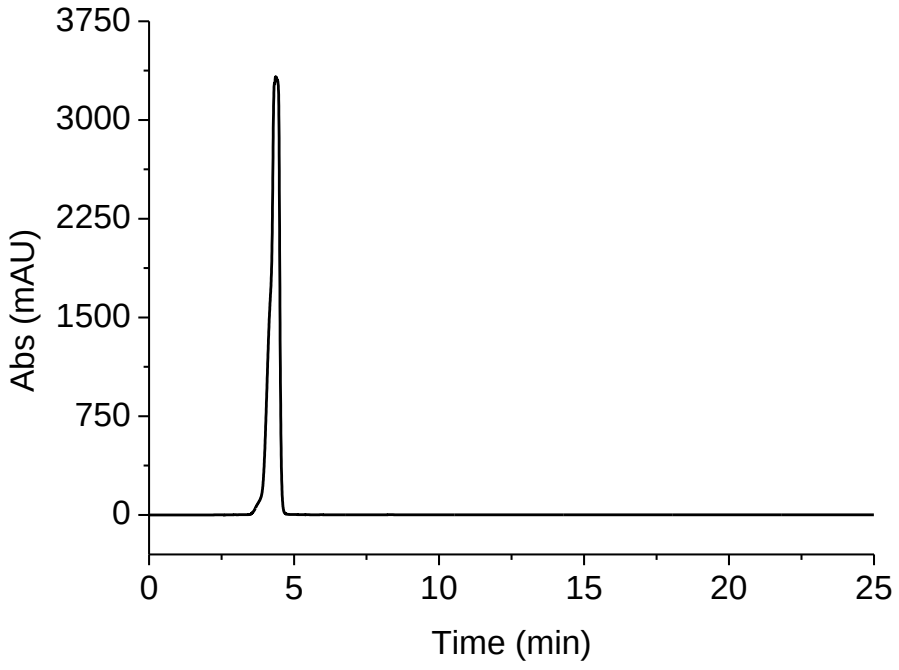

Figure S27. i) ^{1}H NMR spectrum of **hybrid 27** (400 MHz; DMSO-d_6)

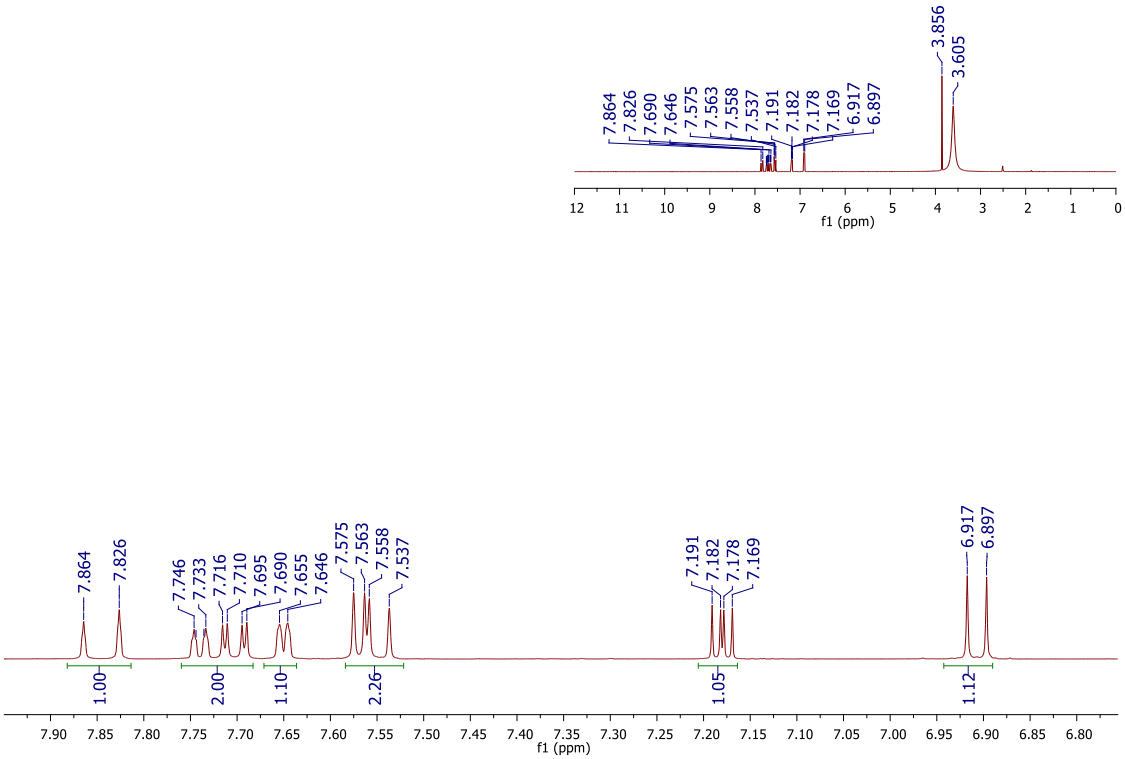

Figure S27. ii) ^{13}C NMR spectrum of **hybrid 27** (150 MHz; DMSO-d_6)

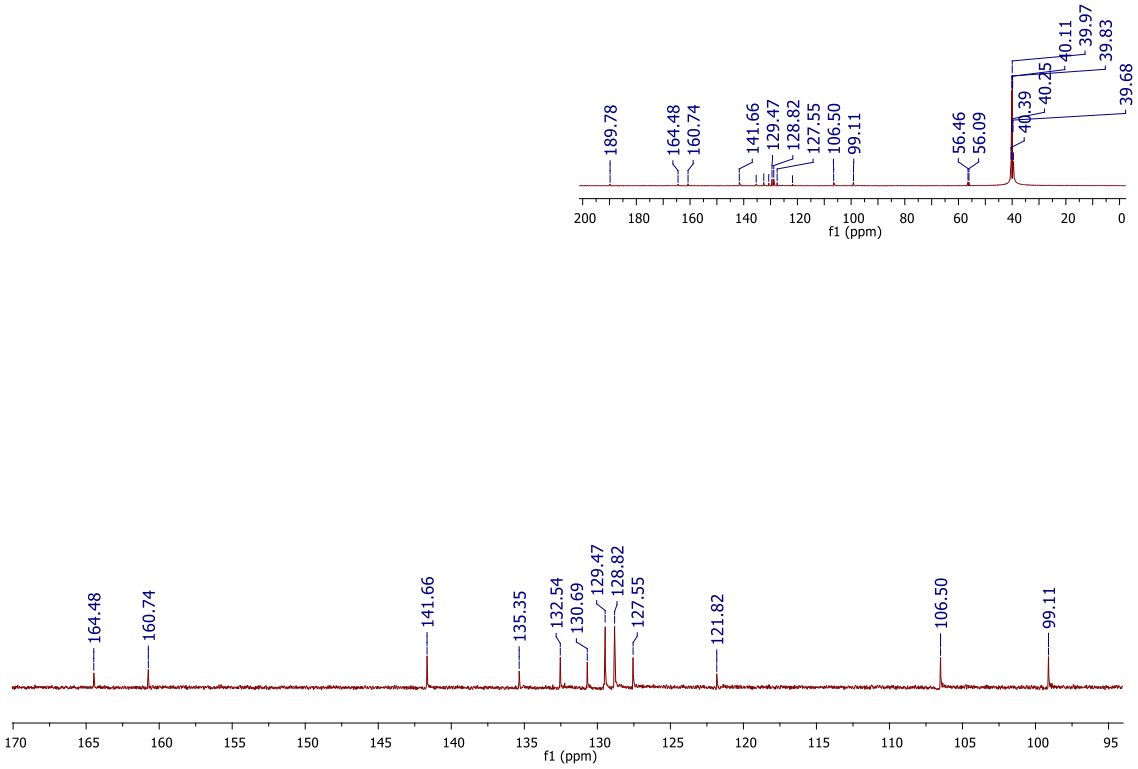

Figure S27. iii) UV-Vis spectrum of **hybrid 27** (MeOH/H_2O (3:1))

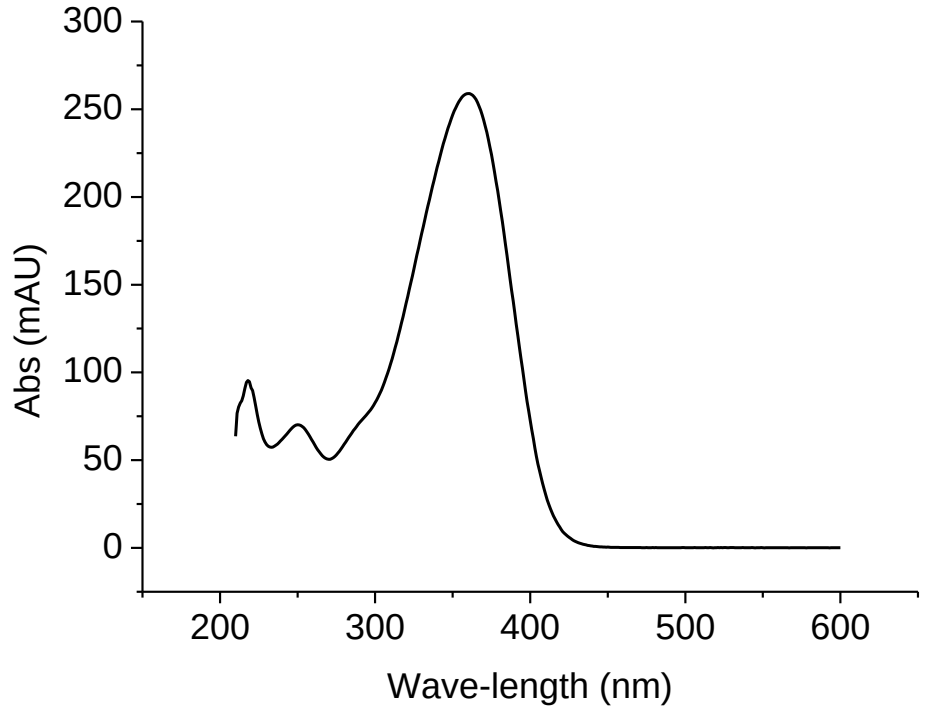

Figure S27. iv) HPLC chromatogram of **hybrid 27** (MeOH/H_2O (3:1))

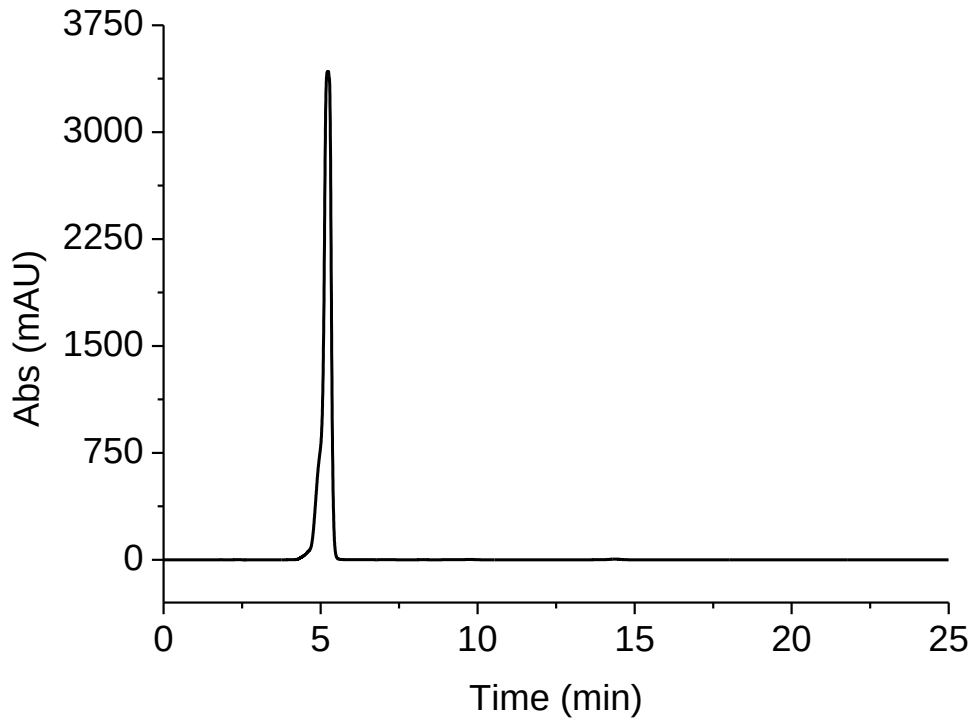

Figure S28. i) ^{1}H NMR spectrum of **hybrid 28** (400 MHz; DMSO-d_6)

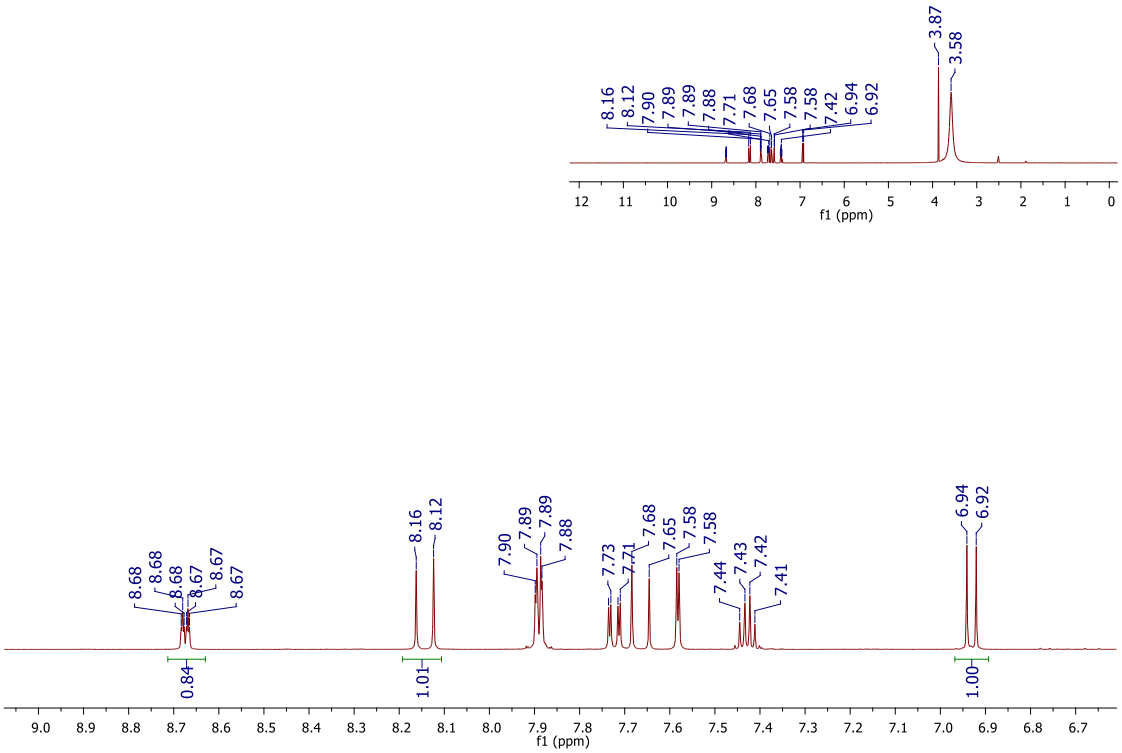

Figure S28. ii) ^{13}C NMR spectrum of **hybrid 28** (150 MHz; DMSO-d_6)

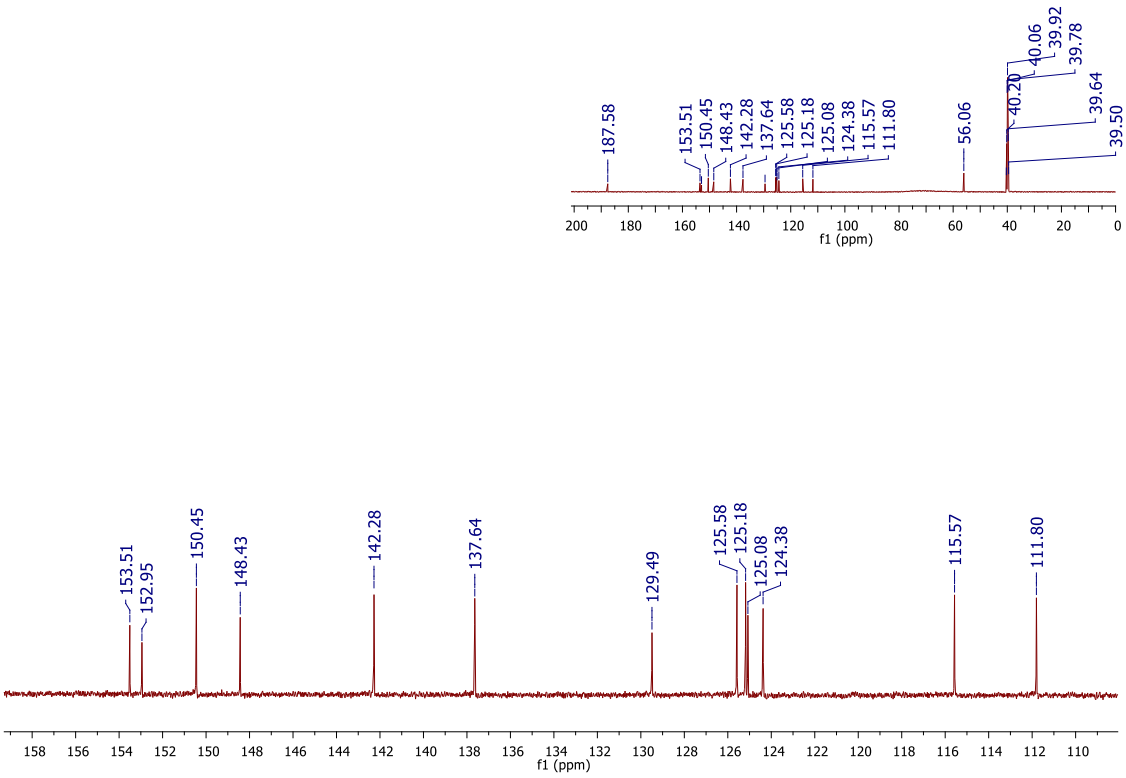

Figure S28. iii) UV-Vis spectrum of **hybrid 28** (MeOH/H_2O (3:1))

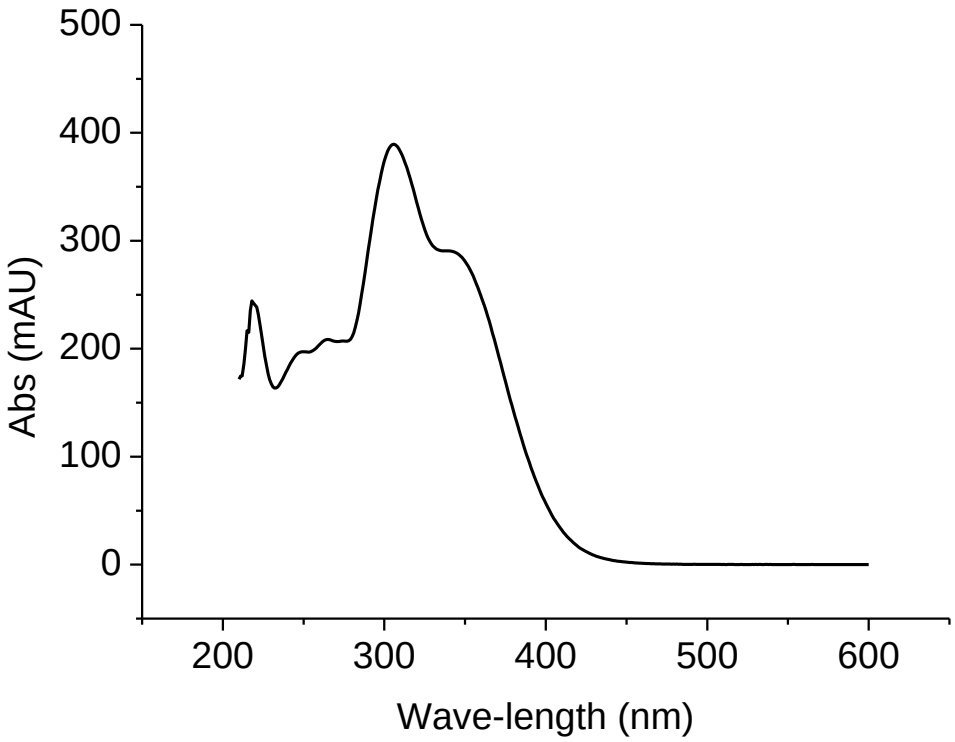

Figure S28. iv) HPLC chromatogram of **hybrid 28** (MeOH/H_2O (3:1))

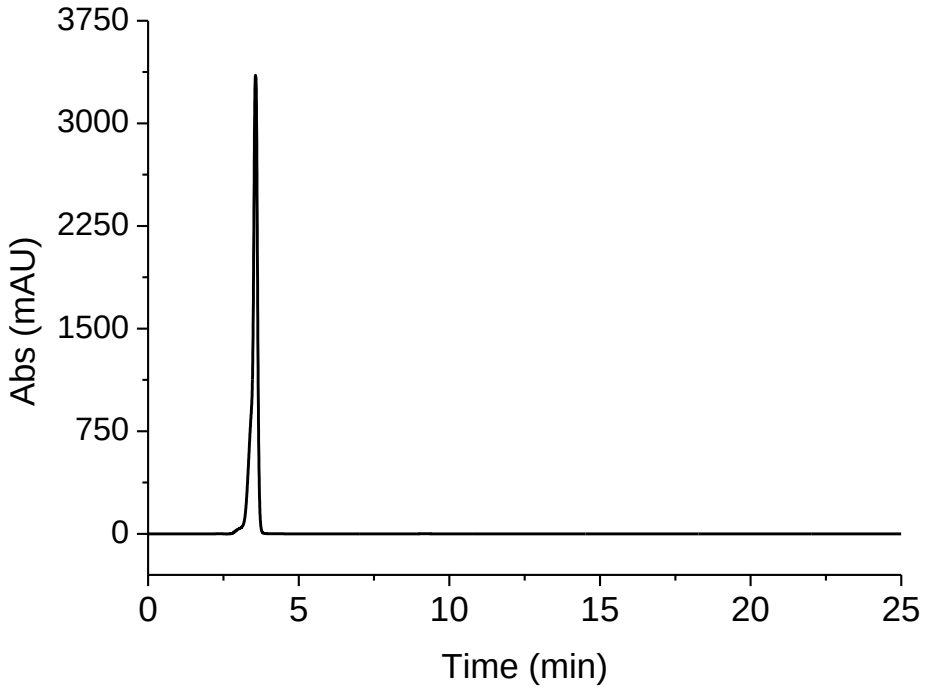

Figure S29. i) ^{1}H NMR spectrum of **hybrid 29** (300 MHz; DMSO-d_6)

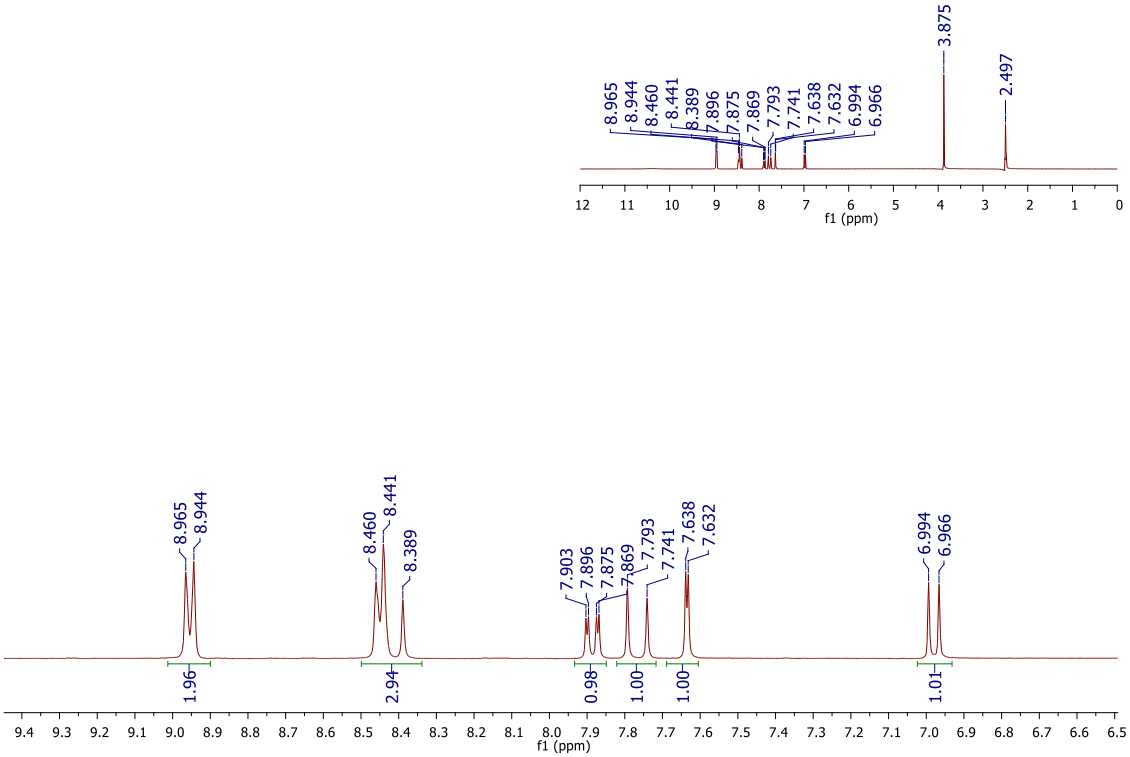

Figure S29. ii) ^{13}C NMR spectrum of **hybrid 29** (150 MHz; DMSO-d_6)

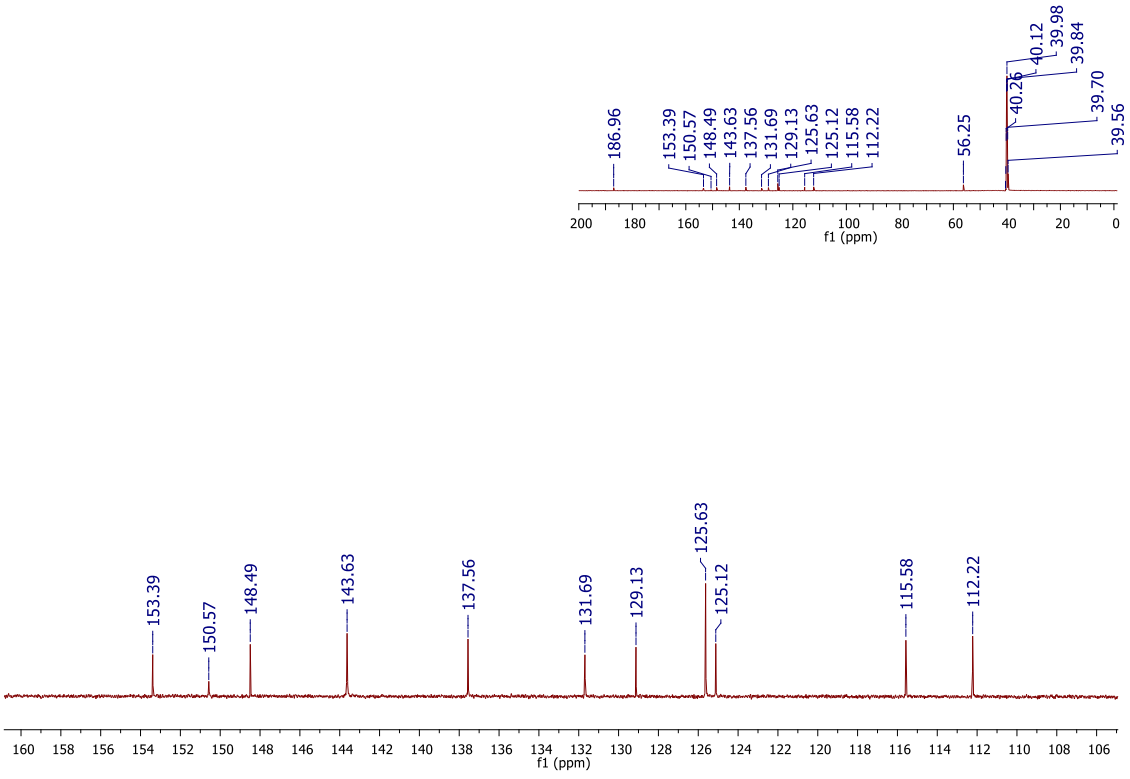

Figure S29. iii) UV-Vis spectrum of **hybrid 29** (MeOH/H_2O (3:1))

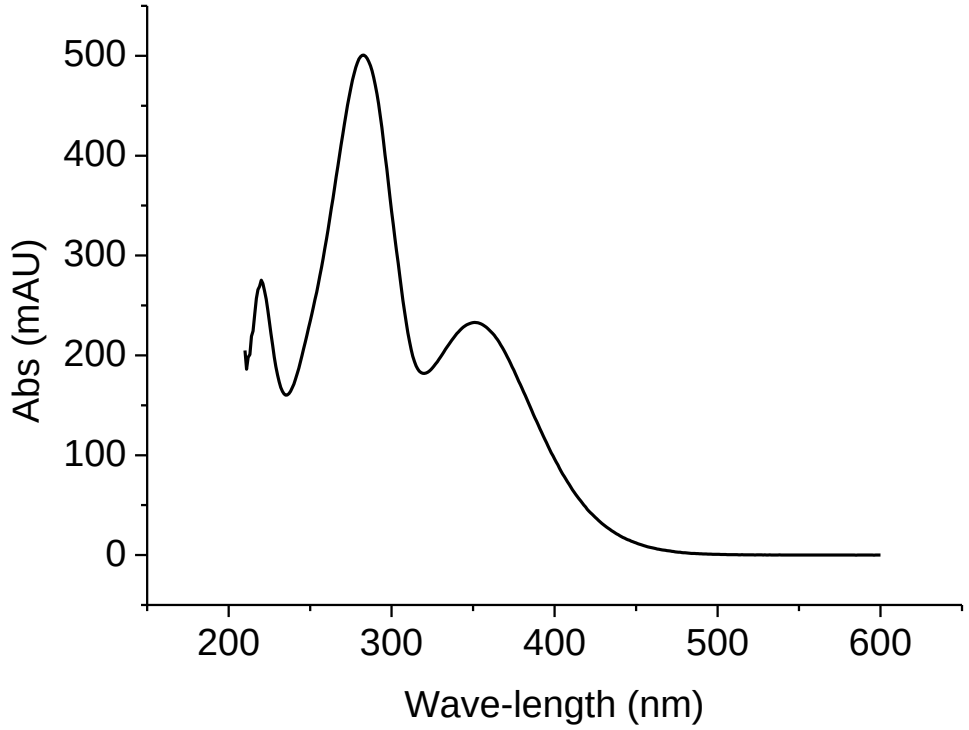

Figure S29. iv) HPLC chromatogram of **hybrid 29** (MeOH/H_2O (3:1))

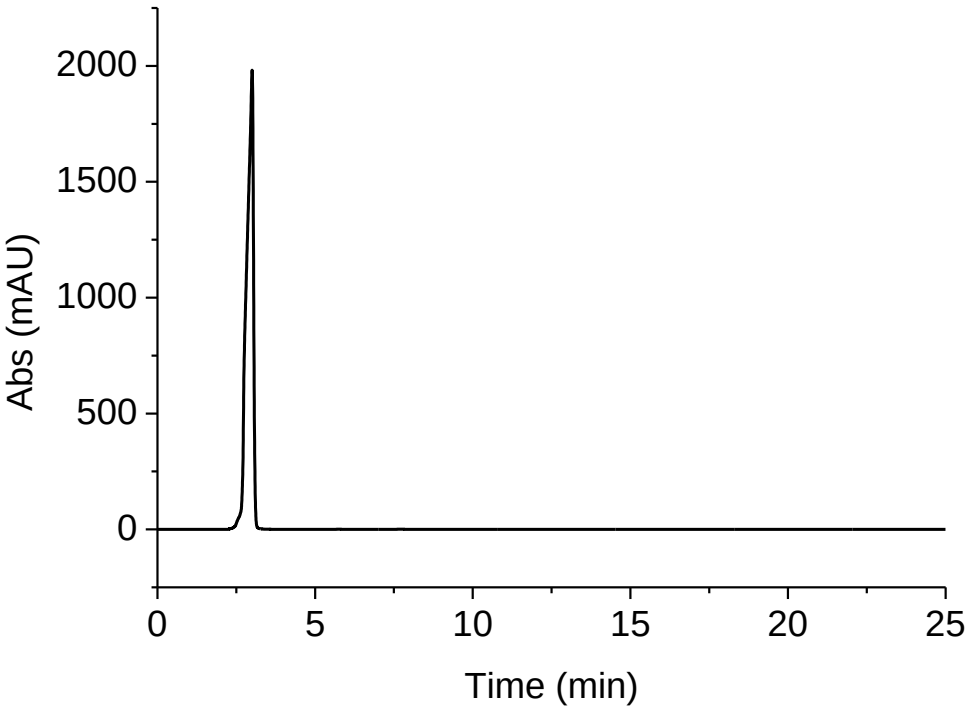

Figure S30. i) ^{1}H NMR spectrum of **hybrid 30** (600 MHz; DMSO-d_6)

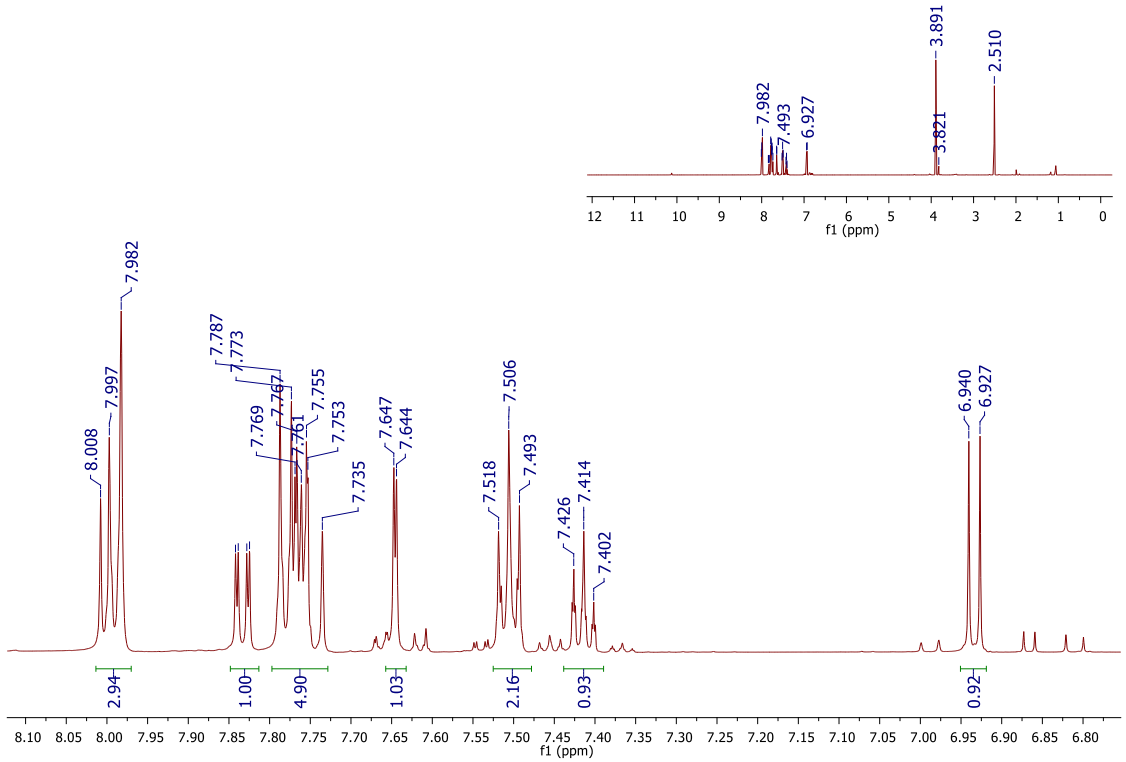

Figure S30. ii) ^{13}C NMR spectrum of **hybrid 30** (150 MHz; DMSO-d_6)

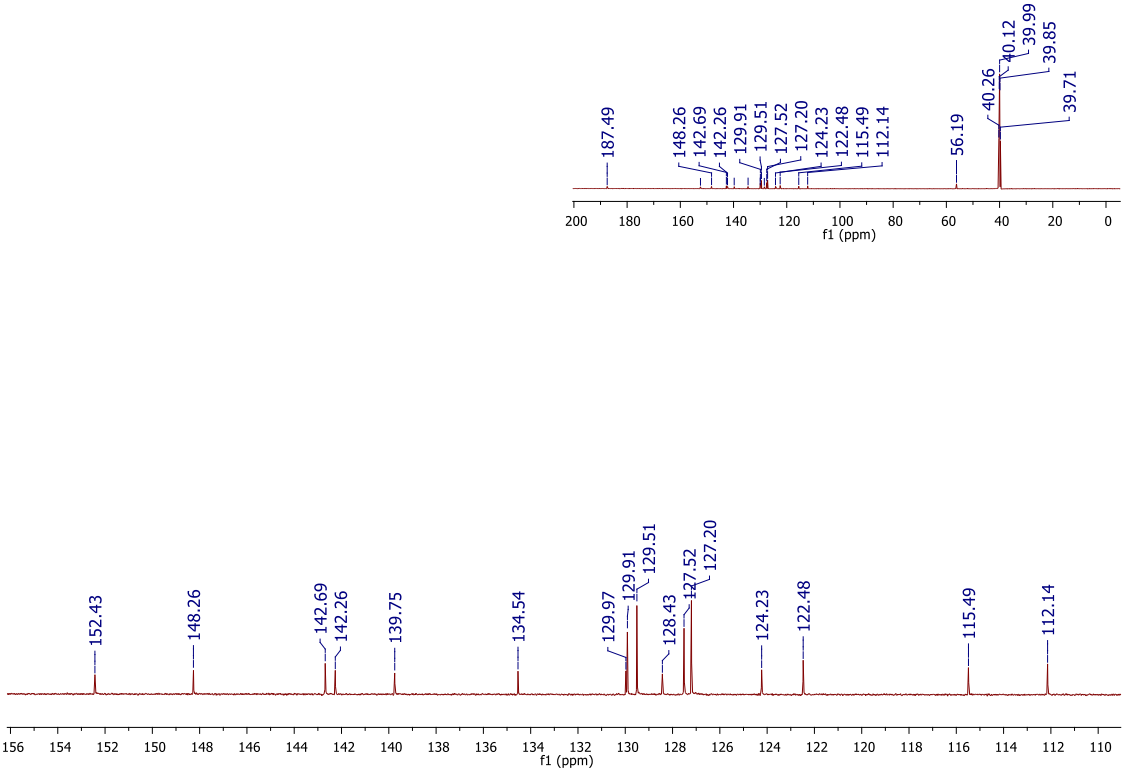

Figure S30. iii) UV-Vis spectrum of **hybrid 30** (MeOH/H_2O (3:1))

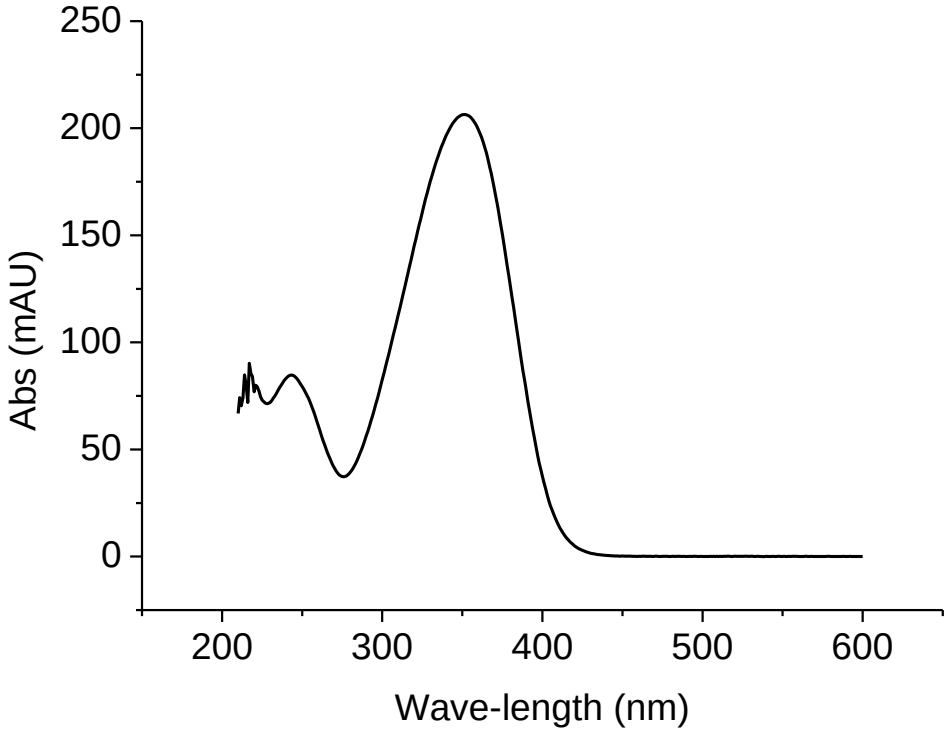

Figure S30. iv) HPLC chromatogram of **hybrid 30** (MeOH/H_2O (3:1))

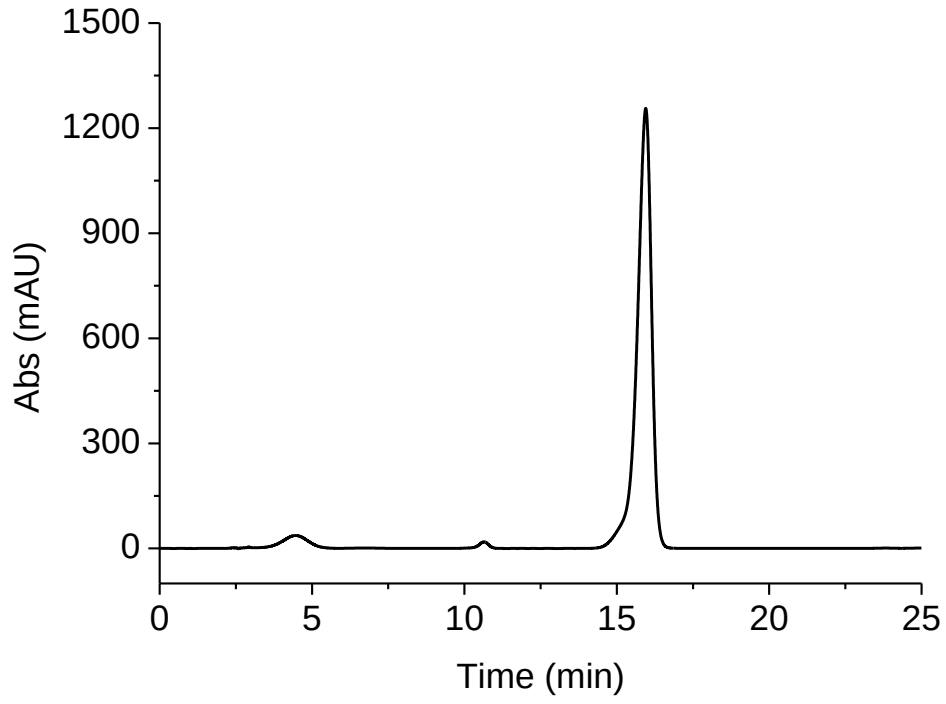

CAPÍTULO III

1. CONCLUSÕES

O presente trabalho discorreu à respeito da atividade antibacteriana de uma série de trinta híbridos curcumina-cinamaldeído. Primeiramente, os híbridos foram sintetizados, purificados e identificados estruturalmente, com posterior avaliação da atividade antibacteriana contra *S. aureus* sensível e resistente à meticilina (MSSA e MRSA), que evidenciou que a hibridação molecular entre a curcumina e o cinamaldeído manteve ou aumentou a atividade dos híbridos e que a lipofilicidade é um fator importante para o aumento da atividade anti-*S. aureus*.

O híbrido mais ativo contra MSSA e MRSA (híbrido **20**) foi selecionado para avaliação da sua combinação com vancomicina e meticilina, e quanto a sua atividade anti-adesão, antibiofilme e no tempo de morte das duas cepas. As associações entre **20** e vancomicina ou meticilina aumentaram a atividade antibacteriana contra MSSA e MRSA. O tratamento com **20** diminuiu a aderência das cepas de MSSA e MRSA, quando comparado ao grupo não tratado. Para os biofilmes, após o tratamento com **20**, verificou-se uma diminuição da sua sobrevivência quando comparado ao controle negativo, apresentando atividade antibiofilme similar ou superior à vancomicina e meticilina nas mesmas concentrações. No ensaio de tempo de morte, o tratamento com **20** diminuiu a população bacteriana ao longo do período experimental, indicando ação bactericida. Além disso, **20** apresentou toxicidade a 90 mg/kg, após 72 horas de tratamento, sendo responsável pela morte de 50% da larvas de *G. mellonella*.

Com relação ao expectro de ação dos híbridos curcumina-cinamaldeído, para *E. faecalis*, *S. epidermidis* e *P. aeruginosa*, os híbridos lipofílicos demonstraram maior atividade, no entanto, os híbridos não apresentaram atividade antibacteriana contra *E. coli*. *A. baumannii* foi a espécie bacteriana mais suscetível aos híbridos. Para *M. tuberculosis*, verificou-se que a inserção de grupos retiradores de elétrons e/ou lipofílicos aumentou a atividade antimicobacteriana.

Com relação aos estudos *in silico*, os híbridos não violaram as regras estabelecidas por Lipinski e Veber, corroborando boas propriedades druglikeness. Além disso, todos os híbridos apresentaram alta porcentagem de absorção intestinal e valores de permeação pela barreira hematoencefálica que indicam boa absorção no sistema nervoso central.

Por meio deste estudo, pode-se realizar estudos preliminares de relação estrutura-atividade e comprovar a atividade antibacteriana de híbridos de curcumina-cinamaldeído, estimulando o estudo dessas substâncias, a fim de buscar novos agentes capazes de atuar contra cepas resistentes.